HIDRAULICA

HYDRAULICS-PNEUMATICS-TRIBOLOGY-ECOLOGY-SENSORICS-MECHATRONICS
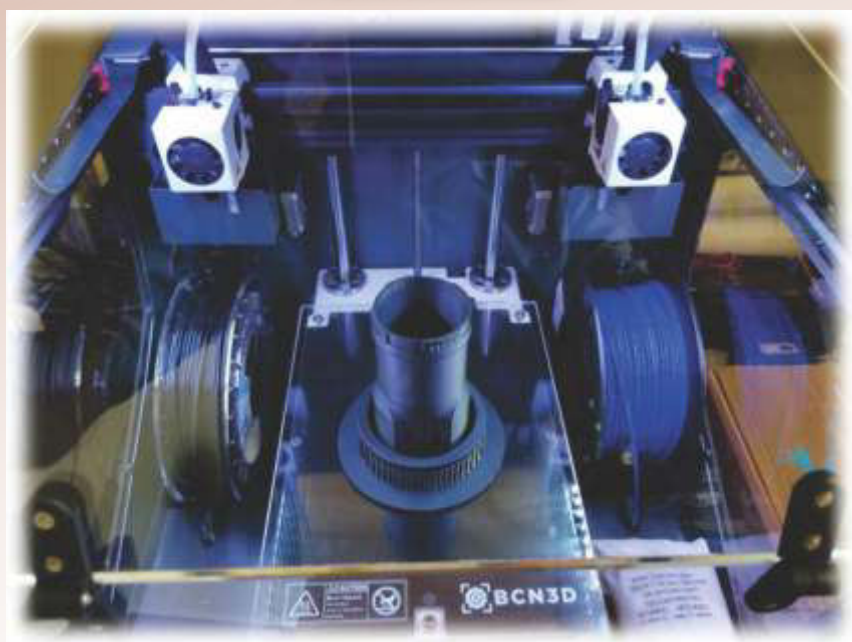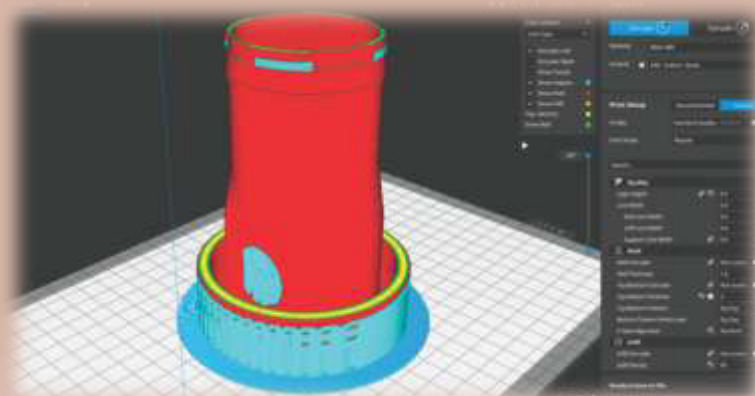
Available online at
hidraulica.fluidas.ro

CONTENTS

EDITORIAL

Hidraulica pe Internet

De ceva timp se tot vorbește de cea de-a patra revoluție industrială, care deși este în desfășurare specialiștii îi tot adaugă în fiecare zi noi valențe. Noile valențe sunt legate mai ales de informatică, senzorică, automatică, dar mai cu seamă de Internet.

Ph.D.Eng. Petrin DRUMEA
MANAGING EDITOR

În aceste zile când omenirea este lovită brutal de pandemia de coronavirus, una din probleme o constituie lipsa de capacitate managerială adecvată în coordonarea și mai ales în menținerea fabricației la un nivel acceptabil atunci când majoritatea lucrătorilor și specialiștilor stau acasă, participând la activitățile curente prin intermediul telefonului și al calculatorului.

Imediat se constată că nu mulți sunt cei bine pregătiti pentru lucrul cu calculatorul, pentru telecomanda sistemelor de producție sau pentru activitățile de concepție. Separarea informaticienilor de personalul de management și de cel implicat în producția concretă creează la această oră multe probleme pe care ni le-am creat singuri.

Probabil că în multe situații nu avem implementate nici măcar elementele unei mentenanțe predictive sau proactive, prin care să putem urmări calitatea în timp real a procesului de producție și situația nivelului de defectare a zonelor cu mare importanță în linia tehnologică de fabricație. Sigur că trebuia să determinam din timp care sunt punctele importante și care sunt situațiile lor de normalitate, să introducem senzoristică eficientă și informatica prin care să transformăm în fapt Internetul întru-un factor activ.

Oricum ar fi situația reală, este usor de realizat sistemul cu cerințele precizate anterior, la care să adăugam managementul potrivit.

În domeniul acționărilor hidraulice, multe din cerințele Industrie 4.0 sunt realizate industrial, de obicei pe zone tehnologice, dar cu mari șanse de trecere rapidă la nivelul întregii fabricații.

Să sperăm că această pandemie, pe lângă nenorocirile aduse, ne-a creat și impulsul progresului industrial de creație și de producție.

Vă doresc multă sănătate!

EDITORIAL

Hydraulics via the Internet

For some time, there has been talk about the fourth industrial revolution, and although it is in progress, specialists are adding new meanings to it every day. The new meanings are mainly related to computer science, sensorics, automation, but especially to the use of the Internet.

Ph.D.Eng. Petrin DRUMEA
MANAGING EDITOR

In these days when humanity is brutally hit by the coronavirus pandemic, one of the problems is lack of adequate managerial capacity in coordinating and especially in maintaining manufacturing at an acceptable level when most workers and specialists stay home, participating in current activities through the telephone and the computer.

It can be immediately noticed that not many of them are well prepared for working with the computer, for remote control of production systems or for design activities. The separation of the computer scientists from the management staff and the one involved in the actual production is currently creating many problems that we have created ourselves.

Probably in many cases we have not even implemented the elements of predictive or proactive maintenance, through which we can track the real-time quality of the production process and the fault level situation for the areas of great importance in the technological manufacturing line. Of course, we had to determine in advance what the critical points are and what their normal situations are, to introduce efficient sensorics and computing by which to actually turn the Internet into an active factor.

Whatever the real situation, it is easy to achieve the system with the requirements specified above, to which we should add the appropriate management.

In the field of hydraulic drives, many of the requirements of Industry 4.0 are achieved industrially, usually on technological areas, but with high chances of rapid transition across the entire manufacturing.

Let us hope that this pandemic, besides the misfortunes brought, has also created the impulse of the industrial progress of creation and production.

I wish you all good health.

Experimental Research on the Processing of Concave Spherical Surfaces with Toroidal Mills Versus Spherical Mills

PhD. Student Eng. **Andrei OȘAN**[1]

[1] Technical University of Cluj-Napoca - North University Center of Baia Mare, Romania,
osan.andrei@yahoo.com

Abstract: *The quality of the surface plays a very important role on the wear layer of the piece. There must be a balance so that the roughness is not too high but not too low. To determine the optimum roughness, several process factors must be correlated so that the results are the desired ones. This work aims to determine the roughness on the concave spherical surfaces. In order to determine it, the process factors but also the geometrical shape of the tool vary. As an additional argument in determining the optimal values, the execution time of each experiment is also pursued.*

Keywords: *Concave spherical surface, toroidal milling, spherical milling, optimum regimes, surface quality*

1. Introduction

Surface roughness is one of the most important parameters for determining product quality [5].
The presence of irregularities on the surface of a part transposes, under harsher operating conditions, a series of disadvantages: the effective contact surfaces are reduced, the conditions of friction and working conditions of the part are reduced, the resistance to alternating stresses of the material is reduced by the concentration of stresses. , reducing sealing, changing the actual dimensions of the part.
On the other hand, their absence makes it impossible to maintain the oil film on the contact surface at normal lubrication.
The roughness is determined according to the conditions of use, depending on: the processing speed, the size of the contact surface, the size and character of the requests, the precision of the dimensions and the geometric shape.
The roughness of the surfaces resulting from the milling operations are influenced by both the milling kinematics and the cutting conditions [3], [8], [1], [2].
The research carried out internationally, analyses the variation of the surface roughness processed with spherical milling cutters according to the following parameters: the angle of inclination of the cutting tool axis in relation to the normal one on the processed surface, the speed applied to the cutting tool, the advance on the tooth, the depth on the tooth, the depth of the tooth step by step etc.
The optimization of the processing strategies on machine tools with 5-axis numerical control is the theme of the work [4], where it is proposed to practice a variable angle of inclination of the tool axis in the direction of the processing advance, depending on the geometry of the processed surface. The results regarding the surface roughness, obtained on the basis of the experimental results are significantly higher.
The quality of the machined surface varies even if the machining strategy and the value of the inclination angle remain unchanged, but the orientation of the machining strategy changes with respect to the contour borders of the machined surface, by rotating the entire strategy with a certain angle, a fact highlighted in the paper [7].
The direction of inclination of the axis of the tool and the value of the angle at which the cutting tool is inclined in relation to the normal on the surface to be machined, is an important factor that determines the evolution of the roughness of the machined surfaces. As we established experimentally in the paper [6] the tool orientations have a great influence on the surface roughness, surface morphology as well as residual loading. For this reason, it is necessary to establish the optimum values of the inclination of the axis of the tool, for which the roughness has the lowest value, respectively avoiding the inclination directions and the angular values that determine high values of the roughness and implicitly low surface quality.

2. Presentation of the experimental stand

The experimental part will be realized on a centre with numerical control in 5 axes OKUMA MU-400VA. This is a fast and precise vertical CNC that offers superior simultaneous workability in 5 axes simultaneously. The Okuma MU-400VA has a rotary table that offers a plus in 5-axis processing as well as a fast and precise positioning and at the same time a rigidity in offering outstanding performance.

The spherical-concave surface is represented by a dome at the top of the plate, it is positioned in the centre of the plate representing the distance of 5mm from the maximum spherical height to the flat surface. The concave spherical shape has a diameter of Ø85 mm as provided in the following figure.
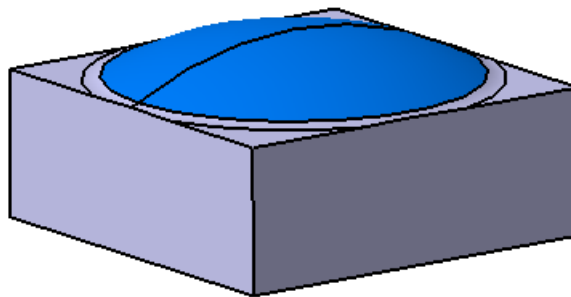
Fig. 1. The concave spherical surface

The two cutting tools used are: toroidal drill JHP780160E2R400.0Z4-M64 and spherical head drill JS534160D1B.0Z4-NXT.

TR200TIME is used to measure the roughness, this tester is applied on the production site and can be used to measure the roughness of the surfaces of the different processed parts, to calculate the parameters according to the selected measuring conditions and to clearly display all the measuring parameters and graphs. profile on the screen.

3. The experimental part

Within this subchapter we will experimentally research the development of 27 concave spherical surfaces with toroidal milling as shown in table 1 and 27 concave spherical surfaces processed with spherical milling as presented in table 2. At the same time, these tables contain a column where the basic times of each test are passed. These times represent strictly the moment spent during the processing, the auxiliary times being considered constant and equal avoiding their debate.

Regarding the cutting regimes only the 3 presented in the tables vary, the rest remain constant. Here the cutting depth equal to 0.5 mm (ap = 0.5 mm) and the radial depth equal to 0.3 mm (ae = 0.3mm) are entered. The emulsion is present as a cooling liquid throughout the process. Regarding the clamping mode, the plates will be attached to a clamp with a fingerprint being a rigid and secure system. For a better organization I decided to note with SFCV-TR the concave spherical surfaces processed with the toroidal milling machine and with SFCV-SF the concave spherical surfaces processed with the spherical milling machine.

Table 1: Carrying out experiments on the processing of concave spherical surfaces with toroidal milling

Nr.	Cutting speed [m/min]	Tilt angle [°]	Feed/tooth [mm/tooth]	Program name SFCV-TR	Time [min]
1	80	15°	0.11	SFCV-TR-1	04:09
2	80	15°	0.15	SFCV-TR-2	03:03
3	80	15°	0.19	SFCV-TR-3	02:24
4	80	35°	0.11	SFCV-TR-4	03:42

5	80	35°	0.15	SFCV-TR-5	02:43
6	80	35°	0.19	SFCV-TR-6	02:08
7	80	55°	0.11	SFCV-TR-7	03:41
8	80	55°	0.15	SFCV-TR-8	02:42
9	80	55°	0.19	SFCV-TR-9	02:08
10	170	15°	0.11	SFCV-TR-10	01:57
11	170	15°	0.15	SFCV-TR-11	01:26
12	170	15°	0.19	SFCV-TR-12	01:08
13	170	35°	0.11	SFCV-TR-13	01:44
14	170	35°	0.15	SFCV-TR-14	01:17
15	170	35°	0.19	SFCV-TR-15	01:01
16	170	55°	0.11	SFCV-TR-16	01:44
17	170	55°	0.15	SFCV-TR-17	01:16
18	170	55°	0.19	SFCV-TR-18	01:00
19	210	15°	0.11	SFCV-TR-19	01:35
20	210	15°	0.15	SFCV-TR-20	01:10
21	210	15°	0.19	SFCV-TR-21	00:55
22	210	35°	0.11	SFCV-TR-22	01:25
23	210	35°	0.15	SFCV-TR-23	01:02
24	210	35°	0.19	SFCV-TR-24	00:49
25	210	55°	0.11	SFCV-TR-25	01:24
26	210	55°	0.15	SFCV-TR-26	01:02
27	210	55°	0.19	SFCV-TR-27	00:49

Table 2: Carrying out experiments on the processing of concave spherical surfaces with spherical milling

Nr.	Cutting speed [m/min]	Tilt angle [°]	Feed/tooth [mm/tooth]	Program name SFCV-SF	Time [min]
1	80	15°	0.11	SFCV-SF-1	03:27
2	80	15°	0.15	SFCV-SF-2	01:55
3	80	15°	0.19	SFCV-SF-3	01:20
4	80	35°	0.11	SFCV-SF-4	03:48
5	80	35°	0.15	SFCV-SF-5	02:07
6	80	35°	0.19	SFCV-SF-6	01:28
7	80	55°	0.11	SFCV-SF-7	04:43
8	80	55°	0.15	SFCV-SF-8	02:37
9	80	55°	0.19	SFCV-SF-9	01:49
10	170	15°	0.11	SFCV-SF-10	02:37
11	170	15°	0.15	SFCV-SF-11	01:27
12	170	15°	0.19	SFCV-SF-12	01:01
13	170	35°	0.11	SFCV-SF-13	02:52
14	170	35°	0.15	SFCV-SF-14	01:36
15	170	35°	0.19	SFCV-SF-15	01:06

16	170	55°	0.11	SFCV-SF-16	03:34
17	170	55°	0.15	SFCV-SF-17	01:59
18	170	55°	0.19	SFCV-SF-18	01:22
19	210	15°	0.11	SFCV-SF-19	02:15
20	210	15°	0.15	SFCV-SF-20	01:15
21	210	15°	0.19	SFCV-SF-21	00:52
22	210	35°	0.11	SFCV-SF-22	02:28
23	210	35°	0.15	SFCV-SF-23	01:22
24	210	35°	0.19	SFCV-SF-24	00:57
25	210	55°	0.11	SFCV-SF-25	03:04
26	210	55°	0.15	SFCV-SF-26	01:42
27	210	55°	0.19	SFCV-SF-27	01:11

3.1 Surface processing

The CAM programs are made using the Powermill software capable of generating the desired trajectory depending on the required inclination, so we decided that the processing should be carried out in one direction, with the contour tracking movement with the interpolation function with the corresponding inputs and outputs having the possibility to create each tool separately. For a better expression in figure 2 are presented 3 images during the simulation of the milling process with the toroidal milling on the concave spherical surface with the 3 types of inclinations and in figure 3 are presented 3 images during the simulation of the concave spherical surface processing using the spherical milling in the 3 types of inclinations.
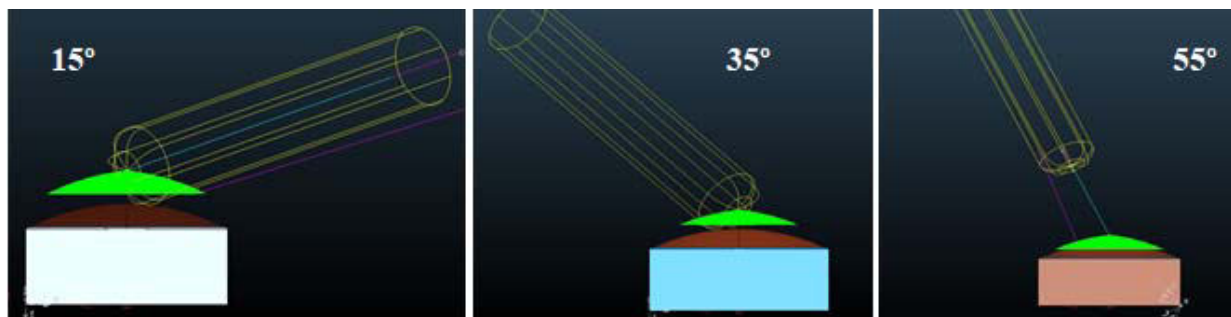
Fig. 2. Images taken following the simulation of the trajectory of the toroidal mill in Powermill on SFCV-TR
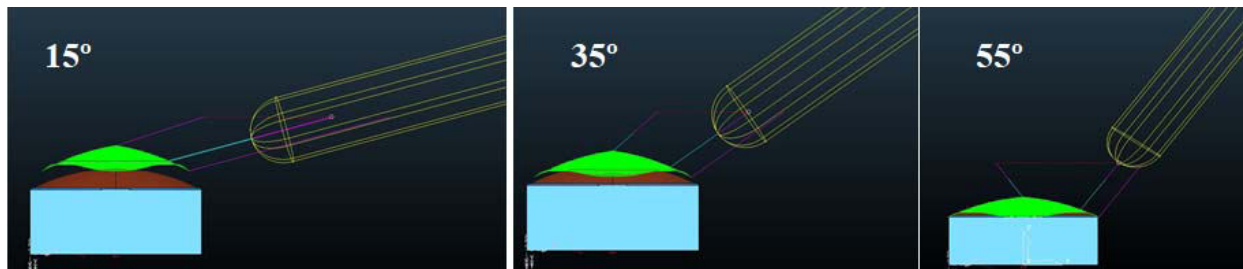
Fig. 3. Images taken following the simulation of the trajectory of the toroidal mill in Powermill on SFCV-SF

The practical experiment will be performed on the center with numerical control in 5 axes OKUMA MU-400VA as shown in figure 4 where 3 images are present during the processing of the concave spherical surface with the toroidal milling machine in the case of the 3 types of inclinations and in figure 5 it is presented processing of concave spherical surfaces with spherical milling for the 3 types of inclinations.

Fig. 4. Processing of the concave spherical surface with the toroidal milling machine in the case of the 3 types of inclinations

Fig. 5. Processing of the concave spherical surface with the spherical mill in the case of the 3 types of inclinations

It is noteworthy that, during the entire processing period, both in the case of toroidal milling and in the case of spherical milling, the axis of the tool keeps its angle of inclination constantly throughout the surface.

At the end of the experimental work performed on 27 concave spherical surfaces processed with toroidal milling and 27 concave spherical surfaces processed with spherical milling in the following figure are presented the plates prepared to be measured in terms of surface quality.

Fig. 6. The concave spherical surfaces processed with the two types of mills prepared for measurement

3.2 Analysis of the execution time

Analyzing the duration of the basic times of the processing of the concave spherical surface in the case of the two types of mills and of the 3 variables, the following was observed:

The maximum time obtained by the toroidal milling machine is 4 minutes and 9 seconds in the case of the minimum processing speeds but at an angle of inclination of 15º. As for the record, the shortest processing time of the concave spherical surface belongs to the toroidal milling of 49 seconds obtained at the maximum speed and at an angle of inclination of 55º.

The longest execution time is the one with spherical milling when the cutting regimes are at a minimum and the inclination angle is 55º with a time of 4 minutes and 43 seconds.

The spherical milling cut obtained the shortest for 57 seconds at maximum speeds and at an inclination angle of 35º.

At the conclusion of the graphical analysis of the basic times, they are close, there is a slight detachment of the toroidal drill for the inclination of 55º but the most important test is the quality of the surface.
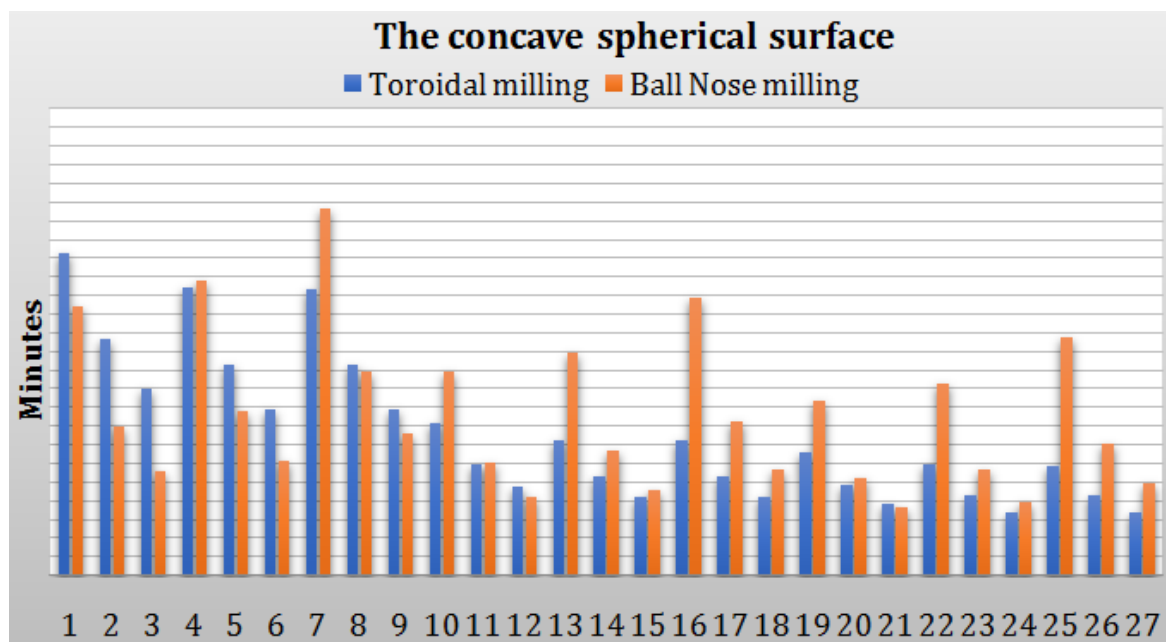
Fig. 7. Graphical analysis of the execution times for the processing of the concave spherical surface

3.3 Surface quality analysis

Regarding the concave spherical surface processed with the spherical milling, the smallest value of the arithmetic roughness Ra, is 0.296 [μm] for the SFCV-SF-10 surface processed with vc = 370 [m / min] fz = 0.05 [mm / tooth] and the inclination of the tool axis of 15º.

The highest roughness value Ra is 0.861 [μm] on the SFCV-SF-25 surface with vc = 430 [m / min] fz = 0.05 [mm / tooth] and the tool axis inclination of 55º.

The minimum value of the total roughness, Rt = 2,140 [μm] also in the case of the SFCV-SF-10 surface and the maximum value Rt = 8.860 [μm] on the SFCV-SF-25 surface.

The concave spherical surface processed with the toroidal milling saw the lowest arithmetic roughness, Ra = 0.220 [μm] measured in the direction parallel to the advance, the surface SFCV-TR-17 processed with vc = 170 [m / min] fz = 0.15 [mm / tooth] and 55º tool axis inclination.

The highest value of arithmetic roughness, Ra = 0.8 [μm] was recorded during SFCV-TR-4 surface processing with vc = 80 [m / min] fz = 0.11 [mm / tooth] and at the slope of 15º.

From the point of view of the total roughness Rt, the minimum value is 1,526 [μm] measured parallel to the advance direction on SFCV-TR-4. It is curious that this surface has the lowest roughness value Rt but it also holds the highest value of roughness Ra measured perpendicular to the feed direction.

The maximum value for the total roughness Rt is 6.433 [μm] measured perpendicular to the SFCV-TR-13 surface with vc = 170 [m / min] fz = 0.11 [mm / tooth] and the tool axis inclination of 35º.

Table 3: The results related to the processing of the concave spherical surface with the spherical mill

Surface type	Roughness Ra[μm]		Roughness Rt[μm]	
	Direction of measurement in relation to the direction of advance			
	Parallel	Perpendicular	Parallel	Perpendicular
SFCV-SF-1	0.429	0.556	3.626	3.496
SFCV-SF-2	0.429	0.493	2.279	3.860
SFCV-SF-3	0.338	0.543	2.786	3.880
SFCV-SF-4	0.392	0.484	3.300	3.803
SFCV-SF-5	0.443	0.606	3.639	3.880
SFCV-SF-6	0.385	0.536	2.927	3.783
SFCV-SF-7	0.448	0.513	3.059	5.093
SFCV-SF-8	0.476	0.495	2.453	3.846
SFCV-SF-9	0.400	0.541	3.166	5.093
SFCV-SF-10	0.296	0.485	2.140	3.867
SFCV-SF-11	0.329	0.543	2.473	4.093
SFCV-SF-12	0.379	0.543	3.053	4.039
SFCV-SF-13	0.383	0.573	2.620	4.466
SFCV-SF-14	0.390	0.555	3.346	4.113
SFCV-SF-15	0.504	0.403	4.206	3.293
SFCV-SF-16	0.413	0.666	3.326	6.399
SFCV-SF-17	0.456	0.771	3.679	7.080
SFCV-SF-18	0.409	0.670	4.220	5.406
SFCV-SF-19	0.370	0.785	3.153	5.313
SFCV-SF-20	0.396	0.683	3.220	5.566
SFCV-SF-21	0.436	0.580	3.146	4.200
SFCV-SF-22	0.479	0.674	3.679	5.246
SFCV-SF-23	0.546	0.660	4.566	5.533
SFCV-SF-24	0.486	0.505	4.700	3.686
SFCV-SF-25	0.522	0.861	3.873	8.860
SFCV-SF-26	0.548	0.614	4.660	4.980
SFCV-SF-27	0.467	0.607	4.312	4.886

Table 4: Results related to the processing of the concave spherical surface with the toroidal milling machine

Surface type	Roughness Ra[μm]		Roughness Rt[μm]	
	Direction of measurement in relation to the direction of advance			
	Parallel	Perpendicular	Parallel	Perpendicular
SFCV-TR-1	0.644	0.655	3.266	5.124
SFCV-TR-2	0.415	0.641	2.399	5.700
SFCV-TR-3	0.440	0.544	2.593	3.683
SFCV-TR-4	0.230	0.800	1.545	7.680
SFCV-TR-5	0.346	0.622	2.013	4.606

SFCV-TR-6	0.339	0.612	2.366	4.866
SFCV-TR-7	0.282	0.731	1.666	4.886
SFCV-TR-8	0.300	0.712	1.907	5.611
SFCV-TR-9	0.265	0.603	2.187	5.692
SFCV-TR-10	0.380	0.558	2.360	3.606
SFCV-TR-11	0.259	0.511	1.526	3.612
SFCV-TR-12	0.291	0.582	2.239	4.306
SFCV-TR-13	0.363	0.797	3.633	6.433
SFCV-TR-14	0.476	0.763	4.120	5.293
SFCV-TR-15	0.250	0.627	3.813	3.553
SFCV-TR-16	0.285	0.613	2.359	4.506
SFCV-TR-17	0.220	0.537	1.960	3.046
SFCV-TR-18	0.333	0.770	2.733	5.407
SFCV-TR-19	0.402	0.537	2.860	4.553
SFCV-TR-20	0.436	0.709	2.686	4.066
SFCV-TR-21	0.280	0.627	1.647	4.586
SFCV-TR-22	0.364	0.618	2.073	4.433
SFCV-TR-23	0.466	0.643	3.486	5.326
SFCV-TR-24	0.367	0.506	2.539	4.399
SFCV-TR-25	0.370	0.673	2.479	5.206
SFCV-TR-26	0.248	0.675	2.659	4.332
SFCV-TR-27	0.342	0.626	1.973	5.519

Comparing the quality of the concave spherical surfaces processed with the spherical mill and the toroidal mill, we can observe a slight advantage of 0.076 [μm] on the arithmetic mean depth for the toroidal mill in the case of surface processing with v_c = 170 [m / min] f_z = 0.15 [mm / tooth] and 55° tool axis inclination. And from the point of view of the total roughness R_t the toroidal mill has an advantage of 0.614 [μm].

The concave spherical surface represented by a dome proved that the best surface quality was obtained by toroidal milling at the inclination angle of 55°. In the case of surface processing at this angle the toroidal mill has developed less wear than the spherical mill.
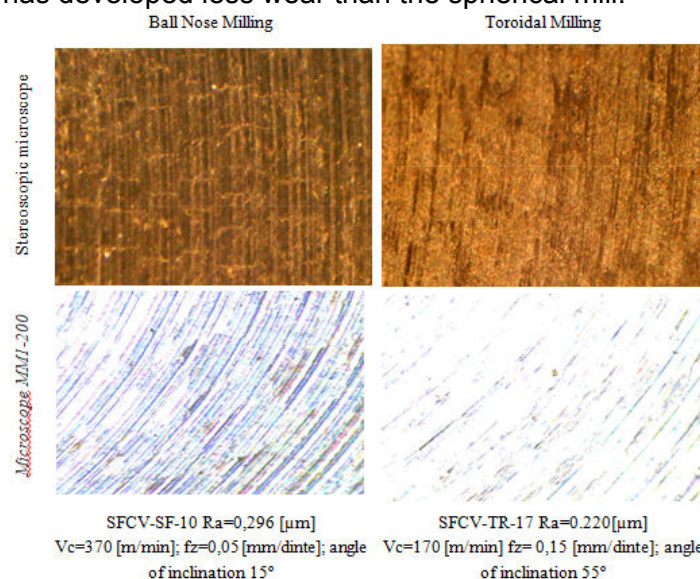

Fig. 8. Microscopic images of the quality of the surfaces processed with the two mills

Figure 8 shows microscopic images obtained with the IOR stereoscopic microscope and with the MM1-200 microscope of the best concave spherical surfaces processed with the toroidal or respective spherical mill.

4. Conclusions

The purpose of this work is to determine the quality of the surface. Surface quality plays a very important role in the precision and lubrication of surfaces. It was chosen to compare the processed surfaces with the toroidal milling, respectively the spherical milling. The surface on which the roughness was investigated is the concave cylindrical surface.

As variable parameters it was decided to juggle with the cutting speed, the feed rate and the inclination angle of the tool. It was decided to process 27 surfaces with toroidal milling and 27 surfaces machined with spherical milling.

From the point of view of the execution time, the fastest processing was performed with the toroidal milling machine within a period of 49 seconds in the case of the maximum speeds at the 55º angle compared to the fastest processing obtained with the spherical milling in 57 seconds. at maximum speeds but at 35º inclination angle.

Regarding the surface quality, the best surface quality was obtained with the toroidal milling machine, having the value Ra = 0.220 [μm] with Vc = 170 [m / min], Fz = 0.15 [mm / tooth] and the inclination angle of 55º. In the case of spherical milling, the best surface quality was recorded using the regimes Vc = 370 [m / min], fz = 0.05 [mm / tooth] and the inclination angle of 15º recording the value Ra = 0.296 [μm].

According to the aspects investigated in this paper, it is proved that depending on the surface geometry and the tool geometry, as regards the processing of concave spherical surfaces, one can exit the pattern to use the toroidal milling instead of the spherical milling. This statement is confirmed both by the evolution of the execution time and by determining the quality of the surface.

Acknowledgments

References

[1] Bieker, R. *CAM-compatible technology for CNC milling of hollow steel molds / CAM-gerechte technologie fuer die NCFraesbearbeitung von stahlhohlformen*. Diss. Thesis. Aachen, 1991.

[2] Bouzakis, K., D. Efstathiou, K. Antoniadis, A. Charachaliou, and P. Aichouh. "Analytical experimental determination of surface roughness in milling." Paper presented at 2nd International Conference on Tribology Balkantrib'96, Thessaloniki, June 5-7, 1996.

[3] Eversheim, W., W. Koenig, R. Bieker, and M.T. Cobanoglou. "NC Fraesbeareitung von vergueteten Schmiedegesenken." *VDI-Z integrierte Produktion* 131, no. 4 (1989): 99-103.

[4] Hikichi, T., K. Nakamoto, T. Ishida, and Y. Takeuchi. "Tool Path Generation for 5-Axis Control Machining Considering the Quality of Machined Surface." Proceedings of 5th International Conference on Leading Edge Manufacturing in 21st Century (LEM 21), Osaka, Japan, December 2-4, 2009, pp.107-112.

[5] Oșan, A. "Experimental Research on the Processing of Convex Spherical Surfaces with Toroidal Mills Versus Spherical Mills." *Magazine of Hydraulics, Pneumatics, Tribology, Ecology, Sensorics, Mechatronics "Hidraulica"*, no. 4 (December 2019): 63-72.

[6] Oșan, A., M. Bănică, and V. Năsui. "The influence of inclination of the axis of the toroidal on a flat surface roughness." Paper presented at the 23rd edition of Innovative Manufacturing Engineering&Energy International Conference – ImanE&E 2019, Pitești, Romania, May 22 – 24, 2019; *IOP Conf. Series: Materials Science and Engineering* 564 (2019): 012003, doi:10.1088/1757-899X/564/1/012003.

[7] Vijayaraghavan, A., A.M. Hoover, J. Hartnett, and. D.A. Dornfeld. "Improving endmilling surface finish by workpiece rotation and adaptive toolpath spacing." *International Journal of Macine Tools&Manufacture* 49 (2009): 89-98.

[8] Werner, A. *Process design and process reliability when using slim end mills / Prozessauslegung und Prozesssicherheit beim einstazt von schlanken schaftfraesern*. Thesis. Aachen, 1993.

Transients in Public Water Supply in Győr-Moson-Sopron County

Assistant professor PhD Student **Nikolett FECSER**[1]

[1] Széchenyi István University, 1 Egyetem tér, Gyor, H-9026, Hungary, e-mail: fecser.nikolett@sze.hu

Abstract: *Transient is a flow condition in which the velocity and pressure change rapidly with time. Transient operating states place such extreme loads on the pipes that they might cause burst water pipes. To highlight the importance of transient phenomena, I present the measurements carried out at Pannon-Víz Zrt and their results in my study. By this research, I aim to raise awareness about the dangers of transient phenomena in water supply systems. Furthermore, I wish to improve the operational safety and efficiency of water supply systems.*

Keywords: *Transient, flow condition, pressure, pipes, measuring instruments.*

1. Introduction

A transient operating state is a kind of flow in time and space which is initiated by the impacts of some occurrence started from a steady state and lasts until the development of another steady state [1]. In extreme situations, transient phenomena can endanger the soundness of the pipe itself. The main reasons of the occurrences of transient phenomena are, for example, a sudden change in flow or, isolating pipeline sections. If the valve openings and closings, pump start/stopping are not carried out slowly enough in the systems of large water pipes at pumping stations, they might generate quick changes in pressure. Due to the reasons mentioned above it is necessary to analyze the transient states developing in the system.

2. The venue of the measuring process

Pannon-Víz ZRt, the largest water and sewage service in Győr-Moson-Sopron county, operates several regional drinking water supply systems. My measuring instruments were installed at the booster station in Táp, and the reservoir at kindergarten in Táp. I applied 2 pieces of TRAREC® measuring instruments to monitor the transient state in the pipeline system. Model number LL1-12079 got installed at the booster station in Táp and LL1-12078 at kindergarten in Táp. The distance between the two measuring devices is 1190 meter. Figure 1 shows the distance between the two measuring instruments.

Fig. 1. Measurement venues

Fig. 2 shows the position of the two measuring instruments.

Fig. 2. Measurement venues

2.1 Describing the measuring instrument

The applied measuring instrument is TRAREC® (TRANSIENT RECORDER).
Main characteristics of the measuring instrument [2,3]:
• patented measurement and evaluation system
• normal or high-frequency measuring method
• selective data storage for long measurements
• variable parameters for different applications.

Figure 3 shows the TRAREC® measuring instrument.

Fig. 3. TRAREC® measuring instrument

Table 1 shows the parameters of the measuring instrument.

Table 1: TRAREC® the parameters of the measuring instrument [4]

Pressure sensor	0 -15 bar; (maximum 40 bar)
Accuracy	0.1%
Measurement frequency	50-1000 measurements / sec
Data storage frequency	1 - 60 s
Data segmentation	20 bit
Duration of measurement	1-2 weeks
Data communication and charging	USB 2

Table 2 shows the calibration data of the measuring instrument and summarizes some measured values.

Table 2: TRAREC® calibration data of the measuring instrument

Parameters of the measuring instrument		
Name	LL1-12078	LL1-12079
Sequence number	12078	12079
Version	1.0	1.0
Serial number	12078	12079
Pressure range (mwc)	211.00 mwc	211.00 mwc
Calibration	0.86111	0.86466
Pressure shifting	-9.58 mwc	-10.20 mwc
Starting date	14.02.2018	14.02.2018
Finishing date	16.02.2018	16.02.2018
Sea level (m)	0.00 m	0.00 m
Frequency of measurements	256 Hz	256 Hz
Frequency of data collection (sec)	1 sec	1 sec

3. Presenting measurement results

I used the PressEval software for evaluating the results of the measurement. Analysing transients I applied a 1- hour method, namely the number of occurrences of transients during an hour was evaluated. Fig. 4 shows the measurements made by the two measuring instruments. (Starting date: 14.02.2018, Finishing date: 16.02.2018).
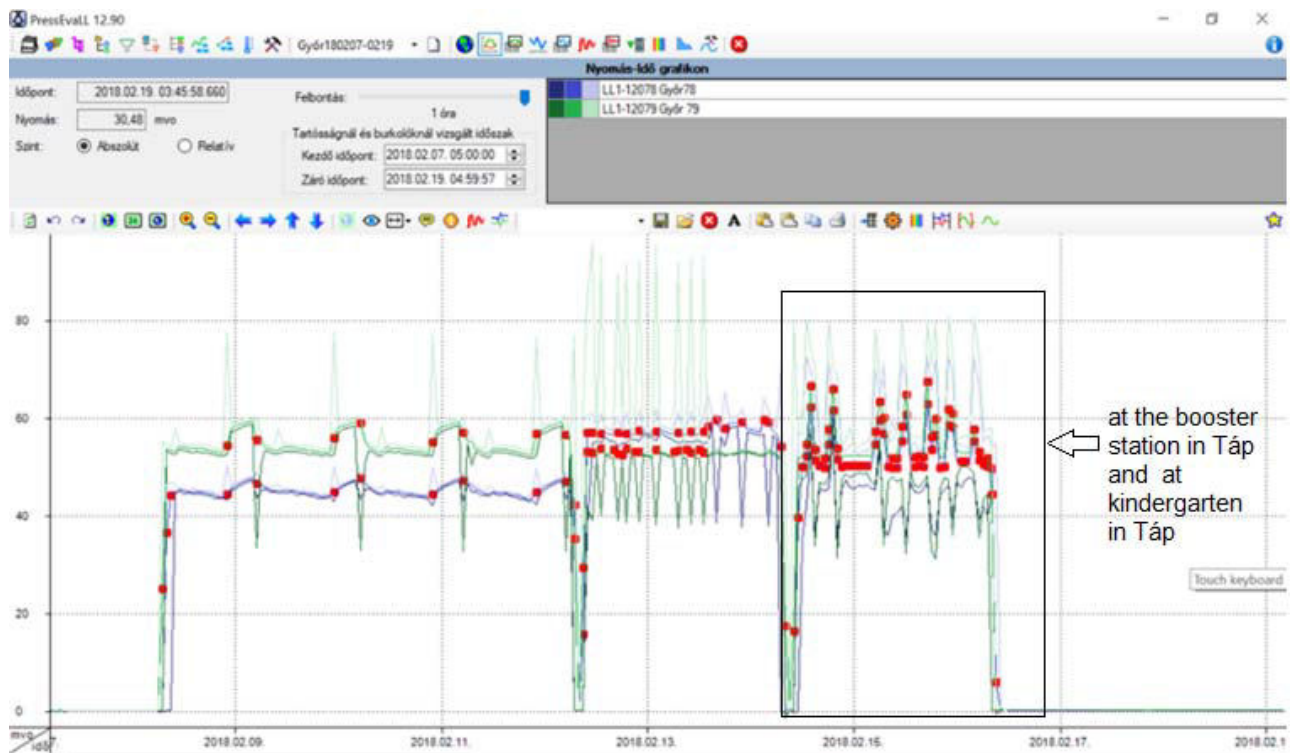
Fig. 4. Program PressEvaLL

In Table 3-4-5. I collected the absolute, minimum and maximum values of pressure changes.

Table 3: Pressure changes

Date (0.2.14-02.16) [h:m:s]		Absolute change [bar/s]	
Measurement instrument 79	Measurement instrument 78	Measurement instrument 79	Measurement instrument 78
	19:58:25		0.479
05:34:15		2548	
06:23:18		0.546	
	07:08:08		0.506
07:24:21		1.042	
	08:59:58		2.335
09:07:37		0.695	
	09:23:11		1.601
	10:17:49		0.927
10:33:01		0.998	
	10:54:09		0.898
11:34:23		2.923	
	11:51:33		0.496
17.22:49		0.408	
19:12:04		2.675	
22:26:49		3.027	
04:42:27	04:42:27	2.762	

Table 4: Pressure changes

Date (0.2.14-02.16) [h:m:s]		Minimum change [bar/s]	
Measurement instrument 79	Measurement instrument 78	Measurement instrument 79	Measurement instrument 78
	19:58:25		-6.615
05:34:15		-6.942	
06:23:18		-5.359	
	07:08:08		-3.066
07:24:21		-7.326	
	08:59:58		-17.744
09:07:37		-1.625	
	09:23:11		-13.415
	10:17:49		-14.309
10:33:01		-6.528	
	10:54:09		-14.039
11:34:23		-7.697	
	11:51:33		-1.221
17.22:49		-5.459	
19:12:04		-7.554	
22:26:49		-7.227	
04:42:27	04:42:27	-7.897	

Table 5: Pressure changes

Date (0.2.14-02.16) [h:m:s]		Maximum change [bar/s]	
Measurement instrument 79	Measurement instrument 78	Measurement instrument 79	Measurement instrument 78
	19:58:25		8.304
05:34:15		39.084	
06:23:18		4.604	
	07:08:08		3.421
07:24:21		7.127	
	08:59:58		14.891
09:07:37		2.053	
	09:23:11		12.151
	10:17:49		15.331
10:33:01		8.638	
	10:54:09		16.878
11:34:23		38.970	
	11:51:33		1.349
17.22:49		5.174	
19:12:04		33.838	
22:26:49		35.734	
04:42:27	04:42:27	36.661	

The process of the transient can be seen clearly from the table. The table demonstrates that the phenomenon of transiency is detectable in the system. The next task is to observe what causes the phenomenon of transiency.

4. Conclusions

The importance of the secure operation of domestic water supply systems is unquestionable. As part of my research, I carried out measurements on pipe sections operated by Pannon-VízZrt., using a sensor specially developed for transient measurements. In my study I intended to draw attention onto the existence of the phenomenon of pressure transiency and its importance. My goal is to reveal what might cause the appearance of transient in the system. Transient, which is a flow condition where the velocity and pressure change rapidly with time, can collapse a water distribution system if that system is not equipped with adequate transient protection devices. It is important to mention that measurements regarding transient phenomena help the detection of critical pipe sections, marking exactly the location where pressure absorbing elements should be mounted.

References

[1] Pandula, Zoltán. *Model describing transient flow behavior of a damper / Csappantyú tranziens áramlásbeli viselkedését leíró modell*. Budapest, Hungary, 2003.
[2] Zimmer, Péter. "Successful application of transient measurement in the field of water loss detection / A tranziens mérés sikeres alkalmazása a vízveszteség-feltárás területén." *Vízmű Panoráma*, no. 5 (2007).
[3] Ludányi, László, Árpád Nagy, and Péter Zimmer. "Trarec Transient Pressure Gauge and PressEval Data Management and Processing Software / A Trarec tranziens nyomásmérő műszer és a PressEval Adatkezelő és feldolgozó szoftver." Budapest, 2004. http://www.muszeroldal.hu/news/trarec.pdf.
[4] Csongrádi, Zoltán, Nikolett Fecser, and Bálint Lajtai. "Studying transients in water supply systems." *Hidraulica*, no. 3 (September 2018): 26-32.

Study of Temperature–Corrosion–Torsion Affecting Factors on the Shape of a Toroidal LPG Tank Using the Finite Element Method

Assoc. Prof. PhD. Eng. **Mihai ŢĂLU**[1], Assoc. Prof. PhD. Eng. **Ştefan ŢĂLU**[2,*]

[1] University of Craiova, Faculty of Mechanics, Department of Applied Mechanics and Civil Engineering, Calea București Street, no. 107, 200512 Craiova, Dolj county, Romania. E-mail: mihai_talu@yahoo.com

[2] Technical University of Cluj-Napoca, The Directorate of Research, Development and Innovation Management (DMCDI), Constantin Daicoviciu Street, no. 15, Cluj-Napoca, 400020, Cluj county, Romania. Corresponding author* e-mail: stefan_ta@yahoo.com

Abstract: *In this paper it is investigated the influence of the temperature–corrosion–torsion affecting factors on the shape of a three-dimensional (3-D) hexagonal toroid with regular hexagonal cross-section used in manufacturing of liquefied petroleum gas (LPG) storage tanks from the automotive industry. A design strategy was proposed to determine based on the finite element method, the change of the torsion angle, temperature and corrosion factors during operation. Numerical simulations were applied to compute the optimum form and sizing of the storage tank based on an objective optimization function to minimize the storage tank mass. The proposed method is demonstrated and numerical tested, demonstrating the potential of the suggested approach.*

Keywords: *3-D hexagonal toroidal LPG fuel tank, automotive industry, industrial engineering design, optimization methods*

1. Introduction

Nowadays, computer-aided design is recognized as a strategic resource in the field of the fuel tank industry [1-3] and a coherent approach regarding the advanced design tools [4-7] for the creation of new products with high performances was applied [8-10].
Diverse methods for manufacturing of LPG storage tanks have been introduced in many academic and industrial fields [11-14]. Most of them were made by approaches depended on the knowledge and experience of the experts concerning qualitative innovation based on 3-D design that offers a competitive advantage [14-17].
In the scientific literature there are presented various multicriteria analyses by evolutionary stages (design, execution and operation) [18-22] of the factors that influence LPG storage tanks from the automotive industry [23-26].
The dynamics of the storage tank markets requires superior engineering CAD designs [27-30], quality construction practices [31-33], and intelligent innovations for optimizing system performance and to meet the customers' requirements [33-36].
Modeling prototypes with computer-aided design (CAD) software [37-40] and advanced design modeling with a widely used interface standard [41-43] allow encouraging the rapid adoption of efficient technologies for LPG storage tanks including credible information, standards, and other management policies. Also, well-designed LPG storage tanks and control strategies can improve reliability, and reduce costs by using modern technologies [44-48].

2. Design methodology

2.1. Basic geometry of the parametric 3-D model

Let's consider the parametric 3-D model generated by revolving of a closed generating curve C_G (a hexagon with rounded corners) along a closed guiding curve C_D (a hexagon with rounded corners) as shown in figs. 1 and 2 [14].
The following parameters were applied as input parameters to the 3-D parametric model (figs. 1 and 2): a) a closed generating curve CG (a hexagon with a side value L = 175 mm, with rounded corners, radius R = 50 mm), and b) the guiding curve CD (a hexagon with a side value L = 430 mm, with rounded corners, radius R = 180 mm), and the thickness = 10 mm.

Fig. 1. The axonometric view of 3-D twisted model   **Fig. 2.** The frontal view of 3-D twisted model
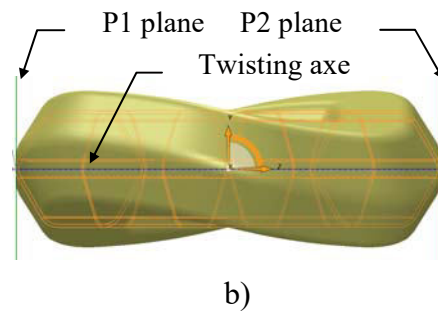
2.2. Numerical analysis of the parametric 3-D model

Based on the physical model, the modeling was done in the AutoCAD Autodesk 2020 software [49] and the numerical analysis was performed with SolidWorks 2020 software [50] with the Static, Thermal and Design Study modules. The design data used were:
- the tank material is AISI 4340 steel;
- the maximum hydraulic test pressure: p_{max} = 30 bar;
- the working temperature between the limits: T = -30 ^{0}C up to T = 60 ^{0}C;
- supporting surfaces located on the inferior side;
- the duration of the tank exploitation: n_a = 15 years;
- the corrosion rate of the material: v_c = 0.07 mm/year.

Numerical calculations were performed for: mesh standard type, solid mesh, curvature-based mesh with quality high, Jacobian in 16 points, element size 6 mm, number of nodes 47767, number of elements 23925.

The parameterized 3-D model used in calculus is a section of ½ (fig. 3) from the initial physical model and the corresponding surfaces to which the constraints and restrictions are applied are shown in fig. 4.

Fig. 3. The corresponding surfaces to which the constraints are applied for half section of the model   **Fig. 4.** The corresponding surfaces to which the constraints are applied for of the whole model

The design data used in this analysis for the tank lateral cover are:
- the maximum pressure p_{max} = 3 N/mm^2 on the inner surface S_1;
- the working temperature between the limits: T = -30 ^{0}C to T = 60 ^{0}C on the exterior surface S_2;
- the fixation of the tank on the six tank supports located at the inferior part of the tank.

The values of the state of stress Von Mises determined by the finite element method for n_a= 0 and 5 years are shown in table 1.

Table 1: The Von Mises resultant effort for n_a= 0 and 5 years

σ [MPa]	n_a= 0 years				n_a= 5 years			
	T [°C]				T [°C]			
φ [°]	-30°	0°	30°	60°	-30°	0°	30°	60°
0	604.130	533.813	441.46	487.942	609.754	513.007	455.0307	506.921
0.25	633.167	524.136	471.115	515.153	646.455	544.486	499.540	549.939
1	632.577	526.742	448.32	497.578	630.826	527.699	499.485	542.929
2	603.872	514.467	435.172	482.933	648.021	556.001	468.075	513.643
4	582.163	491.112	436.272	474.882	647.333	553.428	468.162	506.284
6	614.474	533.706	433.225	461.236	671.966	558.710	455.288	494.191
8	562.664	483.278	434.062	482.022	684.722	593.138	503.395	529.039
10	597.586	508.453	428.215	456.060	646.973	558.237	472.069	520.390

The graphs corresponding to the Von Mises resultant efforts taking into account the results from table 1 are graphically shown in figs. 7, 8, 13 and 14, respectively.
The most important cases of the maximum values of the Von Mises effort taking into account the results from table 2 are graphically shown in figs. 5, 6, 9, 10, 11, 12, 15 and 16, respectively.

Table 2: The maximum values of the Von Mises resultant effort

Case no.	n_a [years]	φ [°]	T [°C]	σ [MPa]
1	0	0.25	-30	633.167
2	5	8	-30	684.722
3	10	0.25	-30	671.250
4	15	8	-30	726.248

a) Case no.1
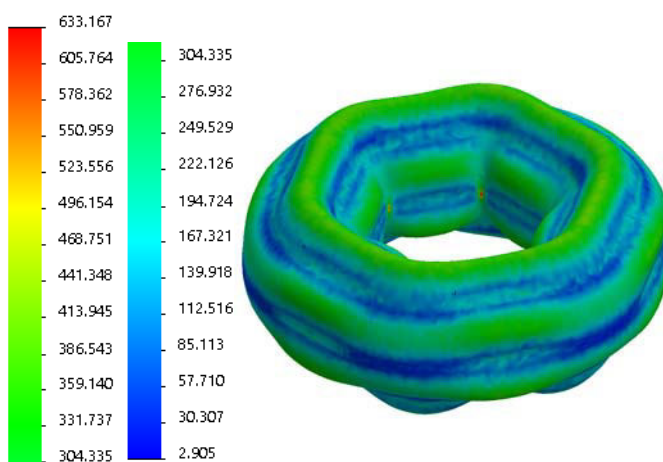
Fig. 5. The graphs of Von Mises stress distribution for n_a = 0 years
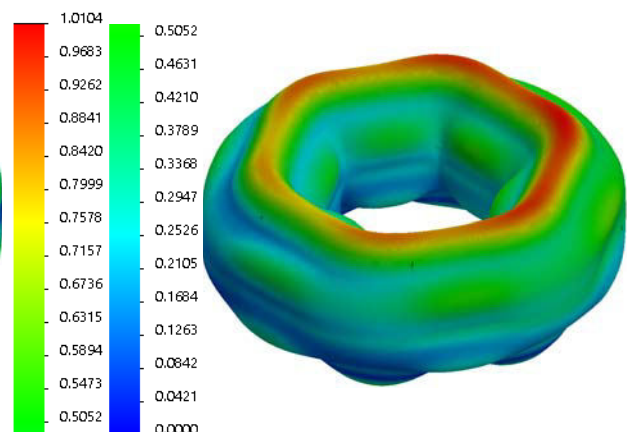
Fig. 6. The graphs of linear deformation distribution for n_a = 0 years

The graphs of 3-D surfaces corresponding to the Von Mises effort $\sigma = f(T, \phi)$ for 0 and 5 years are graphically shown in figs. 7 and 8.

Fig. 7. The graphs of $\sigma = f(T, \phi)$ for $n_a = 0$ years   **Fig. 8.** The graphs of $\sigma = f(T, \phi)$ for $n_a = 5$ years

b) Case no. 2
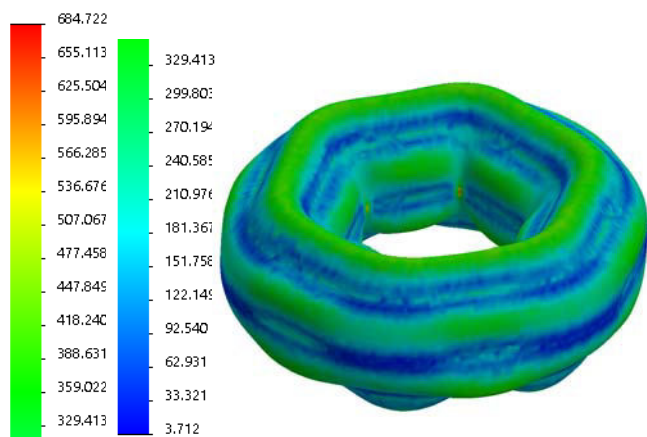
Fig. 9. The graphs of Von Mises stress distribution for $n_a = 5$ years   **Fig. 10.** The graphs of linear deformation distribution for $n_a = 5$ years

The values of the state of stress Von Mises determined by the finite element method for $n_a = 10$ and 15 years are shown in table 3.

Table 3: The Von Mises resultant effort for $n_a = 10$ and 15 years

σ [MPa]	$n_a = 10$ years				$n_a = 15$ years			
	T [°C]				T [°C]			
ϕ [°]	-30°	0°	30°	60°	-30°	0°	30°	60°
0	631.859	536.113	500.095	544.749	664.749	580.277	539.257	593.356
0.25	671.825	580.275	513.908	559.111	720.992	642.609	563.393	609.903
1	656.152	558.748	523.648	572.092	690.050	582.294	575.271	617.743
2	640.331	548.530	499.530	544.232	656.473	556.017	565.732	612.368
4	665.269	566.368	511.877	560.938	697.559	602.885	560.280	614.595
6	618.443	539.903	498.637	551.038	675.154	587.652	540.631	594.554
8	642.592	555.988	519.963	572.506	726.248	633.716	542.715	587.319
10	637.352	547.513	501.518	553.876	677.954	585.842	565.737	613.592

c) Case no. 3
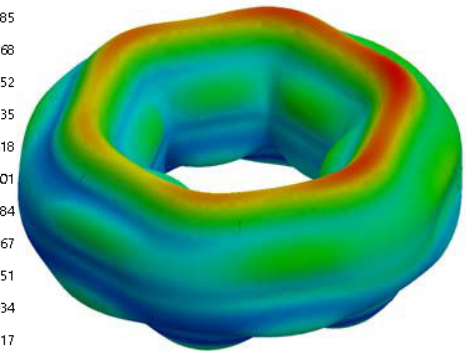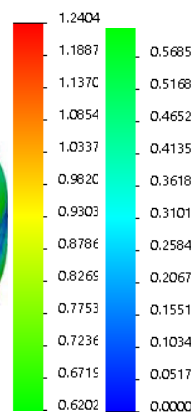
Fig. 11. The graphs of Von Mises stress distribution for n_a = 10 years

Fig. 12. The graphs of linear deformation distribution for n_a = 10 years

The graphs of 3-D surfaces corresponding to the Von Mises effort σ = f(T, ϕ) for 10 and 15 years are graphically shown in figs. 13 and 14.
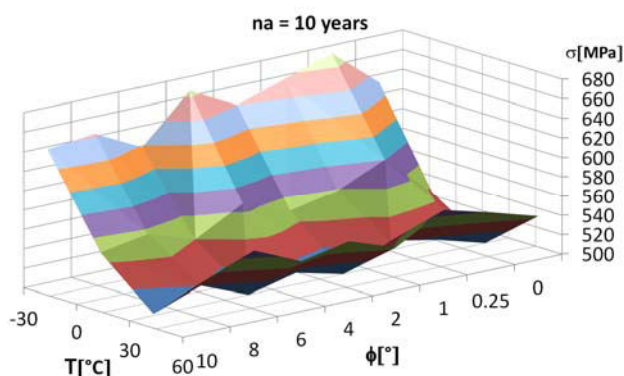
Fig. 13. The graphs of σ = f(T, ϕ) for n_a =10 years
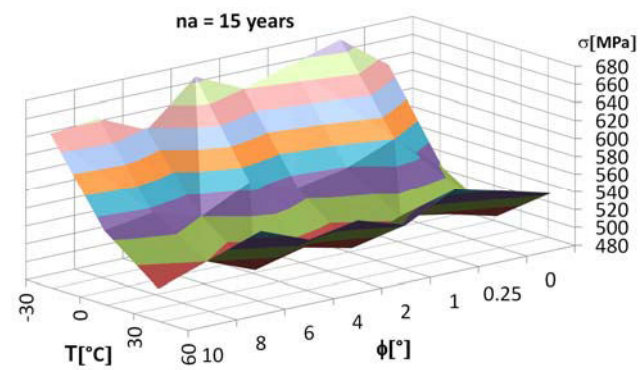
Fig. 14. The graphs of σ = f(T, ϕ) for n_a = 15 years

d) Case no. 4

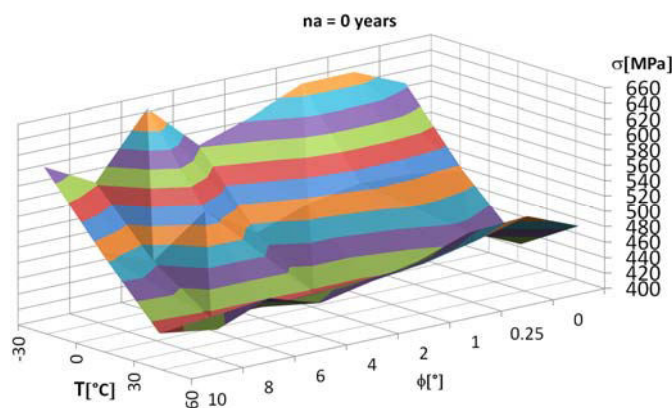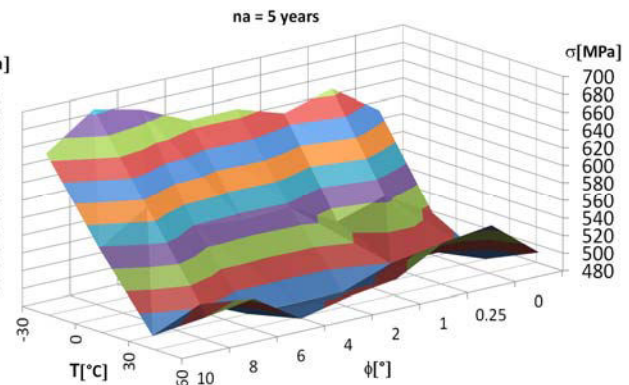**Fig. 15.** The graphs of Von Mises stress distribution for n_a = 15 years

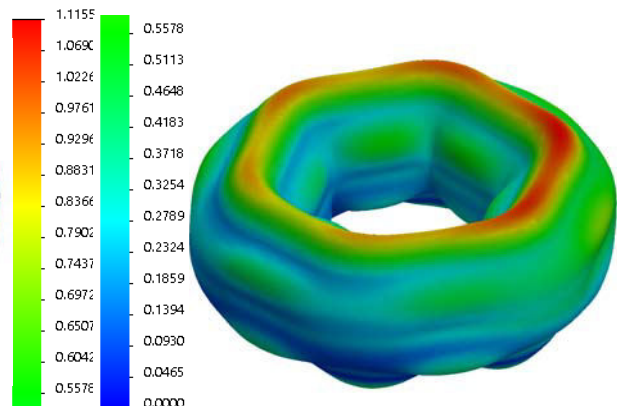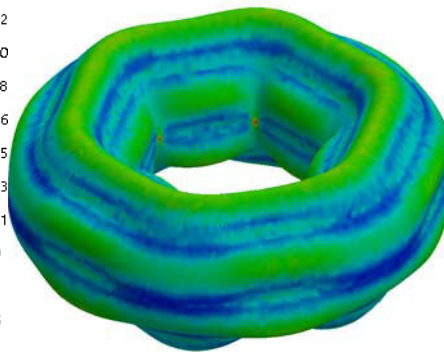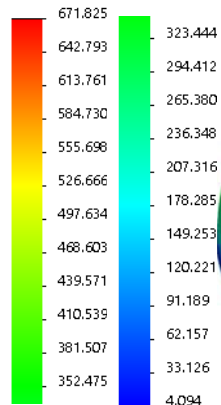**Fig. 16.** The graphs of linear deformation distribution for n_a = 15 years

The percentage variation of Von Mises resultant effort in relation to the initial effort status (tables 4 and 5) and the corresponding graphs are given in figs. 17, 18 and 19.

Table 4: The percentage variation of Von Misess resultant effort for 5 and 10 years

	Δσ [%] for n_a= 5 years				Δσ [%] for n_a= 10 years			
	T [°C]				T [°C]			
φ [°]	-30°	0°	30°	60°	-30°	0°	30°	60°
0	0.93	3.74	3.07	3.89	4.59	4.34	13.28	11.64
0.25	2.10	3.88	6.03	6.75	6.11	10.71	9.08	8.53
1	0.99	0.18	11.41	9.11	3.73	6.08	16.80	14.98
2	7.31	8.07	7.56	6.36	6.04	6.62	14.79	12.69
4	11.19	12.69	7.31	6.61	14.28	15.32	17.33	18.12
6	9.36	4.68	5.09	7.14	0.65	1.16	15.10	19.47
8	21.69	22.73	15.97	9.75	14.21	15.05	19.79	18.77
10	8.26	9.79	10.24	14.11	6.65	7.68	17.12	21.45

Table 5: The percentage variation of Von Misess resultant effort for 15 years

	Δσ [%] for n_a = 15 years			
	T [°C]			
	-30°	0°	30°	60°
φ [°]	10.03	12.94	22.15	21.60
0	13.87	22.60	19.59	18.39
0.25	9.09	10.55	28.32	24.15
1	8.71	8.08	30.00	26.80
2	19.82	22.76	28.42	29.42
4	9.88	10.11	24.79	28.90
6	29.07	31.13	25.03	21.84
8	13.45	15.22	32.12	34.54
10	10.03	12.94	22.15	21.60

Fig. 17. The graphs of Δσ for n_a = 5 years

Fig. 18. The graphs of Δσ for n_a = 10 years

Fig. 19. The graphs of Δσ for n_a = 15 years

The most important cases of the maximum values of the resultant linear deformation taking into account the results from table 6 are graphically shown in figs. 20, 21, 24, 25, 26, 27, 30 and 31, respectively.

The graphs corresponding to the resultant linear deformation *u* taking into account the results from table 6 are graphically shown in figs. 22, 23, 28 and 29, respectively.

The values of the resultant linear deformation *u* determined by the finite element method for 0 and 5 years are shown in table 6.

Table 6: The resultant linear deformation for n_a= 0 and 5 years

u [mm]	n_a= 0 years				n_a= 5 years			
	T [°C]				T [°C]			
ϕ [°]	-30°	0°	30°	60°	-30°	0°	30°	60°
0	1.0170	0.9791	0.9434	0.9117	1.11340	1.0743	1.0369	1.0043
0.25	1.01801	0.97955	0.94958	0.9262	1.12945	1.09517	1.06171	1.03081
1	0.99508	0.96169	0.93050	0.90255	1.08137	1.04716	1.01438	0.98266
2	0.97581	0.94611	0.91779	0.89117	1.06893	1.03666	1.00558	0.97721
4	0.99898	0.96650	0.93499	0.90532	1.08680	1.05429	1.02450	0.99571
6	1.02196	0.98997	0.96063	0.93327	1.12669	1.09292	1.06090	1.02826
8	1.01696	0.98608	0.95619	0.92772	1.11552	1.08383	1.05303	1.02509
10	1.03229	1.00131	0.97133	0.94276	1.13948	1.08960	1.07938	1.05072

Table 7: The maximum values of the resultant linear deformation

Case no.	n_a [years]	ϕ [°]	T [°C]	u [mm]
5	0	0	-30	1.01700
6	5	10	-30	1.13948
7	10	10	-30	1.24760
8	15	10	-30	1.38699

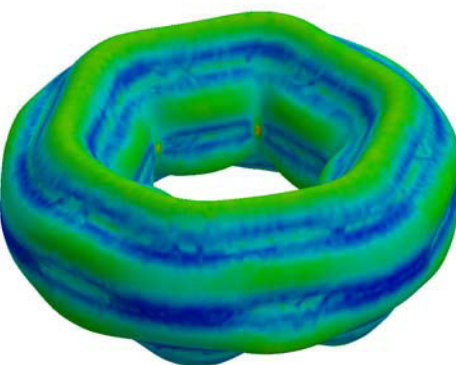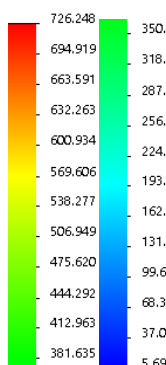e) Case no. 5
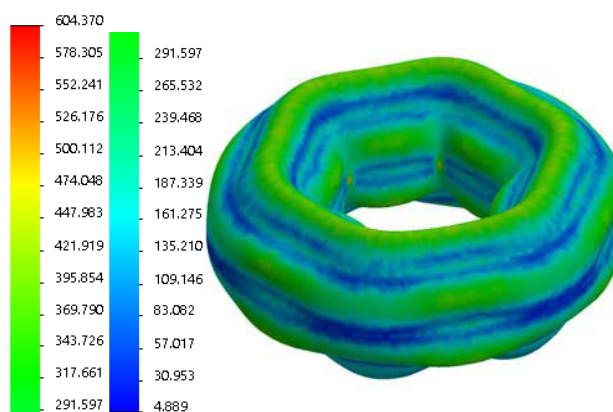
Fig. 20. The graphs of Von Mises stress distribution for n_a = 0 years
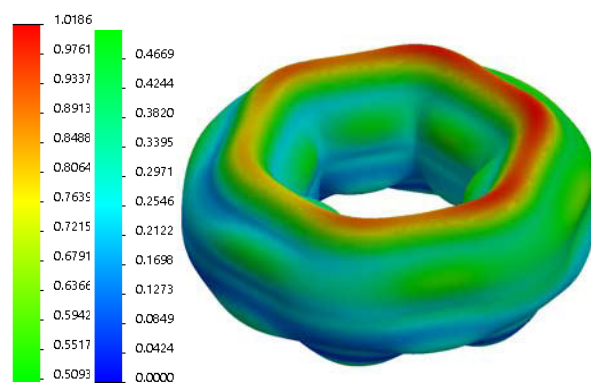
Fig. 21. The graphs of linear deformation distribution for n_a = 0 years

The graphs of 3-D surfaces corresponding to the resultant linear deformation for 0 and 5 years are graphically shown in figs. 22 and 23.
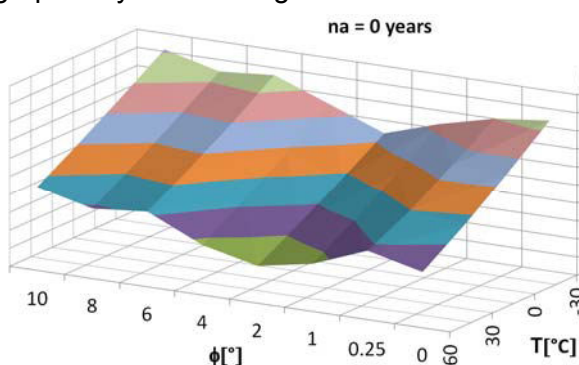
Fig. 22. The graphs of u = f(T, ϕ) for n_a = 0 years
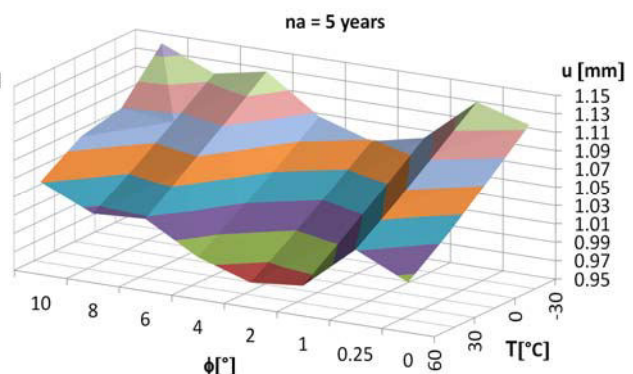
Fig. 23. The graphs of u = f(T, ϕ) for n_a = 5 years

f) Case no. 6
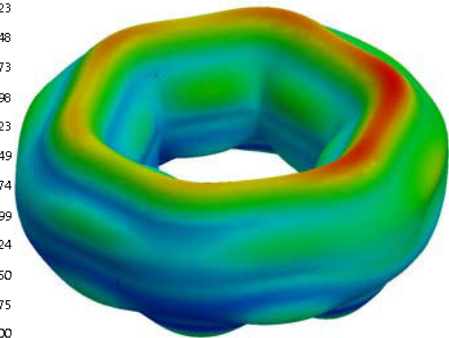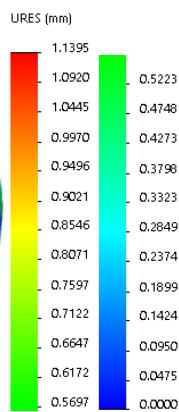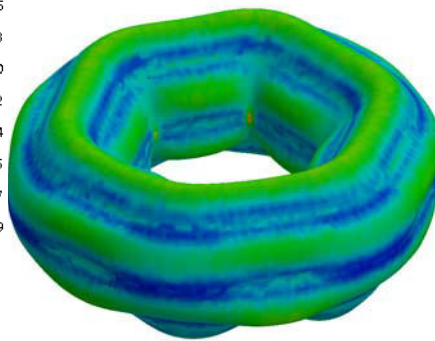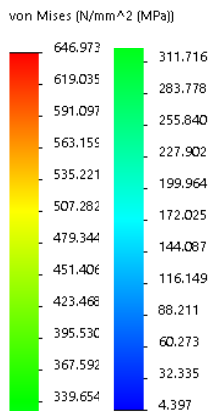
Fig. 24. The graphs of Von Mises stress distribution for n_a = 5 years

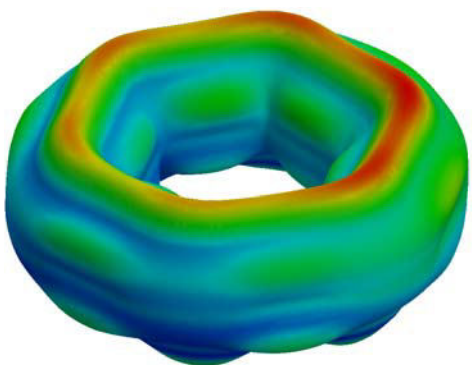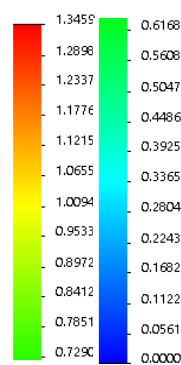**Fig. 25.** The graphs of linear deformation distribution for n_a = 5 years

The values of the resultant linear deformation u determined by the finite element method for 10 and 15 years are shown in table 8.

Table 8: The resultant linear deformation for n_a= 10 and 15 years

u [mm]	n_a= 10 years				n_a= 15 years			
	T [°C]				T [°C]			
φ [°]	-30°	0°	30°	60°	-30°	0°	30°	60°
0	1.2272	1.1873	1.149	1.115	1.350	1.309	1.269	1.234
0.25	1.24041	1.20394	1.16825	1.13343	1.35984	1.32258	1.28607	1.25023
1	1.19863	1.16424	1.13162	1.10273	1.31771	1.28140	1.24605	1.22414
2	1.1848	1.15216	1.12050	1.09030	1.30078	1.26603	1.23383	1.20218
4	1.19040	1.15660	1.12632	1.09682	1.33552	1.27958	1.24871	1.21853
6	1.23481	1.20082	1.16787	1.13583	1.35532	1.32053	1.28648	1.25324
8	1.23110	1.19687	1.16377	1.13202	1.34585	1.31439	1.28365	1.2537
10	1.24760	1.21373	1.18070	1.14858	1.38699	1.35259	1.31891	1.28601

g) Case no. 7
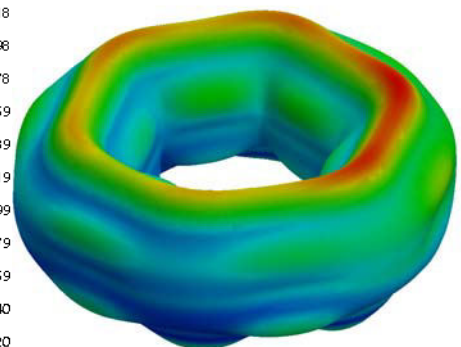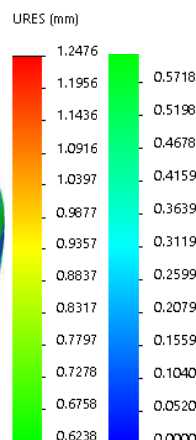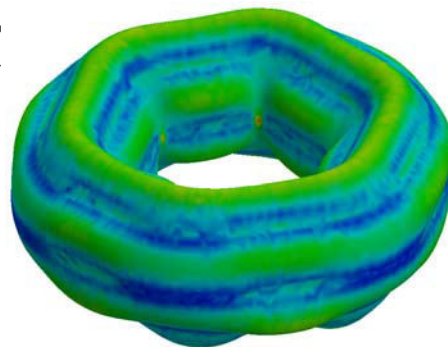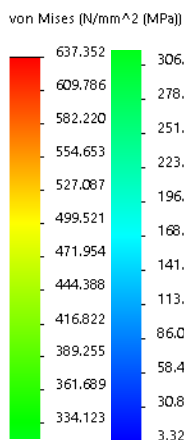
Fig. 26. The graphs of Von Mises stress distribution for n_a = 10 years

Fig. 27. The graphs of linear deformation distribution for n_a = 10 years
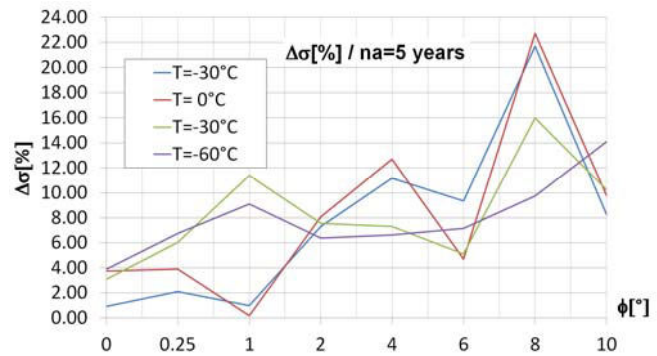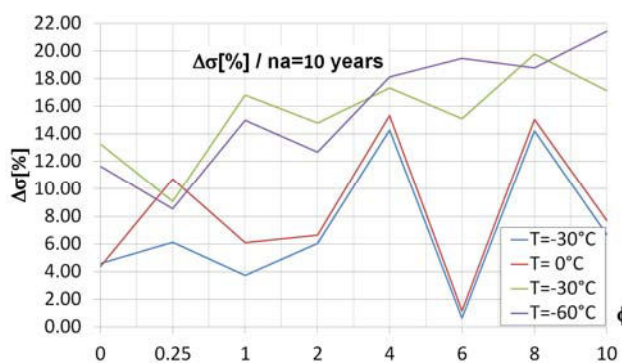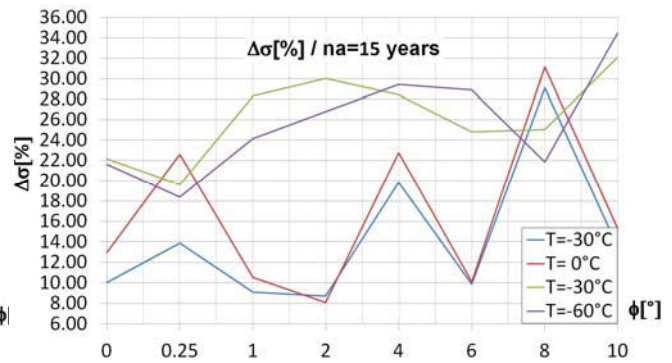
The graphs of 3-D surfaces corresponding to the resultant linear deformation for 10 and 15 years are graphically shown in figs. 28 and 29.
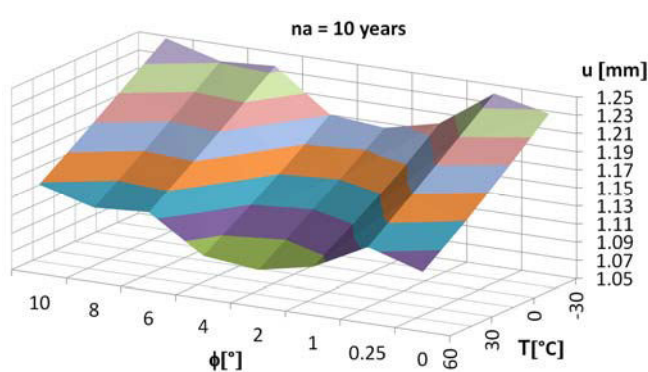
Fig. 28. The graphs of u = f(T, ϕ) for n_a = 10 years   **Fig. 29.** The graphs of u = f(T, ϕ) for n_a = 15 years
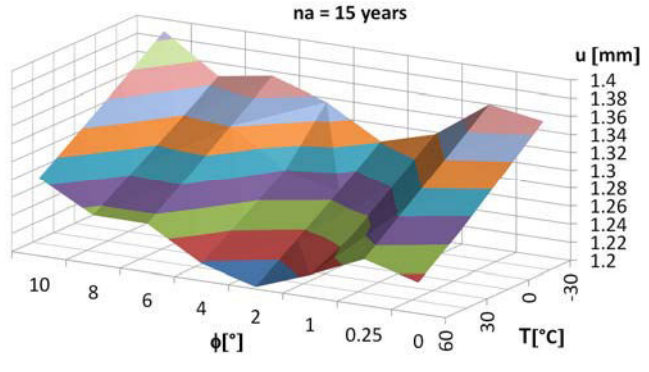
h) Case no. 8
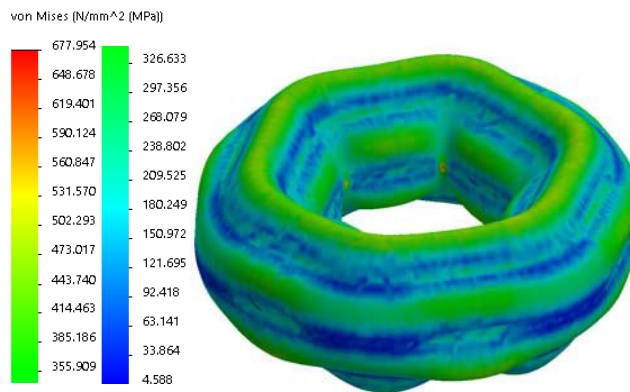
Fig. 30. The graphs of Von Mises stress distribution for n_a = 15 years   **Fig. 31.** The graphs of linear deformation distribution for n_a = 15 years
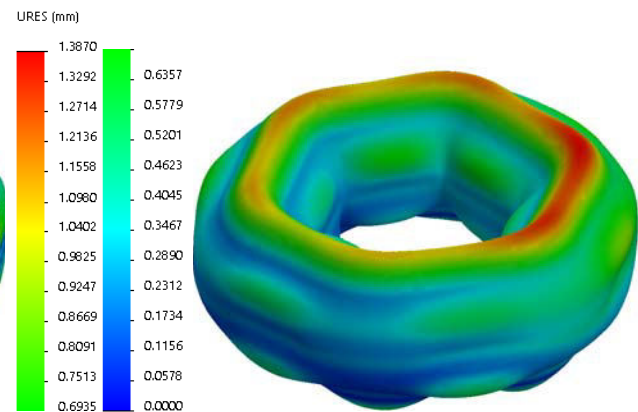
The percentage variation of resultant linear deformation in relation to the initial value (tables 9 and 10) and the corresponding graphs are given in figs. 32, 33 and 34.

Table 9: The percentage variation of resultant linear deformation for 5 and 10 years

ϕ [°]	Δu [%] for n_a= 5 years				Δu [%] for n_a= 10 years			
	T [°C]				T [°C]			
	-30°	0°	30°	60°	-30°	0°	30°	60°
0	9.48	9.72	9.91	10.16	20.67	21.26	21.79	22.30
0.25	11.83	11.80	11.81	11.29	22.81	22.91	23.03	22.37
1	8.67	8.89	9.01	8.88	20.46	21.06	21.61	22.18
2	9.54	9.57	9.57	9.65	21.42	21.78	22.09	22.34
4	8.79	9.08	9.57	9.98	19.16	19.67	20.46	21.15
6	10.25	10.40	10.44	10.18	20.83	21.30	21.57	21.70
8	9.69	9.91	10.13	10.50	21.06	21.38	21.71	22.02
10	10.38	8.82	11.12	11.45	20.86	21.21	21.55	21.83

Table 10: The percentage variation of resultant linear deformation for 15 years

φ [°]	Δu [%] for n_a = 15 years			
	T[°C]			
	-30°	0°	30°	60°
0	32.74	33.69	34.51	35.35
0.25	34.64	35.02	35.44	34.98
1	32.42	33.24	33.91	35.63
2	33.30	33.81	34.43	34.90
4	33.69	32.39	33.55	34.60
6	32.62	33.39	33.92	34.28
8	32.34	33.29	34.25	35.14
10	34.36	35.08	35.78	36.41
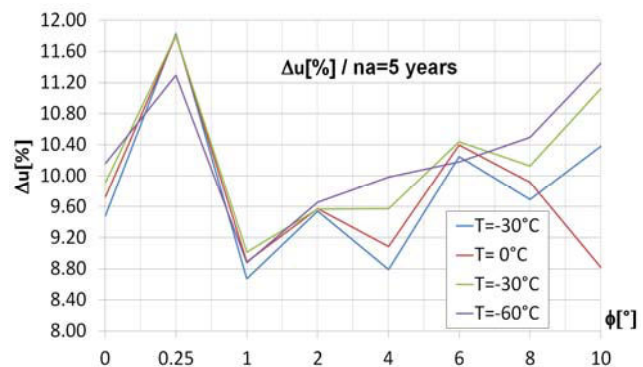
Fig. 32. The graphs of Δu for n_a = 5 years
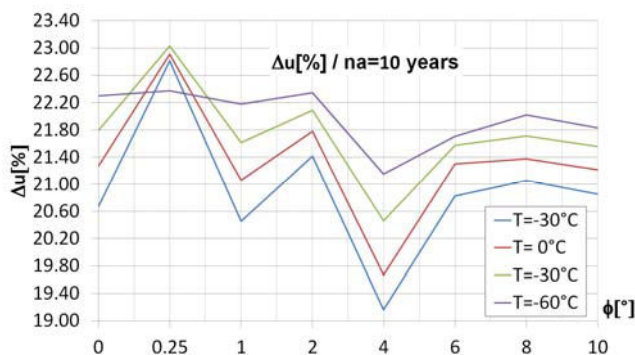
Fig. 33. The graphs of Δu for n_a = 10 years
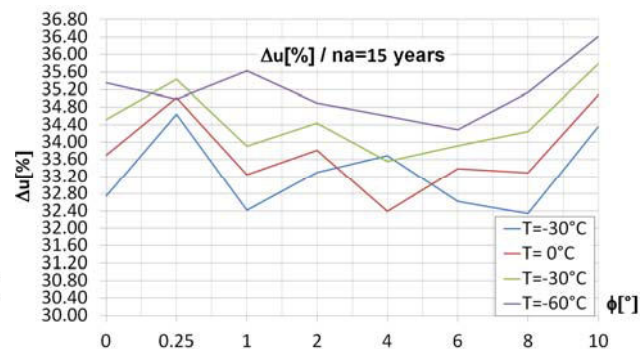
Fig. 34. The graphs of Δu for n_a = 15 years

3. Conclusions

Following the numerical analyses and the resulting graphs it has been found that:
- with the increase of the torsion angle φ, the state of effort increases and reaches maximum values with the decreasing of the temperature, reaching a minimum value for T = -30 ^{0}C;
- the state of efforts are amplified with the increase of corrosion, by decreasing the thickness of the wall of the tank coverings;
- in the last year of exploitation (n_a= 15 years), the maximum value of the Von Mises stress occurs at T = - 30 ^{0}C, φ = 8 [°], and σ = 726.25 MPa > $σ_a$ = 710 MPa;
- the percentage variation of Von Mises resultant effort in report with n_a= 0 years, indicated an increasing of Δσ [%] > 34.54 [%] for T = 60 ^{0}C. Also, the resultant linear deformation *u* has a maximum value for φ = 10 [°] and T = -30 ^{0}C. The percentage variation of resultant linear deformation Δu [%] has a maximum value for maximum values of φ and T.
- the results shows that the angular torsion overlaps over the disadvantageous effects of corrosion and temperature variation leading to higher increases of stress and deformation states.

References

[1] Ghiţă, C. Mirela, Anton C. Micu, Mihai Ţălu and Ştefan Ţălu. "Shape optimization of a thoroidal methane gas tank for automotive industry." *Annals of Faculty of Engineering Hunedoara - International Journal of Engineering, Hunedoara, Romania*, Tome X, Fascicule 3 (2012): 295-297.
[2] Ghiţă, C. Mirela, Anton C. Micu, Mihai Ţălu and Ştefan Ţălu. "Shape optimization of vehicle's methane gas tank." *Annals of Faculty of Engineering Hunedoara - International Journal of Engineering, Hunedoara, Romania*, Tome X, Fascicule 3 (2012): 259-266.
[3] Ghiţă, C. Mirela, Anton C. Micu, Mihai Ţălu, Ştefan Ţălu and Ema I. Adam. "Computer-Aided Design of a classical cylinder gas tank for the automotive industry." *Annals of Faculty of Engineering Hunedoara - International Journal of Engineering, Hunedoara, Romania*, Tome XI, Fascicule 4 (2013): 59-64.

[4] Ghiţă, C. Mirela, Anton C. Micu, Mihai Ţălu and Ştefan Ţălu. "3D modelling of a shrink fitted concave ended cylindrical tank for automotive industry." *Acta Technica Corviniensis – Bulletin of Engineering, Hunedoara, Romania*, Tome VI, Fascicule 4 (2013): 87-92.

[5] Ghiţă, C. Mirela, Anton C. Micu, Mihai Ţălu and Ştefan Ţălu. "3D modelling of a gas tank with reversed end up covers for automotive industry.", *Annals of Faculty of Engineering Hunedoara - International Journal of Engineering, Hunedoara, Romania*, Tome XI, Fascicule 3 (2013): 195-200.

[6] Ghiţă, C. Mirela, Ştefan C. Ghiţă, Ştefan Ţălu and Simona Rotaru, "Optimal design of cylindrical rings used for the shrinkage of vehicle tanks for compressed natural gas." *Annals of Faculty of Engineering Hunedoara - International Journal of Engineering, Hunedoara*, Tome XII, Fascicule 3 (2014): 243-250.

[7] Bică, Marin, Mihai Ţălu and Ştefan Ţălu. "Optimal shapes of the cylindrical pressurized fuel tanks." *Magazine of Hydraulics, Pneumatics, Tribology, Ecology, Sensorics, Mechatronics (HIDRAULICA)*, no. 4 (December 2017): 6-17.

[8] Vintilă, Daniela, Mihai Ţălu and Ştefan Ţălu. "The CAD analyses of a torospheric head cover of a pressurized cylindrical fuel tank after the crash test." *Magazine of Hydraulics, Pneumatics, Tribology, Ecology, Sensorics, Mechatronics (HIDRAULICA)*, no. 4 (December 2017): 57-66.

[9] Ţălu, Ştefan and Mihai Ţălu. "The influence of deviation from circularity on the stress of a pressurized fuel cylindrical tank." *Magazine of Hydraulics, Pneumatics, Tribology, Ecology, Sensorics, Mechatronics (HIDRAULICA)*, no. 4 (December 2017): 34-45.

[10] Ţălu, Mihai. "The influence of the corrosion and temperature on the Von Mises stress in the lateral cover of a pressurized fuel tank." *Magazine of Hydraulics, Pneumatics, Tribology, Ecology, Sensorics, Mechatronics (HIDRAULICA)*, no. 4 (December 2017): 89-97.

[11] Ţălu, Mihai and Ştefan Ţălu. "Analysis of temperature resistance of pressurized cylindrical fuel tanks." *Magazine of Hydraulics, Pneumatics, Tribology, Ecology, Sensorics, Mechatronics (HIDRAULICA)*, no. 1 (March 2018): 6-15.

[12] Ţălu, Mihai and Ştefan Ţălu. "Design and optimization of pressurized toroidal LPG fuel tanks with variable section." *Magazine of Hydraulics, Pneumatics, Tribology, Ecology, Sensorics, Mechatronics (HIDRAULICA)*, no. 1 (March 2018): 32-41.

[13] Ţălu, Ştefan and Mihai Ţălu. "Algorithm for optimal design of pressurized toroidal LPG fuel tanks with constant section described by imposed algebraic plane curves." *Magazine of Hydraulics, Pneumatics, Tribology, Ecology, Sensorics, Mechatronics (HIDRAULICA)*, no. 2 (June 2018): 14-21.

[14] Ţălu, Mihai and Ştefan Ţălu. "The optimal CAD design of a 3D hexagonal toroid with regular hexagonal cross-section used in manufacturing of LPG storage tanks." *Magazine of Hydraulics, Pneumatics, Tribology, Ecology, Sensorics, Mechatronics (HIDRAULICA)*, no. 2 (June 2018): 49-56.

[15] Ţălu, Mihai and Ştefan Ţălu. "The influence of corrosion and temperature variation on the minimum safety factor of a 3D hexagonal toroid with regular hexagonal cross-section used in manufacturing of LPG storage tanks." *Magazine of Hydraulics, Pneumatics, Tribology, Ecology, Sensorics, Mechatronics (HIDRAULICA)*, no. 3 (August 2018): 16-25.

[16] Ţălu, Ştefan and Mihai Ţălu. "The influence of corrosion and pressure variation on the minimum safety factor of a 3D hexagonal toroid with regular hexagonal cross-section used in manufacturing of LPG storage tanks." *Magazine of Hydraulics, Pneumatics, Tribology, Ecology, Sensorics, Mechatronics (HIDRAULICA)*, no. 3 (August 2018): 39-45.

[17] Ţălu, Mihai and Ştefan Ţălu. "The influence of corrosion and temperature variation on a CNG storage tank with a combined form consisting of a torus and a sphere." *Magazine of Hydraulics, Pneumatics, Tribology, Ecology, Sensorics, Mechatronics (HIDRAULICA)*, no. 4 (December 2019): 93-104.

[18] Ţălu, Mihai and Ştefan Ţălu. "Optimal design of a CNG storage tank with a combined form consisting of a torus and a sphere." *Magazine of Hydraulics, Pneumatics, Tribology, Ecology, Sensorics, Mechatronics (HIDRAULICA)*, no. 4 (December 2019): 73-82.

[19] Ţălu, Ştefan and Mihai Ţălu. "Numerical analysis of the influence of uniaxial compression loads on the shape of a toroidal LPG tank." *Magazine of Hydraulics, Pneumatics, Tribology, Ecology, Sensorics, Mechatronics (HIDRAULICA)*, no. 1 (March 2020): 47-58.

[20] Ţălu, Mihai and Ştefan Ţălu. "Stress and deformation analysis under bending and torsional loads of a toroidal LPG tank based on the finite element analysis." *Magazine of Hydraulics, Pneumatics, Tribology, Ecology, Sensorics, Mechatronics (HIDRAULICA)*, no. 1 (March 2020): 88-101.

[21] Ţălu, Mihai and Ştefan Ţălu. "3D geometrical solutions for toroidal LPG fuel tanks used in automotive industry." *Advances in Intelligent Systems Research,* vol. 151 (2018): 189-193. DOI: 10.2991/cmsa-18.2018.44.

[22] Ţălu, Ştefan and Mihai Ţălu. "Constructive CAD variants of toroidal LPG fuel tanks used in automotive Industry." *Advances in Intelligent Systems Research,* vol. 159 (2018): 27-30. DOI: 10.2991/mmsa-18.2018.7.

[23] Ţălu, Ştefan and Mihai Ţălu. "The Influence of corrosion on the vibration modes of a pressurized fuel tank used in automotive industry." *DEStech Transactions on Materials Science and Engineering,* (2018): 1-6. DOI: 10.12783/dtmse/icmsa2018/20560.

[24] Ţălu, Mihai and Ştefan Ţălu. "Optimal engineering design of a pressurized paralepipedic fuel tank." *Annals of Faculty of Engineering Hunedoara - International Journal of Engineering, Hunedoara, Romania*, Tome XVI, Fascicule 2 (2018): 193-200.

[25] Malviya, Rupesh Kumar and Muhamed Rushaid. "Consequence analysis of LPG storage tank." Materials today, vol. 5, issue 2 (2018): 4359-4367. DOI: 10.1016/j.matpr.2017.12.003.

[26] Ejeh, Chukwugozie Jekwu, Akhabue Gbemisola Precious and Isaac Agyeibi. "Effect of transient temperature on 304 stainless steel LPG tank structure using numerical simulation approach." *SN Applied Sciences,* no. 1, (2019): article number: 1690. DOI: 10.1007/s42452-019-1760-1.

[27] Ţălu, Ştefan and Mihai Ţălu. "CAD generating of 3D supershapes in different coordinate systems." *Annals of Faculty of Engineering Hunedoara - International Journal of Engineering, Hunedoara, Romania*, Tome VIII, Fascicule 3 (2010): 215-219.

[28] Ţălu, Ştefan and Mihai Ţălu. "A CAD study on generating of 2D supershapes in different coordinate systems." *Annals of Faculty of Engineering Hunedoara - International Journal of Engineering, Hunedoara, Romania*, Tome VIII, Fascicule 3 (2010): 201-203.

[29] Niţulescu, Theodor and Ştefan Ţălu. *Aplicaţii ale geometriei descriptive şi graficii asistate de calculator în desenul industrial. (Applications of descriptive geometry and computer aided design in engineering graphics).* Cluj-Napoca, Risoprint Publishing house, 2001.

[30] Bîrleanu, Corina and Ştefan Ţălu. *Organe de maşini. Proiectare şi reprezentare grafică asistată de calculator. (Machine elements. Designing and computer assisted graphical representations).* Cluj-Napoca, Victor Melenti Publishing house, 2001.

[31] Ţălu, Ştefan and Mihai Ţălu. *AutoCAD 2006. Proiectare tridimensională. (AutoCAD 2006. Three-dimensional designing)*. Cluj-Napoca, MEGA Publishing house, 2007.

[32] Ţălu, Ştefan. *Geometrie descriptivă. (Descriptive geometry)*, Cluj-Napoca, Risoprint Publishing house, 2010.

[33] Ţălu, Ştefan. *AutoCAD 2017*. Cluj-Napoca, Napoca Star Publishing house, 2017.

[34] Ţălu, Ştefan. *Micro and nanoscale characterization of three dimensional surfaces. Basics and applications*. Napoca Star Publishing House, Cluj-Napoca, Romania, 2015.

[35] Ţălu, Ştefan and Cristina Racocea. *Reprezentări axonometrice cu aplicaţii în tehnică. (Axonometric representations with applications in technique).* Cluj-Napoca, MEGA Publishing house, 2007.

[36] Racocea, Cristina and Ştefan Ţălu. *Reprezentarea formelor geometrice tehnice în axonometrie. (The axonometric representation of technical geometric shapes).* Cluj-Napoca, Napoca Star Publishing house, 2011.

[37] Ţălu, Mihai. *Calculul pierderilor de presiune distribuite în conducte hidraulice. (Calculation of distributed pressure loss in hydraulic pipelines).* Craiova, Universitaria Publishing house, 2016.

[38] Ţălu, Mihai. *Mecanica fluidelor. Curgeri laminare monodimensionale. (Fluid mechanics. The monodimensional laminar flow).* Craiova, Universitaria Publishing house, 2016.

[39] Ţălu, Mihai. *Pierderi de presiune hidraulică în conducte tehnice cu secţiune inelară. Calcul numeric şi analiză C.F.D. (Hydraulic pressure loss in technical piping with annular section. Numerical calculation and C.F.D.)*, Craiova, Universitaria Publishing house, 2016.

[40] Nedelcu, Dorian. *Proiectare şi simulare numerică cu SolidWorks. (Digital Prototyping and Numerical Simulation with SolidWorks)*. Timişoara, Eurostampa Publishing house, 2011.

[41] Florescu-Gligore, Adrian, Ştefan Ţălu and Dan Noveanu. *Reprezentarea şi vizualizarea formelor geometrice în desenul industrial. (Representation and visualization of geometric shapes in industrial drawing).* Cluj-Napoca, U. T. Pres Publishing house, 2006.

[42] Florescu-Gligore, Adrian, Magdalena Orban and Ştefan Ţălu. *Cotarea în proiectarea constructivă şi tehnologică. (Dimensioning in technological and constructive engineering graphics).* Cluj-Napoca, Lithography of The Technical University of Cluj-Napoca, 1998.

[43] Ţălu, Ştefan. *Limbajul de programare AutoLISP. Teorie şi aplicaţii. (AutoLISP programming language. Theory and applications)*. Cluj-Napoca, Risoprint Publishing house, 2001.

[44] Ţălu, Ştefan. *Grafică tehnică asistată de calculator. (Computer assisted technical graphics)*. Cluj-Napoca, Victor Melenti Publishing house, 2001.

[45] Ţălu, Ştefan. *Reprezentări grafice asistate de calculator. (Computer assisted graphical representations).* Cluj-Napoca, Osama Publishing house, 2001.

[46] Ţălu, Ştefan. *Tehnologia de rulare a filetelor. (Thread rolling technology).* Cluj-Napoca, Napoca Star Publishing house, 2019.

[47] *** Certification tests of LPG and CNG. Accessed March 3, 2020. http://vzlutest.cz/en/certification-tests-of-lpg-and-cng-c3.html.

[48] *** TANK software (https://cas.hexagonppm.com/solutions/tank)

[49] *** Autodesk AutoCAD 2020 software.

[50] *** SolidWorks 2020 software.

Procedural and Methodological Example of Gravimetric Measurement of Pollutant Particles in the Environment using Sampling Devices

PhD Candid. **Melania MITUCĂ-CORLECIUC**[1], Assoc.prof.PhD.eng. **Ion DURBACĂ**[1],
PhD Eng. **George SORESCU**[2], PhD Candid. **Cosmin Gheorghe CIOCOIU**[1],
PhD Candid. **Luana NISTEA**[1], PhD Candid. **Vasile SĂCUIU**[1]

[1] POLITEHNICA University of Bucharest; ion.durbaca@yahoo.com

[2] General Inspectorate for Emergency Situations; georgesorescu@yahoo.com

Abstract: *This paper deals, using a demonstrative example, with the methodological procedure of gravimetric measurement of the polluting particles, according to the standard SR EN 12341/2014, for the real evaluation of the 10 μm particle in the biphasic suspensions discharged into the environment. The procedure can be used to compare a non-certified measuring instrument with a reference instrument by verifying that the conditions for the difference between the particle-specific concentration of the particulate immissions (<± 10 μg / m³) and their concentration in the environment (< 100 μg / m³). The mathematical processing of the comparative results through the regression equation must verify that a correlation coefficient value is obtained to validate the fulfillment of the standard requirements.*

Keywords*: Particles, pollutants, immissions, regression, correlation.*

1. Introduction

Atmospheric pollution has become a major issue for today's society, and efforts to breathe clean air are of great importance. In day-to-day life, the introduction into the atmosphere, directly or indirectly, of substances or energy that is harmful to human health and / or the quality of the environment is air pollution. This causes large societal damages due to the serious socio-economic consequences that can affect human health and / or environmental quality.

As a result of the very large influence of the anthropogenic sources with major potential on air pollution (large combustion plants - IMA, transport, petrochemical industry, construction materials industry, etc.), the pollutants in suspension were noted, with PM (Particulate Matter) representing solid substances in the form of powders, which means an amount of substance present in a given volume. They are a category of air pollutants that greatly affect human health because they include harmful substances such as nitrates, sulphates, organic carbon, elemental carbon, dust, etc. in their composition [1].

Because pollutant particles can come from very different sources, they lead to a number of specific morphological, chemical and physical properties, and their distribution according to their dimensions is an important parameter that influences their behavior. Thus, PM10 pollutants, as defined by EPA (Environmental Protection Agency, USA), include more than 50% of particles collected by a 10 μm diameter sampler and the specific shape penetration curve [1, 2].

In recent years, government agencies in many European countries have monitored particulate matter PM10, respectively the total concentration of all particles smaller than 10 μm in diameter, which corresponds to all fine particle areas plus the smallest classes of coarse particles, all these being called, particles that can be inhaled. Pollutants with the PM2.5 index, which includes all fine particles with diameters less than 2,5 μm (inhalable particles), are also monitored. The new term of superfine particles is applied to particles with very small diameters, typically less than 0.05 μm (50 nm) and PM0.05 [3], respectively.

Therefore, it is imperative to step up efforts in order to monitor and control environmental pollution by using advanced methods and techniques to ensure increased quality indicators for all environmental factors, in accordance with applicable norms, standards and regulations.

2. Description of the method of gravimetric measurement of the powders content coming from gaseous pollutant emissions

The gravimetric measurement principle consists in the analysis of a representative volume of gaseous effluent extracted under isokinetic conditions from from an outlet channel. As schematically shown in Fig. 1, several simultaneous and successive thermotechnical determinations are made. Thus, the flow conditions (flow, static and dynamic pressure, humidity, temperature, etc.) must be known and a strategy correlated with the concrete conditions regarding the selection of the sampling section and the representative points [4, 5].
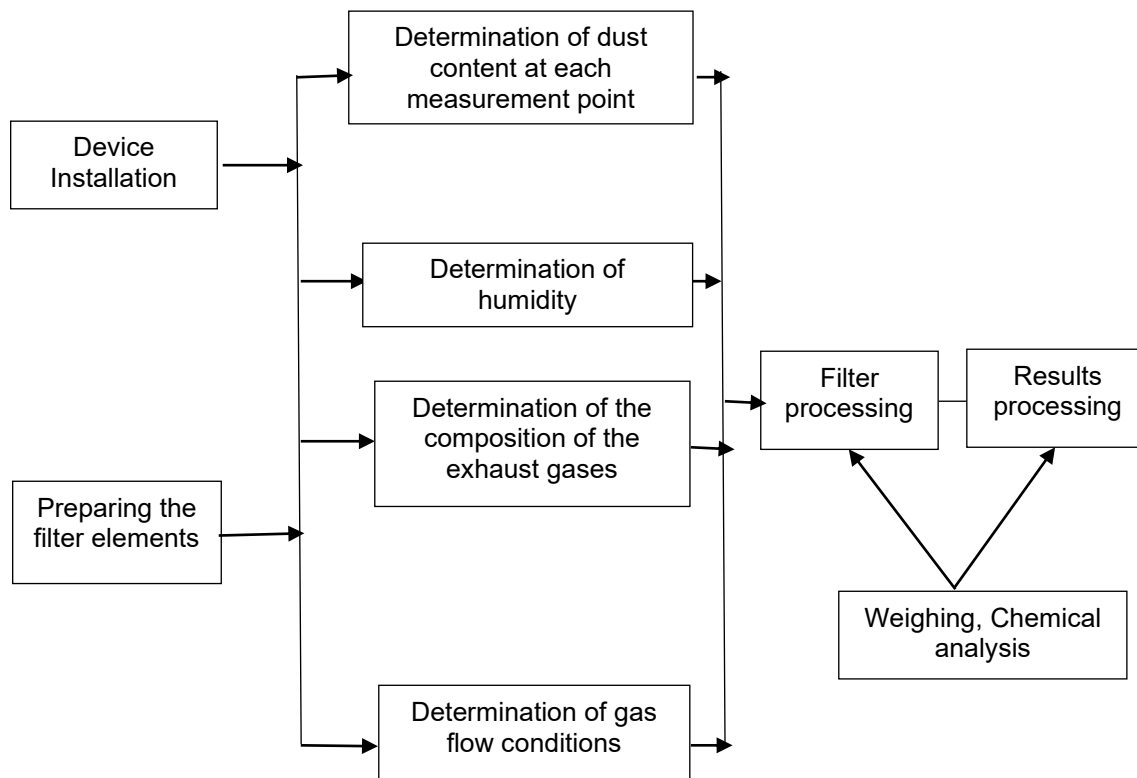
Fig. 1. Scheme of procedures necessary for the experimental determination of the dust content of gaseous pollutant emissions [5].

The installation with which the gravimetric measurement of the amount of dust pollutants from industrial gaseous emissions is carried out through the chimneys (exhaust channels) thereof is complex and basically consists of several independent components [6, 7].
After the installation, it is brought to the operating temperature (120°C), the sealing is checked, operation followed by starting the suction pump. Then, the gas intake through the bypass system. Throughout the measurement, the flow parameters of the effluent are monitored and the data of the measured quantities are periodically noted. At the end of the measurement, the gas suction is switched off, after which the filter element is removed and stored in a specially prepared container. Next, the preparation of filter cartridges or flat filters is followed [8 - 10].
The measurement of the mass of the filter elements (before and after use) is performed with a precision electronic scale, in µg. The filter cartridges used may also be subjected to chemical analysis to determine the component chemical elements. The overall measurement of the particle emission is done over a representative period for the analyzed phenomenon, so the tested facility must be well known by the authorized personnel performing the experiment. It is defined as the individual measurement, the average value of the sum of the point measurements made on the axis or in the grid [8-10].

3. Determination of PM10 powders from the environment using sampling devices

At present, the national regulations represented by Law no. 104/2011 on ambient air quality limits the concentration of particulate matter PM10 from ambient to the daily limit value of 50 μg / m^3 over 24 hours [12].

As defined above, PM 10 represents the mass of particulate matter with a diameter of less than or equal to 10 μm. PM 10 inhalable dusts are harmful to human health because they can be deposited on the upper respiratory tract, causing severe traumatic lesions and illnesses.

Using the model of separator (analyzer) of 10 μm of dust in the environment, according to the requirements of SR EN 12341/2014, we aim to validate it for the current use in long-term determinations of PM10 powders in the environment.

3.1. Description of the sampling device

In order to determine PM 10 powder imissions, the procedure for experimenting with a sampling device, designated MVS6, is considered in accordance with the requirements of SR EN 12341/2014 „Air quality. Standardized gravimetric measurement method for determining the mass fraction of PM10 or PM2.5 of the suspended particles ".

The MSV6 sample is used for the determination of particle immission (PM 10 fractions) in the surrounding air, the principle of determining the concentration of powders in the atmosphere being the determination of their mass, using the gravimetric method. The method complies with the requirements of Law no. 104/2011, as well as with international law and is used as a reference method in the technique of measuring suspended particles.

The particle sampling plant PM 10 in Fig. 2, a) and b) belongs to the company SVEN LECKEL INGENIEURBURG GMBH [12] and consists of the MSV6 analyzer (consisting of the separator, filter port, filter and separator support), the air meter, the vacuum pump and the connection hoses.

The principle of dust collection PM 10 from the ambient air with the mentioned installation takes into account the following: with the aid of the vacuum pump 7, the dust air is sucked in through the separator 1 with which the particles with dimensions larger than 10 μm are retained. The breathable particles below 10 μm are retained on the filter 3. The volume of air sucked through the filter is determined by means of the meter 6. The connection between the components of the system is made with the elastic hoses 5. The flow regulation $Q = 6$ m^3 / h is made by means of the valve 8. The separator has the role of selecting PM 10 particles from ambient air, according to the standard SR EN 12341/2014. In designing and constructing the separator, the basic dimensional elements of the respective standard were considered.

a.   b.

Fig. 2. Particle sampling plant PM10 - MVS6 [12].

Circulation path through the air sampler sucked from the environment and the particle retainer MSV6 PM 10, shown in Fig. 3, and the overview of the apparatus, in Fig. 4.
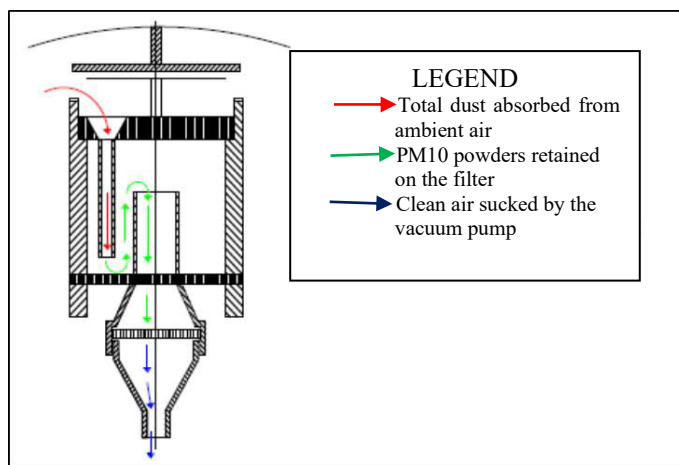
Fig. 3. Trajectory of the suction air from the environment through the MSV6 sampler [12]
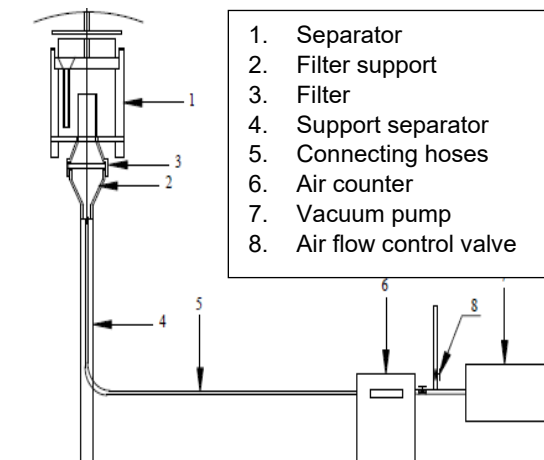
Fig. 4. Overview of the MSV6 sampler [12]

The separator consists of 8 suction tubes, with which the large particles are selected by the impact phenomenon. Particles aspirated from the ambient air stream are retained on the filter.

The impact velocity of the particles at the outlet of the suction tubes with diameter Ø 6.5 mm, results from the fundamental relation of the flow of a fluid through a pipe (Q = w • S), respectively (1):

$$w = \frac{Q}{S} = \frac{Q}{8 \times \frac{\pi \cdot d^2}{4}}$$ (1)

and the particle velocity is obtained: w = 6.28 m / s.

For the determination of the gravimetric concentration PM10 particles, glass fiber filters are used at which the mass is measured before and after sampling. The air meter together with the vacuum pump is metrologically checked and has a calibration certificate.

The gravimetric (C) concentration of PM 10 particles is determined by the relationship (2):

$$C = \frac{G_2 - G_1}{V} \ [mg/m^3]$$ (2)

where: G_2, G_1 represents the final and initial mass of the filter [mg]; V – inlet air volume [m³].

3.2. Description of the validation method of the sampling device

According to SR EN 12341/2014 for the real evaluation of PM 10 powders from the total dust in suspension, 50% particles of 10 μm must be found in the separator and 50% on the filter.

In order to determine the dispersion of the particles (%) depending on their size in [μm], it is necessary to carry out dust from the ambient air with the MSV6 analyzer (having the technical characteristics: flow rate Q = 6 m³ / h; pressure drop of the apparatus / installation: (147 - 196) · 10^5 MPa; electric vacuum pump 220 V, type ACOO with flow rate of 150 l / min; glass fiber filter, diameter Ø42 mm and pore size 0.8 μm), as well as preparation of the samples for reading the dimensions, respectively the dispersion of these particles under a Zeiss microscope. The powder taken from the separator is inserted into a clock bottle with alcohol water (25%), to prevent losses, and after homogenization, a drop is placed on the glass blade. After drying, cover the sample with a blade that is secured to the edge with a tape.

The prepared samples are analyzed under a microscope with a magnification power of about 1000 times. The values of the accumulated retentions and passes in / from the separator, respectively of the accumulated retentions on the filter, are presented in Table 1.

Table 1: The values of the accumulated particles retention and passage (%) in / from the separator and the accumulated particle retention (%) on the filter

Particle size PM x [μm]	The value of retensions (R_s) in separator q_i [%]	The value of cumulative retentions (R_{CS}) in separator Σq_i [%]	The value of cumulative passes from the separator (T_{CS}) 100 - Σq_i [%]	The value of retentions on the filter (R_F), q_i [%]	The value of cumulative retentions on the filter (R_{CF}), Σq_i [%]
20	12	12	88	0	0
19	11	33	67	0	0
18	10	43	57	0	0
17	9	52	48	0	0
16	8	60	40	0	0
15	7	67	33	0	0
14	6	73	27	0	0
13	5	78	22	0	0
12	4	82	18	0	0
11	3	85	15	0	0
10	2	87	13	2	2
9	2	89	11	2	4
8	2	91	9	2	6
7	2	93	7	3	9
6	2	95	5	3	12
5	2	97	3	6	18
4	1	98	2	8	26
3	1	99	1	12	38
2,5	1	100	0	26	64
1	0	100	0	36	100

4. Results and discussions

In order to determine the critical separation size, the graph of cumulative passage (TCS) from the separator [%] and the cumulative filter retention (RCF) of the powders, according to Fig. 5.
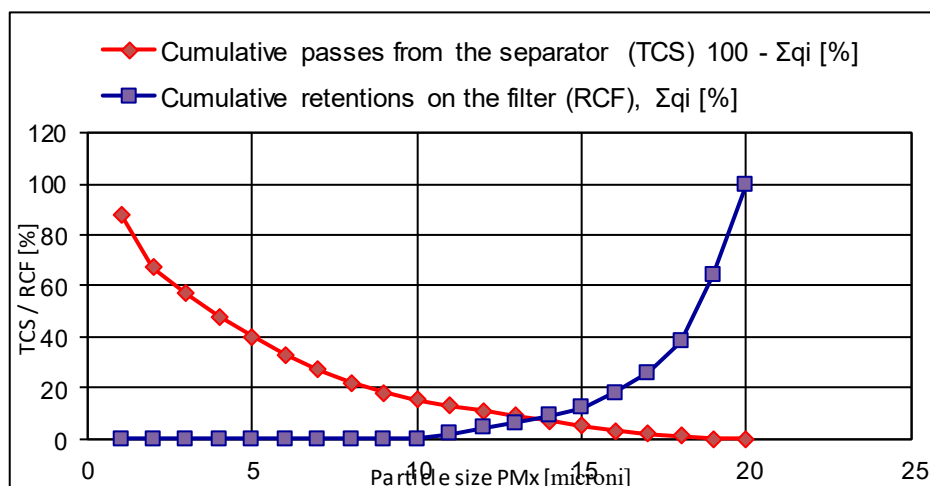
Fig. 5. The graph of the passage from the separator and the retention on the filter

The intersection of the two TCS and RCF curves is about 13 μm from the abscissa.
In another procedural stage comparative determinations are made with a reference device, namely the TEOM 1405, produced by the American company TEOM [11].
According to the standard of SR EN 12341/2014 (ch. 4.2, point B), for the comparison of a non-certified device with a reference device (certified), the following requirements must be met:

- the difference of the concentrations determined by the devices to admit values less than ± 10 μg / m^3, if the concentration in ambient environment Xi is less than 100 μg / m^3;
- the difference of the concentrations determined by the devices to admit values less than ± 10%, if the concentration in the ambient environment Xi is greater than 100 μg / m^3.
The values recorded correspond to concentrations less than 100 μg / m^3. The sampling height is 1.0 m above the ground. For testing, the reference device TEOM 1405 and the non-certified apparatus - MVS6 were considered.
Other equipment and materials used were: gas meter (0.06 - 6 m^3 / h); analytical balance (± 0.2 mg); vacuum pump (0.1 ÷ 120 l / min); filter funnel; desiccator; FM filters with pore diameter Ø0.8 μm; connecting hoses.
It should also be specified: the temperature of the environment with values between 8 ºC and 10 ºC; the relative humidity of the air between 50 - 80%.
The measurements were made in parallel with both devices, the distance between them being a minimum of 2 m. At each measurement, the operating rates for the TEOM 1405 and MVS6 respectively were determined.
The preparation of the filters for both devices must comply with the operational and system procedures of the industrial polluter on which the sampling is carried out. Certified filters were used for both devices. Simultaneous sampling was performed over a period of 24 hours. The results of the comparative measurements made are summarized in Table 2.

Table 2: Results of comparative measurements

Nr. crt.	x_i (TEOM 1405)	y_i (MVS6)
1	96	99
2	64	72
3	74	64
4	42	49
5	85	82
6	11	16
7	53	46
8	21	19
9	32	29

By processing the values in Table 2 with the help of graphical tools in Excel, we obtain the equation of the regression line (3), for estimating a linear model of connection between the results of comparative measurements, according to Fig. 6:

$$y = f(x) = 0.9633 x + 1.7252 \qquad (3)$$

where, x represents the concentrations determined with the reference device TEOM 1405, mg/m^3; y - concentrations determined with MVS6 [mg/m^3].
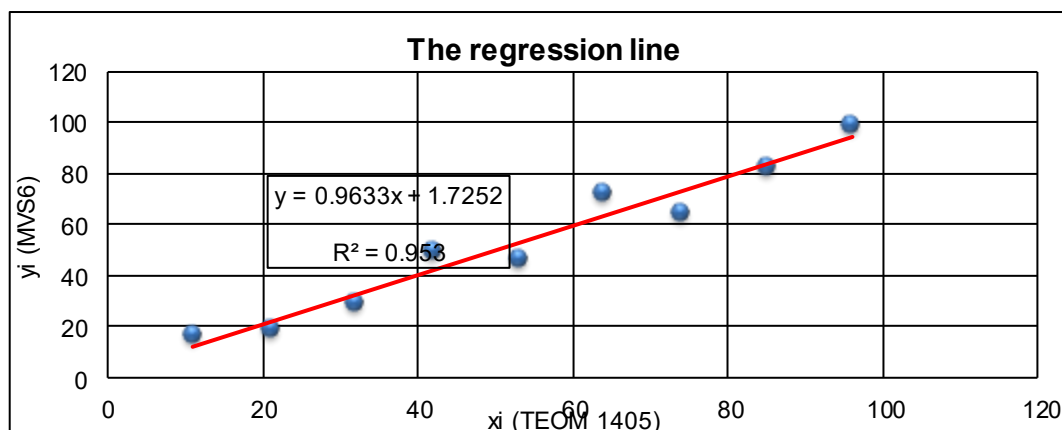
Fig. 6. Correlation between TEOM 1405 and MVS6 sampling devices.

The correlation coefficient (determination) d, results from Fig. 6:

$$d = R^2 \cdot 100 = 95.33\ \%.$$

According to SR EN 12341/2002, the correlation coefficient must be: R2 ≥ 0.95. But, since R2 = 0.9533 ≥ 0.95, it turns out that the requirement in the standard has been met.

5. Conclusions

In conclusion, the comparative determinations made between the TEOM 1405 reference device and the MVS6 analyzer are significantly correlated, respectively the value of the correlation coefficient validates the fulfilment of the requirements of the standard SR EN 12341/2014.
From here, the certification decision for the conformity of the MSV6 powder collection device is also used, in order to use it.
Therefore, the present work can constitute an application guide apt to lead to the possibility to use both for the assessment based on gravimetric measurement of the pollutant particles in the suspensions discharged in the environment and for the validation of the certification of any dust sampling devices compared to those considered as references or basis for meeting the technical-legislative standards and norms in force.

References

[1] Lăzăroiu, Gh. *Impactul CTE asupra mediului*. Bucharest, POLITEHNICA Press, 2005.
[2] Oroian, I., L. Paulette, C. Iederan, P. Burduhos, I. Brașovean, and Cl. Balint. "Modalități de cuantificare a PM10 și PM2,5 din aerul ambiental utilizând metoda standardizată." *ProEnvironment*, no. 2 (2009): 68 – 72.
[3] Căldăraru, Fl., and M. Căldăraru. *Methods for measuring and monitoring environmental quality parameters / Metode de măsurare și monitorizare a parametrilor de calitate a mediului.* Bucharest, Cavallioti Publishing House, 2010.
[4] Ionel, I., Fr. Popescu, D. Bisorca, P.D. Oprișa-Stănescu, and Cl. Gruescu. *Measuring air quality and dispersing noxious. Experimental themes / Măsurarea calității aerului și dispersarea noxelor. Teme experimentale*. Timișoara, Politehnica Publishing House, 2004.
[5] Popescu, Fr., and I. Ionel. *Quality management in environmental protection / Managementul calității în protecția mediului*. Timișoara, Politehnica Publishing House, 2008.
[6] Durbacă, I. "Modelling and simulation of air Pollutant dispartion." Paper presented at "The 7th Conference with International Participation – Constructive and Technological Design Optimizaton in the Machines Buiding Field" OPROTEH 2007, Bacău, Romania, November 1–3, 2007.
[7] Durbacă, I., M. Ştefănescu, and N. Durbacă. "Dispersia emisiilor poluante evacuate în atmosferă prin coșuri înalte – oportunitate majoră de asigurare a calității aerului." Paper presented at National Symposium „Generarea, prevenirea și procesarea emisiilor poluante în mediul industrial" – GEPROPOL 2009, Bucharest, Romania, June 12-13, 2009.
[8] Stănescu-Dumitru, R., R.C. Artenie, and M. Tat. *Evaluation of occupational exposure to powders. Practical guide / Evaluarea expunerii profesionale la pulberi. Ghid practic*. Bucharest, Viața Medicală Românească Publishing House, 2002.
[9] Istrate, M. *Technologies and installations for reducing polluting emissions. Pollution control in thermotechnics / Tehnologii și instalații pentru reducerea emisiilor poluante. Controlul poluării în termoenergetică.* Iași, Setis Publishing House, 2004.
[10] Mihăiescu, R. *Integrated environmental monitoring / Monitoringul integrat al mediului*. Cluj-Napoca, Bioflux Publishing House, 2014.
[11] Ray, A.L., and D.L. Vaughn. "Standard Operating Procedure for the Continuous Measurement of Particulate Matter." Thermo Scientific TEOM® 1405-DF, Sonoma Technology, Inc., 2009.
[12] https://mecrosystem.ro/instrumente-analitice-analizaore/imisii/pulberi/sven-leckel/pm-25-10/#

Gradually Varied Flow in a Trapezoidal Channel, towards a Hydraulics with Fractional Calculation and Finite Differences

Student **Carlos A. SANTAMARÍA DÍAZ**[1], Dra. **Maritza L. ARGANIS JUÁREZ**[2,3],
Dr. **José L. ARAGÓN HERNÁNDEZ**[3], Dr. **José L. HERRERA ALANÍS**[3],
M.A. **Jesús J. CORTÉS ROSAS**[3], M.A. **Miguel E. GONZÁLEZ CÁRDENAS**[3],
M.A. **Víctor D. PINILLA MORÁN**[3], M.I. **Margarita E. PRECIADO JIMÉNEZ**[4]

[1] Universidad Nacional Autónoma de México. Facultad de Ciencias, paladio06@ciencias.unam.mx Av. Universidad 3000 Ciudad Universitaria Coyoacán CDMX México 04510

[2] Universidad Nacional Autónoma de México. Instituto de Ingeniería, MArganisJ@iingen.unam.mx Av. Universidad 3000 Ciudad Universitaria Edificio 17 Cub.328. Coyoacán CDMX México 04510

[3] Universidad Nacional Autónoma de México. Facultad de Ingeniería, jaragonh@unam.mx; jherreraa75@gmail.com; j.javier.cortes@gmail.com; migue_033@yahoo.com.mx; vdpinillam@gmail.com. Av. Universidad 3000 Ciudad Universitaria Edificio 17 Cub.328. Coyoacán CDMX México 04510

[4] Instituto Mexicano de Tecnología del Agua. preciado@tlaloc.imta.mx. Blvd. Paseo Cuauhnáhuac 8532, Progreso, 62550 Jiutepec, Mor México

Abstract: *Several engineering problems involve use a derivative of a function; in recent years, physical phenomena have been reviewed are traditionally considered to be derived with an integer order in their mathematical models, instead derived with fractional order. Gradually varied flow evaluation profile in a free-surface channel is traditionally resolved with differential calculus and integer derivatives solved with finite difference schemes. In this work, equations were obtained relate derivatives of half order derivative of first order for different algebraic functions, resulting in polynomial type models; since there is a proportion between first derivative with derivatives of fractional order through these expressions and observing flow profiles can adjust a y(x) function approximately polynomial it is established various tests must be done to approximate to gradually varied flow equation solution help fractional differential equations can be solved through fractional finite differences.*

Keywords: *Fractional calculation, gradually varied flow, trapezoidal channel, hydraulics, half derivative*

1. Introduction

Gradually varied flow profiles determination has traditionally been approached with first derivative of strut with respect to length *x* recorded by flow [1] (formula 1).

$$\frac{dy}{dx} = \frac{S_0 - S_f}{1 - Fr^2}$$

(1)

Where

S_0, channel bottom slope, dimensionless
S_f, hydraulic slope, dimensionless
Fr, Froude number
$\frac{dy}{dx}$ Deep y first derivative with respect to chain x.

Numerical methods of the Euler method type, Runge-Kutta [2], in finite differences used to solve differential equation are traditionally used with proven results with laboratory tests; direct step method is a scheme that also provides solution to this problem. Currently, fractional calculation has begun to be studied to find solutions to these problems under approach to dependent variable behavior with respect to dependent implies a variation of non-integer order.

In recent years, questions have been raised regarding derivatives consideration of integer order in mechanical and engineering problems such as free fall, simple pendulum movement, parabolic launch; soil drag phenomenon problem in diffusion wave problems, before these analysis studies and hydraulics area, diffusion equation studies resolution were made using fractional calculation [3,4,5,6,7,8].

An interpretation fractional order derivatives geometric is not yet clear [9], graphs have been made to represent them, but an interpretation curves obtained (Figure 1) has not been fully achieved.
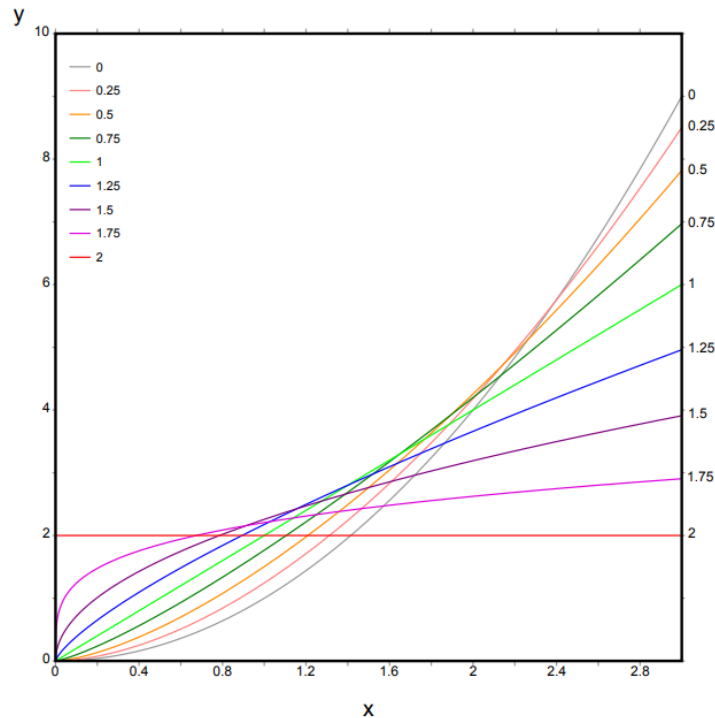
Fig. 1. Derivative of different fractional Behavior order in polynomial equation $y = x^2$. Source page 84 [3] and page 63 [9]

In this paper is proposed to obtain various functions that relate the behavior of a half derivative respect to a first order derivative of simple polynomial functions of degree p; when these functions were found, it was possible to obtain how a derivative of fractional order relates with a derivative of first order which allows this result to be transferred to a differential equation of first order to transform it into a differential equation of fractional order that can be solved with a scheme in finite fractional differences [4]. Rectangular laboratory channel geometry data were taken into account, in which an expense was passed and measurements of its braces were taken with a certain ΔX chain; adjustment was made profile measured best trend line by observing a polynomial behavior.

The method of Runge Kutta [2] was used with data for a hypothetical trapezoidal canal example [1]. This flow profile was obtained by solving a gradually varied flow differential equation; a polynomial type trend line was adjusted to profile obtained. Taking into account profiles can have polynomial behaviors and on the other hand a derivative of order one keeps a direct proportion with fractional derivative, it is possible to propose use of fractional derivatives to find an approximate solution to gradually varied flow profiles.

2. Methodology

2.1 Relationships between fractional derivative of order p and derivative of order one in polynomial functions

Santamaría, 2019 [10] when carrying out the GeoGebra © program [11] and half derivative to polynomial function are obtaining from $y=x^p$ form found two important observations:

a) As the order of the polynomial increases, the first order derivative tends to be equal to original function, as does the half order derivative

b) While first derivative has exponent p-1, half derivative has exponent p-0.5, it means first order derivative is equal to the half derivative raised to (p-1) / (p-0.5) and then divided by a constant determined with the gamma function as follows (formula 2):

$$D_x y = C\left(D_x^{1/2} y\right)^{\frac{p-1}{p-0.5}}$$

(2)

Half derivative is no longer valid around p = 170.25, but it remains to be verified if this is due to the used expression involving gamma function or is a software limitation.

On the other hand, when it drawing half behavior derivative respect to first order derivative polynomial functions degrees two and three, polynomial trend lines were determined (Figures 2 and 3).
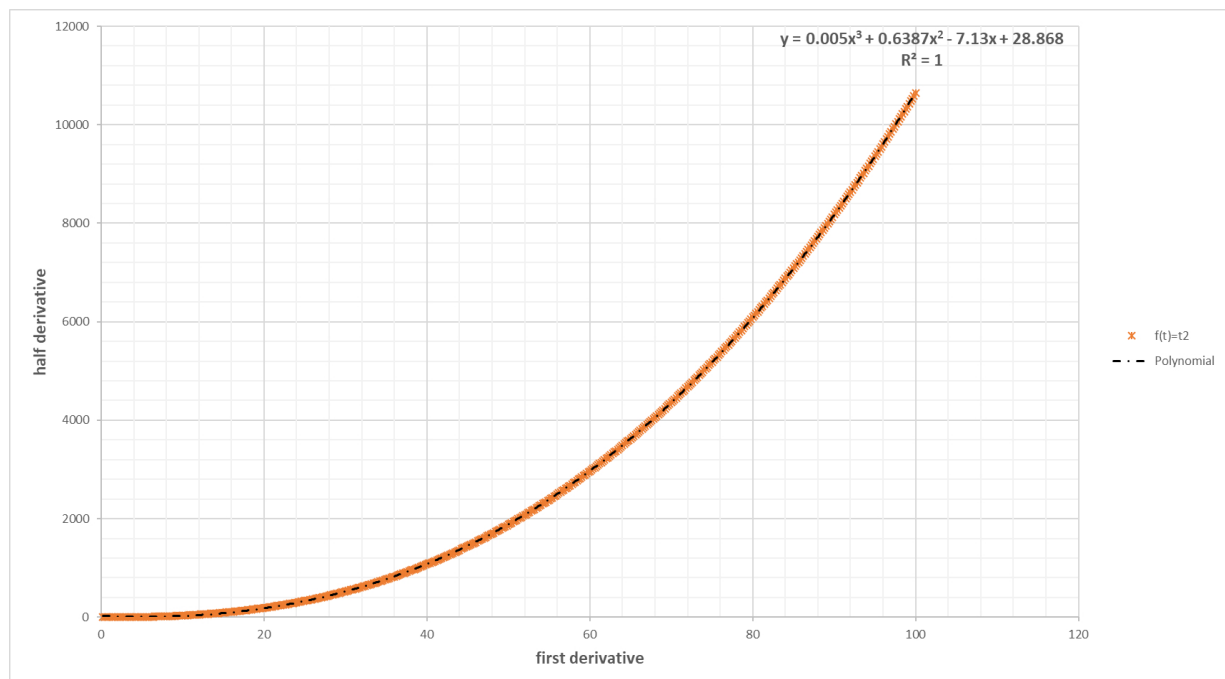
Fig. 2. Half derivative Graph vs first order derivative for function $y = x^2$
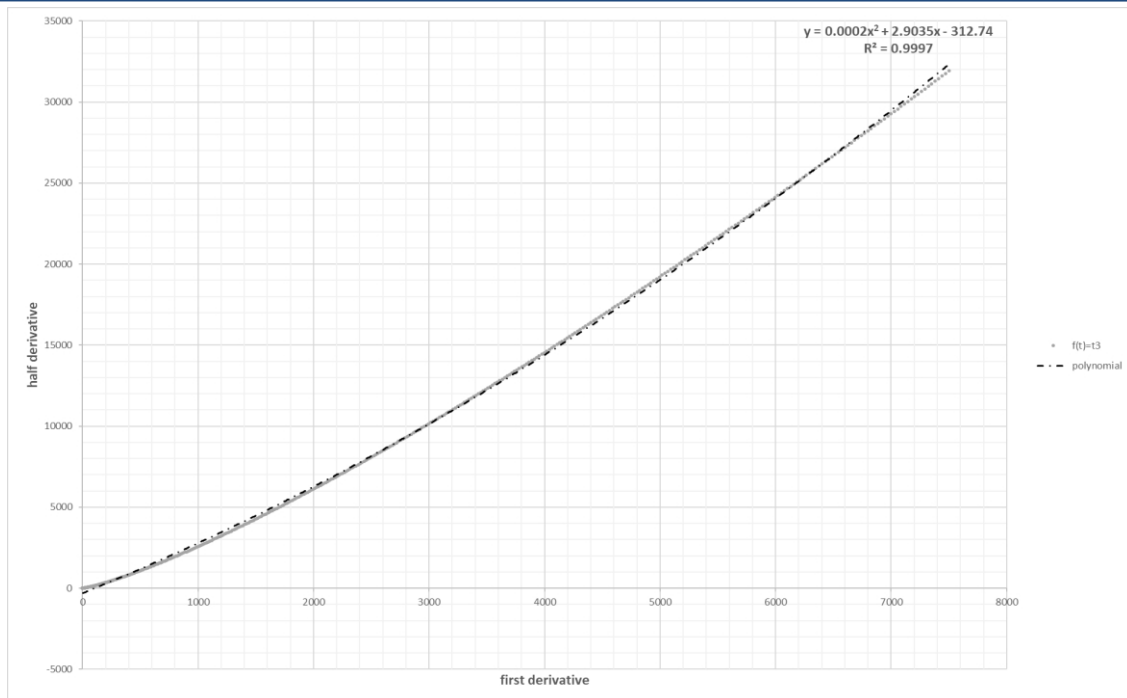
Fig. 3. Half derivative Graph vs first order derivative for function $y = x^3$

2.2 Theoretical gradually varied flow profile behavior

When taking into account measured data in laboratory from trapezoidal canal gradually varied flow profile and looking for trend line between variable x and strap and it was found the best curved portion profile trend line is a third-grade polynomial (Figure 4).
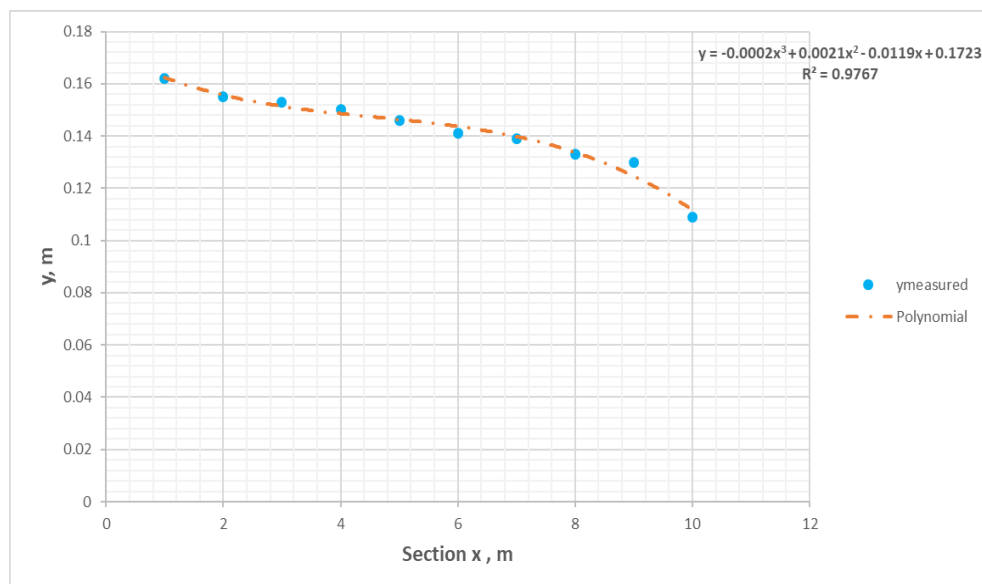
Fig. 4. Y Deep behavior Graph vs x chain in a laboratory trapezoidal channel

When considering data from hypothetical trapezoidal channel and numerical estimation performing to tie and against x-chain using Runge Kutta numerical method, a trend line corresponding to a degree two polynomial with a determination high coefficient is obtained (Figure 5).
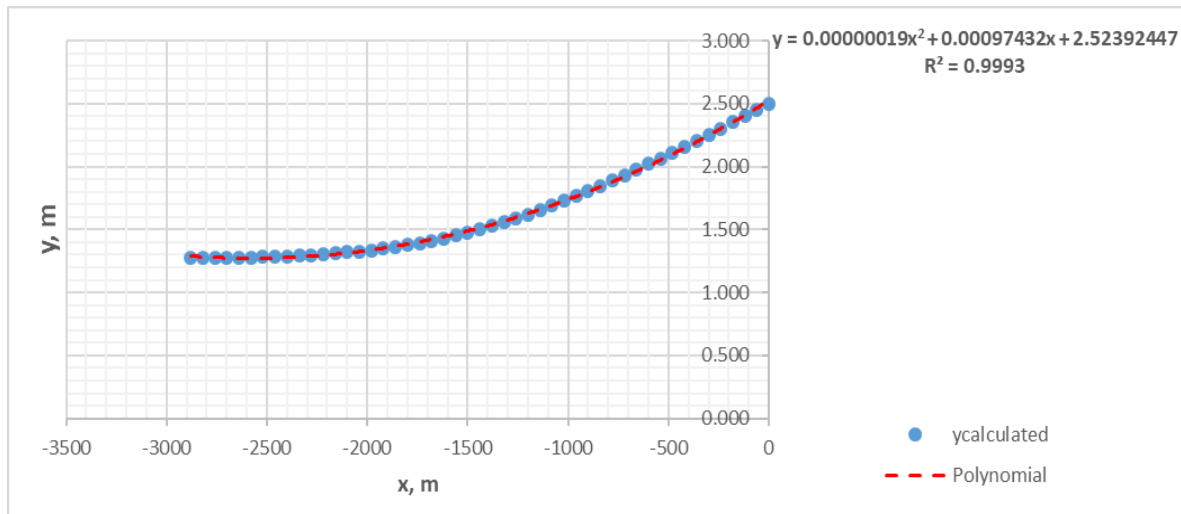
Fig. 5. Y Deep behavior Graph vs x chain in a hypothetical trapezoidal channel

3. Conclusions

Analyzing figures 4 and 5 we can conclude that flow profile can approximated by a polynomial function of grades between 1 and 3, so the first order derivative function y'(x) can be related to a fractional derivative of half order $y^{1/2}(x)$ according to equation 1 or with transformations expressed by equations 2 and 3. Schemes in fractional finite differences such as cited in Appendix A can also be used to approximate gradually varied flow profile solution.

4. Appendix A

A.1 Fourth order Runge Kutta method

Runge Kutta's methods numerically solve a first-order ordinary differential equation with initial conditions to form [2] (formula A.1):

$$y' = f(x,y); \text{ Subject to } y(x_0) = y_0 \tag{A.1}$$

In a range of values $x_0 \leq x \leq x_n$, it considering a constant increment h in independent variable x.

To do this, use following recurrence equations applied at each solution point:

$$
\begin{aligned}
k_1 &= f(x_i, y_i) \\
k_2 &= f(x_i + 0.5h, y_i + k_1 h) \\
k_3 &= f(x_i + 0.5h, y_i + k_2 h) \\
k_4 &= f(x_i + h, y_i + k_3 h) \\
y_{i+1} &= y_i + \frac{h}{6}(k_1 + 2k_2 + 3k_3 + k_4) \\
i &= 0,1,2,..n-1
\end{aligned}
\tag{A.2}
$$

A2. Finite fractional differences corrective predictive method

Corrective predictive method obtains differential equation numerical solution of fractional order [11]:

$$cD_o^\alpha u(t) = f\big(t, u(t)\big), t \in [0, T] \tag{A.3}$$

Subject to initial condition

$$u^{(j)}(o) = u_0^{(j)}, j = 0,1,2, \ldots, n-1$$

Where $\alpha > 0$, n is first integer not less than α

Form of a corrective predictive method, obtained from Adams-Bashford-Moulton method is:

$$u_{k+1}^p = \sum_{j=0}^{n-1} \frac{t_{k+1}^j}{j!} u_0^j + \frac{1}{\Gamma(\alpha)} \sum_{j=0}^{k} b_{j,k+1} f(t_j, u_j) \tag{A.4}$$

$$u_{k+1} = \sum_{j=0}^{n-1} \frac{t_{k+1}^j}{j!} u_0^j + \frac{1}{\Gamma(\alpha)} \Big[\sum_{j=0}^{k} a_{j,k+1} f(t_j, u_j) + a_{k+1,k+1} f(t_{k+1}, u_{k+1}^p) \Big] \tag{A.5}$$

Where

$$a_{j,k+1} = \frac{\Delta t^\alpha}{\alpha(\alpha+1)} \begin{cases} k^{\alpha+1} - (k-\alpha)(k+1)^\alpha, & j = 0 \\ (k-j+2)^{\alpha+1} + (k-j)^{\alpha+1} - 2(k-j+1)^{\alpha+1} - 2(k-j+1)^{\alpha+1}, & 1 \le j \le k \\ 1, & j = k+1 \end{cases} \tag{A.6}$$

and

$$b_{j,k+1} = \frac{\Delta t^\alpha}{\alpha} \big[(k-j+1)^\alpha - (k-j)^\alpha \big], \qquad\qquad 0 \le j \le k \tag{A.7}$$

Where
u_j Is approximate solution of $u(t_j)$

This method applies prediction equation (A.4) to estimate an approximate value of u_{k+1} subsequently used in corrective equation (A.5) to obtain an improved approximation value.

Acknowledgments

References

[1] Sotelo Ávila, Gilberto. *Open Channel Hydraulics. / Hidráulica de canales*. México. UNAM, Facultad de Ingeniería, 2002.
[2] Chapra, Steven C., and Raymond P. Canale. *Numerical Methods for Engineers. / Métodos numéricos para ingenieros*. México D.F., McGraw Hill, 2007.
[3] Lombardero Ozores, Antón "Cálculo fraccionario y dinámica newtoniana." *Revista de Investigación. Pensamiento Matemático* 4, no. 1 (2014): pp 77-106.
[4] Pérez Contreras, Pablo José. *Finite Differences for the Solution of Fractional Ordinary Differential Equations. / Diferencias Finitas Para la Solución de Ecuaciones Diferenciales Ordinarias Fraccionarias*. Mater's Tesis. Tesis de maestría. Colombia, 2014.
[5] Hermosillo Arteaga, Armando Rafael. *Modeling by differential equations and fractional rheology of the creep phenomenon in reconstituted clay soils. / Modelación mediante ecuaciones diferenciales y reología fraccionarias del fenómeno de creep en suelos de arcilla reconstituida*. Tesis doctoral. Posgrado en Ingeniería, UNAM. 2013.

[6] Pierantozzi, Teresa. *Study of fractional generalizations of the standard diffusion and wave equations / Estudio de generalizaciones fraccionarias de las ecuaciones estándar de difusión y de ondas*. Doctoral Thesis. Tesis Doctoral. Universidad Complutense De Madrid, Madrid, 2006.

[7] Pérez Gómez, Jorge Alberto, Jair Servin Aguilar, and Marcos González Olvera. "Adaptive Fractional Order Control Applied to a Hydraulic System"/"Control Adaptable de Orden Fraccionario Aplicado a un Sistema Hidráulico." Memorias del Congreso Nacional de Control Automático. San Luis Potosí, San Luis Potosí, México, 10-12 de Octubre de 2018.

[8] Guía-Calderón, Manuel, J. Juan Rosales-García, Rafael Guzmán-Cabrera, Adrián González-Parada, and J. Antonio Álvarez-Jaime. "The differential and integral fractional calculation and its applications"/"El cálculo diferencial e integral fraccionario y sus aplicaciones." *Acta Universitaria* 25, no. 2 (2015): 20-27. doi: 10.15174/au.2015.688.

[9] Coronel Frías, Elmer, and Marlon Tomas Moreno Chapoñán. *Equivalences between the properties of fractional derivatives and classical derivatives./Equivalencias entre Las propiedades de las derivadas fraccionariasy las derivadas clásicas*. Bachelor thesis. Tesis De Licenciatura. Universidad Nacional "Pedro Ruiz Gallo" Facultad de Ciencias Físicas y Matemáticas Escuela Profesional De Matemática Lambayeque Perú, 2016.

[10] Santamarina, Carlos. "Online trials with GeoGebra."/"Ensayos en línea con GeoGebra". Own design notes. Notas de diseño propio. 2019.

[11] GeoGebra software..https://www.geogebra.org/?lang=es.

[12] Li, C.P., and F. Zeng. "Finite difference methods for fractional differential equations." *Int. J. Bifurcation Chaos* 22, no. 04 (2012): Article 1230014-1-28.

Numerical Analysis of the Influence of Uniaxial Compression Loads on the Shape of a Toroidal LPG Tank

Assoc. Prof. PhD. Eng. **Ștefan ȚĂLU**[1], Assoc. Prof. PhD. Eng. **Mihai ȚĂLU**[2,*]

[1] Technical University of Cluj-Napoca, The Directorate of Research, Development and Innovation Management (DMCDI), Constantin Daicoviciu Street, no. 15, Cluj-Napoca, 400020, Cluj county, Romania. E-mail: stefan_ta@yahoo.com

[2] University of Craiova, Faculty of Mechanics, Department of Applied Mechanics and Civil Engineering, Calea București Street, no. 107, 200512 Craiova, Dolj county, Romania. Corresponding author* e-mail: mihai_talu@yahoo.com

Abstract: This study focuses on investigations of the influence of uniaxial compression loads on the shape of a three-dimensional (3-D) hexagonal toroid with regular hexagonal cross-section used in manufacturing of liquefied petroleum gas (LPG) storage tanks from the automotive industry. In order to improve the computing efficiency and to minimize the storage tank mass, the finite element method was applied to study the effect of every affecting factor (temperature, corrosion and compression loads) on the LPG storage tank model. Results show that analysis based on the finite element method can improve the simulation accuracy while greatly reduce the computing cost.

Keywords: 3-D hexagonal toroidal LPG fuel tank, automotive industry, industrial engineering design, optimization methods

1. Introduction

In the last decades, intense international competition has forced companies to apply CAD/CAM (Computer-aided design/ Computer-aided manufacturing) systems [1-3] to assist in automating tasks within design and manufacturing of the fuel storage tanks [4-7] to increase productivity and improve quality end product [8-11].

The dynamics of the storage tank markets require superior engineering CAD designs [12-15], advanced materials [16-18], advanced manufacturing processes [19-21], novel design approaches [22-24], intelligent innovations [25, 26], quality assurance, and quality control to meet the customers' requirements.

The CAD multivariable models of LPG storage tanks, defined by geometrical parameters, offer several advantages and can be tested by simulating real-world conditions to reduce the time required to design and prototype, and ultimately improve profitability.

LPG storage tanks are manufactured based on a well-integrated project management approach to various design standards [27-29] using special expertise, technology, and strict quality control measures, in a wide range of various capacities [6-10]. In the literature, there are various theories (continuum damage mechanics approaches, and energy-based damage methods) to predict the life of LPG storage tanks and to calculate the crack initiation probability.

By constructing virtual prototypes with advanced CAD software [30-34] and applying accurate exploitation assessments, different variants of LPG storage tanks with good technical-functional characteristics can be designed (based on descriptive geometry concepts [35-39]), as well as control strategies that can improve reliability and can reduce production costs [40-44].

This paper studies the influence of uniaxial compression loads applied normally on one side of the 3-D hexagonal toroid with regular hexagonal cross-section used in manufacturing of LPG storage tanks using the finite element analysis.

2. Design methodology

2.1. Basic geometry of the parametric 3-D model

Let's consider the parametric 3-D model generated by revolving of a closed generating curve C_G (a hexagon with rounded corners) along a closed guiding curve C_D (a hexagon with rounded corners) as shown in figs. 1 and 2 [14].

The following parameters were applied as input parameters to the 3-D parametric model (figs. 1 and 2): a) a closed generating curve CG (a hexagon with a side value L = 175 mm, with rounded corners, radius R = 50 mm), and b), the guiding curve CD (a hexagon with a side value L = 430 mm, with rounded corners, radius R = 180 mm), and the thickness = 10 mm.

Fig. 1. The isometric representation of 3-D model, not deformed, before the uniaxial compression
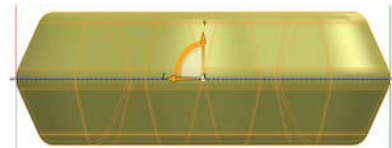
Fig. 2. The lateral representation of 3-D model not deformed, before the uniaxial compression
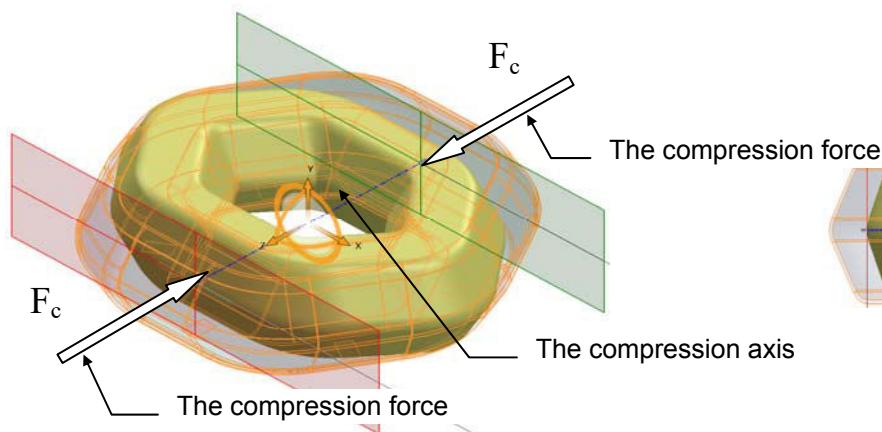
Fig. 3. The isometric representation of 3-D model, deformed, after the uniaxial compression
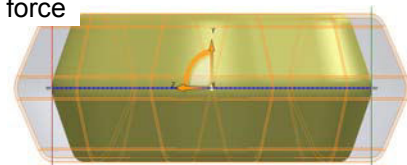
Fig. 4. The lateral representation of 3-D model deformed, after the uniaxial compression

2.2. Numerical analysis of the parametric 3-D model

Based on the physical model, the modeling was done in the AutoCAD Autodesk 2020 software [45] and the numerical analysis was performed with SolidWorks 2020 software [46] with the Static, Thermal and Design Study modules. The design data used were:
- the tank material is AISI 4340 steel;
- the maximum hydraulic test pressure: p_{max} = 30 bar;
- the working temperature between the limits: T = -30 ^{0}C up to T = 60 ^{0}C;
- supporting surfaces located on the inferior side;
- the duration of the tank exploitation: n_a = 15 years;
- the corrosion rate of the material: v_c = 0.07 mm/year.

Numerical calculations were performed for: mesh standard type, solid mesh, curvature-based mesh with quality high, Jacobian in 16 points, element size 6 mm, number of nodes 47767, number of elements 23925. The parameterized 3-D model used in calculus is a section of ½ (fig. 5) from the initial physical model and the corresponding surfaces to which the constraints and restrictions are applied are shown in fig. 5.

This methodology is applied in the simulation of stress analysis of the 3-D parametric model using a displacement-based finite element method.

a)   b)
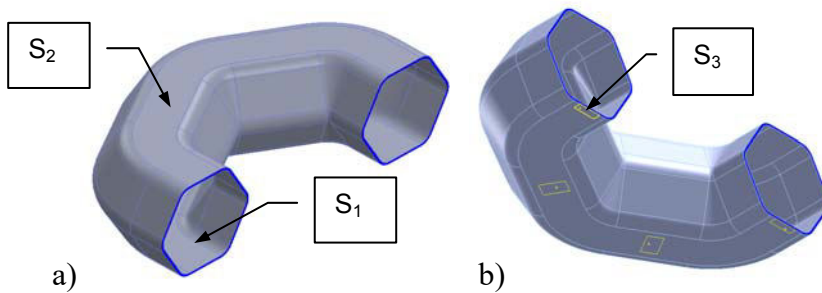
Fig. 5. The surfaces to which the constraints were applied.

Fig. 6. The discretization of the model

The design data used in this analysis for the tank lateral cover are:
- the maximum pressure p_{max} = 3 N/mm^2 on the inner surface S_1;
- the working temperature between the limits: T = -30 ^{0}C to T = 60 ^{0}C on the exterior surface S_2;
- the fixation of the tank on the six tank supports located at the inferior part of the tank.
The finite element discretization for the 3-D parametric model is shown in fig. 6.
The values of the state of stress Von Mises determined by the finite element method for n_a= 0, 5, 10 and 15 years are shown in table 1.

Table 1: The Von Misess resultant effort for n_a= 0, 5, 10 and 15 years

Lc [mm]	T [^{0}C]				T [^{0}C]			
	-30^0	0^0	30^0	60^0	-30^0	0^0	30^0	60^0
	n_a = 0 [years]				n_a = 5 [years]			
	σ_c [MPa]				σ_c [MPa]			
0	665.40	565.66	479.29	527.43	610.22	514.24	511.09	560.58
1	639.82	542.94	515.96	557.23	532.28	510.09	552.49	598.10
2	627.93	527.30	500.92	546.85	564.98	521.91	562.62	606.45
3	531.38	467.79	507.29	549.93	631.33	538.41	557.01	600.40
4	509.47	464.14	508.40	556.37	678.74	578.54	544.43	591.21
5	589.15	499.13	448.13	452.74	665.32	564.82	559.06	604.03
6	674.86	570.83	512.66	561.59	674.56	570.71	512.09	542.58
7	651.59	550.74	504.76	547.34	679.16	578.01	478.09	488.02
8	525.77	472.30	516.00	563.23	674.37	570.86	494.20	528.26
9	523.78	529.17	521.79	570.21	646.48	550.40	559.13	600.81
10	568.13	533.82	498.05	543.62	649.97	555.16	560.20	596.27
	n_a = 10 [years]				n_a = 15 [years]			
0	656.26	615.97	591.97	641.72	654.50	655.70	636.94	688.12
1	566.98	568.67	606.88	647.44	760.74	661.69	677.69	720.92
2	577.49	580.21	623.99	670.84	733.97	630.11	636.39	671.18
3	680.81	585.12	611.01	658.16	608.07	618.41	658.21	700.28
4	690.24	589.25	601.49	655.87	618.59	636.51	681.17	728.32
5	703.44	600.73	635.70	675.09	644.32	579.84	618.48	662.06
6	698.80	601.83	608.11	652.30	633.14	632.84	599.81	627.73
7	677.61	593.07	639.09	690.45	640.52	627.79	669.36	713.72
8	657.19	565.88	533.39	570.39	667.74	655.60	703.00	754.60
9	589.70	547.00	578.70	613.37	624.54	623.04	667.02	713.53
10	581.48	563.95	606.61	652.00	599.76	618.13	661.29	707.00

The uniaxial displacement under compression loads is noted with L_c.

The graphs corresponding to the Von Mises resultant efforts σ_c (L_c, T) taking into account the results from table 1 are graphically shown in figs. 7-10, respectively.
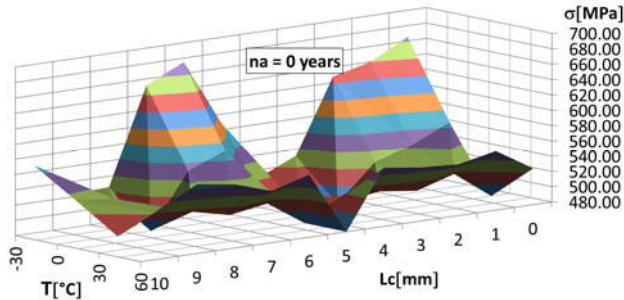
Fig. 7. The graphs of $\sigma = f(L_c, T)$ for $n_a = 0$ years
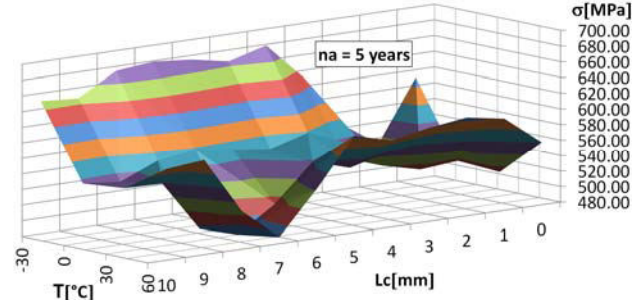
Fig. 8. The graphs of $\sigma = f(L_c, T)$ for $n_a = 5$ years
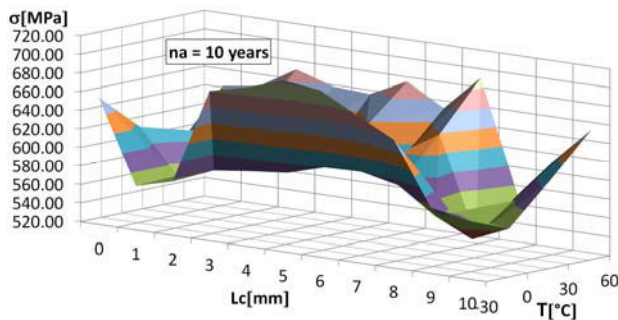
Fig. 9. The graphs of $\sigma = f(L_c, T)$ for $n_a = 10$ years
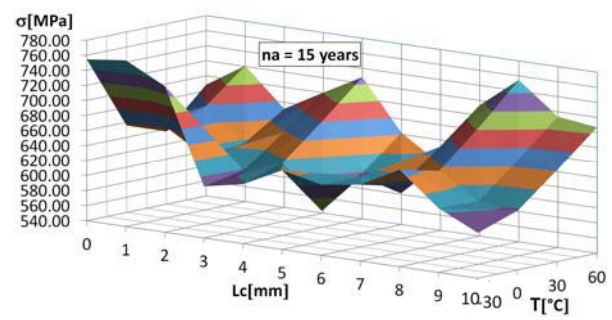
Fig. 10. The graphs of $\sigma = f(L_c, T)$ for $n_a = 15$ years

The graphs of curves corresponding to the Von Mises resultant efforts σ_c (L_c, T) for n_a = {0, 5, 10, and 15 years}, are graphically shown in fig. 11.
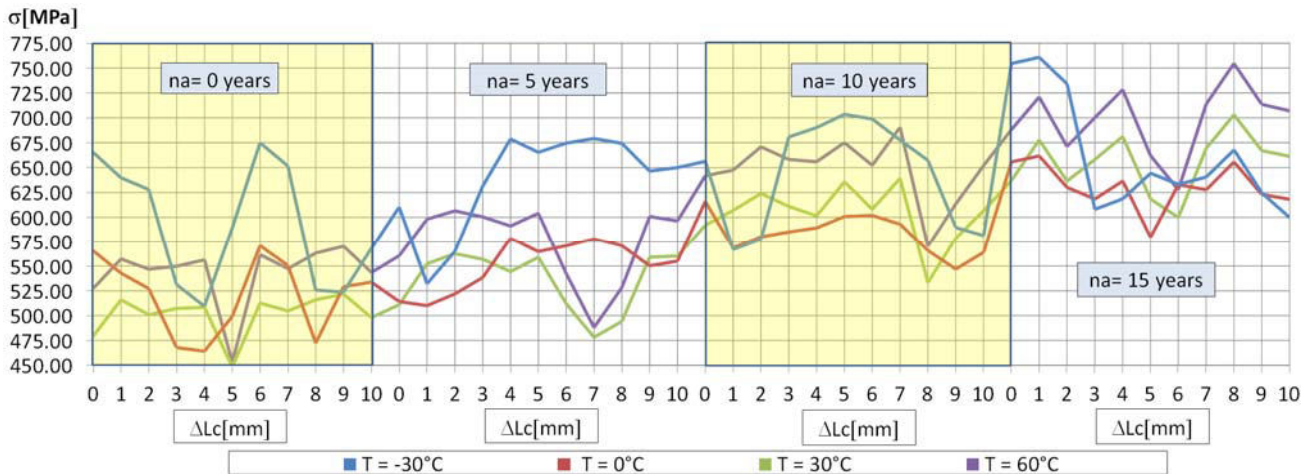
Fig. 11. The graphs of σ_c (L_c, T) for: T = {-30 ^{0}C, 0 ^{0}C, 30 ^{0}C, 60 ^{0}C} and n_a= {0, 5, 10 and 15 years}

The results show the Von Mises resultant efforts has a maximum value corresponding for T = -30 ^{0}C. It was calculated the percentage variation of the Von Mises effort $\Delta\sigma_c$ (L_c, T) versus the resulting stress state of the non-deformed tank (for L_c = 0), using the following formula:

$$\Delta\sigma = \frac{(\sigma_{Lc=0} - \sigma)}{\sigma_{Lc=0}} \cdot 100 \ [\%]$$ (1)

The percentage variation of Von Mises resultant effort $\Delta\sigma_c$ in relation to the initial effort status (computed in table 2) and the corresponding graphs (in 2-D) are shown in fig. 12, while the corresponding graphs (in 3-D) are shown in figs. 13-16.

Table 2: The percentage variation of Von Mises resultant effort for n_a= 0, 5, 10 and 15 years

Lc [mm]	T [^{0}C]				T [^{0}C]			
	-30^0	0^0	30^0	60^0	-30^0	0^0	30^0	60^0
	n_a = 0 [years]				n_a = 5 [years]			
	$\Delta\sigma_c$ [%]				$\Delta\sigma_c$ [%]			
1	-3.84	-4.02	7.65	5.65	-12.77	-0.81	8.10	6.69
2	-5.63	-6.78	4.51	3.68	-7.41	1.49	10.08	8.18
3	-20.14	-17.30	5.84	4.27	3.46	4.70	8.98	7.10
4	-23.43	-17.95	6.07	5.49	11.23	12.50	6.52	5.46
5	-11.46	-11.76	-6.50	-14.16	9.03	9.84	9.39	7.75
6	1.42	0.91	6.96	6.48	10.54	10.98	0.20	-3.21
7	-2.08	-2.64	5.31	3.78	11.30	12.40	-6.46	-12.94
8	-20.98	-16.51	7.66	6.79	10.51	11.01	-3.31	-5.77
9	-21.28	-6.45	8.87	8.11	5.94	7.03	9.40	7.18
10	-14.62	-5.63	3.91	3.07	6.51	7.96	9.61	6.37
	n_a = 10 [years]				n_a = 15 [years]			
	$\Delta\sigma_c$ [%]				$\Delta\sigma_c$ [%]			
1	-13.61	-7.68	2.52	0.89	0.83	0.91	6.40	4.77
2	-12.00	-5.81	5.41	4.54	-2.72	-3.90	-0.09	-2.46
3	3.74	-5.01	3.22	2.56	-19.41	-5.69	3.34	1.77
4	5.18	-4.34	1.61	2.21	-18.01	-2.93	6.94	5.84
5	7.19	-2.47	7.39	5.20	-14.60	-11.57	-2.90	-3.79
6	6.48	-2.30	2.73	1.65	-16.09	-3.49	-5.83	-8.78
7	3.25	-3.72	7.96	7.59	-15.11	-4.26	5.09	3.72
8	0.14	-8.13	-9.90	-11.12	-11.50	-0.02	10.37	9.66
9	-10.14	-11.20	-2.24	-4.42	-17.23	-4.98	4.72	3.69
10	-11.40	-8.44	2.47	1.60	-20.51	-5.73	3.82	2.74
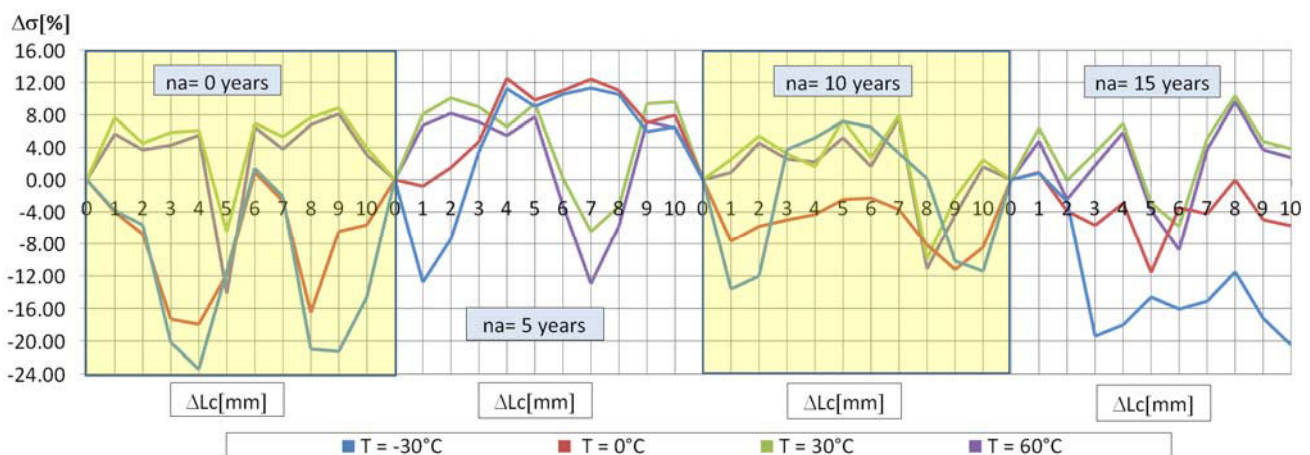
Fig. 12. The graphs of $\Delta\sigma$ (L_c, T) for: T = {-30 ^{0}C, 0 ^{0}C, 30 ^{0}C, 60 ^{0}C } and n_a= {0, 5, 10 and 15 years}
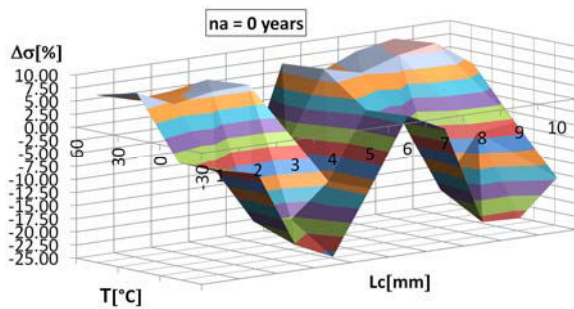
Fig. 13. The graphs of $\Delta\sigma$ (L_c, T) for n_a = 0 years
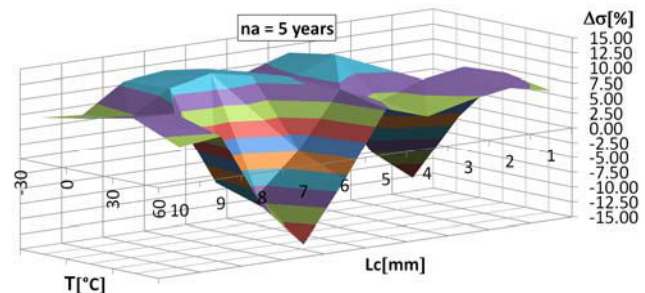
Fig. 14. The graphs of $\Delta\sigma$ (L_c, T) for n_a = 5 years
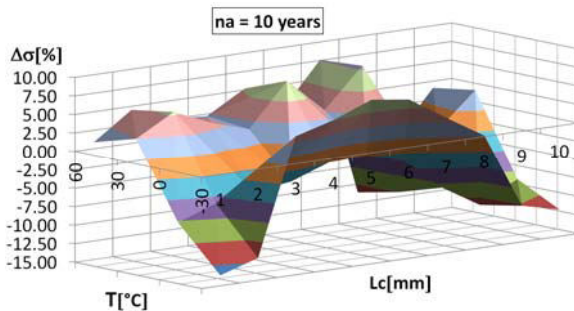
Fig. 15. The graphs of $\Delta\sigma$ (L_c, T) for n_a = 10 years
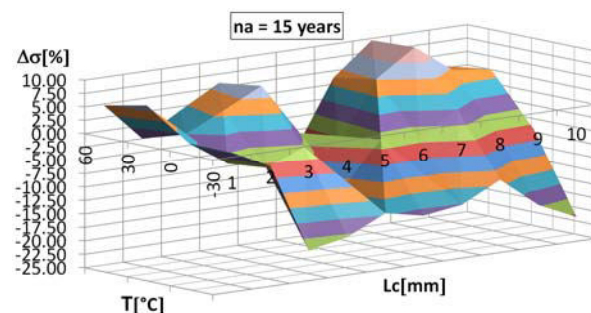
Fig. 16. The graphs of $\Delta\sigma$ (L_c, T) for n_a = 15 years

For the most important cases of the uniaxial compression loads, the Von Mises resultant efforts σ_c (L_c, T) was calculated taking into account the results from table 3, while the corresponding graphs are shown in figs. 17-20.

Table 3: The maximum values of the Von Misess resultant effort

No. case	n_a [years]	Lc [mm]	T [°C]	σ_c [MPa]
1	0	10	-30	568.13
2	5	5	30	559.06
3	10	6	0	601.83
4	15	8	60	754.60
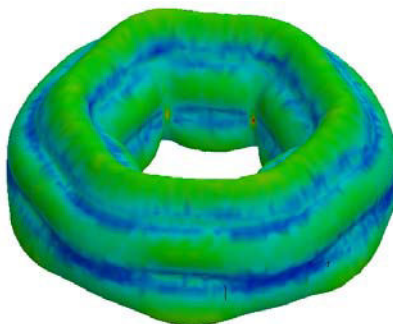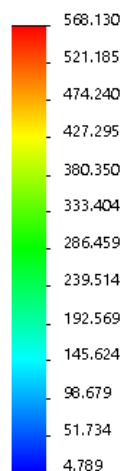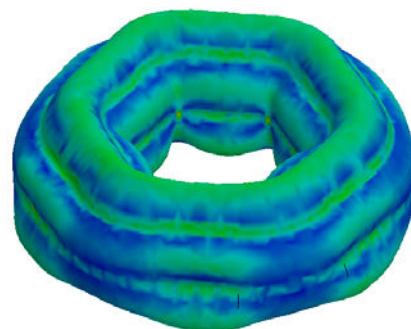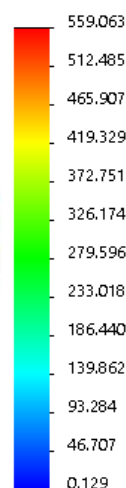
Fig. 17. The graphs of σ = f(L_c, T) for case 1
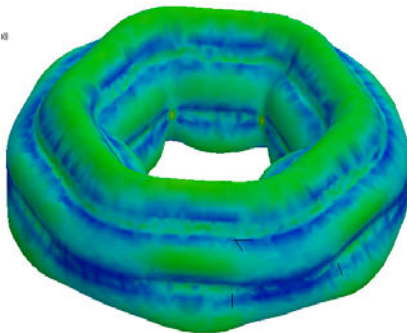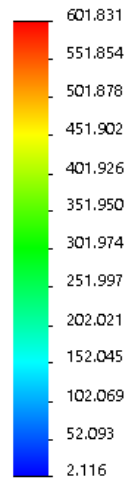
Fig. 18. The graphs of σ = f(L_c, T) for case 2
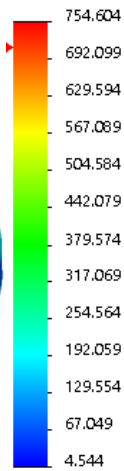
Fig. 19. The graphs of $\sigma = f(L_c, T)$ for case 3   **Fig. 20.** The graphs of $\sigma = f(L_c, T)$ for case 4

The values of the resultant linear deformation u determined by the finite element method for $n_a = \{0, 5, 10$ and 15 years$\}$ are shown in table 4.

Table 4: The resultant linear deformation for $n_a = \{0, 5, 10$ and 15 years$\}$

Lc [mm]	T [^{0}C]				T [^{0}C]			
	-30^0	0^0	30^0	60^0	-30^0	0^0	30^0	60^0
	$n_a = 0$ [years]				$n_a = 5$ [years]			
	u_c [mm]				u_c [mm]			
0	0.869	0.837	0.805	0.777	0.938	0.904	0.871	0.841
1	0.695	0.704	0.715	0.728	0.761	0.769	0.780	0.793
2	0.675	0.683	0.693	0.704	0.728	0.736	0.745	0.757
3	0.673	0.681	0.690	0.700	0.727	0.735	0.745	0.757
4	0.656	0.664	0.673	0.684	0.708	0.712	0.720	0.730
5	0.635	0.626	0.619	0.614	0.697	0.702	0.709	0.718
6	0.623	0.632	0.645	0.659	0.720	0.719	0.719	0.720
7	0.669	0.676	0.685	0.694	0.727	0.720	0.713	0.706
8	0.654	0.661	0.670	0.680	0.718	0.707	0.699	0.696
9	0.636	0.644	0.655	0.666	0.687	0.695	0.704	0.714
10	0.671	0.678	0.686	0.696	0.693	0.699	0.707	0.719
	$n_a = 10$ [years]				$n_a = 15$ [years]			
0	1.011	0.974	0.944	0.916	1.106	1.076	1.047	1.020
1	0.836	0.845	0.855	0.866	0.927	0.933	0.941	0.952
2	0.805	0.815	0.825	0.837	0.887	0.891	0.887	0.884
3	0.807	0.816	0.826	0.839	0.905	0.914	0.924	0.935
4	0.805	0.811	0.819	0.828	0.873	0.882	0.893	0.905
5	0.791	0.796	0.807	0.817	0.843	0.835	0.829	0.831
6	0.784	0.790	0.797	0.807	0.882	0.873	0.872	0.877
7	0.788	0.796	0.80	0.814	0.932	0.938	0.948	0.960
8	0.795	0.793	0.795	0.802	0.871	0.879	0.888	0.898
9	0.797	0.789	0.783	0.779	0.833	0.839	0.847	0.855
10	0.804	0.811	0.820	0.831	0.899	0.904	0.910	0.917

The graphs of curves (in 2-D) corresponding to the resultant linear deformation $u = (L_c, T)$ for $n_a =$ {0, 5, 10 and 15 years}; are graphically shown in fig. 21, while the corresponding graphs (in 3-D) are shown figs. 22-25.
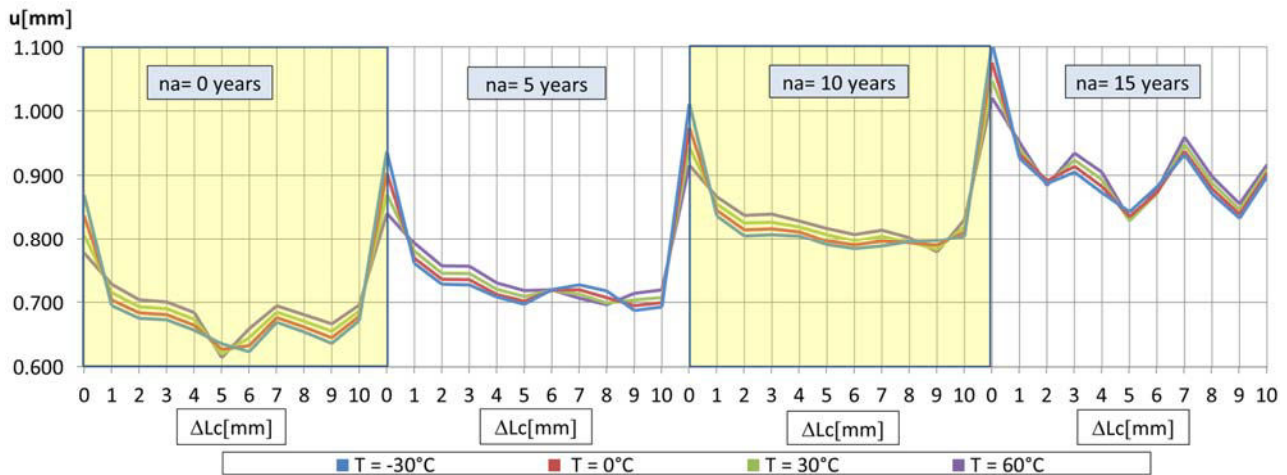
Fig. 21. The graphs of $u = (L_c, T)$ for: T = {-30 ^{0}C, 0 ^{0}C, 30 ^{0}C, 60 ^{0}C} and n_a= {0, 5, 10 and 15 years}
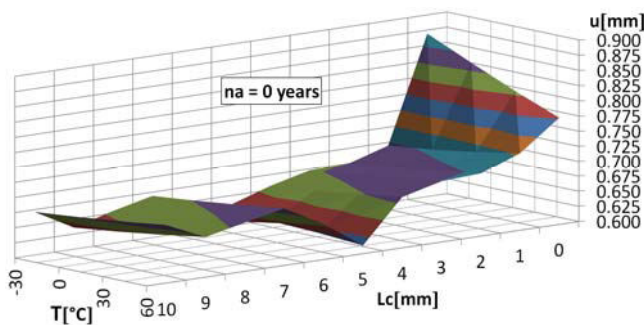
Fig. 22. The graphs of u (L_c, T) for n_a = 0 years
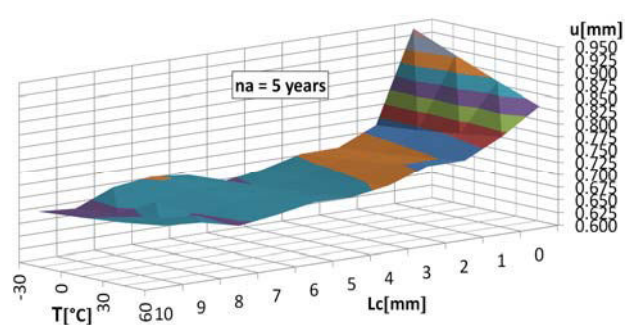
Fig. 23. The graphs of u (L_c, T) for n_a = 5 years
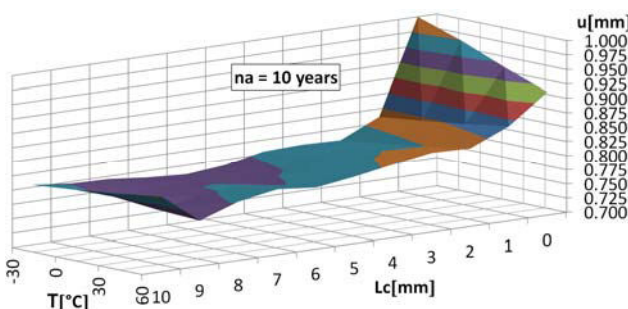
Fig. 24. The graphs of u = f(L_c, T) for n_a = 10 years
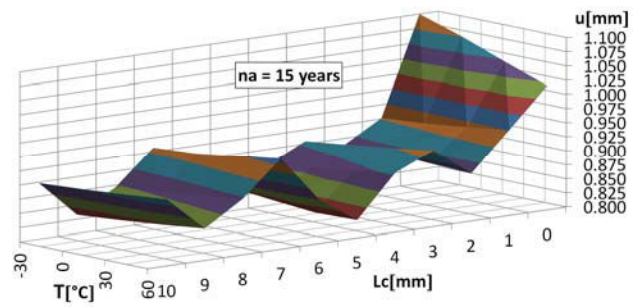
Fig. 25. The graphs of u = f(L_c, T) for n_a = 15 years

For the most important cases of the uniaxial compression loads, the resultant linear deformation $u = (L_c, T)$ was calculated taking into account the results from table 5, while the corresponding graphs are shown in figs. 26-29.

Table 5: The representation cases chosen for different linear deformation states

No. case	n_a [years]	Lc [mm]	T [°C]	u [mm]
1	0	10	-30	0.671
2	5	5	30	0.709
3	10	6	0	0.790
4	15	8	60	0.898
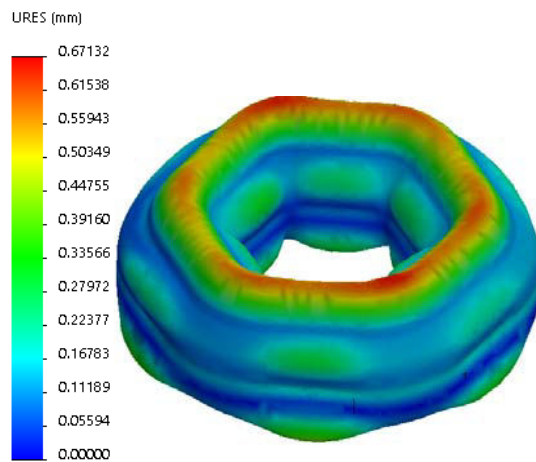
Fig. 26. The graphs of u = f(L_c, T) for case 1   **Fig. 27.** The graphs of u = f(L_c, T) for case 2
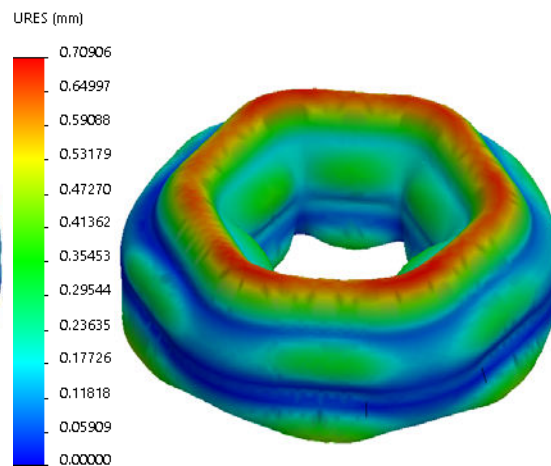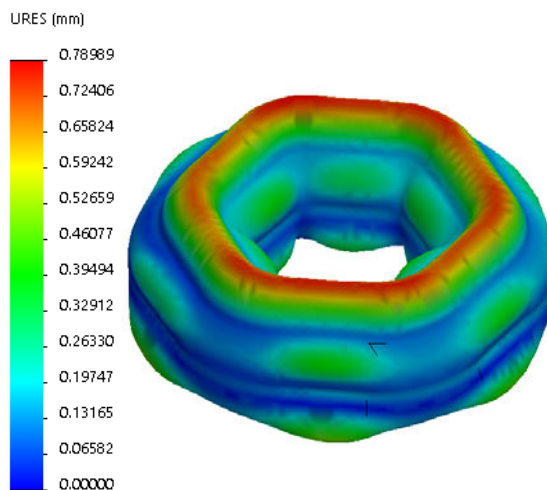
Fig. 28. The graphs of u = f(L_c, T) for case 3   **Fig. 29.** The graphs of u = f(L_c, T) for case 4
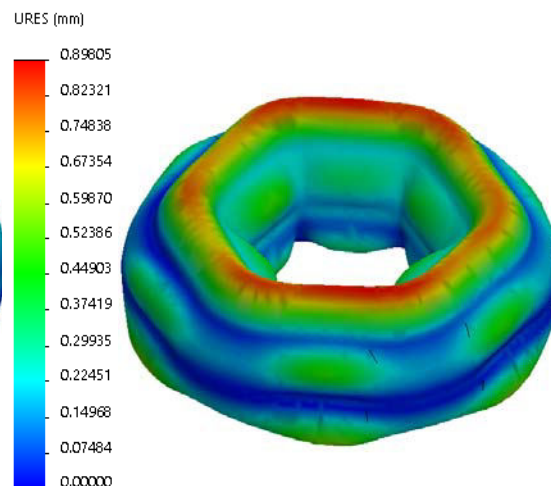
It was calculated the percentage variation of the resultant linear deformation Δu (L_c, T) versus the resulting state of the non-deformed tank (for u_{Lc}= 0), using the following formula:

$$\Delta u = \frac{(u_{Lc=0} - u)}{u_{Lc=0}} \cdot 100 \; [\%] \tag{2}$$

The percentage variation of resultant linear deformation Δu in relation to the initial value was calculated in table 6 and the corresponding graphs are given in fig. 30.

Table 6: The percentage variation of resultant liniar deformation Δu for n_a= 0, 5, 10 and 15 years

Lc [mm]	T [^{0}C]				T [^{0}C]			
	-30^0	0^0	30^0	60^0	-30^0	0^0	30^0	60^0
	n_a = 0 [years]				n_a = 5 [years]			
	Δu [%]				Δu [%]			
1	-20.06	-15.91	-11.23	-6.28	-18.82	-14.89	-10.42	-5.67
2	-22.33	-18.32	-13.96	-9.41	-22.31	-18.56	-14.41	-9.95
3	-22.61	-18.66	-14.34	-9.84	-22.43	-18.62	-14.43	-10.00
4	-24.48	-20.64	-16.41	-11.97	-24.44	-21.19	-17.29	-13.12
5	-26.93	-25.16	-23.19	-21.03	-25.66	-22.35	-18.57	-14.55
6	-28.35	-24.45	-19.96	-15.20	-23.22	-20.46	-17.47	-14.40
7	-23.05	-19.21	-15.00	-10.62	-22.42	-20.37	-18.17	-15.97

8	-24.80	-20.98	-16.80	-12.41	-23.45	-21.75	-19.75	-17.16
9	-26.85	-22.98	-18.72	-14.25	-26.70	-23.13	-19.19	-15.05
10	-22.76	-18.96	-14.80	-10.45	-26.11	-22.60	-18.76	-14.42
	n_a = 10 [years]				n_a = 15 [years]			
	Δu [%]				Δu [%]			
1	-17.29	-13.28	-9.41	-5.42	-16.23	-13.26	-10.10	-6.69
2	-20.38	-16.41	-12.56	-8.58	-19.79	-17.11	-15.32	-13.34
3	-20.18	-16.25	-12.44	-8.37	-18.19	-15.03	-11.79	-8.38
4	-20.41	-16.75	-13.22	-9.55	-21.11	-17.97	-14.73	-11.30
5	-21.81	-18.29	-14.51	-10.83	-23.82	-22.35	-20.86	-18.54
6	-22.44	-18.94	-15.57	-11.86	-20.24	-18.80	-16.76	-14.05
7	-22.04	-18.35	-14.79	-11.12	-15.71	-12.83	-9.45	-5.91
8	-21.35	-18.59	-15.80	-12.41	-21.26	-18.28	-15.21	-11.97
9	-21.17	-18.99	-17.09	-14.98	-24.71	-21.99	-19.16	-16.15
10	-20.44	-16.74	-13.12	-9.30	-18.77	-15.99	-13.15	-10.15
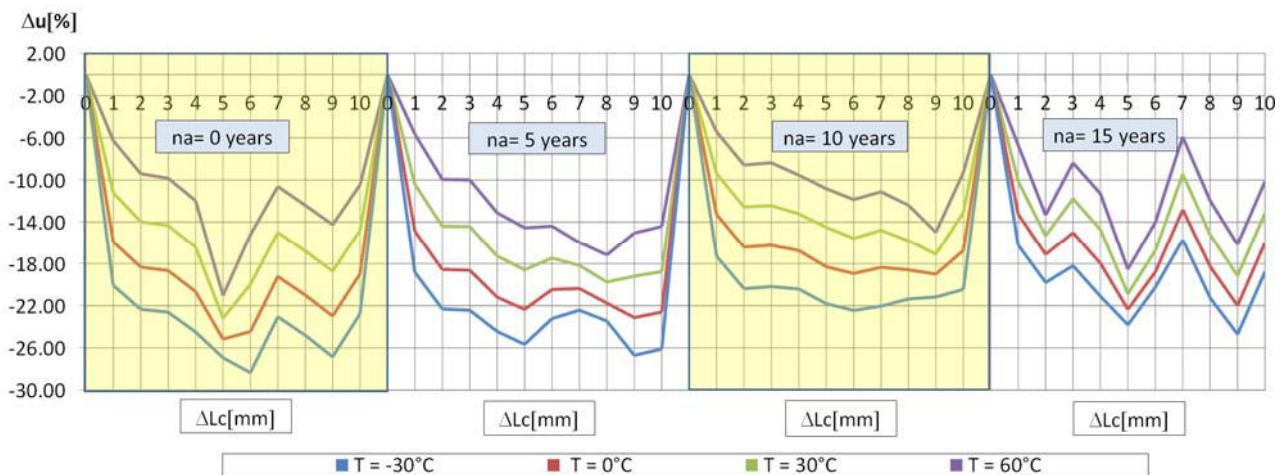
Fig. 21. The graphs of Δu = (L_c, T) for: T = {-30 ^{0}C, 0 ^{0}C, 30 ^{0}C, 60 ^{0}C} and n_a= {0, 5, 10 and 15 years}

3. Conclusions

Finite element analyses of stress and linear deformation has attracted a strong interest in the storage tank design. Following the numerical analyses and the resulting graphs it has been found that:
- for n_a= 15 years, σ_{max} = 760.64 MPa > σ_a = 710 MPa. Also, the state of efforts are amplified with the increase of corrosion and compression loads, and by the decreasing of the working temperature;
- the increase of the working temperature determines the decrease of the stress state, while the compression and corrosion process increase the stress state;
- $\Delta\sigma$ [%] $\cong$ 12% for T = 0 ^{0}C and n_a= 5 years, while $\Delta\sigma$ [%] $\cong$ -23.43% for T = -30 ^{0}C and n_a= 0 years;
- the highest values of resulting linear deformations and the Von Mises stress occur in the middle area of the torus sides. Also, the resultant linear deformation u is amplified with the increase of corrosion, compression loads, and the working temperature;
- u_{max} $\cong$ 1.1 mm for T = -30 ^{0}C and n_a= 10 years. Δu_{max} [%] $\cong$ 28.35% for T = -30 ^{0}C and n_a= 0 years;
- for ΔL < 1.33% of the diameter of the torus, the stress state increases by $\Delta\sigma$ $\cong$ 25% and the percentage variation of resultant linear deformation Δu = 28%.

References

[1] Ghiţă, C. Mirela, Anton C. Micu, Mihai Ţălu and Ştefan Ţălu. "Shape optimization of a thoroidal methane gas tank for automotive industry." *Annals of Faculty of Engineering Hunedoara - International Journal of Engineering, Hunedoara, Romania*, Tome X, Fascicule 3 (2012): 295-297.

[2] Ghiţă, C. Mirela, Anton C. Micu, Mihai Ţălu and Ştefan Ţălu. "Shape optimization of vehicle's methane gas tank." *Annals of Faculty of Engineering Hunedoara - International Journal of Engineering, Hunedoara, Romania*, Tome X, Fascicule 3 (2012): 259-266.

[3] Ghiţă, C. Mirela, Anton C. Micu, Mihai Ţălu, Ştefan Ţălu and Ema I. Adam. "Computer-Aided Design of a classical cylinder gas tank for the automotive industry." *Annals of Faculty of Engineering Hunedoara - International Journal of Engineering, Hunedoara, Romania*, Tome XI, Fascicule 4 (2013): 59-64.

[4] Ghiţă, C. Mirela, Anton C. Micu, Mihai Ţălu and Ştefan Ţălu. "3D modelling of a shrink fitted concave ended cylindrical tank for automotive industry." *Acta Technica Corviniensis – Bulletin of Engineering, Hunedoara, Romania*, Tome VI, Fascicule 4 (2013): 87-92.

[5] Ghiţă, C. Mirela, Anton C. Micu, Mihai Ţălu and Ştefan Ţălu. "3D modelling of a gas tank with reversed end up covers for automotive industry.", *Annals of Faculty of Engineering Hunedoara - International Journal of Engineering, Hunedoara, Romania*, Tome XI, Fascicule 3 (2013): 195-200.

[6] Ghiţă, C. Mirela, Ştefan C. Ghiţă, Ştefan Ţălu and Simona Rotaru, "Optimal design of cylindrical rings used for the shrinkage of vehicle tanks for compressed natural gas." *Annals of Faculty of Engineering Hunedoara - International Journal of Engineering, Hunedoara*, Tome XII, Fascicule 3 (2014): 243-250.

[7] Bică, Marin, Mihai Ţălu and Ştefan Ţălu. "Optimal shapes of the cylindrical pressurized fuel tanks." *Magazine of Hydraulics, Pneumatics, Tribology, Ecology, Sensorics, Mechatronics (HIDRAULICA)*, no. 4 (December 2017): 6-17.

[8] Vintilă, Daniela, Mihai Ţălu and Ştefan Ţălu. "The CAD analyses of a torospheric head cover of a pressurized cylindrical fuel tank after the crash test." *Magazine of Hydraulics, Pneumatics, Tribology, Ecology, Sensorics, Mechatronics (HIDRAULICA)*, no. 4 (December 2017): 57-66.

[9] Ţălu, Ştefan and Mihai Ţălu. "The influence of deviation from circularity on the stress of a pressurized fuel cylindrical tank." *Magazine of Hydraulics, Pneumatics, Tribology, Ecology, Sensorics, Mechatronics (HIDRAULICA)*, no. 4 (December 2017): 34-45.

[10] Ţălu, Mihai. "The influence of the corrosion and temperature on the Von Mises stress in the lateral cover of a pressurized fuel tank." *Magazine of Hydraulics, Pneumatics, Tribology, Ecology, Sensorics, Mechatronics (HIDRAULICA)*, no. 4 (December 2017): 89-97.

[11] Ţălu, Mihai and Ştefan Ţălu. "Analysis of temperature resistance of pressurized cylindrical fuel tanks." *Magazine of Hydraulics, Pneumatics, Tribology, Ecology, Sensorics, Mechatronics (HIDRAULICA)*, no. 1 (March 2018): 6-15.

[12] Ţălu, Mihai and Ştefan Ţălu. "Design and optimization of pressurized toroidal LPG fuel tanks with variable section." *Magazine of Hydraulics, Pneumatics, Tribology, Ecology, Sensorics, Mechatronics (HIDRAULICA)*, no. 1 (March 2018): 32-41.

[13] Ţălu, Ştefan and Mihai Ţălu. "Algorithm for optimal design of pressurized toroidal LPG fuel tanks with constant section described by imposed algebraic plane curves." *Magazine of Hydraulics, Pneumatics, Tribology, Ecology, Sensorics, Mechatronics (HIDRAULICA)*, no. 2 (June 2018): 14-21.

[14] Ţălu, Mihai and Ştefan Ţălu. "The optimal CAD design of a 3D hexagonal toroid with regular hexagonal cross-section used in manufacturing of LPG storage tanks." *Magazine of Hydraulics, Pneumatics, Tribology, Ecology, Sensorics, Mechatronics (HIDRAULICA)*, no. 2 (June 2018): 49-56.

[15] Ţălu, Mihai and Ştefan Ţălu. "The influence of corrosion and temperature variation on the minimum safety factor of a 3D hexagonal toroid with regular hexagonal cross-section used in manufacturing of LPG storage tanks." *Magazine of Hydraulics, Pneumatics, Tribology, Ecology, Sensorics, Mechatronics (HIDRAULICA)*, no. 3 (August 2018): 16-25.

[16] Ţălu, Ştefan and Mihai Ţălu. "The influence of corrosion and pressure variation on the minimum safety factor of a 3D hexagonal toroid with regular hexagonal cross-section used in manufacturing of LPG storage tanks." *Magazine of Hydraulics, Pneumatics, Tribology, Ecology, Sensorics, Mechatronics (HIDRAULICA)*, no. 3 (August 2018): 39-45.

[17] Ţălu, Mihai and Ştefan Ţălu. "The influence of corrosion and temperature variation on a CNG storage tank with a combined form consisting of a torus and a sphere." *Magazine of Hydraulics, Pneumatics, Tribology, Ecology, Sensorics, Mechatronics (HIDRAULICA)*, no. 4 (December 2019): 93-104.

[18] Ţălu, Mihai and Ştefan Ţălu. "Optimal design of a CNG storage tank with a combined form consisting of a torus and a sphere." *Magazine of Hydraulics, Pneumatics, Tribology, Ecology, Sensorics, Mechatronics (HIDRAULICA)*, no. 4 (December 2019): 73-82.

[19] Ţălu, Mihai and Ştefan Ţălu. "Study of temperature–corrosion–torsion affecting factors on the shape of a toroidal LPG tank using the finite element method." *Magazine of Hydraulics, Pneumatics, Tribology, Ecology, Sensorics, Mechatronics (HIDRAULICA)*, no. 1 (March 2020): 21-32.

[20] Ţălu, Mihai and Ştefan Ţălu. "Stress and deformation analysis under bending and torsional loads of a toroidal LPG tank based on the finite element analysis." *Magazine of Hydraulics, Pneumatics, Tribology, Ecology, Sensorics, Mechatronics (HIDRAULICA)*, no. 1 (March 2020): 88-101.

[21] Ţălu, Mihai and Ştefan Ţălu. "3D geometrical solutions for toroidal LPG fuel tanks used in automotive industry." *Advances in Intelligent Systems Research,* vol. 151 (2018): 189-193. DOI: 10.2991/cmsa-18.2018.44.

[22] Ţălu, Ştefan and Mihai Ţălu. "Constructive CAD variants of toroidal LPG fuel tanks used in automotive Industry." *Advances in Intelligent Systems Research,* vol. 159 (2018): 27-30. DOI: 10.2991/mmsa-18.2018.7.

[23] Ţălu, Ştefan and Mihai Ţălu. "The Influence of corrosion on the vibration modes of a pressurized fuel tank used in automotive industry." *DEStech Transactions on Materials Science and Engineering,* (2018): 1-6. DOI: 10.12783/dtmse/icmsa2018/20560.

[24] Ţălu, Mihai and Ştefan Ţălu. "Optimal engineering design of a pressurized paralepipedic fuel tank." *Annals of Faculty of Engineering Hunedoara - International Journal of Engineering, Hunedoara, Romania*, Tome XVI, Fascicule 2 (2018): 193-200.

[25] Ţălu, Ştefan and Mihai Ţălu. "CAD generating of 3D supershapes in different coordinate systems." *Annals of Faculty of Engineering Hunedoara - International Journal of Engineering, Hunedoara, Romania*, Tome VIII, Fascicule 3 (2010): 215-219.

[26] Ţălu, Ştefan and Mihai Ţălu. "A CAD study on generating of 2D supershapes in different coordinate systems." *Annals of Faculty of Engineering Hunedoara - International Journal of Engineering, Hunedoara, Romania*, Tome VIII, Fascicule 3 (2010): 201-203.

[27] Niţulescu, Theodor and Ştefan Ţălu. *Aplicaţii ale geometriei descriptive şi graficii asistate de calculator în desenul industrial. (Applications of descriptive geometry and computer aided design in engineering graphics).* Cluj-Napoca, Risoprint Publishing house, 2001.

[28] Bîrleanu, Corina and Ştefan Ţălu. *Organe de maşini. Proiectare şi reprezentare grafică asistată de calculator. (Machine elements. Designing and computer assisted graphical representations).* Cluj-Napoca, Victor Melenti Publishing house, 2001.

[29] Nedelcu, Dorian. *Proiectare şi simulare numerică cu SolidWorks. (Digital Prototyping and Numerical Simulation with SolidWorks).* Timişoara, Eurostampa Publishing house, 2011.

[30] Ţălu, Ştefan and Mihai Ţălu. *AutoCAD 2006. Proiectare tridimensională. (AutoCAD 2006. Three-dimensional designing).* Cluj-Napoca, MEGA Publishing house, 2007.

[31] Ţălu, Ştefan. *AutoCAD 2017.* Cluj-Napoca, Napoca Star Publishing house, 2017.

[32] Ţălu, Ştefan. *Grafică tehnică asistată de calculator. (Computer assisted technical graphics).* Cluj-Napoca, Victor Melenti Publishing house, 2001.

[33] Ţălu, Ştefan. *Reprezentări grafice asistate de calculator. (Computer assisted graphical representations).* Cluj-Napoca, Osama Publishing house, 2001.

[34] Ţălu, Ştefan. *Limbajul de programare AutoLISP. Teorie şi aplicaţii. (AutoLISP programming language. Theory and applications).* Cluj-Napoca, Risoprint Publishing house, 2001.

[35] Ţălu, Ştefan. *Geometrie descriptivă. (Descriptive geometry)*, Cluj-Napoca, Risoprint Publishing house, 2010.

[36] Ţălu, Ştefan and Cristina Racocea. *Reprezentări axonometrice cu aplicaţii în tehnică. (Axonometric representations with applications in technique).* Cluj-Napoca, MEGA Publishing house, 2007.

[37] Racocea, Cristina and Ştefan Ţălu. *Reprezentarea formelor geometrice tehnice în axonometrie. (The axonometric representation of technical geometric shapes).* Cluj-Napoca, Napoca Star Publishing house, 2011.

[38] Florescu-Gligore, Adrian, Ştefan Ţălu and Dan Noveanu. *Reprezentarea şi vizualizarea formelor geometrice în desenul industrial. (Representation and visualization of geometric shapes in industrial drawing).* Cluj-Napoca, U. T. Pres Publishing house, 2006.

[39] Florescu-Gligore, Adrian, Magdalena Orban and Ştefan Ţălu. *Cotarea în proiectarea constructivă şi tehnologică. (Dimensioning in technological and constructive engineering graphics).* Cluj-Napoca, Lithography of The Technical University of Cluj-Napoca, 1998.

[40] Ţălu, Ştefan. *Micro and nanoscale characterization of three dimensional surfaces. Basics and applications.* Napoca Star Publishing House, Cluj-Napoca, Romania, 2015.

[41] Ţălu, Mihai. *Calculul pierderilor de presiune distribuite în conducte hidraulice. (Calculation of distributed pressure loss in hydraulic pipelines).* Craiova, Universitaria Publishing house, 2016.

[42] Ţălu, Mihai. *Mecanica fluidelor. Curgeri laminare monodimensionale. (Fluid mechanics. The monodimensional laminar flow).* Craiova, Universitaria Publishing house, 2016.

[43] Ţălu, Mihai. *Pierderi de presiune hidraulică în conducte tehnice cu secţiune inelară. Calcul numeric şi analiză C.F.D. (Hydraulic pressure loss in technical piping with annular section. Numerical calculation and C.F.D.)*, Craiova, Universitaria Publishing house, 2016.

[44] Ţălu, Ştefan. *Tehnologia de rulare a filetelor. (Thread rolling technology).* Cluj-Napoca, Napoca Star Publishing house, 2019.

[45] *** Autodesk AutoCAD 2020 software.

[46] *** SolidWorks 2020 software.

Continuous Lubrication Systems for Machine Tools

Prof. PhD Eng. **Anca BUCUREŞTEANU**[1], Prof. PhD Eng. **Dan PRODAN**[1],
Assoc. Prof. PhD Eng. **Adrian MOTOMANCEA**[1], Assistant **Alina OVANISOF**[1]

[1] University POLITEHNICA of Bucharest, ancabucuresteanu@gmail.com, prodand2004@yahoo.com, adrian.motomancea@deltainfo.ro, alinaovanisof@yahoo.com

Abstract: *This paper describes some of the results obtained by the authors in the design, simulation and testing of the lubrication units for machine tools. The paper is based on the data collected during the manufacture of a boring and milling machine tool with numerical control (AF 105 CNC). The study includes theoretical considerations, calculations and simulation of unit operation but also explanations on the actual manufacture of the unit. Several machines were built on the basis of this project. The proper selection of the components, the making of calculations and simulation helped to the manufacture of an efficient unit with low noise and reduced heat.*

Keywords: Lubrication unit, machine tools

1. Lubrication unit

The unit is meant to lubricate the following mechanisms from the machine housing: two-speed gearbox, nut of the ball screw of the W axis feed kinematic chain [1, 2, 3], guideways of W axis and the boring spindle. Figure 1 shows the kinematic diagram of the AF105 machine housing and the points where the lubrication is required, noted OIL1.1, OIL1.2, OIL3.1, OIL3.2, OIL4.
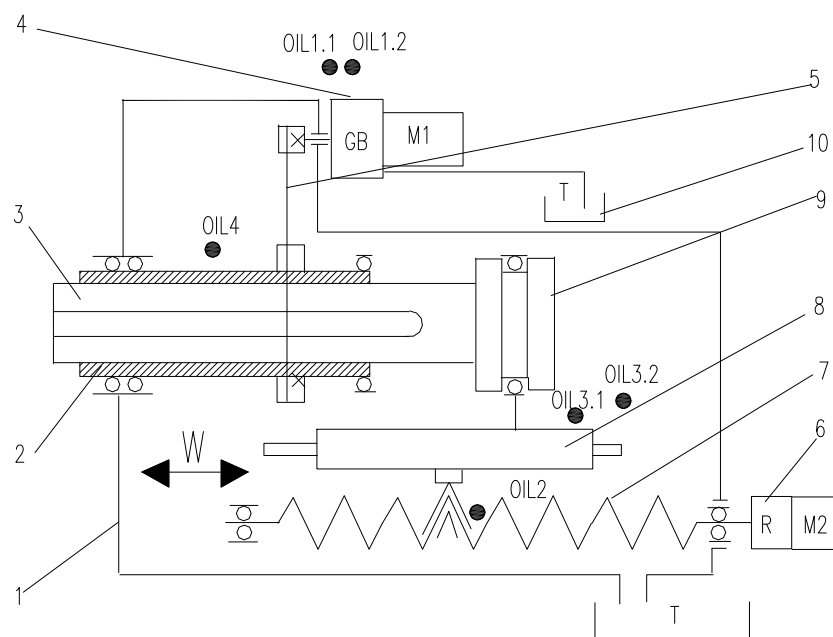
Fig. 1. Kinematic diagram of AF 105 machine housing

The main spindle 2 is supported on bearings related to housing 1 where the boring spindle 3 moves. The main spindle is the last element of the main kinematic chain [1] which also includes the main motor M1 and the GB two-speed gearbox [1, 4]. This one rotates the main spindle by means of the toothed belt 5 [2, 3, 4]. The feed kinematic chain 6 for W axis includes the M2 servomotor, the R reducer and the ball screw 7. This screw actuates the saddle 8 which, thanks to a specific supporting on bearings, moves the boring spindle 3. The oil which will ensure the lubrication is supplied from the tank 10.

The hydraulic diagram of the lubrication unit is shown in Figure 2.
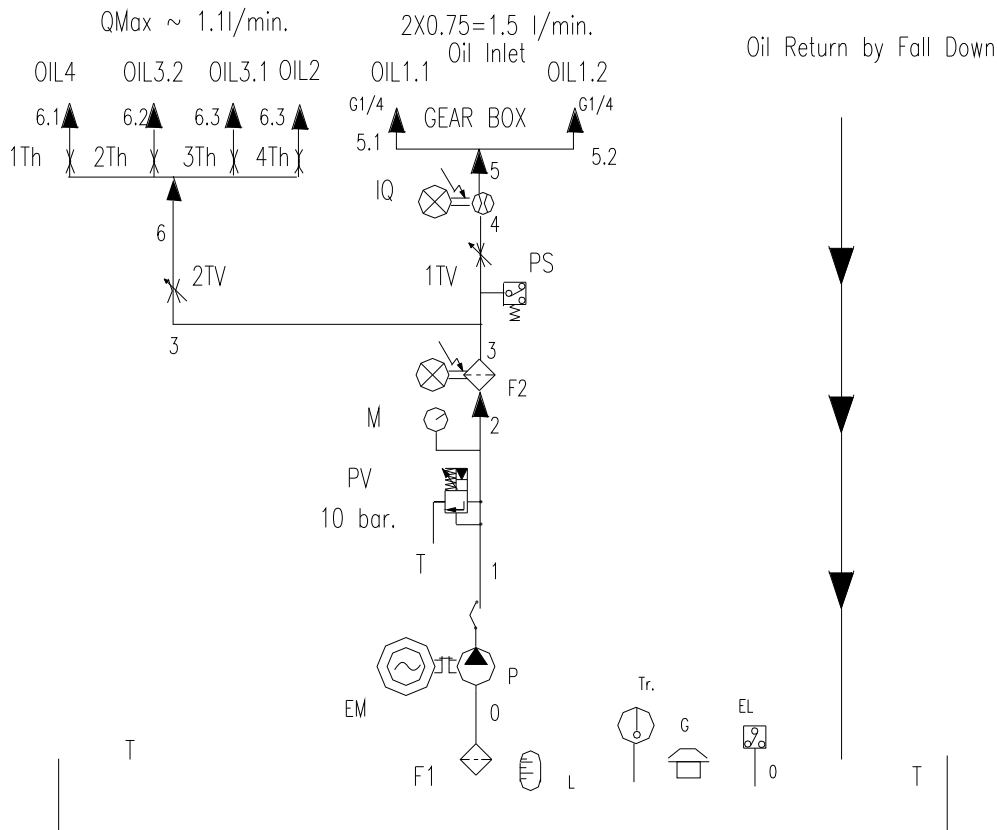
Fig. 2. Hydraulic diagram of the lubrication unit of AF 105 machine housing

The EM electromotor actuates the P gear pump [5, 6, 7]. The maximum operating pressure is regulated by the PV pressure relief valve and is visualized with the help of the M pressure gauge. The purity of the lubrication oil is ensured by the F1 suction filter and the F2 pressure filter. This latter is provided with an electric clogging indicator [6, 7]. The existence of a minimum operating pressure in the CNC machines must be confirmed to allow the corresponding phase of the working program to be carried out. The PS pressure switch was provided to confirm this pressure. The manufacturer of gearboxes recommend that these ones are lubricated at a certain flow rate [5, 4]. The regulation of the flow is made by means of the 1TV throttle valve. The flow rate (1.5 l/min) is confirmed by the IQ flowmeter. The necessary flow summed for the other lubrication points is regulated with the help of the 2TV throttle valve and does not exceed the value of 1 l/min. The following elements are located on the T tank: filling cap G, temperature probe Tr, sight glass L and the minimum level electric indicator EL.

2. Calculation and simulation of the lubrication unit

For the lubrication of the necessary points mentioned above, a constant flow pump will be used. This pump will be driven by a three-phase asynchronous motor which has the sync speed of n = 470 RPM. If the necessary flow is Q_E, the pump capacity will meet the condition:

$$q > \frac{Q_E}{n} \times 1000 \ [cm^3] \tag{1}$$

In the relation above, the Q_E flow is introduced in [l/min]. From the specialty catalogues, the $q_P > q$ is chosen. In this case, the actual available flow is:

$$Q_R = q_P \times \frac{n}{1000} \text{ [l/min]} \tag{2}$$

The maximum operating pressure will not exceed the p_{Max} value imposed. In this case, it is recommended to have p_{Max} = 20 bar.
The required power of the electric motor is determined by means of the relation:

$$P_{EM} = \frac{Q_P}{450} p_{Max} \text{ [KW]} \tag{3}$$

The electric motor is chosen from the specialized catalogues. The flange foot motors are recommended [4]. Taking into consideration the operating flow rate, the nominal size DN4 or DN6 is recommended for the devices used.
The tank will have the minimum useful volume V_0, that must verify the condition [5, 6]:

$$V_0 > 5 \, Q_R \text{ [l]} \tag{4}$$

In order to verify and to eventually correct the diagram, a simulation in AUTOMATION STUDIO [8] was conducted.
The characteristics in Figure 3 show the desired flow values following up the simulation.
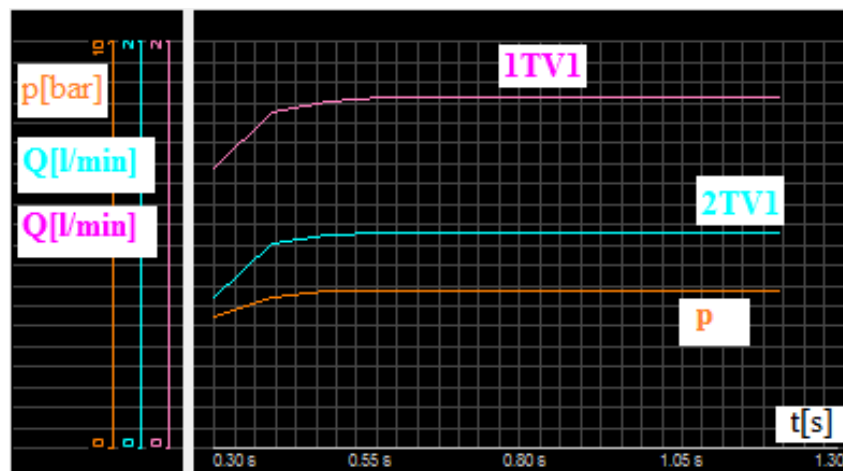
Fig. 3. Results of the simulation

We observe from the characteristics of Figure 3 that after less than 1s the pressure reaches the value of 4 bar for the regulated flow rates. Thus, downstream the 1TV1 throttle valve (at the gear box) a flow rate equal to 1.67 l/min is obtained. Downstream the 2TV1 throttle valve, a flow valve of 1.1 l/min is obtained.
Studying the results of the simulation and observing that less than 10% of the throttle valves regulation capacity was used, we considered that the designed diagram met the requirements and the manufacture was started.

3. Presentation of the unit

Due to constructive reasons, the manufactured tank has a useful volume V_0 = 30 l. The electric motor, the pump and a part of the components were assembled on the tank. Their location – keeping the same notations as in Figure 2 – is shown in Figure 4.
The lubrication points are presented in Figure 5 together with some of the elements of the kinematic diagram in Figure 1.
After making the unit, this one was adjusted. During the operation, the real pressure is 5-6 bar, the flow rate downstream the 1TV1 throttle valve, measured at gearbox output, is 1.6 l/min. The flow rate, regulated at the 2TV1 throttle valve output, cannot be measured because the discharge is freely made and the oil is recovered by falling.

a.   b.
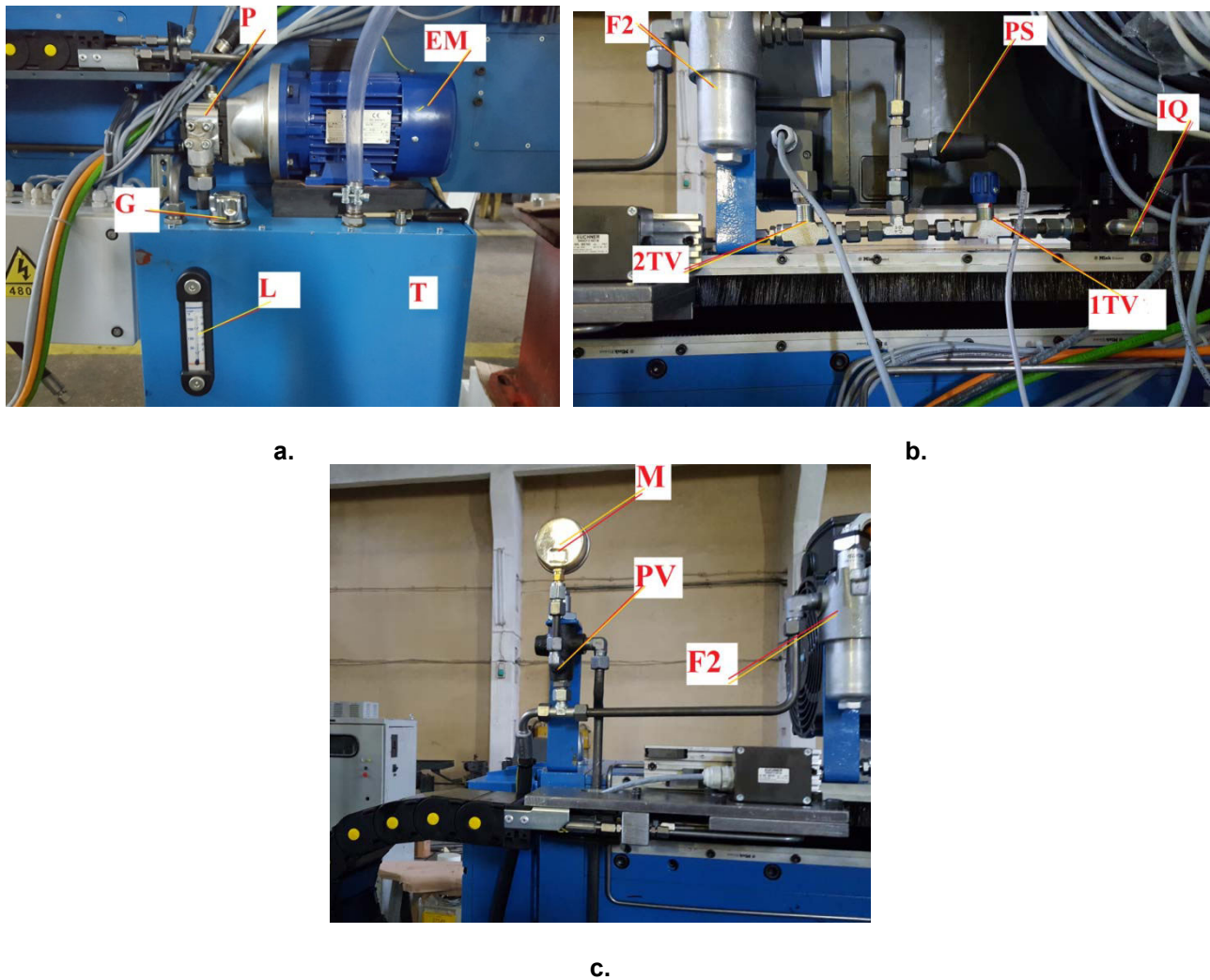
c.
Fig. 4. Presentation of the unit
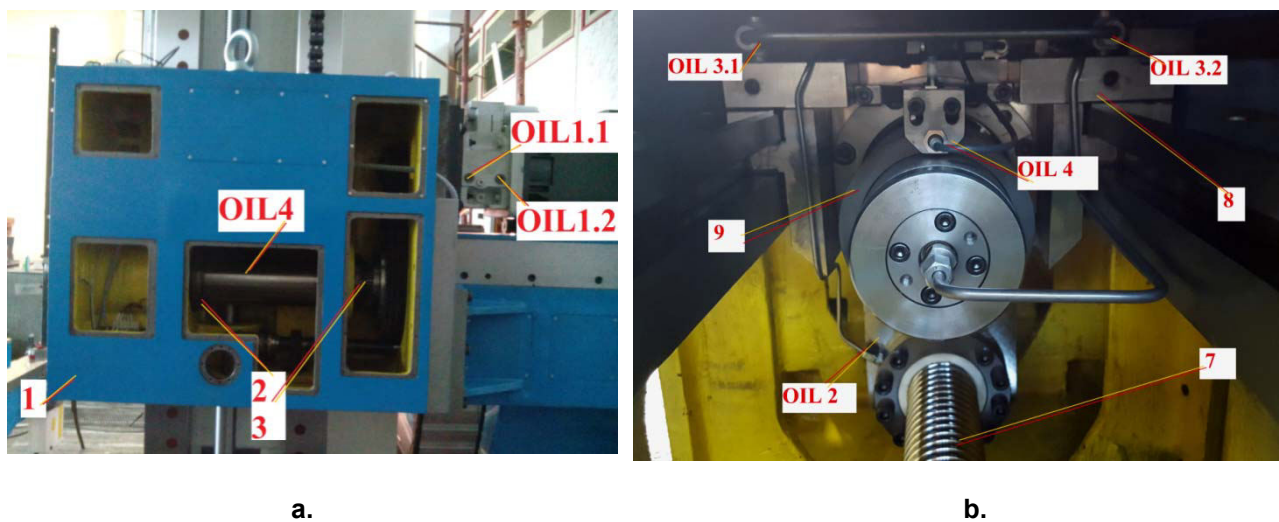
a.   b.
Fig. 5. Presentation of the lubrication points

4. Conclusions

The lubrication units belong to the category of subsidiary systems of the machine tools.

These ones include a pump (usually a constant flow one) and the equipment for measurement and control. Generally, the operating pressure does not exceed 20 - 25 bar. The adjustment of the flow rates, in the case of the permanent flow lubrication, is made using fixed or adjustable throttle valves.

In the case of the numerical control machines, the minimum pressure is confirmed by pressure switches.

If standard gearboxes are used, it is important to comply with the recommendations of the manufacturers regarding the value of the necessary flow. The existence of the recommended flow is confirmed by means of flowmeters. These ones and the pressure switches as well shall be calibrated periodically.

By using simulation programs in the design phase of the lubrication units, one can study the behavior of the elements in the diagram and also its operation. It is also possible to determine the capacities for regulation of the flow and pressure.

The results of the simulations are indicative ones; therefore, they must be compared with the results obtained experimentally.

References

[1] Prodan, Dan. *Heavy machine tools. Mechanical and Hydraulic Systems/Maşini-unelte grele. Sisteme mecanice si hidraulice*. Bucharest, Printech Publishing House, 2010.
[2] Joshi, P.H. *Machine tools handbook*. New Delhi, McGraw-Hill Publishing House, 2007.
[3] Perovic, Bozina. *Machine tools handbook/Handbuch Werkzeug-Maschinen*. Munchen, Carl Hanser Verlag, 2006.
[4] *** Catalogues and leaflets BOSCH REXROTH, BARUFFALDI, ZF, REDEX, PIRELLI.
[5] Bucureşteanu, Anca. *Adjacent Installation for Machine-Tools and Manufacturing Systems/Instalaţii conexe pentru maşini-unelte şi sisteme de producţie*. Bucharest, Printech Publishing House, 2009.
[6] Prodan, Dan, Mircea Duca, Anca Bucureşteanu and Tiberiu Dobrescu. *Hydrostatic drives-machine parts/Acţionări hidrostatice – Organologie*. Bucharest, AGIR Publishing House, 2005.
[7] Bucureşteanu, Anca. *Hydraulic and Pneumatic Driving/Acţionări hidraulice şi pneumatice*. Bucharest, Printech Publishing House, 2003.
[8] *** Software package AUTOMATION STUDIO.

Establishing the Mathematical Relation between the Rotor Radius and the Height of the Rotating Piston for a Rotating Machine with Profiled Rotors

PhD Student **Mariana Mirela STOICAN (PRISECARU)**[1]**,** Prof. Dr. Eng. **Nicolae BĂRAN**[1]**,**
PhD Student **Almaslamani Ammar Fadhil SHNAWA**[1]

[1] University Politehnica of Bucharest, mirela.prisecaru@yahoo.com

Abstract: Mathematically, the paper establishes a link between the constructive elements, the rotor radius and the height of the rotating piston, which is part of the construction of a machine with profiled rotors that transports fluids.
For a certain constructive solution, the maximum height of the rotating piston is set; the influence of the height of the piston on the flow rate and the driving power of the machine are highlighted.
A constructive solution which allows the maximum power of the machine is presented.

Keywords: Rotating machine, profiled rotor, rotating piston

1. Introduction

This paper is part of the category of scientific paper that addresses the research field of rotating machines that transports fluids.
A type of rotating working machine with profiled rotors is presented; it can work as [1], [2]:
- a fan, for driving different gas mixtures with or without suspensions;
- a low pressure compressor;
- a rotating volumetric pump for the conveyance of any type of liquid or gas fluid, namely:
  - general fluids: water, air, steam, etc.
  - multiphase fluids: water + air, water + sand, water + ash etc.
  - viscous fluids: oil, diesel, petroleum, etc.

The advantage of the rotating working machine is that the entire torque received from the drive motor is used to transport the fluid.
There are no reciprocating parts; there are no large friction between the movable and the fixed part of the rotating machine [3].
Generally, the machines are divided into two categories [1]:
    I. Power machines that produce energy; they transform a certain form of energy into mechanical energy.
    II. Working machines, which consume mechanical energy and produce another form of energy.
Fans, compressors, pumps are part of the category of machines that consume mechanical energy to create the potential increase of potential pressure energy of fluids (liquids or gases, vapors).
This paper offers new researches directions in the field of fluid transport by rotating machines.

2. The operating principle and the constructive solution of the rotating machine

The fluid sucked into the suction connection (1) (figure 1) is transported by a rotational movement by the pistons (4) to the discharge connection (7); the fluid may be polyphase (air + water, water + sand, water + steam, water + ash, etc.) or may be viscous, or with high density.
The machine has two profiled rotors that rotate counterclockwise inside some housing (figure 1).
The synchronous rotation of the two rotors (3, 8) is ensured by means of two gear wheels which form a cylindrical gear with straight teeth, gear located outside the machine.
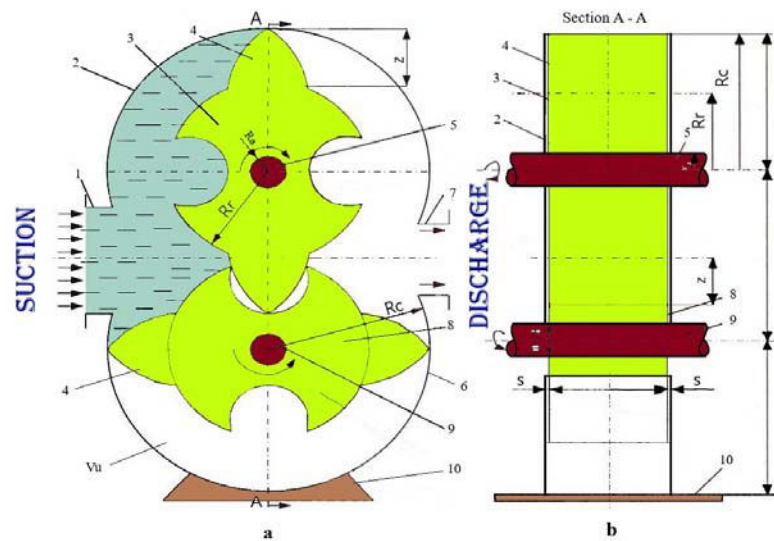
Fig. 1. Cross section (a) and longitudinal section (b) through the rotating machine
1 - suction connection; 2 - upper housing; 3 - upper rotor; 4 - rotating piston; 5 - driven shaft; 6 - lower housing; 7 - fluid discharge connection; 8 - lower rotor; 9 - driving shaft; 10 – support

In figure 1 was noted:
R_c - housing radius; R_r - rotor radius; R_a - shaft radius; z - rotating piston height;
V_u - the useful volume between two successive pistons and the inner wall of the housing.

3. Deduction of the calculation formula for the flow rate transported by the machine and for the driving power of the machine

At a complete rotation of the shafts (5.9), two such volumes (V_u) will be transported from the suction to the discharge.

$$\overset{\Box}{V}_u = 2\left(\frac{\pi R_c^2}{2} - \frac{\pi Rr^2}{2}\right) \cdot l \quad \left[m^3/rot\right] \tag{1}$$

The housing radius (R_c) is the sum of the rotor radius (R_r) and the height of the piston (z) (figure 1).

$$R_c = R_r + z \quad [m] \tag{2}$$

From relation (1) and (2) results:

$$\overset{\Box}{V}_u = \pi \cdot l \cdot z(z + 2\,R_r) \quad \left[m^3/rot\right] \tag{3}$$

The volumetric fluid flow rate flowed by a single rotor of length l [m] and speed n_r [rot / min] will be:

$$\overset{\Box}{V}_u = \pi \cdot l \cdot z\left(z + 2R_r\right) \cdot \frac{n_r}{60} \quad \left[m^3/s\right] \tag{4}$$

The rotating machine has two identical rotors, so the fluid flow rate will be:

$$\overset{\Box}{V}_m = 2\overset{\Box}{V}_m = \pi l z\left(z + 2R_r\right) \cdot \frac{n_r}{30} \quad \left[m^3/s\right] \tag{5}$$

From relation (5) one can observe that the fluid flow rate conveyed by the machine varies according to the following parameters:
    • Geometrical hydraulic parameters: l - rotor length [m]; R_r - rotor radius [m]; z - rotating piston height [m].
    • Functional parameters: n_r - speed of the rotating machine [rot / min].

4. Establishing the mathematical relation between the rotor radius and the height of the rotating piston

It is considered one piston (4) fixed to the lower rotor (figure 2).
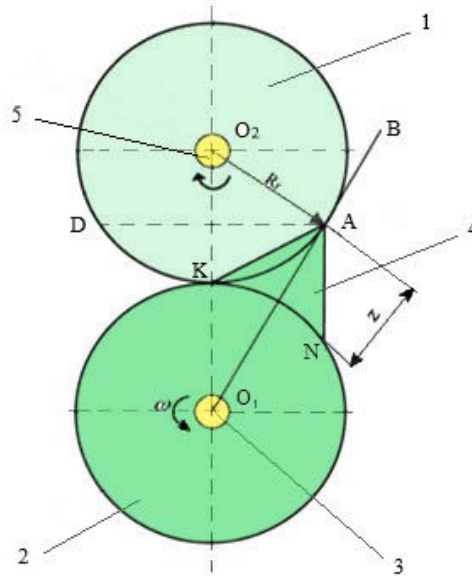
Fig. 2. Calculation notations
1 - upper rotor; 2 - lower rotor; 3 - driving shaft; 5 - driven shaft;
4 - rotating piston of triangular shape

The rotor radius (1) is extended by a length (z) and thus the line O1B reaches the rotor (2) at point A. Theoretically, when point K reaches point D, point A reaches K, respectively point N reaches K, because the length of the circle arcs AK, KD and KN is the same. When the piston (5) exits the gap created in the rotor (2), points A and N reach point K; the sealing between the two rotors being ensured by the direct contact between the lateral surfaces of the rotors.
From the right triangle O1O2A results:

$$O_1O_2^2 = AO_2^2 + AO_1^2 \tag{6}$$

$$(2R_r)^2 = R_r^2 + (R_r + z)^2 \tag{7}$$

relation that becomes:

$$z^2 + 2R_r z - 2R_r^2 = 0 \tag{8}$$

$$z_{1,2} = \frac{-2R_r \pm \sqrt{4R_r^2 + 8R_r^2}}{2} \tag{9}$$

Performing the calculations, from relation (9) results
$$\begin{cases} z_1 = 0.732R_r \\ z_2 = -2.73R_r \end{cases}$$

The relation (8) specifies the correlation between the height of the piston (z) and the rotor radius (R_r); thus, the housing radius will be:

$$R_c = R_r + z = R_r + 0.732R_r = 1.732R_r \ [m] \tag{10}$$

or:

$$R_c = \frac{z}{0.732} + z = 2.366z \quad [m] \tag{11}$$

The relations (8), (10) and (11) give the mathematical connection between R_r, z and R_c.

From the mathematical analysis [6] it is known that between two roots of the function there is a maximum or minimum point of the function; for this purpose, the relation (3) is derived according to z and one can obtain:

$$2z + 2R_r = 0 \tag{12}$$

$$z = -R_r \tag{13}$$

The function f (z) (figure 3) is graphically represented, choosing for R_r the value of 0.05 m which was adopted when constructing a prototype in the laboratories of the Department of Thermotechnics, Engines, Thermal and Refrigeration Equipment's of University Politehnica of Bucharest.

From relation (3) the data from table 1 are obtained.

Table 1: Values for z and f (z)

$z \cdot 10^{-2}$ [m]	-15	-10	-5	0	5
$f(z) \cdot 10^{-3}$ [m]	25	-50	-75	-50	25

Respectively, one can obtain:

$$z_1 = 0.732 R_r = 0.732 \cdot 0.05 = 0.0366 \; [m]$$

$$z_2 = -2.73 R_r = -2.73 \cdot 0.05 = -0.1366 \; [m]$$

The intersection of the function with the oz axis is given by the points: A (0.366; 0), B (- 0.1366; 0).
The end point of the function is C (- 0.0075; - 0.05)
With the data in table 1 and having the coordinates of the intersection points of the function with the oz axis, the function f (z) is plotted in figure 3.
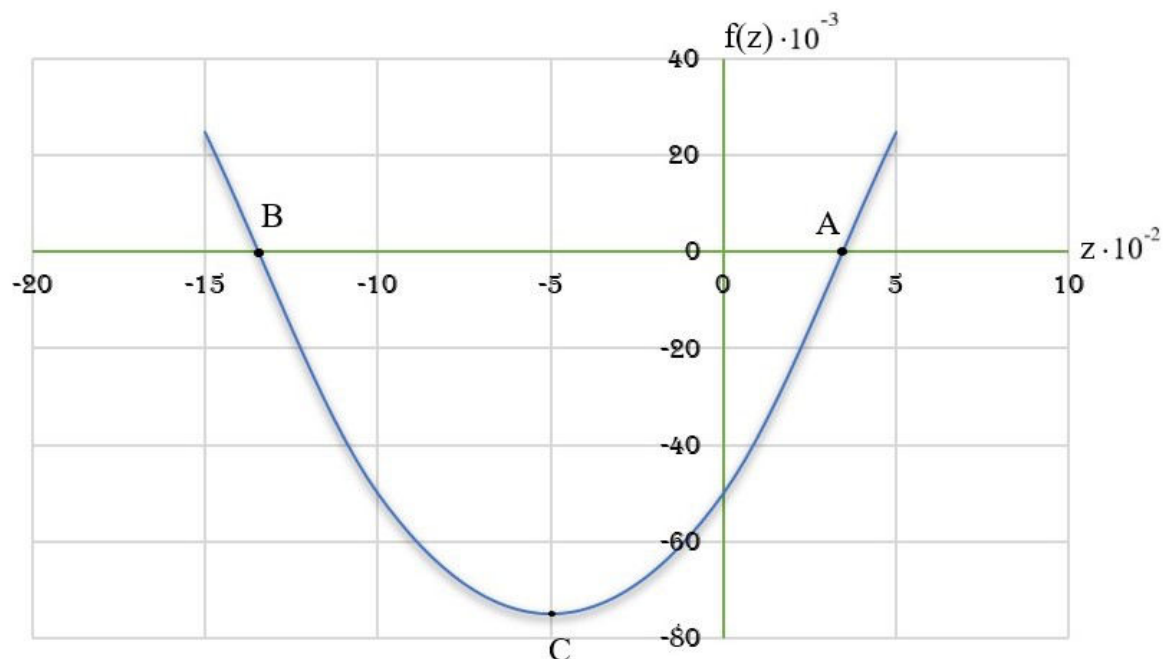
Fig. 3. Graphical representation of the function f (z)

From figure 3 one can observe that the function f (z) has the extreme point for z = - R_r = - 5 cm; the same thing is also given by the relation (8): $P' = f(z)$ from which the same value results: z = - R_r.

In conclusion, the driving power of the machine is maximum when z = R_r technically acceptable result [7].

5. The constructive solution of the machine when the height of the piston tends towards the rotor radius

The constructive solution presented in figure 4 has the following particularities:
    a) The piston height is smaller by 1-2 mm than the rotor radius;
    b) The shaft for each rotor does not penetrate inside the rotor, thus z → R_r;
    c) The shaft drives the lower rotor through a flange fixed with rotor screws; the flange rotates inside the side wall of the housing (figure 4.b);
    d) In the figure 4 the side wall of the housing on the right side is not drawn, which is similar to the wall on the left side; in this way, in view (a) the two rotors are observed.
The elaboration of this constructive solution aims to validate the previously established conclusion, namely that the value of z must tend to R_r.
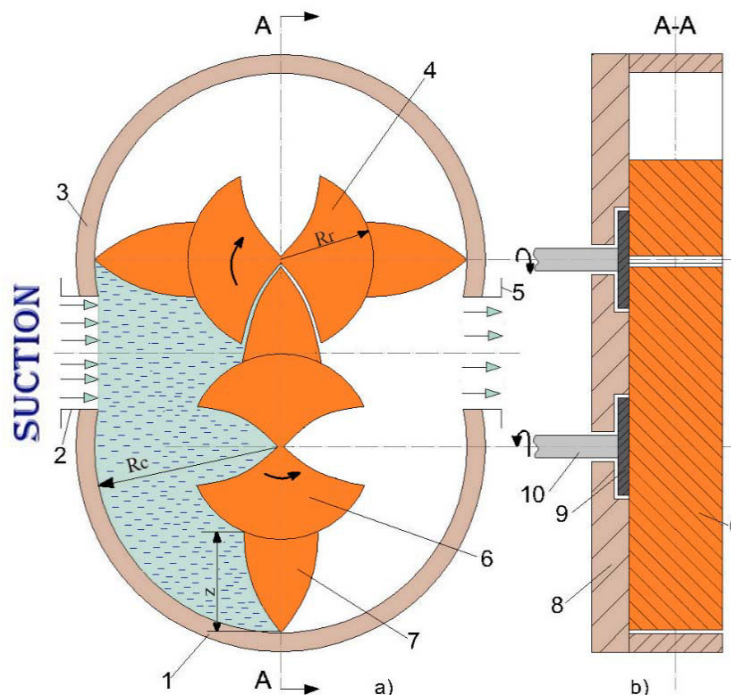
Fig. 4. View (a) and longitudinal section (b) through the rotating machine
a: 1 - lower housing; 2 - fluid suction connection; 3 - upper housing; 4 - upper rotor;
5 - fluid discharge connection; 6 - lower rotor; 7 - rotating piston;
b: 8 - housing side wall (left); 9 - flanges fixed by the rotor; 10 - shaft fixed by the flanges.

Previous researches in the field of rotating machines [8], [9], [10] continue with this new constructive solution where the value of z tends towards R_r.

6. Conclusions

a) Both by deriving the power formula of the machine and by graphically representing the function f (z) = 0 resulted:
    - If the rotating machine acts as a working machine (pump, compressor) the required drive power from the outside is maximum if z = R_r; of course, and the flow rate transported by the machines is maximum.

- If the rotating machine acts as a motor machine (steam engine, pneumatic motor), the power developed by it is maximum when $z \to R_r$.

b) In figure 4 a constructive solution of the machine was presented, a solution that allows z to tends towards R_r.

References

[1] Băran, N., P. Răducanu, et. al. *Bases of Technical Thermodynamics*. Bucharest, Politehnica Press Publishing House, 2010.

[2] Băran, N., D. Duminică, D. Besnea, and A. Detzotzis. "Theoretical and experimental researches regarding the performances of a new type of rotating machine with profiled rotors." *Advanced Materials Research* 488-489 (March 2012): 1757-1761.

[3] Hawas, M. *The influence of fluid viscosity on the performance of rotating machine with profiled rotors*. PhD Thesis. Politehnica University of Bucharest, 2015.

[4] Detzortzis, A., N. Băran, and M. Hawas. "The influence of the rotor architecture of a rotating working machine on the driving power." *U.P.B. Sci. Bull. Series D* 77, no. 1 (2015): 155-166.

[5] Exarhu, M. *Pneumatic and hydraulic machines and installations.* (in Romanian). S.C. Andor SRL, Bucharest, 2011.

[6] Goleţ, Ioan, Ciprian Hedrea, and Camelia Petrişor. *Mathematical analysis. Theoretical synthesis and applications / Analiză matematică. Sinteze teoretice şi aplicaţii*. Bucharest, Politehnica Press Publishing House, 2014.

[7] Motorga, A. *Influence of constructive and functional parameters on the performances of rotating machines with profiled rotors*. PhD Thesis. Faculty of Mechanical Engineering and Mechatronics, Politehnica University of Bucharest, 2011.

[8] Băran, N., I. Căluşaru, and A. Detzortzis. "Research Regarding the Testing of a New Type of Rotating Machine with Profiled Rotors." *Journal of Materials Science and Engineering A* 2, no. 3 (2012): 372-376.

[9] Hawas, M., N. Băran, and A. Detzortzis. "Influence of the rotor architecture and of the speed on the volumetric efficiency of a new type of rotating volumetric machine." *Advanced Materials Research* 905, (2014): 487-491.

[10] Hawas, M. "Research regarding the establishment of efficiency for a new type of rotating volumetric pump." *International Research Journal of Engineering and Technology (IRJET)* 2, no. 2 (2015): 796-800.

Applicability of Video-Based Water Velocity Measurements on Ice-Drifting River Sections

PhD student **Gábor KERÉK**[1]

[1] Deputy Head of Department, North Transdanubian Water Directorate, Győr, Hungary, kerek.gabor@eduvizig.hu

Abstract: *Video-based velocity analysis is a novel, experimental procedure onto the definition of the surface water velocity of water flows. The method may be effective to ground data collections, when any other measurement procedure inapplicable, i.e. flash-flood events, analysis of longer water flow sections, monitoring places which can be difficult to approach.*
In this paper I take an overview of the theoretical bases of the video-based velocity analysis (LSPIV), then, according to the application of two numerical methods I take an estimate onto the cross-sectional distribution of the water velocity and the discharge using the measured LSPIV velocities.
At last I make proposals concerning the practical adaptability of the method.

Keywords: *Large Scale Particle Image Velocimetry, Ice-drifting, Water discharge measurement*

1. Introduction

The LSPIV-method is an indirect way to analyse the surface velocity conditions of a river or a free-surface flow. Opposed to the common hydrometric practice, this process doesn't require using any mechanical or acoustic device that physically contacts the flowing water. The usability of conventional water velocity and flow measuring instruments are strongly influenced by measurement conditions. Due to safety issues these instruments have limited usability in case of flash floods or ice-covered water surfaces. As a result, in most cases the hydrological-hydraulic parameters of such hydrological events can only be determined by estimates or approximate calculations, with no measured parameters. The LSPIV procedure can be an approximate method onto these hardly measurable situations, because this method requires only a video, which records the flowing water surface.

2. Large Scale Particle Image Velocimetry (LSPIV) – Theoretical foundations

The method is based on a captured a video of a particular section of the watercourse. In order to analyse the flow a series of pictures have to be done from the video, which has a determined Δt gap in time between the particular pictures. By analysing this sequence of images, a processing software determines an instantaneous velocity field by tracking the trace of a tracer floating on the surface.[1] It is obligate that the video has to be taken from that kind of section of a watercourse where sufficient tracer (leaf, foam made by turbulence, tiny cane debris, other sediment, ice) floats on the surface, as their absence impairs the mapping of the velocity field. As the video is usually made from an external viewpoint, the images that captured from the video must be transformed into a 2D orthogonal coordinate system. This method is called orthorectification. The method base is to find well-defined points that can be seen on the images, and can be identify in real conditions as well. It is also crucial to know the geographic coordinates (or the physical distance components in a North-East coordinate system) of these reference points (called GRPs - Ground Reference Points). Using the field and image points, the coordinates between the two reference systems can be determined using the following conventional photogrammetric relationship: [2]

$$x = \frac{A_1 X + A_2 Y + A_3 Z + A_4}{C_1 X + C_2 Y + C_3 Z + 1} \tag{1}$$

$$y = \frac{B_1 X + B_2 Y + B_3 Z + B_4}{C_1 X + C_2 Y + C_3 Z + 1} \tag{2}$$

where

x, y – the coordinates of GRPs in the coordinate system of the image,

X, Y, Z – the coordinates of the GRPs in the real space

A1 … C3 – transformation coefficients using field reference points

There are many options to define the coordinates of ground reference points, e.g. GNSS-based measurements or to identify the points from a well-detailed aerial image (e.g. Google Earth).The LSPIV procedure determines the surface water velocity of a stream by analyzing the similarity of patterns on each image pairs, determining a so-called similarity index. The comparison made in a pixel-defined query area defined in the first image of the sequence of images (This is called interrogation area - [hereinafter IA]) in the same area of the next image of the sequence in relation to the search area ([hereinafter SA]) also defined in pixels. The maximum value of the similarity index represents the most likely movement of a tracer between two consecutive frames. With orthorectification the extent of displacement of a tracer is determined, and knowing the Δt sampling frequency between the two frames, the surface water velocity can be calculated. [1]

The method used in my analysis determines the similarity index by the following cross-correlation algorithm:

$$R_{ab} = \frac{\sum_{x=1}^{MX}\sum_{y=1}^{MY}\{(a_{xy}-\overline{a_{xy}})(b_{xy}-\overline{b_{xy}})\}}{\sqrt{\sum_{x=1}^{MX}\sum_{y=1}^{MY}\{a_{xy}-\overline{a_{xy}}\}^2 \sum_{x=1}^{MX}\sum_{y=1}^{MY}\{b_{xy}-\overline{b_{xy}}\}^2}}$$

(3)

Cross-correlation is determined between the areas of the first frame IA and the IAs within the SA of the subsequent frame.

In the equation:

MX, MY – IA size in pixels,

a_{xy}, b_{xy} – Change of 8-bit grayscale (0 to 255) in IA; the values marked with the upper sign are the average values for IA

The advantage of this method is to able to estimate the water speed conditions from a low-resolution video.[1]

As a result of this procedure, the instantaneous surface velocity field of the test area can be obtained. The LSPIV vector field hereinafter allows further analysis, e.g. it is suitable for determining the average surface velocity and also to estimate the direction and turbulence of the flow; or with the geodetic measurement of the riverbed (even after the particular event) onto the calculation of the water discharge.[1]

Videos (i.e., sequences of images with a defined sampling time) can be analyzed by using FUDAA-LSPIV, a free software specifically designed to support LSPIV-based velocity vector field definition. The program is freeware and its graphical user interface runs under Java Runtime Environment.

The program analyzes 8-bit grayscale images (pgm extension) as input format, and performs orthorectification and velocity field computation on a defined sequence of images with the mentioned cross-correlation analysis. A pgm image (actually an ASCII text file) can be created from a video file of any length and resolution using free converter programs. A sample cube of the input image sequence is shown in Figure 1.
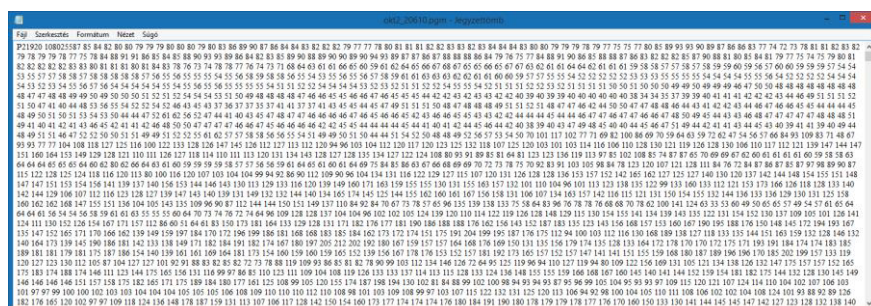
Fig. 1. FUDAA-LSPIV input file format

To perform 2D orthorectification, at least 6 interface points per image sequence have to be selected. The orthorectification can be done in one step in case of static reference points for the whole sequence, or even frame by frame in case of moving camera.

2.1 Define the instantaneous velocity field and filter the results

To calculate the instantaneous velocity field on an image sequence the parameters needs to be defined in FUDAA-LSPIV are as follows: [3], [4]

- discretization of computational grid

- defining correlation parameters

- defining Δt time step

The correct setting of these parameters basically determines the correctness of the final result of the analysis thus their determination requires attention.

The basis of determination of the instantaneous surface velocity field is that the motion of the tracer in the 2D image sequence can be followed by the best possible correlation. The most important step in this procedure is to determine the size of the IA and SA query fields in pixels in the FUDAA-LSPIV program. Defining these parameters requires considerable caution and care. If the IA value is too small, the physical size of the surface tracer, and its change between two frames will impair the identification of the displacement, a too high IA value will dramatically increase the software's runtime, but its result will not be necessarily more reliable.

Before the analysis the detection area (the flowing water surface) also have to discretized, which means a fixed grid in pixels in the orthogonal image sequence. An example of grid points is shown in Figure 2.
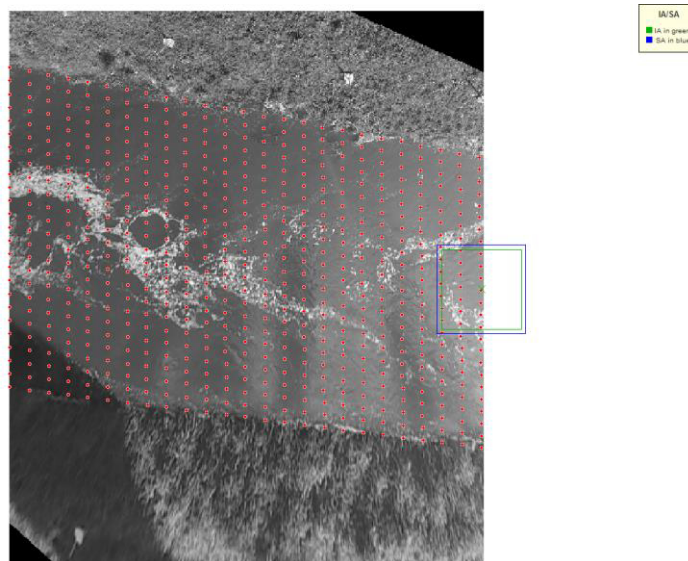
Fig. 2. Computational grid, FUDAA-LSPIV

Finding the optimal value for IA and SA parameters is an experimental procedure in almost every case. It's expedient to perform some sensitivity testing onto the determination of these values. Several tests have shown that 1 second sample rate for some rapidly changing tracers is not sufficient to detect their track continuously, since the turbulence of the flow between two consecutive images rearranges the surface tracer to such an extent that the process cannot reproduce the locally experienced velocity conditions.

The result of the sequence analysis is a surface velocity field defined for the grid points. With the knowledge of the velocity field, additional numerical methods can be used to make an approximate calculation of the water discharge, which is the most important measure of hydrological practice.

3. Velocity profile estimation, determining water discharge

The calculated LSPIV velocity field will be useful in practice if we can determine the flow of the river with sufficient accuracy. To do this, it is essential to know the geometry of the wetted cross section, the water level at the time of video recording, and the distribution of the velocity profile along the Z (depth) axis. Such tasks can usually occur during the subsequent reproduction of the hydraulic characteristics of extreme flow events. Subsequent determination of riverbed geometry and water levels (e.g. from water traces) is a routine activity at the state of the art. In the following part I'm going to introduce two numerical methods for determining the assumed shape of a velocity profile in a preferred transverse section of the LSPIV surface velocity field.

3.1 Estimation of velocity profile using turbulent boundary layer theory

A generally used method of vertical velocity profile estimation is to determine a logarithmic velocity distribution based on the turbulent boundary layer theory.
Along a flat boundary (e.g. wall, riverbed) the flow state is considered to be fully fledged when the velocity doesn't change in time or along the boundary (x axis of the flow), only in the direction perpendicular to the boundary (z-axis). For this case, the simplified Reynolds equation has the following form (omitting the zero derivatives) [5]

$$0 = -\frac{1}{\rho} * \frac{\partial P}{\partial x} + \frac{\partial}{\partial z}\left(v \frac{\partial U}{\partial z} - \overline{u' * w'}\right) = \frac{1}{\rho} * \frac{\partial P}{\partial x} + \frac{1}{\rho} * \frac{\partial \tau_v}{\partial z} + \frac{1}{\rho} * \frac{\partial \tau_t}{\partial z} \tag{4}$$

where we separate the shear stresses due to viscosity and turbulence, and from which

$$0 = -\frac{\partial P}{\partial x} + \frac{\partial \tau_e}{\partial z} \tag{5}$$

we get a simple bivariate differential equation.
Since the pressure gradient in the equation is only a function of x and the resultant shear stress is only the function of z, both of them have to be constant for an existing solution. Consequently, they are linear functions on x or z axes. Along the above-mentioned simplifications, now let's evaluate the case of a frequently used, so-called hydraulically rough boundary. The shear stress resulting from the viscosity is generally negligible relative to the turbulence, particularly in the case of rough boundary.
After the simplification we can consider the only part that does not even require indexing

$$\tau = -\rho * \overline{u' * w'} \tag{6}$$

the turbulent shear stress. Introducing l (concept of mixing length [Prandtl, 1925], which means that distance at which a characteristic change in velocity u' can occur, [5]

$$u = U(z) + u' = U(z + l) \tag{7}$$

whereof,

$$u' = U(z + l) - U(z) \tag{8}$$

The latter equation is solved along the z-axis in Taylor-series and keeping the first two terms

$$U(z + l) = U(z) + \frac{\partial U}{\partial z} * l \tag{9}$$

that is,

$$u' = U(z) + \frac{\partial U}{\partial z} * l - U(z) = \frac{\partial U}{\partial z} l \tag{10}$$

Substituting this into the shear stress formula and applying time averaging rules:

$$\tau = -\rho * \overline{\frac{\partial U}{\partial z} * l * w'} = -\rho * \overline{l * w'} * \frac{\partial U}{\partial z} \tag{11}$$

$$sign(\tau) = sign\left(\frac{\partial U}{\partial z}\right), sign\,(w') = -sign\,(l), \tag{12}$$

assuming isotropy, o(u')=o(w') that is $u' = \frac{\partial U}{\partial z} * l\ and\ u' = -w'$ relations

$$w' = -\frac{\partial U}{\partial z} * l \tag{13}$$

Substituting this into the latest formula for shear stress and dividing it by density

$$\frac{\tau}{\rho} = -\overline{u' * w'} = l^2 * \left|\frac{\partial U}{\partial z}\right| * \frac{\partial U}{\partial z} \tag{14}$$

results this equation, which defines the shear stress as the multiplication of the mixing length and the square of time-averaged velocity gradient.
Let's introduce the concept of sliding speed, as follows:

$$u_* = \sqrt{\left|\frac{\tau}{\rho}\right|} = \sqrt{\left|\overline{u' * w'}\right|} = l * \left|\frac{\partial U}{\partial z}\right| \tag{15}$$

whereof

$$\tau = \rho * u_*^2\ \text{és}\ \left|\frac{\partial U}{\partial z}\right| = \frac{u_*}{l} \tag{16}$$

We also introduce the approach that mixing length, as a kind of free path length, increases linearly with the distance from the boundary, so that

$$l = \kappa * z \tag{17}$$

where κ is the so-called Kármán-constant, it's value with good accuracy is 0.4. As we use it for velocity gradient:

$$\frac{\partial U}{\partial z} = \frac{u_*}{\kappa * z} \tag{18}$$

we get a first order differential equation which is rearrangeable (by separating the variables)

$$\partial U = \frac{u_*}{\kappa} * \frac{\partial z}{z} \tag{19}$$

we get an equation which solution is

$$U(z) = \frac{u_*}{\kappa} * (ln z + C) \tag{20}$$

We can introduce z0, called roughness-height, that is, the distance from the rough boundary where the U velocity is still considered to be zero, and using it as a boundary condition

$$0 = \frac{u_*}{\kappa} * (ln z_0 + C) \tag{21}$$

the analytical solution of the velocity profile of the turbulent boundary layer is as follows.

$$U(z) = \frac{u_*}{\kappa} * ln \frac{z}{z_0} \tag{22}$$

By using this formula, the velocity profile of a section in the LSPIV velocity field can be determined. The u* bottom sliding speed can be estimated with the following formula [5]

$$u^* = \sqrt{g * R * I} \tag{23}$$

where

  g – gravitational acceleration (9,81 m/s²)
  R – hydraulic radius
  I – riverbed slope

Using boundary layer theory and LSPIV surface velocity field the vertical velocity profile of a chosen cross section can be derived using the analytical solution of the velocity profile of the turbulent boundary layer. The sliding velocity (u*) is derivable by estimating the roughness height (z0) in the knowledge of riverbed geometry with the following formula [5]

$$\frac{v_{LSPIV} \cdot \kappa}{\ln\frac{H}{z_0}} = u_*$$

(24)

Based on this, the depth-averaged velocities of each vertical profile can be calculated with the following formula: [5]

$$U_{átl} = \frac{u_*}{\kappa} * \left[-\ln\left(\frac{z_0}{H}\right) - 1 \right]$$

(25)

3.2 Derivation of the velocity profile from LSPIV velocity

This procedure is used for the calibration of built-in Doppler acoustic water velocity probes (H-ADCP). [6],[7]
With some modification the method can be adaptable to estimate the vertical velocity profile based on LSPIV velocity data.
Based on this numerical method, the velocity of each vertical profile in a certain cross section can be estimated as follows:

$$v_{i,j} = \alpha_i * [\gamma * (h_{max} - h_{i,j})]^\beta$$

(26)

where

β - coefficient for bed roughness and flow profile shape (1/6 … 1/12)

$$\alpha_i = \frac{v_i^{LSPIV}}{(h_i^{max})^\beta}$$

(27)

$$\gamma = \frac{v_{max}^{becs}}{v_i^{LSPIV}}$$

(28)

(γ= 1.1 … 1.3)

The meaning of these factors is shown graphically in Figure 3.
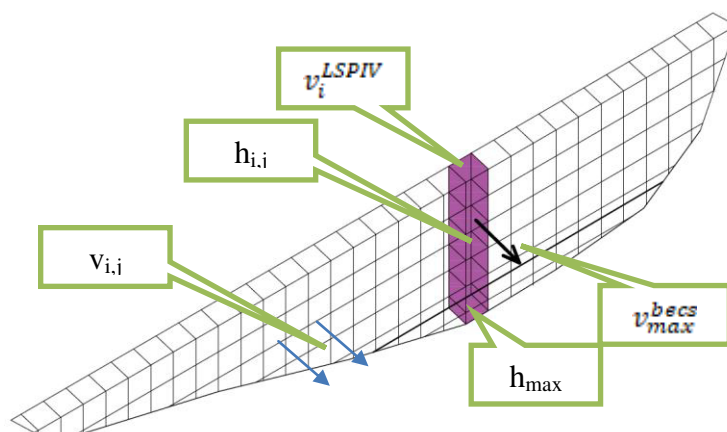
Fig. 3. Estimation of velocity distribution in a vertical profile

Applying this numerical method to a particular cross section of the LSPIV velocity field, water discharge can be calculated within the knowledge of the wetted area of the cross section.
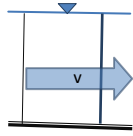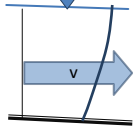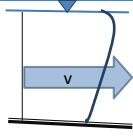
$$Q = \sum_{i=1}^{n} \sum_{j=1}^{n} \Delta s * \Delta h * v_{i,j}$$

(29)

By setting parameters β and γ, you can calibrate the shape of the vertical velocity profile to the shape of the velocity profile of a control ADCP measurement. Table 1 shows three typical speed profiles with the parameter values.

   I.   linear velocity distribution $v^{LSPIV} = v_i,$

  II.   estimation with a power function $v^{LSPIV} = v_{max},$

 III.   estimation that may best fits to a natural free surface flow, whereby the highest velocity zone occurs in the upper third of the velocity profile

Table 1: Vertical velocity profile estimation

	β	γ	velocity profile
I	**0**	**1**	
II	**1/6**	**1**	
III	**1/12**	**1.3**	

These procedures have been tested several times under controlled conditions (control flow measurements with ADCP, accurate GRPs on the video measured via GNSS RTK, appropriate tracer, prismatic riverbed) [8], [9] and all tests showed good agreement with the control results using either of the two numerical methods. However, the question may arise that if we do not explicitly accomplish LSPIV's specific information needs (correct GRPs, appropriate camera position, proper video-resolution, accurate riverbed geometry, control water discharge measurements, etc.) are we still capable of using this method with an adequate result? To prove this, I made an evaluation of a video what is captured from the Danube in an ice drifting period.

4. Evaluation of ice drifting on the Danube

The Lower Danube Valley Water Directorate (Baja, Hungary) operates a webcam at Baja, Hungary at the bank of the Danube to examine the ice conditions of the lower Danube section in Hungary. [10], [11] The directorate has provided me a full day (11 February 2012) of series of 30-second shots, which was recorded during an intense Danube ice drifting.

They also provided me a previously measured cross section of this section of the river. My goal was to determine the daily mean water discharge using the sequence of images and the cross section.

The first difficulty, of course, was the orthorectification of the sequence of images, since measured points were not found in the images. The transformation was done with the help of Google Earth using the pillars of the Danube bridge shown on the pictures, as well as two points that can be identified along the shores. The points used in the images and their alignment under Google Earth are shown in Figures 4 and 5.
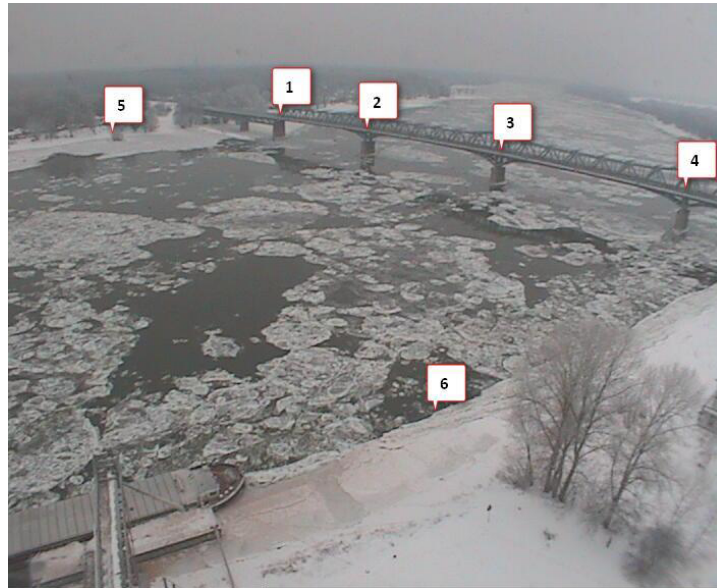
Fig. 4. Danube-Baja February 11, 2012; points used for transformation
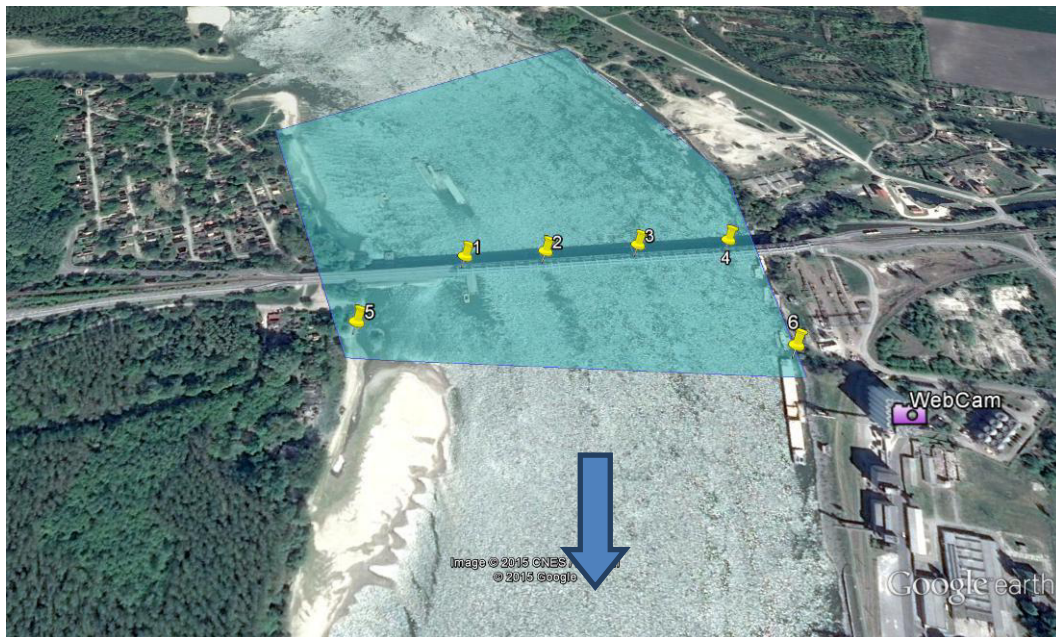
Fig. 5. The captured area with the defined GRPs (Google Earth)

Google Earth determines the points in WGS84 coordinate system with latitude-longitude values. In order to make a correct orthorectification the points have to be transformed into a local planimetric coordinate system, called EOV. It's available with a free converter program, called EHT2. The surface velocity field was determined by the parameters IA = 36 px and SA = 20 px, discretized on a 25x25 m grid on 100 images of the available series, which means an average of about 8 hours taking into account the 30 s sampling time of the images. The results were filtered above the 0,6 value of R_{ab} similarity index.

The calculated surface velocity field and the orthorectified image are shown on Figure 6.
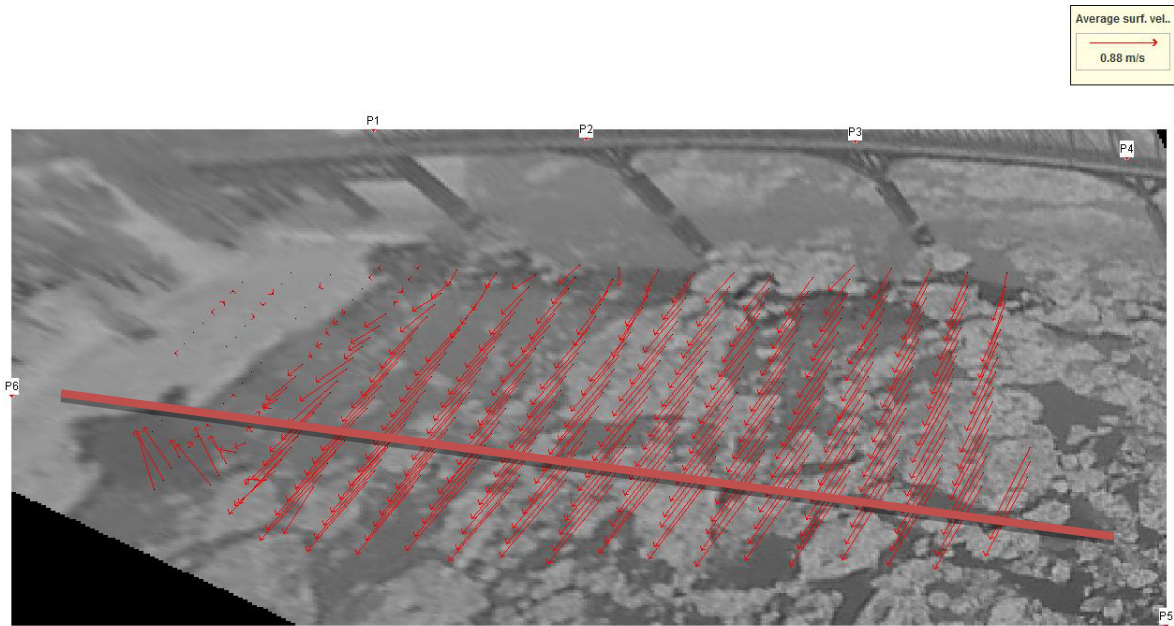
Fig. 6. Calculated LSPIV surface velocity field (Baja, Hungary, February 11, 2012)

The transverse surface velocity distribution of the orange-marked cross section is shown on figure 7.
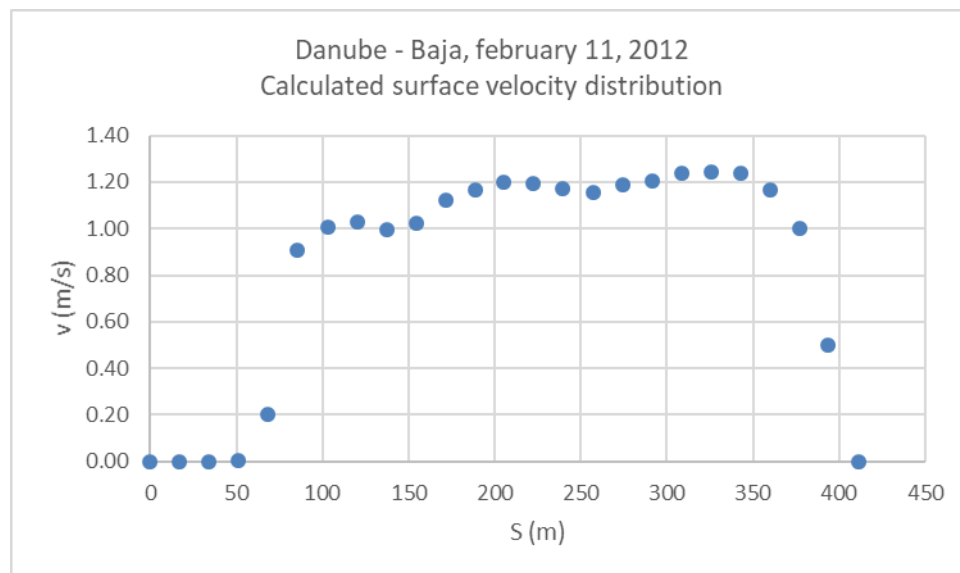
Fig. 7. Danube - Baja, february 11, 2012, Calculated surface velocity distribution

The water levels of the Danube are available in the Hungarian Hydrologic Database (MAHAB), thus the water level at the day of video-capture is known.
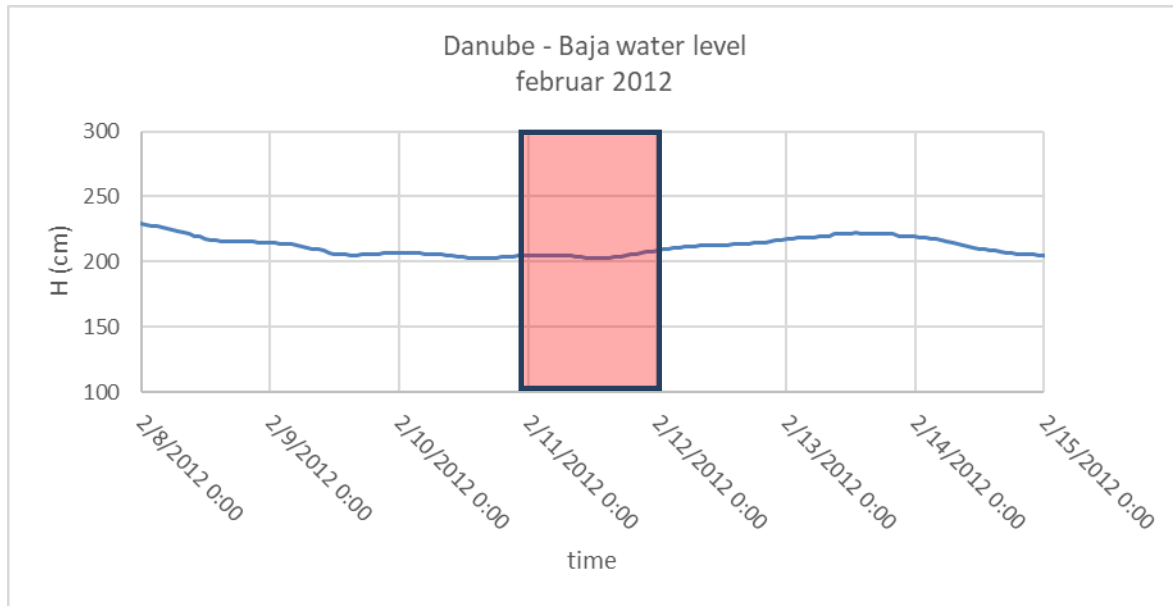
Fig. 8. Danube-Baja water level, februar 2012

Within the knowledge of the water level and a previously measured cross section of this river section, an approximate cross section can be estimated for the evaluation:
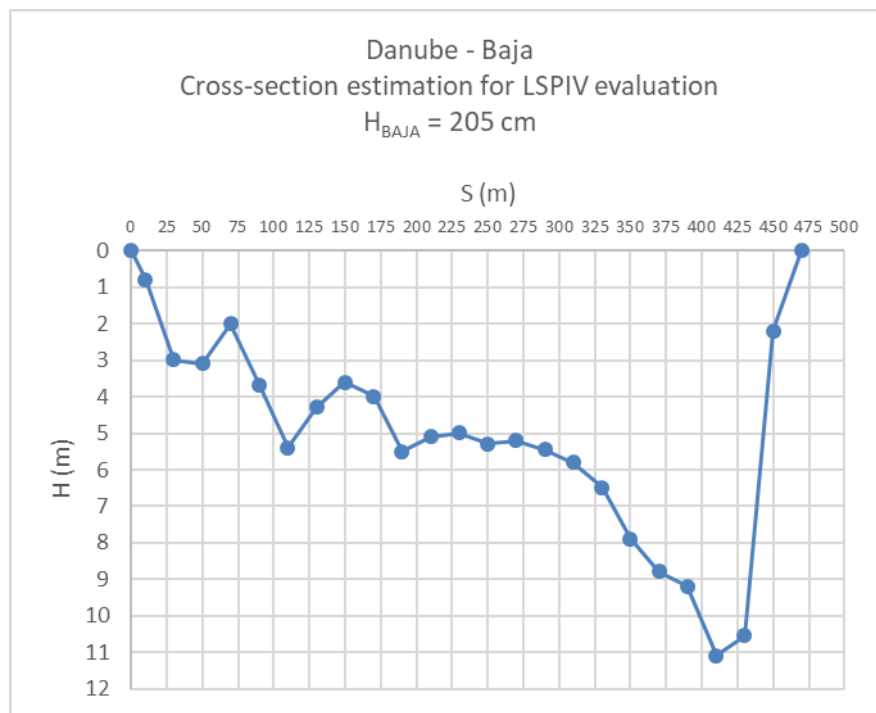
Fig. 9. Cross-section estimation for LSPIV evaluation, Danube - Baja

In view of all this the water discharge can be computable with the help of the previously mentioned LSPIV III velocity profile estimation method. The water discharge for the whole profile resulted 1994 m3/s. The result plotted on Danube - Baja profile's rating curve is the following:
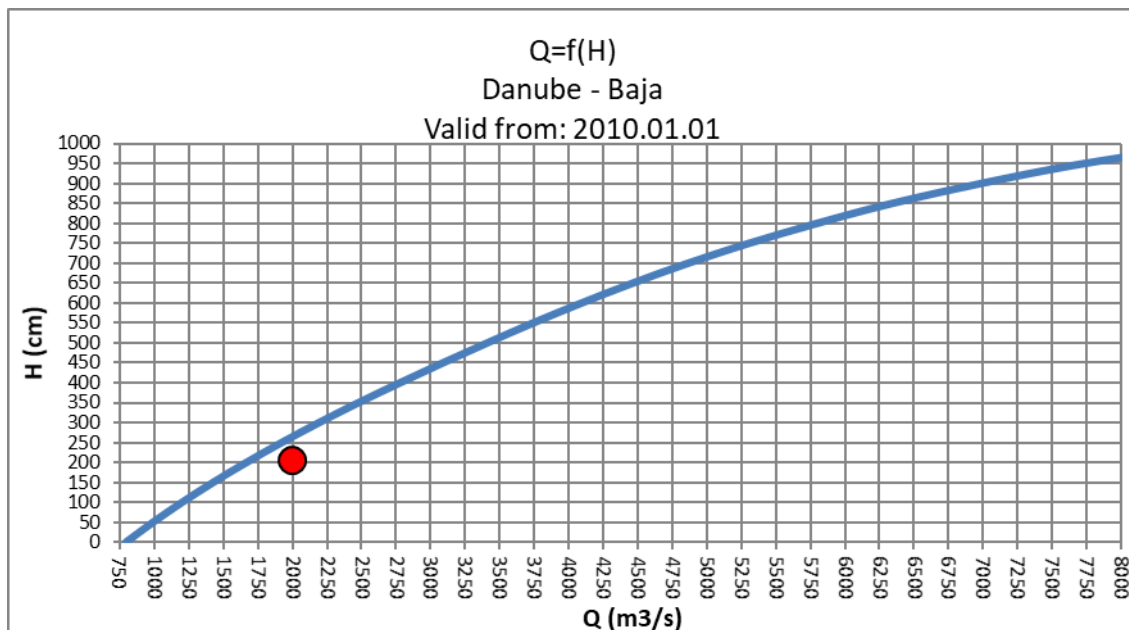
Fig. 10. Rating curve of Danube – Baja profile with the LSPIV discharge

The estimated LSPIV discharge is approximately 15% higher than the rating curve, which is above the usually agreed standard in the hydrographic practice, but according to the uncertainty of the used information and data in the calculations, it means a satisfactory match.

Conclusions

One of the most important conclusions of the analysis of ice-drifting video is that orthorectification can be performed on the images even in the absence of properly measured reference points, if the images containing clearly identifiable terrain points. A similarly important conclusion is that the quality of the surface tracer materially determines the feasibility of the analysis. In case of previously processed measurements, it was an important experience that the observed natural foaming on water surface was a relatively fast changing pattern. Real velocity field hasn't been realized even beside 1second image sampling rate, only with its 3-times densified frequency (3 frames per second) was enough to reproduce the real velocity conditions, however this method necessarily increasing the runtime of the analysis. On the other hand, the ice-floats on the Danube represent a much more constant pattern on the river surface, so in this case the 30 second image sampling rate and the relatively small image resolution of 704x576 pixels did not make it impossible to determine the velocity field. Of course, the determination of the wetted cross-section is essential for the calculation of the water discharge.

Hydrometric devices of the present day - especially acoustic velocity and flowmeters - are high-tech, robustly designed tools for everyday use, which multiplies the measurement efficiency of the previous - mostly mechanical - instruments. They can be used over a very wide range of water courses; they are suitable for high definition determination of water flow and many other flow characteristics.

One might well ask, with such technical knowledge and high-tech instruments, where can be the benefit of the LSPIV method, which is a fundamentally technical estimation procedure?

In the recent years in context with the climate changing there's a significant growth in the number of flash-floods, because of the increasing number of the heavy torrential rainfalls mainly in the summer period. These events mean a great challenge to the hydrologic experts, because these floods' behaviour not really known in their practice. The main problem with these events is that the

hydrological measurement groups of the water directorates usually cannot "reach" the peak of the floods, partly due to lack of capacity and mainly due to the short duration of the flash floods. So, in most cases the whole flood wave drains immeasurably, and in small river basins usually no hydrographic measurement station operates to reconstruct the peak discharge, or any hydraulic parameters of these floods. Thus only a few, low-confidence hydrological estimation methods are available to determine the hydrological characteristics of the floods. Video-based procedures can be an effective tool for such cases. As some 10-second video recording from a suitable location is sufficient to estimate the surface velocity magnitude, the method can be done by anyone even via social media channels. There are some great examples to the strength of the social media e.g. Waze - a social media-based navigation application, or idokep.hu - a meteorological site, also based on social media.

The method can also be integrated into the work of the water directorates. These events usually generate an extraordinary need of information, which hardly can be performed with the current workforce. In recent years on several occasions such events occurred that have exceeded the resources available for this purpose (flood discharge measurement). The method can be successfully applied in all cases where any mechanical or acoustic measurement method fails to work. In the case of a well-organized measurement and data collection campaign, where several members of the defense organization are involved in the data collection beyond hydrographic measurement groups, significantly more numerical hydrographic information may be available for hydrological assessment of a major meteorological event. Of course, after the floods all cross sections have to be measured geodetically, including the signs of the peak water levels. In the knowledge of all these factors the peak discharges can be assessed retrospectively.

The advantage of this method is that a measurement is actually means a video recording, so it can be done by anyone.

Summarizing the results of the measurements and data processing, the LSPIV-based water velocity measurement and discharge calculation can be an appropriate complement to traditional water discharge measurement methods, even with subsequent determination of the wetted cross section.

References

[1] Muste, M., I. Fujita, and A. Hauet. "Large-scale particle image velocimetry for measurements in riverine environments." *Water Resources Research* 44, no. 4, doi:10.1029/2008WR006950 (April 2008): W00D19.

[2] Mikhail, E.M., and F. Ackermann. *Observation and Least Squares*. Dun-Donnelley, New York, 1976.

[3] Fujita, I., M. Muste, and A. Kruger. "Large-scale particle image velocimetry for flow analysis in hydraulic applications." *J. Hydraul. Res.* 36, no. 3 (1998): 397 – 414.

[4] Jodeau, M., A. Hauet, and J. Le Coz. *FUDAA-LSPIV 1.3.2 User Guide*, 2013.

[5] Budapesti Műszaki és Gazdaságtudományi Egyetem. *Hydromorphology, Lecture notes / Hidromorfológia, Egyetemi jegyzet*. Budapest, 2011.

[6] Huang, H. "River Discharge Monitoring Using Horizontal Acoustic Doppler Current Profiler (H-ADCP)." 2014. http://citeseerx.ist.psu.edu/viewdoc/download?doi=10.1.1.559.2922&rep=rep1&type=pdf.

[7] Ghitescu, M.A., and A.T. Constatin. "Studying the Influence of River Works on River Flow Regime with 1-D Hydraulic Modelling." *"HIDRAULICA" Magazine of Hydraulics, Pneumatics, Tribology, Ecology, Sensorics, Mechatronics*, no. 3 (September 2018): 33-38.

[8] Lükő, G. *Analysis of video-based discharge measurement method for streams*. Budapesti Műszaki és Gazdaságtudományi Egyetem, 2015.

[9] Kerék, G. "Videó alapú vízhozammérések alkalmazhatósága kisvízfolyásokon / Applicability of video-based flow measurements in small streams." *MSc Thesis*. Budapesti Műszaki és Gazdaságtudományi Egyetem, 2015.

[10] Keve, G. "Space-time ice monitoring of the Hungarian Lower-Danube." *Periodica PolytechnicA-Civil Engineering* 61, no. 1 (2017): 27-38.

[11] Keve, G. "A jégmegfigyelések korszerűsítési lehetőségei/Opportunities for modernizing ice observation." *Vízügyi Közlemények* 84, no. 3 (2002): 358-378.

Green Energy from Wind Action

Assistant professor **Fănel Dorel ȘCHEAUA**[1]**,** Prof. PhD Eng. **Ion DAVID**[2]

[1] "Dunărea de Jos" University of Galați, fanel.scheaua@ugal.ro

[2] Technical University of Civil Engineering of Bucharest

Abstract: *The atmospheric air front movements determine the winds occurrence. Due to the continuous action of the sun on the atmospheric air masses exposed successively as a result of the earth's rotational motion, different values of the air temperature are obtained, which correlate with the atmospheric pressure values, are forming air masses zonal movements. Over time, special constructive units have been developed that can take the air motion energy in order to achieve continuous rotational motion at a turbine shaft. At present, the wind force ensures a significant amount of necessary energy production for human communities but far from using the whole winds potential worldwide. The constructive and operational characteristics of the wind turbines provide a solution of obtaining green energy with reduced environmental damage. Aspects presented in this paper are related to fluid mechanics elements describing the air motion at the wind turbine blades level that is capable to determine the shaft rotational motion. Also, an air flow analysis is performed on a virtual model of a wind turbine propeller in order to highlight the flow regime according to specific values of the air circulation velocity.*

Keywords: *Air flow, energy recovery, three-dimensional modelling, CFD*

1. Introduction

Every human activity was made in order to satisfy community needs over the times so that every possible resource was taken into account so far. For energy needs traditional fuels have been used during a long period but in time this solution became unfriendly with the environment. So another solutions had to be developed in order to obtain energy from wind action, wave action, water falls or sun power. In this paper is presented a solution of wind power plant from the operational point of view and a model of horizontal axis turbine which use the wind action in order to acquire the axial shaft rotation, necessary for energy production.

The energy produced on the basis of air currents has great potential and represents a sustainable production method by means of which the energy conversion that takes place at the level of the wind power plant rotor. The major advantage that result from the use of wind power plants is related to the carbon dioxide amount that is avoided to be discharged into the atmosphere due to the energy production by using the traditional burning fossil fuels production methods. Even if only 2.5% of the total energy consumed globally is now produced by the wind action, there must be considered the development and increase of the wind energy production amounts ensuring in this way a cleaner environment for the future.

2. Wind turbine operational aspects

The general aspects that characterize the movement of the atmospheric air and the possibilities of capturing and converting the energy within the constructive units of electricity generation used at the present time worldwide are presented.

Depending on the size of the turbine rotor, optimal results regarding the energy values produced in the wind power stations are obtained.

A classification of the wind turbines can be made from the position of the rotor axis. This includes turbines with horizontal and vertical axis. Horizontal axis turbines have the peculiarity of taking the air stream lines from the wind in a direction parallel to the rotor axis, while the turbines with the vertical axis take the air flow path lines in a direction perpendicular to the rotational axis.

Most commonly used with higher installed power are the horizontal axis turbines for power generation worldwide, while vertical axis turbines are used less with much lower installed power.

a) horizontal axis turbine   b) Darrieus H vertical axis   c) Savonius vertical axis   d) Darrieus vertical axis
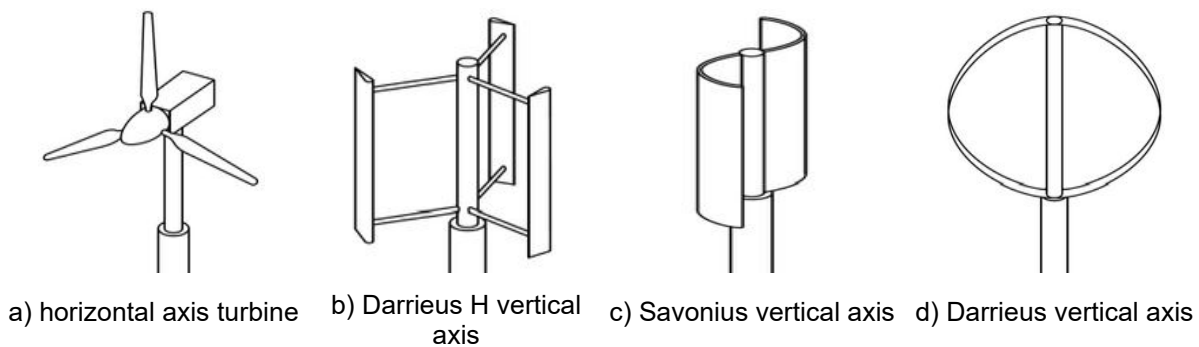
Fig. 1. Principal wind turbine constructive types [8]

The operating performance of a wind turbine is related to the wind velocity values and its direction. Wind turbines have great operating efficiency when there is optimum airflow velocity and must be positioned to be able to receive directly and take over the power from the optimum wind direction.

In order to install a wind turbine, it is important to establish the economic conditions of energy production related to the duration of action and the wind velocity within a respective region, which describes the wind resources present per year.

The wind power density value expressed in power units per unit area $\left(W/m^2\right)$ is described. This parameter comprises the combined effects of the frequency distribution of the wind velocity together with the dependence on the air properties related to density.

The total power value of the wind acting on the surface of the turbine rotor is described by the relation: [1]

$$\frac{dm_a}{dt} = \rho S v \tag{1}$$

$$P_T = \frac{1}{2}\frac{dm_a}{dt}v^2 = \frac{1}{2}\rho S v^3 \tag{2}$$

where: S -rotor surface area, v -wind velocity, ρ -air density.

The average value of the power density of the air circulation over the surface unit can be described as follows: [1]

$$\frac{P_T}{S} = \frac{1}{2}\rho v^3 \tag{3}$$

It is obvious that the wind power density values are proportional to air density, turbine rotor diameter and the cube of air velocity.

The power potential produced by a wind turbine is based on the laws of fluid mechanics that describe the air circulation through the turbine impeller and the aerodynamic characteristics of the rotor.

Some values of available power per surface unit are presented in table 1 according with wind velocity.

Table 1: Values for available power function on wind velocity

Wind velocity *(m/s)*	Available power/area unit $\left(W/m^2\right)$
5	80
10	610
15	2070
20	4900
25	9560
30	16550

For some regions the wind velocity values during the year are measurable and known so that the wind turbines positioning can be established in order to obtain optimal results characterized by high efficiency in the energy production. The estimated average values of the available power can thus be determined based on the average hourly velocities available for a whole year:[1]

$$\frac{\bar{P}}{S} = \frac{1}{2}\rho \bar{v}^3 C_E$$ (4)

where $\bar{v}$ - represents the average value of wind velocity and C_E is the energy factor coefficient described by the relation: [1]

$$C_E = \frac{1}{n_h \bar{v}^3}\sum_{i=1}^{n_h} v_i^3$$ (5)

Relation that consider the total number of hours (n_h) in a year.

A realistic evaluation regarding the total amount of wind power on surface unit available for a certain region is made: [1]

$$\left(\frac{\bar{P}}{S}\right) < 100 \, \frac{W}{m^2} - Low \, potential \, values$$

$$\left(\frac{\bar{P}}{S}\right) \cong 400 \, \frac{W}{m^2} - Good \, potential \, values$$

$$\left(\frac{\bar{P}}{S}\right) > 700 \, \frac{W}{m^2} - Great \, potential \, values$$

.

3. Air circulation velocity and flow rate along rotor blade surface

It is considered the case of air potential movement at the level of a curve delimited by the points A and B positioned on the rotor propeller blade within the air stream.

At each contour point an air stream line passes. A fluid particle has a velocity that passes at some point P and the components *(u)* and *(v)* with respect to the *OXY* coordinate system and (v_n) and (v_t) relative to a system with the origin at point P and the normal and tangential axes at the blade contour curve. [2]
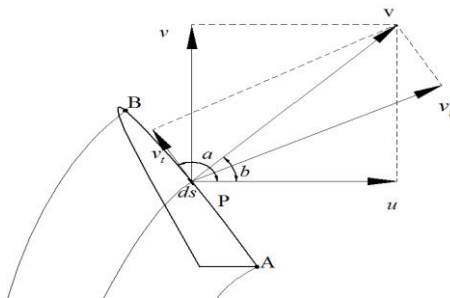
Fig. 2. Schematically representation of air circulation velocity and flow rate [2]

The air velocity circulation along the contour curve AB can be written as follows: [2]

$$\Gamma_{AB} = \int_{AB} v_t ds$$ (6)

On the schematically representation of air circulation in figure 2 the following relations are considered: [2]

$$v_t ds = \mathrm{v}\cos(a-b)ds = \mathrm{v}(\cos a \cos b + \sin a \sin b)ds = udx + vdy \tag{7}$$

$$\Gamma_{AB} = \int_{AB} udx + vdy \tag{8}$$

Expressing the two velocity values in another form can be than written the relation for the air velocity circulation: [2]

$$u = \frac{\partial \varphi}{\partial x}; \quad v = \frac{\partial \varphi}{\partial y} \tag{9}$$

$$\Gamma_{AB} = \int_{AB} \frac{\partial \varphi}{\partial x}dx + \frac{\partial \varphi}{\partial y}dy = \int_{AB} d\varphi = \varphi_B - \varphi_A \tag{10}$$

For the case of a closed curve such as the case of the wind turbine rotor blade, the air flow velocity is equal to the potential increase on the contour curve.
For the values of circulated air flow rates at the contour curve level of the wind turbine rotor blade, can be written the relation for the fluid area between points A and B: [2]

$$Q_{AB} = \int_{AB} v_n ds \tag{11}$$

The following relations can be written from the conditions described by the calculation model presented in figure 1, where the air flow rate equation results: [2]

$$v_n ds = \mathrm{v}\sin(a-b)ds = \mathrm{v}(\sin a \cos b - \sin b \cos a)ds = udy - vdx \tag{12}$$

$$Q_{AB} = \int_{AB} udy - vdx \tag{13}$$

Expressing the two velocity values in another form can be written the relation for the air circulated flow rate in another form: [2]

$$u = \frac{\partial \phi}{\partial y}; \quad v = -\frac{\partial \phi}{\partial x} \tag{14}$$

$$Q_{AB} = \int_{AB} \frac{\partial \phi}{\partial x}dx + \frac{\partial \phi}{\partial y}dy = \int_{AB} d\phi = \phi_B - \phi_A \tag{15}$$

The relations obtained for the air velocity circulation and flow rate show that these values are directly dependent on the functions (φ) and (ϕ) calculated at the contour curve extreme points of the wind turbine rotor blade and not depending on the curve shape.

4. Air flow analysis on virtual model

The potential of air mass circulation can ensure the continuous rotational motion of a turbine's rotor shaft so that electricity is generated through the use of a generator.
A three-dimensional rotor model for wind turbine is constructed and analyzed with ANSYS CFX from the air flow point of view in order to highlight the flow pattern and the operational mode based on the air circulation over the rotor blades.
Air velocity values characteristic of regions with relatively constant wind action during the year are adopted, measurable values that are declared as analysis initial values.
The wind velocity range is considered between 3.5-5 m/s corresponding to the hill regions, the plain area and the coastal area where the wind velocities are in higher values.
The adopted value for air velocity is 4 and 5 m/s for the two analysis conducted.

The rotor model is included in a cylindrical enclosure having a diameter of 7 m that coincides with the propeller blades width.

a) turbine rotor and air enclosure   b) mesh network
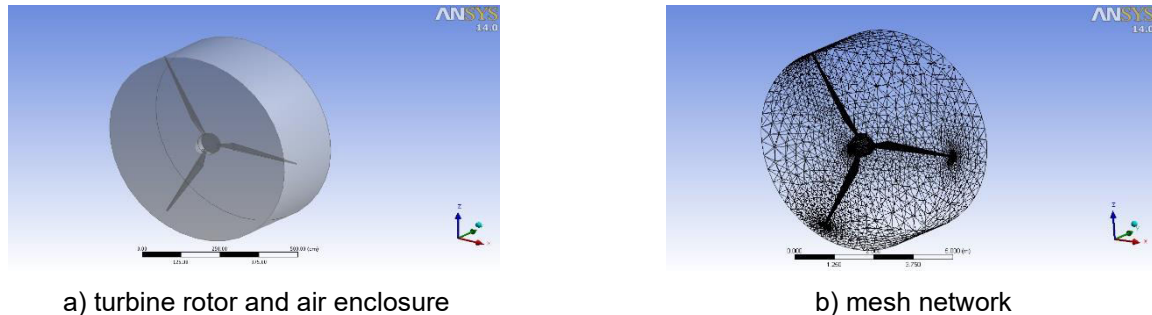
Fig. 3. Analysis main domains and mesh network

Based on the values initially introduced, flow results were obtained with specific values of air circulation velocities at the level of the rotor blades and characteristic pressure being presented in figure 4.

The total force acting on the rotor blades in normal direction is calculated at 233.5 N for the inlet air velocity of 4 m/s and 246,3 N for the inlet air velocity of 5 m/s.

a) air velocity within rotor enclosure   b) total pressure values
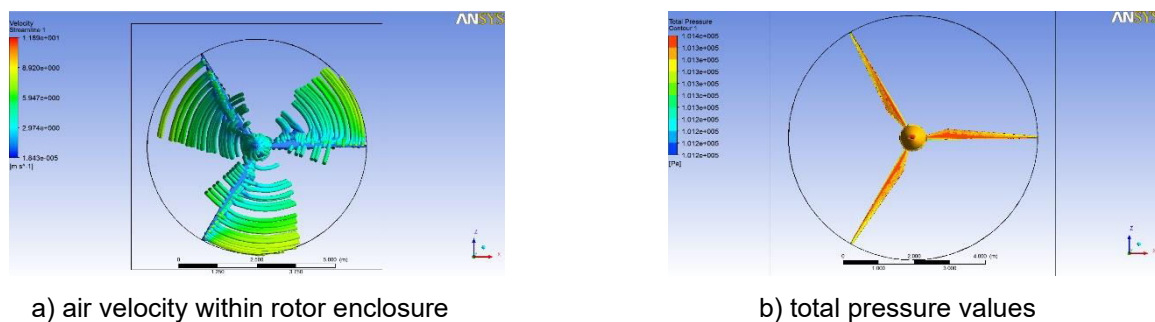
Fig. 4. Air flow analysis results

The air specific path-lines inside the fluid region are also presented emphasizing the principal parameters specific values related to air velocity, static and total pressure.

According with the air flow motion model are met the required conditions for the rotor blade entrainment in motion necessary to form a continuous rotary motion due to hydrostatic forces action on propeller blade.

5. Conclusion

The method of obtaining energy from wind force is highlighted as a viable alternative to the burning of fossil fuels. It has been several decades since the wind energy has registered an increase but more especially in the last period when the wind energy share in the total production reached the maximum values. Wind power plants have been continuously developed over the years in terms of rotor design and diameter, starting from about 12 m at the end of the 80s to approximately 120 m in diameter today, allowing the high power production of about 5 MW of green energy, thus reducing the energy consumption that comes from the sources with a negative effect on the environment.

In this paper were presented theoretical aspects regarding the wind turbines operation method as well as a calculation model of velocity circulation and flow rate specific values of circulated air at the rotor blade contour level.

Also, on the basis of a three-dimensional model, an air flow analysis inside the rotor enclosure was performed based on the declared values for the air input velocity characteristic to regions of plains, hills and coastal areas in Romania.

The results are presented in terms of air flow velocity, static pressure and total air pressure over the analyzed fluid area. Also the force values on the rotor blades are calculated allowing to establish the proper value of rotor torque according with inlet air velocity and analyzed model constructive type.

According to the obtained values it can be said that the conditions necessary for the displacement of the rotor blade are fulfilled based on the result of the hydrostatic forces that act directly on the blade surface and the blade geometry which allows the air to flow in a tangential direction to the contour curve.

References

[1] Manwell, James F., Jon G. McGowan, and Anthony L. Rogers. *Wind energy explained: theory, design and application*. John Wiley & Sons, 2010.

[2] Florea, J., and V. Panaitescu. *Fluid Mechanics / Mecanica fluidelor*. Bucharest, Didactic and Pedagogical Publishing House, 1979.

[3] Axinti, G., and A.S. Axinti. *Hydraulic and pneumatic drives - Components and systems, functions and characteristics / Actionari hidraulice si pneumatice – Componente si sisteme, functii si caracteristici*. Chisinau, Tehnica-Info Publishing House, 2008.

[4] Naccache, G. *CFD Based Analysis and Parametric Study of a Novel Wind Turbine Design: the Dual Vertical Axis Wind Turbine*. Thesis in the Department of Mechanical and Industrial Engineering Presented in Partial Fulfillment of the Requirements For the Degree of Master of Applied Science (Mechanical Engineering) at Concordia University Montreal, Quebec, Canada, 2016.

[5] Scurtu, Ionut Cristian. "Manufacturing and design of the offshore structure Froude scale model related to basin restrictions." *IOP Conference Series: Materials Science and Engineering* 95, no. 1 (2015): art. no. 012068, DOI: 10.1088/1757-899X/95/1/012068.

[6] Dragomir, George, et al. "Wind energy in Romania: A review from 2009 to 2016." *Renewable and Sustainable Energy Reviews* 64 (October 2016):129-143.

[7] Pintilie, Viorel, and Eugen Rusu. "A brief overview of the renewable energy potential in Romania." *Mechanical Testing and Diagnosis* 7, no. 2 (June 2017): 24-29.

[8] Kozak, P. *Effects of unsteady aerodynamics on vertical-axis wind turbine performance*. PhD Thesis, Illinois Institute of Technology, 2014.

Stress and Deformation Analysis under Bending and Torsional Loads of a Toroidal LPG Tank Based on the Finite Element Analysis

Assoc. Prof. PhD. Eng. **Mihai ŢĂLU**[1], Assoc. Prof. PhD. Eng. **Ştefan ŢĂLU**[2,*]

[1] University of Craiova, Faculty of Mechanics, Department of Applied Mechanics and Civil Engineering, Calea București Street, no. 107, 200512 Craiova, Dolj county, Romania. E-mail: mihai_talu@yahoo.com

[2] Technical University of Cluj-Napoca, The Directorate of Research, Development and Innovation Management (DMCDI), Constantin Daicoviciu Street, no. 15, Cluj-Napoca, 400020, Cluj county, Romania. Corresponding author* e-mail: stefan_ta@yahoo.com

Abstract: In this study, the stress and deformation behaviors of a three-dimensional (3-D) hexagonal toroid with regular hexagonal cross-section used in manufacturing of liquefied petroleum gas (LPG) storage tanks from the automotive industry under bending and torsional stress are investigated using the finite element simulations. The effects of bending or torsional loads, and temperature were systematically explored. Numerical calculations have been carried out to compute the optimal form of the LPG storage tank to minimize the storage tank mass in terms of safety. The 3-D parametric models may be used to qualitatively evaluate the variation of stress intensity factor and strain energy release rates. The research results provide important theoretical support for the stress threshold setting and deformation controlling of the LPG storage tanks in the production practice. The results show that this research method is helpful for use of design specifications, standards and knowledge of LPG storage tanks in order to product updates and diversification.

Keywords: 3-D hexagonal toroidal LPG fuel tank, bending and torsional loads, automotive industry, industrial engineering design, optimization methods, finite element analysis

1. Introduction

From a global perspective, due to the increase in vehicle production, there has been a growing demand for automotive fuel storage tanks to meet the increasing service demands, quality requirements and safety legislation [1-3].

In the last decade, much progress and open innovation have been made in the flexible manufacturing of LPG storage tanks in different geometrical variants [4-7]. LPG storage tanks require a sufficiently flexible manufacturing technology, precise and qualified, permanently perfected by the R&D results, constantly in progress, and to ensure the repeatability of standard products, through an effective process of production, traceability and upgrading [8-12].

The knowledge and experience gained in the field of the design and manufacture of LPG storage tanks, in general, and in internal geometry, in particular, were supported by innovative methods calculation and simulation [12-14], which allowed the optimization of the different one's product parameters from the design phase [15-17], and which it ensures good operation during operation and a lifetime of extended life, depending on the specificity of the applications [18-20].

Quantitative and qualitative research based on 3-D computer-aided design of LPG storage tanks offers a competitive advantage and can help establish the importance of specific customer needs and validate the best product concept and geometry of LPG storage tanks [21-23].

Finite element analysis is an important tool used in design to obtain insights into the mechanical properties and deformation behaviors of LPG storage tanks under various loads [24-26].

The integration of advanced knowledge of 3D modelling (CAD) [27-30] with manufacturing processes has found significant benefits in increased productivity within the design [31-34], improved product quality [35-37], and high competitiveness of LPG storage tanks [38-41].

According to the technical literature, relatively rare studies (direct mechanical testing experiments and simulations) were devoted to the bending and torsional loads, or combined deformation behaviors. Our numerical model provides a straightforward prediction of the stress and the resultant linear deformation is proved as an effective tool for LPG storage tanks design due to a great reduction of time-consuming in numerical simulations.

2. Design methodology

2.1. Basic geometry of the parametric 3-D model

Let's consider the parametric 3-D model generated by revolving of a closed generating curve C_G (a hexagon with rounded corners) along a closed guiding curve C_D (a hexagon with rounded corners) as shown in figs. 1 and 2 [14].

The following parameters were applied as input parameters to the 3-D parametric model (figs. 1 and 2): a) a closed generating curve CG (a hexagon with a side value L = 175 mm, with rounded corners, radius R = 50 mm), and b) the guiding curve CD (a hexagon with a side value L = 430 mm, with rounded corners, radius R = 180 mm), and the thickness = 10 mm.

Based on the physical model, the modeling was done in the AutoCAD Autodesk 2020 software [42] and the numerical analysis was performed with SolidWorks 2020 software [43] with the Static, Thermal and Design Study modules. The design data used were:

- the tank material is AISI 4340 steel;
- the maximum hydraulic test pressure: p_{max} = 30 bar;
- the working temperature between the limits: T = -30 ^{0}C up to T = 60 ^{0}C;
- supporting surfaces located on the inferior side;
- the duration of the tank exploitation: n_a = 15 years;
- the corrosion rate of the material: v_c = 0.07 mm/year.

The shape of the parametric storage tank model, not deformed, dimensioned by optimization, is shown in fig. 1 as an isometric view and as a lateral view (fig. 2).
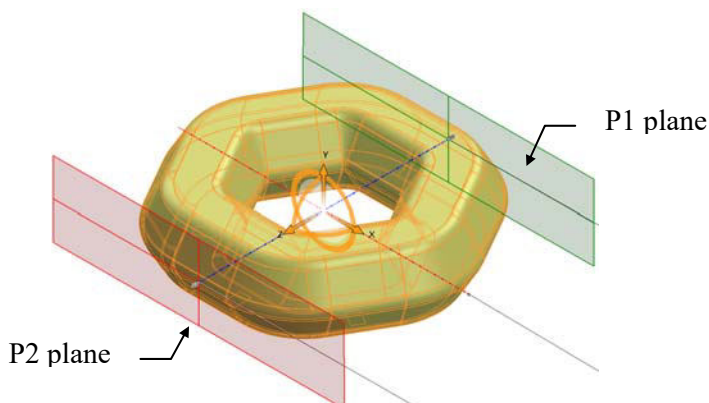
Fig. 1. The isometric representation of 3-D model, not deformed, dimensioned by optimization
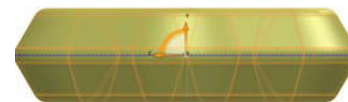
Fig. 2. The lateral representation of 3-D model not deformed, dimensioned by optimization

The manner in which the qualitative deformation of the storage tank shape takes place in the case of bending as a result of the action of a bending moment is shown in fig. 3 and fig. 4.
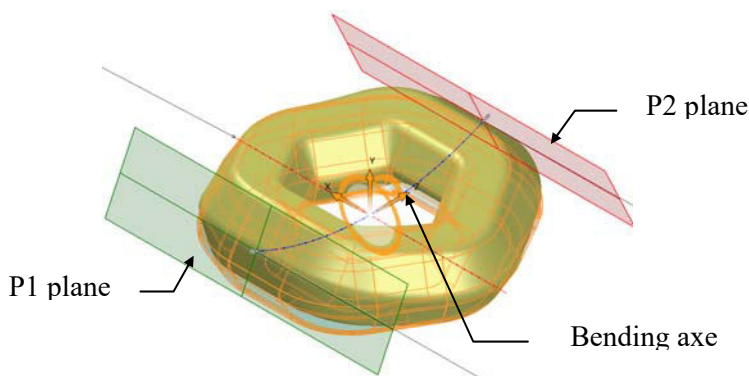
Fig. 3. The isometric representation of 3-D model as a result of the action of a bending moment
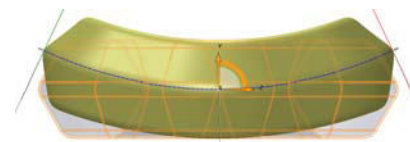
Fig. 4. The lateral representation of 3-D model as a result of the action of a bending moment

The manner in which the qualitative deformation of the storage tank shape takes place in the case of twisting as a result of the action of a twisting moment is shown in fig. 5 and fig. 6.
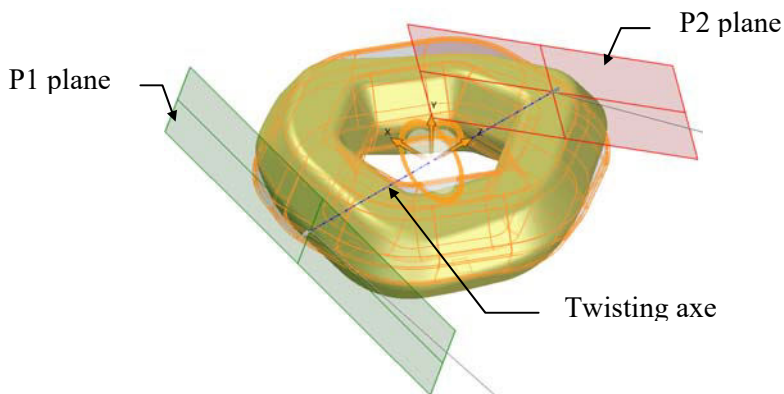
Fig. 5. The isometric representation of 3-D model as a result of the action of a twisting moment
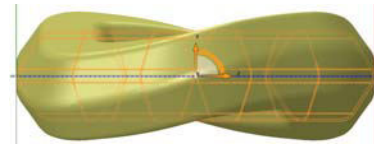
Fig. 6. The lateral representation of 3-D model as a result of the action of a twisting moment

As a result of a road accident in which the vehicle can be involved, the storage tanks after mechanical loads can have a simple bending or twisting deformation or both types.

It is noteworthy that in both cases of deformation calculations were made to determine the stress state and the deformation state, for the same moment corresponding for n_a = {0 years, 5 years, 10 years and 15 years}; and for the same value of the bending or twisting angle: ϕ = {0.25^0, 1^0, 2^0, 4^0, 6^0, 8^0 and 10^0} (fig. 7 and fig. 8).
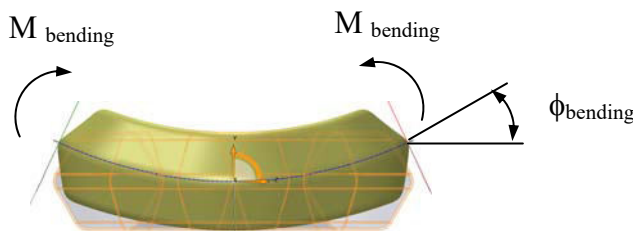
Fig. 7. The axonometric representation of 3-D model and the bending angle ($\phi_{bending}$)
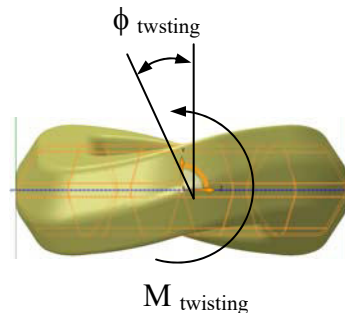
Fig. 8. The frontal representation of 3-D model and the twisting angle ($\phi_{twsting}$)

2.2. Numerical analysis of the parametric 3-D model

Numerical calculations were performed for: mesh standard type, solid mesh, curvature-based mesh with quality high, Jacobian in 16 points, element size 6 mm, number of nodes 47767, number of elements 23925.

The values of the state of stress Von Mises for bending and twisting determined by the finite element method for n_a= 0 and 5 years are shown in table 1, and for n_a = 10 and 15 years in table 2.

Table 1: The Von Mises resultant effort for n_a= 0 and 5 years

ϕ [°]	T [°C]	n_a = 0 years				n_a = 5 years			
		-30°	0°	30°	60°	-30°	0°	30°	60°
0	σ [MPa]	604.130	513.813	441.460	487.942	609.754	513.007	455.0307	506.921
0.25	Bending	442.967	402.354	367.684	402.303	476.814	424.192	380.605	425.947
	Twisting	633.167	524.136	471.115	515.153	646.455	544.486	499.54	549.939
1	Bending	488.906	440.955	396.644	403.908	530.217	482.336	437.783	421.500
	Twisting	632.577	526.742	448.320	497.578	630.826	527.699	499.485	542.929

2	Bending	488.906	440.955	396.644	403.908	501.985	450.381	401.721	412.022
	Twisting	603.872	514.467	435.172	482.933	648.021	556.001	468.075	513.643
4	Bending	550.017	466.968	435.906	470.532	551.485	476.887	455.962	495.63
	Twisting	582.163	491.112	436.272	474.882	647.333	553.428	468.162	506.284
6	Bending	564.078	471.655	431.488	462.456	544.817	461.509	464.226	493.763
	Twisting	644.474	533.706	433.225	461.236	671.966	558.710	455.288	494.191
8	Bending	557.426	467.669	421.722	454.871	584.454	497.238	525.941	565.523
	Twisting	562.664	483.278	434.062	482.022	684.722	593.138	503.395	529.039
10	Bending	459.991	415.98	374.398	374.52	523.966	480.525	443.654	432.795
	Twisting	597.586	508.453	428.215	456.06	646.973	558.237	472.069	520.390

Table 2: The Von Mises resultant effort for n_a= 10 and 15 years

ϕ [°]	T [°C]	n_a = 10 years				n_a = 15 years			
		-30°	0°	30°	60°	-30°	0°	30°	60°
0	σ [MPa]	631.859	536.113	500.095	544.749	664.749	580.277	539.257	593.356
0.25	Bending	501.696	454.657	410.976	451.969	533.786	485.66	440.704	476.922
	Twisting	671.825	580.275	513.908	559.111	720.992	642.609	563.393	609.903
1	Bending	575.507	527.073	481.699	448.798	629.543	580.439	534.174	491.55
	Twisting	656.152	558.748	523.648	572.092	630.050	582.294	575.271	617.743
2	Bending	479.139	427.909	385.301	433.090	516.429	467.660	421.772	460.625
	Twisting	640.331	548.530	499.530	544.232	656.473	556.017	565.732	612.368
4	Bending	595.403	510.138	491.384	535.976	632.426	533.338	572.433	626.159
	Twisting	665.269	566.368	511.877	560.938	697.559	602.885	560.280	614.595
6	Bending	582.945	496.902	495.935	534.353	620.499	544.402	586.990	633.040
	Twisting	618.443	539.903	498.637	551.038	675.154	587.652	540.631	594.554
8	Bending	584.454	497.238	525.941	565.523	619.644	546.724	580.126	615.802
	Twisting	642.592	555.988	519.963	572.506	726.248	633.716	542.715	587.319
10	Bending	523.966	480.525	443.654	432.795	567.888	528.245	490.211	454.101
	Twisting	637.352	547.513	501.518	553.876	677.954	585.842	565.737	613.592

The values of the resultant linear deformation *u* for bending and twisting determined by the finite element method for n_a= 0 and 5 years are shown in table 3, and for n_a= 10 and 15 years in table 4.

Table 3: The resultant linear deformation for n_a= 0 and 5 years

ϕ [°]	u [mm]	n_a = 0 years				n_a = 5 years			
		T [°C]				T [°C]			
		-30°	0°	30°	60°	-30°	0°	30°	60°
0		1.01700	0.97910	0.9434	0.9117	1.1134	1.0743	1.0369	1.0043
0.25	Bending	0.66101	0.64168	0.62444	0.60879	0.71848	0.69716	0.69972	0.66404
	Twisting	1.01000	0.97955	0.94958	0.9262	1.12945	1.09517	1.06171	1.03081
1	Bending	0.66554	0.65167	0.63930	0.62851	0.72933	0.71502	0.70207	0.69057
	Twisting	0.99508	0.96169	0.93050	0.90255	1.08137	1.04716	1.01438	0.98266
2	Bending	0.78179	0.78864	0.79774	0.80987	0.72880	0.7098	0.69290	0.67731
	Twisting	0.97581	0.94611	0.91779	0.89117	1.06893	1.03666	1.00558	0.97721
4	Bending	0.78854	0.79728	0.80724	0.81838	0.87615	0.88465	0.89426	0.90494
	Twisting	0.99898	0.9665	0.93499	0.90532	1.08680	1.05429	1.0245	0.99571
6	Bending	0.79353	0.80305	0.81375	0.82561	0.88274	0.8897	0.89776	0.90686

	Twisting	1.02196	0.98997	0.96063	0.93327	1.12669	1.09292	1.0609	1.02826
8	Bending	0.80324	0.81117	0.82028	0.83051	0.89097	0.89823	0.90709	0.91697
	Twisting	1.01696	0.98608	0.95619	0.92772	1.11552	1.08383	1.05303	1.02509
10	Bending	0.69279	0.66939	0.65723	0.64675	0.75547	0.74217	0.73064	0.72025
	Twisting	1.03229	1.00131	0.97133	0.94276	1.13948	1.0896	1.07938	1.05072

Table 4: The resultant linear deformation for n_a= 10 and 15 years

ϕ [°]	u [mm]	n_a = 10 years T [°C]				n_a = 15 years T [°C]			
		-30°	0°	30°	60°	-30°	0°	30°	60°
0		1.2272	1.1873	1.149	1.115	1.350	1.309	1.269	1.234
0.25	Bending	0.77366	0.7552	0.73816	0.72248	0.85164	0.83065	0.81152	0.7941
	Twisting	1.24041	1.20394	1.16825	1.13343	1.35984	1.32258	1.28607	1.25023
1	Bending	0.79510	0.78095	0.76806	0.75651	0.85524	0.84237	0.83142	0.82191
	Twisting	1.19863	1.64240	1.13162	1.10273	1.31771	1.28140	1.24605	1.12414
2	Bending	0.79109	0.77242	0.75505	0.73889	0.85889	0.84037	0.82289	0.80652
	Twisting	1.1848	1.15216	1.12050	1.09030	1.30078	1.26603	1.23383	1.20218
4	Bending	0.96917	0.97821	0.98824	0.99924	1.08660	1.09410	1.10250	1.11780
	Twisting	1.19040	1.1566	1.12632	1.09682	1.13355	1.27958	1.24871	1.21853
6	Bending	0.98008	0.98897	0.99885	1.00967	1.09767	1.10397	1.11114	1.11919
	Twisting	1.23481	1.20082	1.16787	1.13583	1.35532	1.32053	1.28648	1.25324
8	Bending	0.98923	0.99746	1.00664	1.01676	1.10663	1.11324	1.12073	1.12906
	Twisting	1.23110	1.19687	1.16377	1.13202	1.34585	1.31439	1.28365	1.2537
10	Bending	0.83282	0.82092	0.81052	0.80138	0.93383	0.92238	0.91184	0.90221
	Twisting	1.24760	1.21373	1.18070	1.14858	1.38699	1.35259	1.31891	1.28601

In order to plot the graphs corresponding to the Von Mises resultant efforts, the results are shown in table 5.

Table 5: The Von Mises resultant effort for n_a= 0 years, 5 years, 10 years and 15 years

n_a [years]	ϕ [°]	T [°C]				T [°C]			
		-30°	0°	30°	60°	-30°	0°	30°	60°
		Bending σ_b [MPa]				Twisting σ_t [MPa]			
0	0.25	442.967	402.354	367.684	402.303	633.167	524.136	471.115	515.153
	1	488.906	440.955	396.644	403.908	632.577	526.742	448.32	497.578
	2	522.333	461.709	413.926	453.816	603.872	514.467	435.172	482.933
	4	550.017	466.968	435.906	470.532	582.163	491.112	436.272	474.882
	6	564.078	471.655	431.488	462.456	614.474	533.706	433.225	461.236
	8	557.426	467.669	421.722	454.871	562.664	483.278	434.062	482.022
	10	459.991	415.98	374.398	374.52	597.586	508.453	428.215	456.06
5	0.25	476.814	424.192	380.605	425.947	646.455	544.486	499.54	549.939
	1	530.217	482.336	437.783	421.5	638.826	527.699	499.485	542.929
	2	501.985	450.381	401.721	412.022	648.021	556.001	468.075	513.643
	4	551.485	476.887	455.962	495.63	647.333	553.428	468.162	506.284
	6	544.817	461.509	464.226	493.763	671.966	558.71	455.288	494.191
	8	584.454	497.238	525.941	565.523	684.722	593.138	503.395	529.039

	10	523.966	480.525	443.654	432.795	646.973	558.237	472.069	520.39
10	0.25	501.696	454.657	410.976	451.969	671.825	580.275	513.908	559.111
	1	575.507	527.073	481.699	448.798	656.152	558.748	523.648	572.092
	2	479.139	427.909	385.301	433.09	640.331	548.53	499.53	544.232
	4	595.403	510.138	491.384	535.976	665.269	566.368	511.877	560.938
	6	582.945	496.902	495.935	534.353	618.443	539.903	498.637	551.038
	8	584.454	497.238	525.941	565.523	642.592	555.988	519.963	572.506
	10	523.966	480.525	443.654	432.795	637.352	547.513	501.518	553.876
15	0.25	533.786	485.66	440.704	476.922	720.992	642.609	563.393	609.903
	1	629.543	580.439	534.174	491.55	690.05	582.294	575.271	617.743
	2	516.429	467.66	421.77	460.625	656.473	556.017	565.732	612.368
	4	632.426	533.338	572.433	626.159	697.559	602.885	560.28	614.595
	6	620.499	544.402	586.99	633.04	675.154	587.652	540.631	594.554
	8	619.644	546.724	580.126	615.802	726.248	633.716	542.715	587.319
	10	567.888	528.245	490.211	454.101	677.954	585.842	565.737	613.592

The graphs of curves corresponding to the Von Mises resultant efforts $\sigma = f(T, \phi)$ for n_a = {0 years, 5 years, 10 years and 15 years}; and for the same value of the bending or twisting angle: $\phi = \{0.25^0, 1^0, 2^0, 4^0, 6^0, 8^0$ and $10^0\}$ are graphically shown in fig. 9.
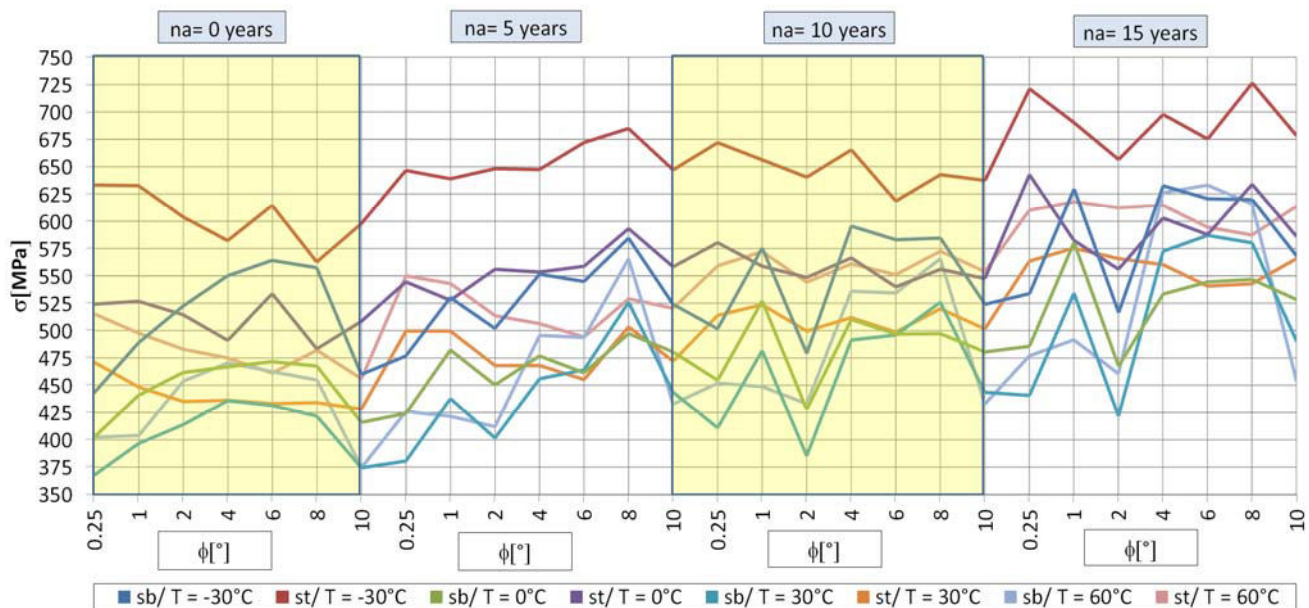
Fig. 9. The graphs of the Von Mises resultant efforts (b index for bending and t index for twisting)

As can be seen from the graphs, the Von Mises resultant effort increases simultaneously with the increase of the duration of the storage tank exploitation and with the increase of the bending or twisting angle of deformation of the storage tank shape.

For a clear representation of the decisive influence of the type of loads of the storage tank shape on the resulting effort Von Mises, the representation was made considering the variation of the resulting effort Von Mises for a constant temperature (T = ct.), the same bending or twisting angle of deformation (ϕ = ct.) and for the same moment of the operating period n_a.

The graphs of curves $\sigma = f(T, \phi)$ with these highlighted details are shown in figs. 10-13.

Fig. 10. The graphs of the Von Mises resultant efforts with highlighted details:
(T = 60 ^{0}C; n_a= {0, 5, 10 and 15 years}; ϕ = {0.25^0, 1^0, 2^0, 4^0, 6^0, 8^0 and 10^0})
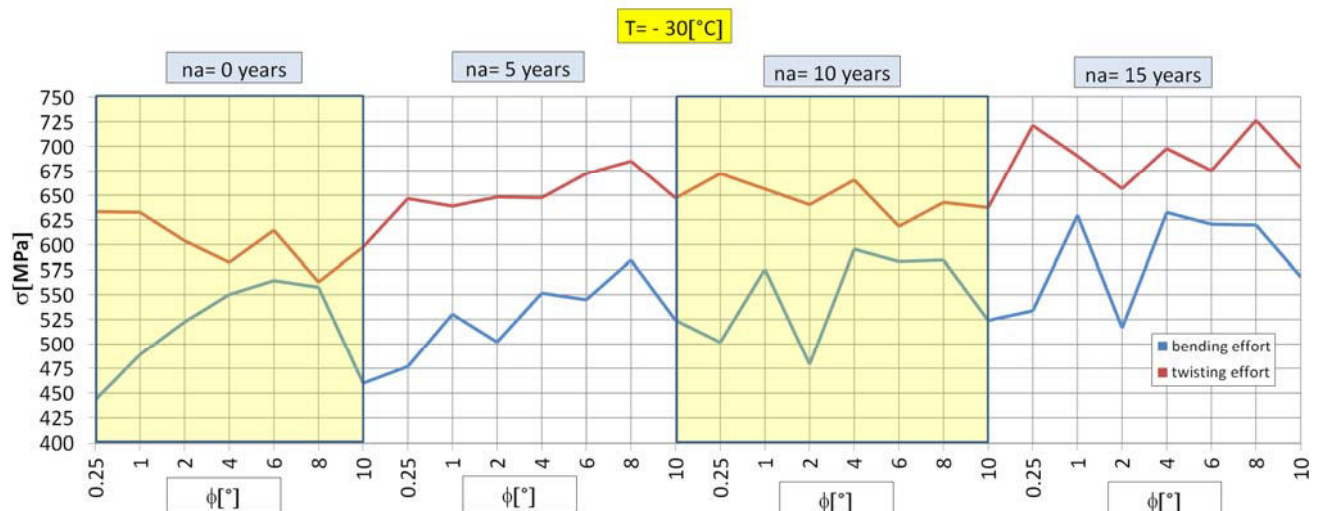
Fig. 11. The graphs of the Von Mises resultant efforts with highlighted details:
(T = - 30 ^{0}C; n_a= {0, 5, 10 and 15 years}; ϕ = {0.25^0, 1^0, 2^0, 4^0, 6^0, 8^0 and 10^0})

Fig. 12. The graphs of the Von Mises resultant efforts with highlighted details:
(T = 0 ^{0}C; n_a= {0, 5, 10 and 15 years}; ϕ = {0.25^0, 1^0, 2^0, 4^0, 6^0, 8^0 and 10^0})
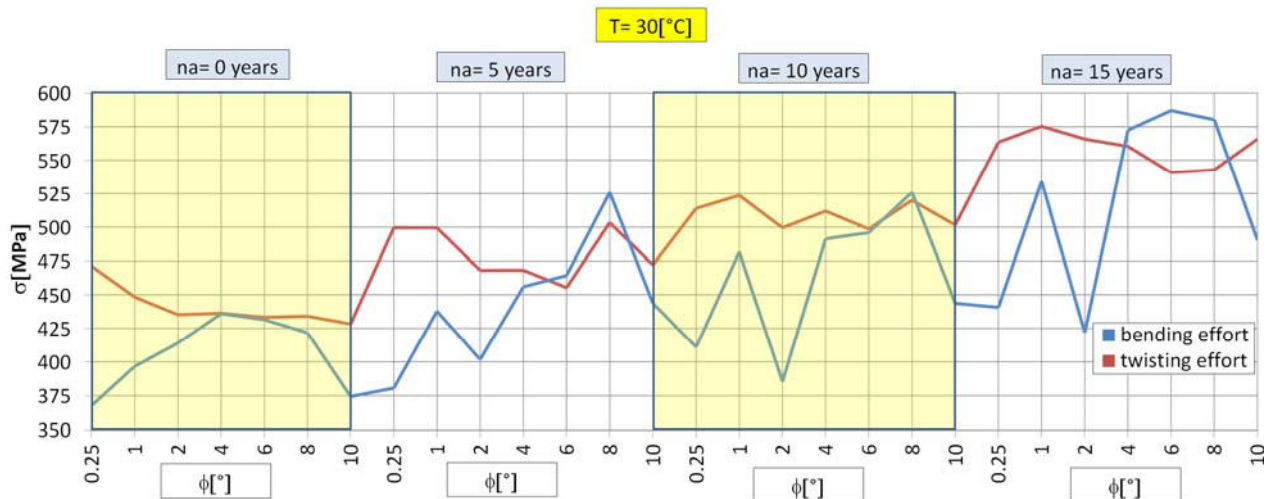
Fig. 13. The graphs of the Von Mises resultant efforts with highlighted details:
(T = 30 ^{0}C; n_a= {0, 5, 10 and 15 years}; ϕ = {0.25^0, 1^0, 2^0, 4^0, 6^0, 8^0 and 10^0})

In order to better highlight the evolution of the Von Mises effort was calculated the percentage variation of Von Mises resultant effort in relation to the initial effort status (table 4).

Table 6: The percentage variation ($\Delta\sigma$) of the Von Mises effort for n_a= 0; 5; 10 and 15 years

n_a [years]	$\Delta\sigma$ [%] ϕ [°]	T [°C] -30°	0°	30°	60°	n_a [years]	$\Delta\sigma$ [%] ϕ [°]	T [°C] -30°	0°	30°	60°
0	0.25	42.94	30.27	28.13	28.05	10	0.25	33.91	27.63	25.05	23.71
	1	29.39	19.45	13.03	23.19		1	14.01	6.01	8.71	27.47
	2	15.61	11.43	5.13	6.42		2	33.64	28.19	29.65	25.66
	4	5.84	5.17	0.08	0.92		4	11.73	11.02	4.17	4.66
	6	8.93	13.16	0.40	-0.26		6	6.09	8.65	0.54	3.12
	8	0.94	3.34	2.93	5.97		8	9.95	11.82	-1.14	1.23
	10	29.91	22.23	14.37	21.77		10	21.64	13.94	13.04	27.98
5	0.25	35.58	28.36	31.25	29.11	15	0.25	35.07	32.32	27.84	27.88
	1	20.48	9.40	14.09	28.81		1	9.61	0.32	7.69	25.67
	2	29.09	23.45	16.52	24.66		2	27.12	18.89	34.13	32.94
	4	17.38	16.05	2.68	2.15		4	10.30	13.04	-2.12	-1.85
	6	23.34	21.06	-1.93	0.09		6	8.81	7.94	-7.90	-6.08
	8	17.16	19.29	-4.29	-6.45		8	17.20	15.91	-6.45	-4.63
	10	23.48	16.17	6.40	20.24		10	19.38	10.90	15.41	35.12

The graphs of the percentage variation of Von Mises resultant effort ($\Delta\sigma$) in relation to the initial effort status for a constant temperature (T = ct.), the same bending or twisting angle of deformation (ϕ = ct.) and for the same moment of the operating period n_a are shown in fig. 14.
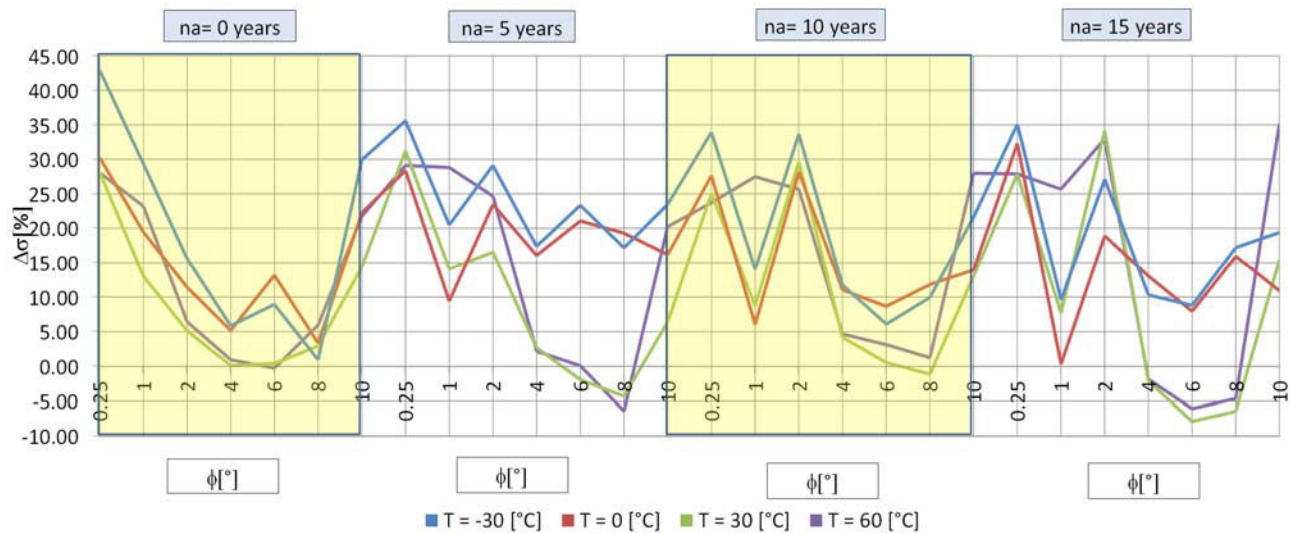
Fig. 14. The graphs of $\Delta\sigma$ for n_a= 0; 5; 10 and 15 years

The results of the variation of the resulting linear deformations *u* from table 5 are shown in a unitary structure in table 7.

Table 7: The variation of the resulting linear deformations *u* for n_a= 0, 5, 10 and 15 years

n_a [years]	ϕ [°]	T [°C]				T [°C]			
		-30°	0°	30°	60°	-30°	0°	30°	60°
		Bending				Twisting			
		u [mm]				u [mm]			
0	0.25	0.661	0.642	0.624	0.609	1.010	0.980	0.950	0.926
	1	0.666	0.652	0.639	0.629	0.995	0.962	0.931	0.903
	2	0.782	0.789	0.798	0.810	0.976	0.946	0.918	0.891
	4	0.789	0.797	0.807	0.818	0.999	0.967	0.935	0.905
	6	0.794	0.803	0.814	0.826	1.022	0.990	0.961	0.933
	8	0.803	0.811	0.820	0.831	1.017	0.986	0.956	0.928
	10	0.693	0.669	0.657	0.647	1.032	1.001	0.971	0.943
5	0.25	0.718	0.697	0.700	0.664	1.129	1.095	1.062	1.031
	1	0.729	0.715	0.702	0.691	1.081	1.047	1.014	0.983
	2	0.729	0.710	0.693	0.677	1.069	1.037	1.006	0.977
	4	0.876	0.885	0.894	0.905	1.087	1.054	1.025	0.996
	6	0.883	0.890	0.898	0.907	1.127	1.093	1.061	1.028
	8	0.891	0.898	0.907	0.917	1.116	1.084	1.053	1.025
	10	0.755	0.742	0.731	0.720	1.139	1.090	1.079	1.051
10	0.25	0.774	0.755	0.738	0.722	1.240	1.204	1.168	1.133
	1	0.795	0.781	0.768	0.757	1.199	1.162	1.132	1.103
	2	0.791	0.772	0.755	0.739	1.185	1.152	1.121	1.090
	4	0.969	0.978	0.988	0.999	1.190	1.157	1.126	1.097
	6	0.980	0.989	0.999	1.010	1.235	1.201	1.168	1.136
	8	0.989	0.997	1.007	1.017	1.231	1.197	1.164	1.132
	10	0.833	0.821	0.811	0.801	1.248	1.214	1.181	1.149
15	0.25	0.852	0.831	0.812	0.794	1.360	1.323	1.286	1.250
	1	0.855	0.842	0.831	0.822	1.318	1.281	1.246	1.224
	2	0.859	0.840	0.823	0.807	1.301	1.266	1.234	1.202

4	1.087	1.094	1.103	1.118	1.336	1.280	1.249	1.219
6	1.098	1.104	1.111	1.119	1.355	1.321	1.286	1.253
8	1.107	1.113	1.121	1.129	1.346	1.314	1.284	1.254
10	0.934	0.922	0.912	0.902	1.387	1.353	1.319	1.286

The graphs of curves corresponding to the resultant linear deformation $u = f(T, \phi)$ for $n_a = \{0$ years, 5 years, 10 years and 15 years$\}$; and for the same value of the bending or twisting angle: $\phi = \{0.25^0, 1^0, 2^0, 4^0, 6^0, 8^0$ and $10^0\}$ are graphically shown in fig. 15.
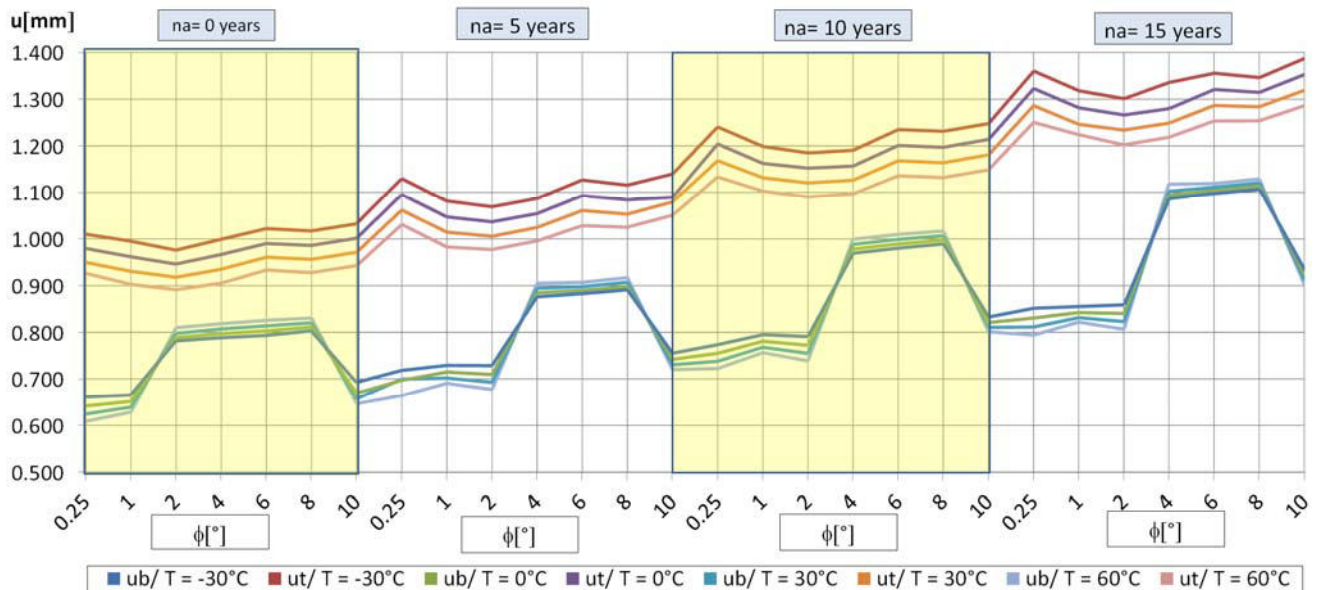
Fig. 15. The graphs of the variation of the resulting linear deformations u (b index for bending and t index for twisting)

For a clear representation of the decisive influence of the type of loads of the storage tank shape on the resulting linear deformation, the representation was made considering the variation of the resulting linear deformation for a constant temperature (T = ct.), the same bending or twisting angle of deformation (ϕ = ct.) and for the same moment of the operating period n_a.
The graphs of curves $u = f(T, \phi)$ with these highlighted details are shown in figs. 16-19.
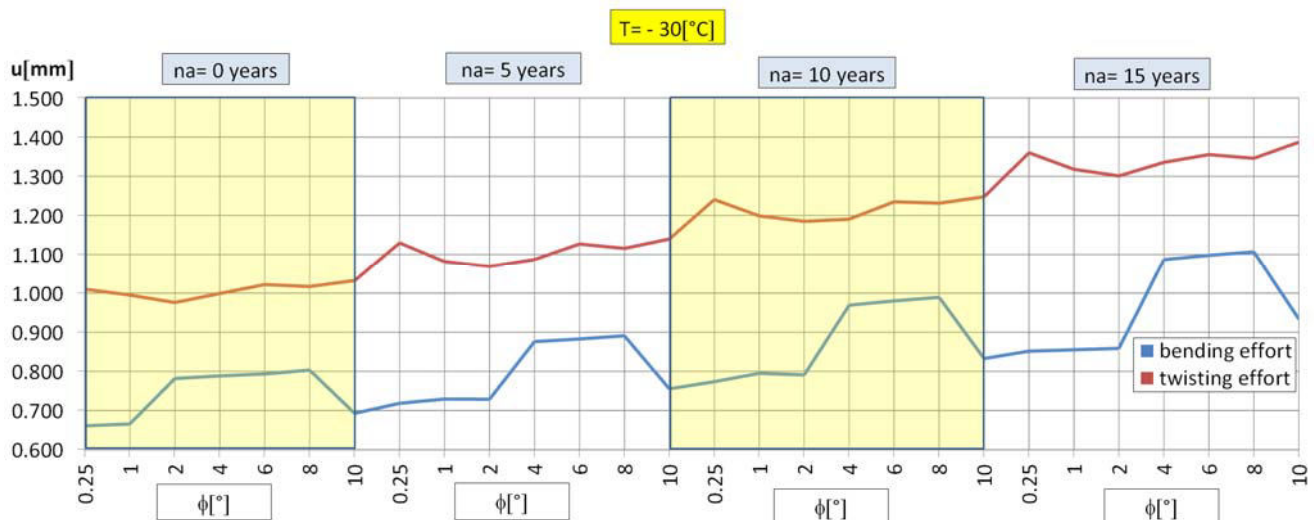
Fig. 16. The graphs of the variation of the resulting linear deformations u with highlighted details:
(T = -30 ^{0}C; $n_a = \{0, 5, 10$ and 15 years$\}$; $\phi = \{0.25^0, 1^0, 2^0, 4^0, 6^0, 8^0$ and $10^0\}$)
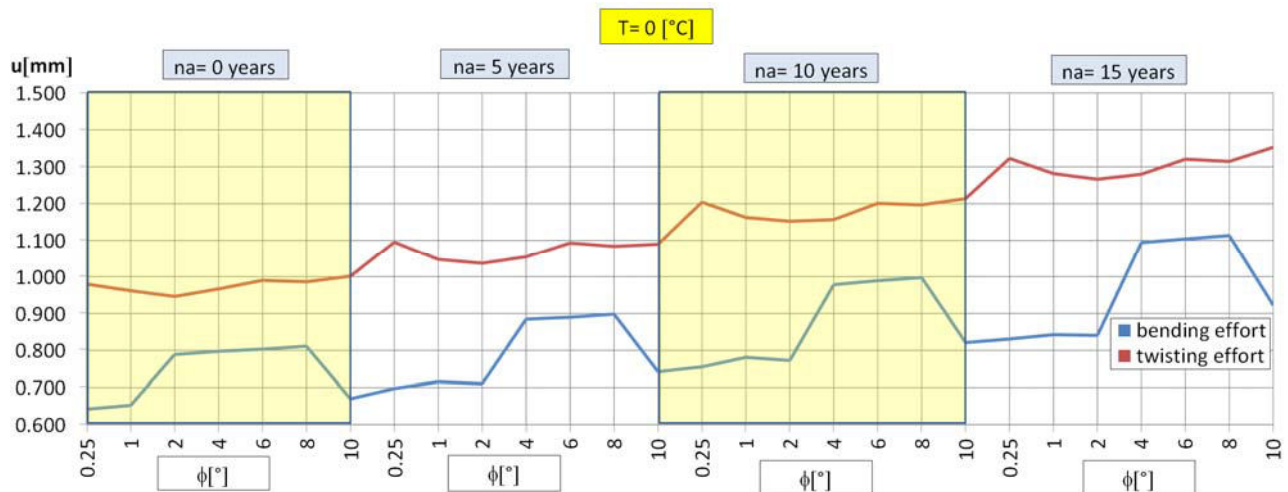
Fig. 17. The graphs of the variation of the resulting linear deformations u with highlighted details:
(T = 0 ^{0}C; n_a= {0, 5, 10 and 15 years}; ϕ = {0.25^0, 1^0, 2^0, 4^0, 6^0, 8^0 and 10^0})

Fig. 18. The graphs of the variation of the resulting linear deformations u with highlighted details:
(T = 30 ^{0}C; n_a= {0, 5, 10 and 15 years}; ϕ = {0.25^0, 1^0, 2^0, 4^0, 6^0, 8^0 and 10^0})

Fig. 19. The graphs of the variation of the resulting linear deformations u with highlighted details:
(T = 60 ^{0}C; n_a= {0, 5, 10 and 15 years}; ϕ = {0.25^0, 1^0, 2^0, 4^0, 6^0, 8^0 and 10^0})

In order to better highlight the evolution of the resultant linear deformation *u* was calculated the percentage variation to the resultant linear deformation *u* in relation to the initial status (table 4).

Table 8: The percentage variation (Δu) of the resulting linear deformations for n_a= 0; 5; 10 and 15 years

n_a [years]	Δu [%] ϕ [°]	T [°C] -30°	0°	30°	60°	n_a [years]	Δu [%] ϕ [°]	T [°C] -30°	0°	30°	60°
0	0.25	52.80	52.65	52.07	52.14	10	0.25	60.33	59.42	58.27	56.88
	1	49.51	47.57	45.55	43.60		1	50.75	48.84	47.33	45.77
	2	24.82	19.97	15.05	10.04		2	49.77	49.16	48.40	47.56
	4	26.69	21.22	15.83	10.62		4	22.83	18.24	13.97	9.77
	6	28.79	23.28	18.05	13.04		6	25.99	21.42	16.92	12.50
	8	26.61	21.56	16.57	11.70		8	24.45	19.99	15.61	11.34
	10	49.00	49.59	47.79	45.77		10	49.80	47.85	45.67	43.33
5	0.25	57.20	57.09	51.73	55.23	15	0.25	59.67	59.22	58.48	57.44
	1	48.27	46.45	44.48	42.30		1	54.07	52.12	49.87	48.94
	2	46.67	46.05	45.13	44.28		2	51.45	50.65	49.94	49.06
	4	24.04	19.18	14.56	10.03		4	22.91	16.95	13.26	9.01
	6	27.64	22.84	18.17	13.39		6	23.47	19.62	15.78	11.98
	8	25.20	20.66	16.09	11.79		8	21.62	18.07	14.54	11.04
	10	50.83	46.81	47.73	45.88		10	48.53	46.64	44.64	42.54

The graphs of the percentage variation of the resultant linear deformation (Δu) in relation to the initial status for a constant temperature (T = ct.), the same bending or twisting angle of deformation (ϕ = ct.) and for the same moment of the operating period n_a (from table 8) are shown in fig. 20.
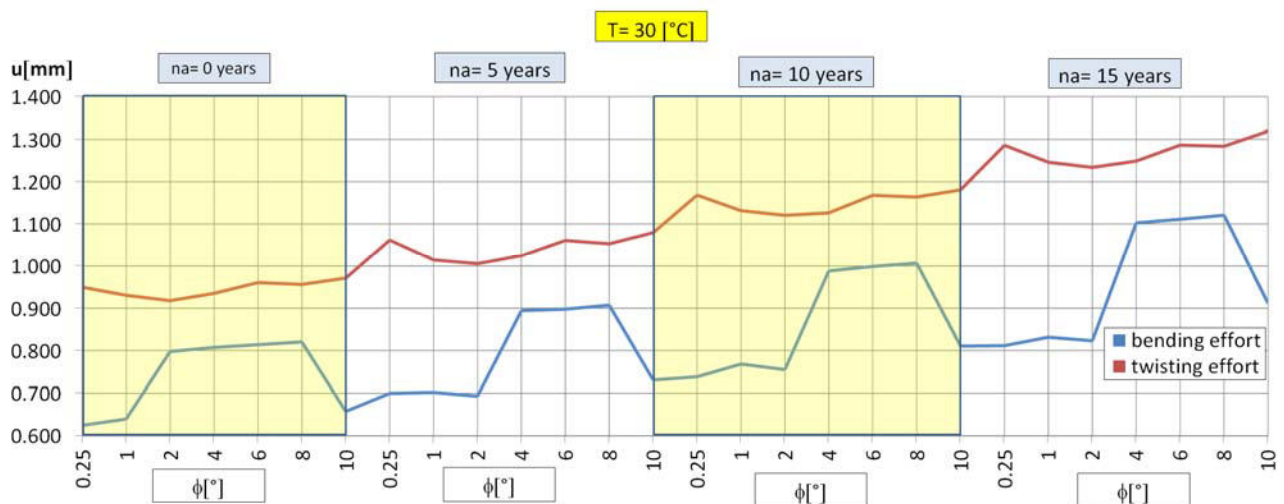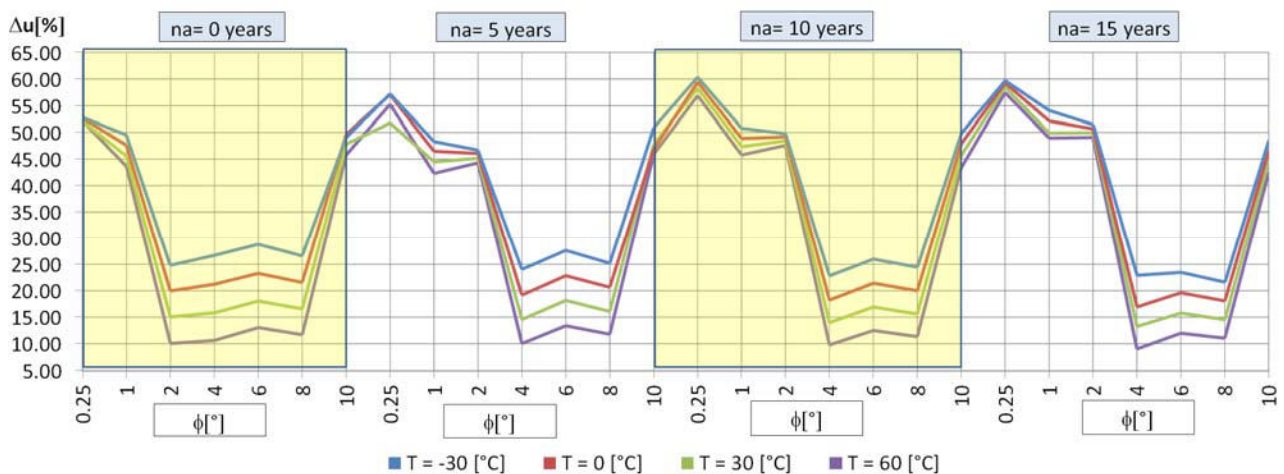

Fig. 20. The graphs of Δu for n_a= 0; 5; 10 and 15 years

3. Conclusions

Following the numerical analyses and the resulting graphs it has been found that:
- the values of the state of stress Von Mises for the twisting process are greater than the bending process. These graphs have an increasing character with maximum values for T = -30 ^{0}C.
- the percentage variation of Von Mises resultant effort ($\Delta\sigma$) has a maximum value of 42.94% for T = -30 ^{0}C. Also, an oscillatory variation is found in the range of -7.9 ≤ $\Delta\sigma$ ≤ 42.94 %.
- the values of the resultant linear deformation *u* for twisting process are greater than bending process. These graphs have an increasing character with a maximum value of *u* = 1.387 mm for

ϕ = 10 [°] and n_a = 15 years. Also, these graphs have an oscillatory variation in the variation range of 0.609 ≤ u ≤ 1.129 mm (the bending process) or of 0.891 ≤ u ≤ 1.387 mm (the twisting process).
- the percentage variation of resultant linear deformation (Δu) has a maximum value of Δu = 59.67 [%] for n_a = 15 years. These graphs have an oscillatory variation with maximum values for T = -30 ^{0}C.

References

[1] Ghiţă, C. Mirela, Anton C. Micu, Mihai Ţălu and Ştefan Ţălu. "Shape optimization of a thoroidal methane gas tank for automotive industry." *Annals of Faculty of Engineering Hunedoara - International Journal of Engineering, Hunedoara, Romania*, Tome X, Fascicule 3 (2012): 295-297.

[2] Ghiţă, C. Mirela, Anton C. Micu, Mihai Ţălu and Ştefan Ţălu. "Shape optimization of vehicle's methane gas tank." *Annals of Faculty of Engineering Hunedoara - International Journal of Engineering, Hunedoara, Romania*, Tome X, Fascicule 3 (2012): 259-266.

[3] Ghiţă, C. Mirela, Anton C. Micu, Mihai Ţălu, Ştefan Ţălu and Ema I. Adam. "Computer-Aided Design of a classical cylinder gas tank for the automotive industry." *Annals of Faculty of Engineering Hunedoara - International Journal of Engineering, Hunedoara, Romania*, Tome XI, Fascicule 4 (2013): 59-64.

[4] Ghiţă, C. Mirela, Anton C. Micu, Mihai Ţălu and Ştefan Ţălu. "3D modelling of a shrink fitted concave ended cylindrical tank for automotive industry." *Acta Technica Corviniensis – Bulletin of Engineering, Hunedoara, Romania*, Tome VI, Fascicule 4 (2013): 87-92.

[5] Ghiţă, C. Mirela, Anton C. Micu, Mihai Ţălu and Ştefan Ţălu. "3D modelling of a gas tank with reversed end up covers for automotive industry.", *Annals of Faculty of Engineering Hunedoara - International Journal of Engineering, Hunedoara, Romania*, Tome XI, Fascicule 3 (2013): 195-200.

[6] Ghiţă, C. Mirela, Ştefan C. Ghiţă, Ştefan Ţălu and Simona Rotaru, "Optimal design of cylindrical rings used for the shrinkage of vehicle tanks for compressed natural gas." *Annals of Faculty of Engineering Hunedoara - International Journal of Engineering, Hunedoara*, Tome XII, Fascicule 3 (2014): 243-250.

[7] Vintilă, Daniela, Mihai Ţălu and Ştefan Ţălu. "The CAD analyses of a torospheric head cover of a pressurized cylindrical fuel tank after the crash test." *Magazine of Hydraulics, Pneumatics, Tribology, Ecology, Sensorics, Mechatronics (HIDRAULICA)*, no. 4 (December 2017): 57-66.

[8] Bică, Marin, Mihai Ţălu and Ştefan Ţălu. "Optimal shapes of the cylindrical pressurized fuel tanks." *Magazine of Hydraulics, Pneumatics, Tribology, Ecology, Sensorics, Mechatronics (HIDRAULICA)*, no. 4 (December 2017): 6-17.

[9] Ţălu, Mihai. "The influence of the corrosion and temperature on the Von Mises stress in the lateral cover of a pressurized fuel tank." *Magazine of Hydraulics, Pneumatics, Tribology, Ecology, Sensorics, Mechatronics (HIDRAULICA)*, no. 4 (December 2017): 89-97.

[10] Ţălu, Ştefan and Mihai Ţălu. "The influence of deviation from circularity on the stress of a pressurized fuel cylindrical tank." *Magazine of Hydraulics, Pneumatics, Tribology, Ecology, Sensorics, Mechatronics (HIDRAULICA)*, no. 4 (December 2017): 34-45.

[11] Ţălu, Mihai and Ştefan Ţălu. "Design and optimization of pressurized toroidal LPG fuel tanks with variable section." *Magazine of Hydraulics, Pneumatics, Tribology, Ecology, Sensorics, Mechatronics (HIDRAULICA)*, no. 1 (March 2018): 32-41.

[12] Ţălu, Mihai and Ştefan Ţălu. "Analysis of temperature resistance of pressurized cylindrical fuel tanks." *Magazine of Hydraulics, Pneumatics, Tribology, Ecology, Sensorics, Mechatronics (HIDRAULICA)*, no. 1 (March 2018): 6-15.

[13] Ţălu, Ştefan and Mihai Ţălu. "Algorithm for optimal design of pressurized toroidal LPG fuel tanks with constant section described by imposed algebraic plane curves." *Magazine of Hydraulics, Pneumatics, Tribology, Ecology, Sensorics, Mechatronics (HIDRAULICA)*, no. 2 (June 2018): 14-21.

[14] Ţălu, Mihai and Ştefan Ţălu. "The optimal CAD design of a 3D hexagonal toroid with regular hexagonal cross-section used in manufacturing of LPG storage tanks." *Magazine of Hydraulics, Pneumatics, Tribology, Ecology, Sensorics, Mechatronics (HIDRAULICA)*, no. 2 (June 2018): 49-56.

[15] Ţălu, Mihai and Ştefan Ţălu. "The influence of corrosion and temperature variation on a CNG storage tank with a combined form consisting of a torus and a sphere." *Magazine of Hydraulics, Pneumatics, Tribology, Ecology, Sensorics, Mechatronics (HIDRAULICA)*, no. 4 (December 2019): 93-104.

[16] Ţălu, Mihai and Ştefan Ţălu. "Optimal design of a CNG storage tank with a combined form consisting of a torus and a sphere." *Magazine of Hydraulics, Pneumatics, Tribology, Ecology, Sensorics, Mechatronics (HIDRAULICA)*, no. 4 (December 2019): 73-82.

[17] Ţălu, Mihai and Ştefan Ţălu. "The influence of corrosion and temperature variation on the minimum safety factor of a 3D hexagonal toroid with regular hexagonal cross-section used in manufacturing of LPG storage tanks." *Magazine of Hydraulics, Pneumatics, Tribology, Ecology, Sensorics, Mechatronics (HIDRAULICA)*, no. 3 (August 2018): 16-25.

[18] Ţălu, Ştefan and Mihai Ţălu. "The influence of corrosion and pressure variation on the minimum safety factor of a 3D hexagonal toroid with regular hexagonal cross-section used in manufacturing of LPG

storage tanks." *Magazine of Hydraulics, Pneumatics, Tribology, Ecology, Sensorics, Mechatronics (HIDRAULICA)*, no. 3 (August 2018): 39-45.

[19] Ţălu, Mihai and Ştefan Ţălu. "Study of temperature–corrosion–torsion affecting factors on the shape of a toroidal LPG tank using the finite element method." *Magazine of Hydraulics, Pneumatics, Tribology, Ecology, Sensorics, Mechatronics (HIDRAULICA)*, no. 1 (March 2020): 21-32.

[20] Ţălu, Ştefan and Mihai Ţălu. "Numerical analysis of the influence of uniaxial compression loads on the shape of a toroidal LPG tank." *Magazine of Hydraulics, Pneumatics, Tribology, Ecology, Sensorics, Mechatronics (HIDRAULICA)*, no. 1 (March 2020): 47-58.

[21] Ţălu, Ştefan and Mihai Ţălu. "Constructive CAD variants of toroidal LPG fuel tanks used in automotive Industry." *Advances in Intelligent Systems Research,* vol. 159 (2018): 27-30. DOI: 10.2991/mmsa-18.2018.7.

[22] Ţălu, Mihai and Ştefan Ţălu. "3D geometrical solutions for toroidal LPG fuel tanks used in automotive industry." *Advances in Intelligent Systems Research,* vol. 151 (2018): 189-193. DOI: 10.2991/cmsa-18.2018.44.

[23] Ţălu, Mihai and Ştefan Ţălu. "Optimal engineering design of a pressurized paralepipedic fuel tank." *Annals of Faculty of Engineering Hunedoara - International Journal of Engineering, Hunedoara, Romania*, Tome XVI, Fascicule 2 (2018): 193-200.

[24] Ţălu, Ştefan and Mihai Ţălu. "The Influence of corrosion on the vibration modes of a pressurized fuel tank used in automotive industry." *DEStech Transactions on Materials Science and Engineering,* (2018): 1-6. DOI: 10.12783/dtmse/icmsa2018/20560.

[25] Ţălu, Ştefan and Mihai Ţălu. "CAD generating of 3D supershapes in different coordinate systems." *Annals of Faculty of Engineering Hunedoara - International Journal of Engineering, Hunedoara, Romania*, Tome VIII, Fascicule 3 (2010): 215-219.

[26] Ţălu, Ştefan and Mihai Ţălu. "A CAD study on generating of 2D supershapes in different coordinate systems." *Annals of Faculty of Engineering Hunedoara - International Journal of Engineering, Hunedoara, Romania*, Tome VIII, Fascicule 3 (2010): 201-203.

[27] Niţulescu, Theodor and Ştefan Ţălu. *Aplicaţii ale geometriei descriptive şi graficii asistate de calculator în desenul industrial. (Applications of descriptive geometry and computer aided design in engineering graphics).* Cluj-Napoca, Risoprint Publishing house, 2001.

[28] Bîrleanu, Corina and Ştefan Ţălu. *Organe de maşini. Proiectare şi reprezentare grafică asistată de calculator. (Machine elements. Designing and computer assisted graphical representations).* Cluj-Napoca, Victor Melenti Publishing house, 2001.

[29] Ţălu, Ştefan and Mihai Ţălu. *AutoCAD 2006. Proiectare tridimensională. (AutoCAD 2006. Three-dimensional designing)*. Cluj-Napoca, MEGA Publishing house, 2007.

[30] Ţălu, Ştefan. *Geometrie descriptivă. (Descriptive geometry)*, Cluj-Napoca, Risoprint Publishing house, 2010.

[31] Ţălu, Ştefan. *AutoCAD 2017*. Cluj-Napoca, Napoca Star Publishing house, 2017.

[32] Ţălu, Ştefan. *Micro and nanoscale characterization of three dimensional surfaces. Basics and applications*. Napoca Star Publishing House, Cluj-Napoca, Romania, 2015.

[33] Țălu, Mihai. *Calculul pierderilor de presiune distribuite în conducte hidraulice. (Calculation of distributed pressure loss in hydraulic pipelines).* Craiova, Universitaria Publishing house, 2016.

[34] Ţălu, Mihai. *Mecanica fluidelor. Curgeri laminare monodimensionale. (Fluid mechanics. The monodimensional laminar flow).* Craiova, Universitaria Publishing house, 2016.

[35] Ţălu, Mihai. *Pierderi de presiune hidraulică în conducte tehnice cu secţiune inelară. Calcul numeric şi analiză C.F.D. (Hydraulic pressure loss in technical piping with annular section. Numerical calculation and C.F.D.)*, Craiova, Universitaria Publishing house, 2016.

[36] Florescu-Gligore, Adrian, Ştefan Ţălu and Dan Noveanu. *Reprezentarea şi vizualizarea formelor geometrice în desenul industrial. (Representation and visualization of geometric shapes in industrial drawing).* Cluj-Napoca, U. T. Pres Publishing house, 2006.

[37] Ţălu, Ştefan and Cristina Racocea. *Reprezentări axonometrice cu aplicaţii în tehnică. (Axonometric representations with applications in technique).* Cluj-Napoca, MEGA Publishing house, 2007.

[38] Racocea, Cristina and Ştefan Ţălu. *Reprezentarea formelor geometrice tehnice în axonometrie. (The axonometric representation of technical geometric shapes).* Cluj-Napoca, Napoca Star Publishing house, 2011.

[39] Florescu-Gligore, Adrian, Magdalena Orban and Ştefan Ţălu. *Cotarea în proiectarea constructivă şi tehnologică. (Dimensioning in technological and constructive engineering graphics).* Cluj-Napoca, Lithography of The Technical University of Cluj-Napoca, 1998.

[40] Nedelcu, Dorian. *Proiectare şi simulare numerică cu SolidWorks. (Digital Prototyping and Numerical Simulation with SolidWorks)*. Timişoara, Eurostampa Publishing house, 2011.

[41] Ţălu, Ştefan. *Tehnologia de rulare a filetelor. (Thread rolling technology).* Cluj-Napoca, Napoca Star Publishing house, 2019.

[42] *** Autodesk AutoCAD 2020 software.

[43] *** SolidWorks 2020 software.

Recycling Household Waste

Prof. Dipl. Eng. **Elena SURDU**[1], Prof. Dipl. Eng. **Dana-Claudia FARCAȘ-FLAMAROPOL**[1]

[1] "Ion I.C. Bratianu" Technological High School in Bucharest, elena.surdu@yahoo.com;
claudia.flamaropol@gmail.com

Abstract: Waste management refers to the temporary storage, reuse, collection, transport, treatment, recycling and disposal of waste, the main purpose being the saving of the raw material by reusing recyclable waste, thus contributing to reducing the pressure on natural resources.
The most effective approaches to reduce the environmental impact are to prevent the uncontrolled disposal of waste and also to collect and recycle them.
Also, by recycling we can obtain new raw materials and also even thermal energy.
The social education of young people is a decisive factor to increase efficiency of long-term waste, collecting and recycling.

Keywords: Waste, recycling, collecting, environment

1. Introduction

A strong impact on natural resources has, first of all, the demographic expansion, which entails the necessity of an economic growth based on technological progress in the productive processes, responsible for ensuring the necessity of material consumer goods. There is a direct, proportional link between the pace of economic growth and that of the volume of waste, which contributes to the exacerbation of the conflict between the technosphere and the sphere.

With the demographic explosion and the revolution in agriculture and industry, waste has exceeded the capacity of the environment to absorb and neutralize them at a rate close to the rate at which they are generated. Demographic growth has led to an increase in the pace of expansion of habitable areas. Urbanization, as a phenomenon with profound implications in contemporary society, requires a significant and concentrated consumption of material and energy resources. Their transformation into goods and services, in addition to meeting material requirements, produces a large and diverse pollutant quantity, which requires, as a necessity increase the capacity to assimilate the environmental factors. The urban and the productive system extend on the basis of the protective and assimilative-dissipative systems.[1]

Unfortunately, a high rate of industrialization, beyond the positive perception in the direction of increasing the degree of civilization, contributes to the aggravation of the environmental and health problems by concentrating in a certain perimeter the different types of waste - urban and industrial.

The concept of waste, generally difficult to define, includes a wide category of products, variable in time and space, which, at least in relation to the intention and the degree of current use, has no special economic value, raising general problems of separation, storage and possibly revaluation.

Recycling is important both for the preservation of this healthy environment and for the reintroduction into the economic circuit of materials that are becoming increasingly difficult to find.

Waste recycling has become a major issue for the overall sanitation of the Earth, the magnitude of the phenomenon largely conditioning the economic development.

Waste recycling is defined as a process of reusing used or old materials and products for the creation of others, without resorting to new raw materials, considerably reducing the energy consumption needed to extract the raw materials, or to destroy any kind of waste.

The waste to be collected and recycled is [2]:

1. Non-hazardous waste from packaging (paper-cardboard, plastic, glass, metal) obtained from storage, handling, tertiary repacking and shipment of primary prepackaged products, as well as from current office activity.

  ➢ Paper waste (paper and cardboard packaging waste): cardboard boxes from various materials and products (from furniture, supplies, food, etc.), wrapping paper, scrap paper: documents, newspapers, magazines.

> ➤ Plastic waste: packaging waste from various products, consumables, foil type, PET, other plastic containers.
> ➤ Metal waste: packaging waste for beverages and food.
> ➤ Glass waste: packaging waste from food containers.

2. Hazardous waste and its packaging (mineral oils, car supplies, detergents, batteries and accumulators; fluorescent light bulbs and tubes; printer cartridges and toners, etc.).

3. Wastes from electrical and electronic equipment, resulting from the failure of office equipment during current activity or such products, damaged during storage or handling, as well as from electrical and electronic products returned by customers.

4. Household waste and assimilated to them, arising from current office, cleaning and maintenance activities.

Domestic waste contains large quantities of reusable materials that can be collected and used.

Waste is any object that is no longer used and thrown away.

2. Reduction of household waste

Recycling is the process of processing waste for reuse; almost all materials that enter the waste composition: paper, glass, plastic packaging, metal boxes can be recycled;

For the purpose of recycling, the waste is collected on a minimum of 4 fractions (paper-cardboard, plastic, glass, metal);

Selective collection is one of the recycling stages, together with the separation and processing of some of the waste components, in order to transform them into useful products; selective waste collection is a process that is available to everyone and involves storing waste in special places for recycling.

Natural resources are limited and do not regenerate very quickly, while the amount of waste increases reaching large areas of land. It is very important to understand that almost half of the waste we dispose of can be reused. The environment is increasingly polluted, and we, by recycling waste, are trying to save the environment and the earth. [3, 4]

Advantages of selective collection:
> ➤ Conservation of natural resources;
> ➤ Reducing the level of harmful emissions from the air - reducing pollution;
> ➤ Decreasing the quantity of waste;
> ➤ Eliminating the transformation of some areas into outbreaks of infection;
> ➤ Energy saving;
> ➤ Keeping a cleaner environment for us and future generations;
> ➤ Increasing the quality of life and health of children;
> ➤ Reducing costs, including the degree of sustainability.
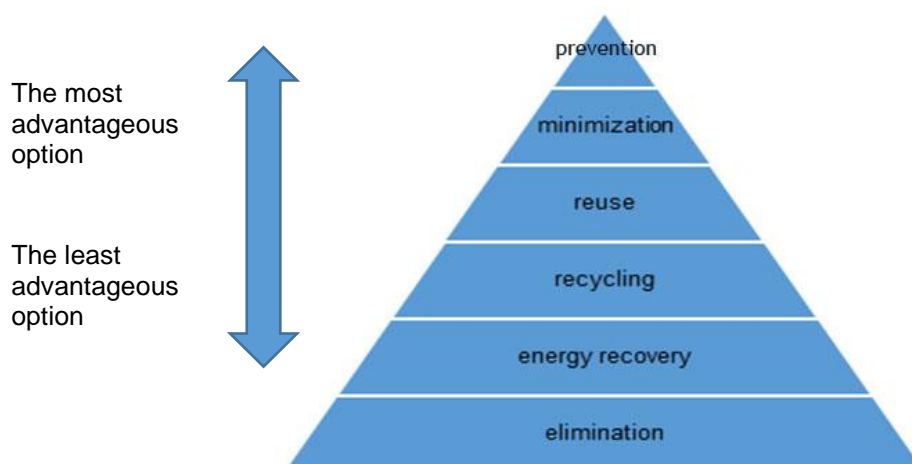
3. Waste management

Fig. 1. The hierarchy of waste management [5]

Waste hierarchy refers to: reduction (prevention and minimization), reuse and recycling (energy recovery), which classifies waste management strategies according to their opportunity in terms of waste minimization. This waste hierarchy aims to obtain maximum practical benefits from products and to generate a minimum amount of waste.
The most effective environmental solution is to reduce (by preventing and minimizing) the generation of waste, and the products and materials can sometimes be reused for the same or different purpose.

4. Methods of municipal waste management

According to the hierarchy, the most efficient environmental solution is to reduce (by preventing and minimizing) the generation of waste, and the products and materials can sometimes be reused for the same or different purpose. Recovery of resources from waste (recycling and composting), recovery and capitalization through energy generation from waste (anaerobic digestive, incineration) are the first options used, and the last option is the disposal of waste. [6]
In addition to the methods mentioned above, the following treatment methods are also used:
1. Recycling - involves the processing of used materials into new products, in order to prevent the transformation into waste of potentially useful material (figure 2). Recyclable materials include many types of glass, paper, metal, plastic, textile and electronics. Separate waste at the source is transferred to waste sorting facilities. In these specialized installations, recyclable materials are received, separated and prepared for marketing to end-user producers.
2. Biological treatment - uses live microorganisms for the decomposition of organic waste either in water, CO_2 and simple inorganic materials or in simple organic materials (aldehydes and acids). The main biological treatment methods used in the EU are aerobic (composting) and anaerobic treatment. The resulting products are compost used in agriculture or landscaping, and in the case of anaerobic digestion, biogas that can be used for energy production (figure 3).
3. Incineration - it is used as a treatment for a very wide range of waste. Waste incineration is to treat waste in such a way as to reduce its volume and hazard, to capture or destroy potentially hazardous substances that are or may be released during incineration. Incineration processes can provide means to enable the recovery of energy, mineral and / or chemical content from waste. Thus, during incineration, combustion gases are created that contain most of the available energy in the form of heat (figure 4)
4. Waste landfill - landfill, which involves waste management, with a reduced or non-existent prior treatment (figure 5). Biodegradable waste landfill has as a result the formation of the storage gas. The main impact of municipal waste management is considered the existing methane in the waste gas, in the form of greenhouse gas. The storage at the landfill must be reserved for stable waste, which can no longer be used. The storage gas can be collected or disposed of by combustion or it can be used as fuel. All municipal waste components are accepted for storage, including the residual fractions remaining after the separation of the recycling materials and the residues from the processes prior to the treatment (incineration and biological treatment).

Fig. 2. Waste recycling [10]

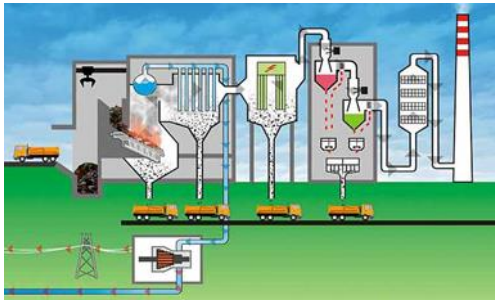**Fig. 3.** Biological waste treatment station [11]

Fig. 4. Waste incineration [12]

Fig. 5. Waste disposal [13]

5. Methods of municipal waste management

The environmental legislation establishes that the application of a hierarchy of waste, a hierarchy through which the actions of waste generation and management are efficient, thus reducing the negative effects on the environment and population health, by:
- Prevention of waste generation;
- Preparation for reuse;
- Waste recycling;
- Other operations of recovery (energy recovery);
- Disposal of waste.
The management of household waste is based on legislation:
  ➢ OUG 1955 regarding the protection of the environment, with the subsequent modifications and completions
  ➢ OUG no 196 2005 on the Environmental Fund with subsequent amendments and completions
  ➢ Law no. 211 2011 on the regime of waste republished with amendments and completions transposes the Waste Framework Directive 2008 98 / as well as the Directive no 851 2018 amending the 2008 Directive 98 / CE on waste
  ➢ Law No 249 2015 on the regime of packaging and packaging waste with subsequent amendments and completions transposes Directive 94 62 1994 CE on packaging and packaging waste as well as Directive 852 2018 which amends Directive 94 62 1994 CE
  ➢ Commission Decision 2014 955 / EU of 18 December 2014 amending Decision 2000 532 / CE establishing a list of waste under Directive 2008 98 / CE
  ➢ Government Decision no. 856 2002 on the records of waste management
  ➢ Government Decision no 1061 2008 on the transport of hazardous and non-hazardous waste on the territory of Romania
  ➢ Order no 1362 2018 regarding the approval of the Procedure for authorization, annual approval and withdrawal of the right of operation of the organizations that implement the obligations regarding the extended liability of the producer
  ➢ Law on sanitation services for localities no 101 2006. [7]

6. Statistical data

Romania produces 5.8 million tonnes of waste per year, with an average of 272 kilograms per year per capita and with a collection rate of only 82.3% (as Waste Atlas study shows). Of the total waste, 56% is organic matter, 9.9% paper and cardboard, another 9.9% represents plastic waste, 4% glass, 2.3% metal and 17.8% other types of waste. Romania recycles only 3%, followed by Bulgaria with a recycling rate of 0%. The collection rate of Romania is 82.3%, followed by Bulgaria with 81% and Estonia 79%.
Of the total 5.8 million tons of waste per year, only Bucharest is responsible for producing 709,720 tons per year, with an average of 375kg per capita.

Table 1: Amount of waste in different countries [9]

Countries	Amount of waste produced		Recycling rate %	Collection rate %
	tons / year	Kg / inhabitant		
Germany	50.5 mil	617	47	100
Slovenia	852.075	414	55	100
Sweden	4.3 mil	458	33	100
Denmark	4.1 mil	747	28	100

The figures on the amount of waste per capita mentioned nationally in the Waste Atlas are similar to those reported by Eurostat for 2016, of 261 kg.

The EU Member State that produces the largest amount of waste is Germany, with a figure of 50.5 million tonnes per year and 617 kg per capita. However, Germany also has the second highest recycling rate of 47%, plus a collection rate of 100%.

Slovenia is the EU Member State with the highest percentage of recycled waste, 55%, plus a collection rate of 100%. However, Slovenia produces only 852,075 tonnes of waste per year, with 414 kg per capita. Sweden produces 4.3 million tonnes per year, i.e. 458 kg per capita, but also has a recycling rate of 33%, plus a collection rate of 100%.

According to the number of inhabitants, Denmark has the highest rate of waste per capita, of 747 kg per year, which amounts to 4.1 million tonnes per year. It also has a collection rate of 100% and a recycling rate of 28%.

Also, worth mentioning are the United Kingdom, which has a recycling rate of 28% at a total amount of 30.7 million tonnes per year, the Netherlands and Austria - both with a recycling rate of 24% - or Italy with 26%.

Table 2: Evolution of waste generation [8]

Residence environment	Generation indicator (kg / inhabitant / day)				
	2015	2016	2017	2018	2019
Urban	0.66	0.66	0.65	0.65	0.64
Rural	0.31	0.31	0.30	0.30	0.29

Table 3: Amounts of municipal waste at national level [8]

Types of municipal waste	Quantity (tonnes / year)				
	2015	**2016**	**2017**	**2018**	**2019**
Domestic waste mixed and separated	3615166	3598678	3586583	3506695	3498851
Assimilable waste collected in the mix and separately	903791	899670	896646	876674	874713
Waste from gardens and parks	97400	97400	97400	97400	97400
Waste from markets	71800	71800	71800	71800	71800
Waste from the street	336800	336800	336800	336800	336800
Total of municipal waste	5024957	5004348	4989229	4889369	4879563
Indicators for municipal waste generation (kg/loc x an)	253	253	253	248	248

Table 4: Composition of household waste and assimilation [8]

Types of waste	Ratio (%)				
	2015	**2016**	**2017**	**2018**	**2019**
Paper and cardboard	11.9	11.9	11.9	12.0	12.2
Metals	2.7	2.7	2.7	1.8	2.0
Plastic	11.7	11.7	11.7	11.5	11.3

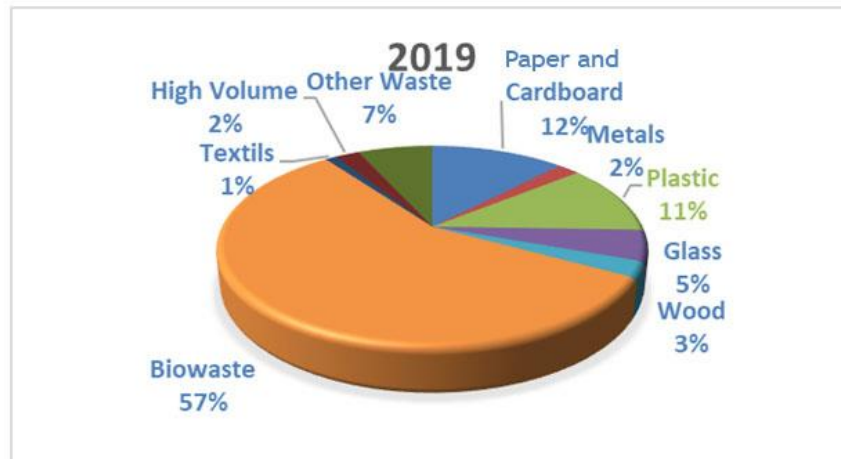| Glass	5.1	5.1	5.1	5.0	5.0
Wood	2.2	2.2	2.2	2.5	2.5
Bio-waste	57.9	57.9	57.9	57.5	57.0
Textiles	0.9	0.9	0.9	1.0	1.0
High Volume	0.9	0.9	0.9	2.0	2.2
Other Waste	6.7	6.7	6.7	6.7	6.8

Fig. 6. Waste collection weight at national level [8]

7. Conclusions

In the socio-economic systems, the largest share of waste was and continues to be considered unusable, the main concern related to their management being the identification of disposal solutions. Waste management is based on the four major principles (prevention, recycling, recovery and disposal), which must lead to the continuous improvement of the quality of life for present and future generations, by creating sustainable communities, capable of managing and using resources in a way efficient and to harness the potential of ecological and social invocation of the economy, in order to ensure environmental protection and social cohesion.

The selective collection of waste at the locality level, regardless of its type and the methods of waste disposal by incineration so as to obtain thermal energy that can be used for heating the houses or for heating the domestic water leads to a successful recycling of the domestic waste.

As a member state of the European Union, Romania has to meet, by 2020, according to European directives, the following objectives: minimum 50% rate of reuse and recycling from the total mass of the quantities of waste (paper, metal, plastic and glass), minimum 70% level of preparation for reuse, recycling and other material recovery operations of minimum 70% by mass of non-hazardous waste from construction and demolition activities, 60% recovery of packaging waste from total packaging introduced on the national market. Also, our country will have to reach, annually, a collected quantity of electronic waste of 4 kg / inhabitant and to collect separately the bio-waste in order to compost and ferment them.

References

[1] Constantinescu, N.N. *Dilemmas of transition to market economy / Dileme ale tranziţiei la economia de piaţă*. Bucharest, AGER – Economistul Publishing House, 1992.
[2] Angelescu, A., I. Ponoran, and V Ciobotaru. *Environment and sustainable development / Mediul ambiant şi dezvoltarea durabilă*. Bucharest, ASE Publishing House, 2003.
[3] Cămășoiu, C. *Economy and the defiance of nature / Economia şi sfidarea naturii*. Bucharest, Economic Publishing House, 1994.
[4] Părăușanu, V., and I Ponoran. *Environmental Economics / Economia mediului*. Bucharest, Sylvi Publishing House, 1997.

[5] Vișan, S., A. Angelescu, and C. Alpopi. *The environment. Pollution and protection / Mediul înconjurător. Poluare şi protecţie*. Bucharest, Economic Publishing House, 2000.

[6] Antonescu, N.N., N. Antonescu, P.-D. Stănescu, and L.L. Popescu. *Management and treatment of urban waste / Gestiunea si tratarea deseurilor urbane.* Bucharest, Matrix Rom Publishing House, 2006.

[7] http://www.anpm.ro/web/apm-constanta/cadru-general/.

[8] http://www.mmediu.ro/app/webroot/uploads/files/PNGD_vers5.pdf.

[9] http://www.ecoteca.ro/compostarea-deseurilor-aspecte-esentiale.html.

[10] http://www.business24.ro/software/produse-software/secretul-eficientei-companiilor-de-reciclare-o-solutie-software-pentru-managementul-deseurilor-1586518.

[11] https://republikanews.ro/statia-de-tratare-mecano-biologica-de-la-ploiesti-este-gata-acum-se-cauta-operatorul-care-sa-o-puna-in-functiune/.

[12] http://greenly.ro/deseuri/procedeul-de-tratarea-a-deseurilor-incinerarea.

[13] http://www.radioresita.ro/311265/amenajarea-depozitului-de-deseuri-inerte-din-zona-fantanele-arad-pe-fagas-normal.

Wastewater Purging. Case Study

Prof. Dipl. Eng. **Dana-Claudia FARCAȘ-FLAMAROPOL**[1], Prof. Dipl. Eng. **Elena SURDU**[1]

[1] "Ion I.C. Bratianu" Technological High School in Bucharest, claudia.flamaropol@gmail.com; elena.surdu@yahoo.com

Abstract: The treatment of the used water is a vital component in any industrial process, because it provides the necessary conditions so that the water can be reused under optimal conditions. In addition to traditional methods and procedures, more and more advanced methods are being sought to complete these processes, making them more efficient and faster, but with lower costs. Of these methods, an effective one is adsorption which has a good efficiency, although it cannot remove pollutants in very small or very high concentrations. Among the most commonly used adsorption treatment methods are the one with active carbon and the one by ion exchange on cations.
One of the concrete solutions found is the use of pure oxygen in the decanting technique. This is exemplified by the BASF decanting facility in Ludwigshafen care using pure oxygen for nitrification through Messer gaskets.
Another concrete case for the depollution of waste water refers to those arising from the processes of manufacturing smoke-free powders by adsorption on activated carbon. In this case, the materials used were Nano carbon powders and activated carbon obtained from charcoal grinded beech wood.

*Keywords: Adsorbents, adsorption, pollutant, water depollution*

1. Introduction

In modern era, it was reached the step in which it utilizes the water, the key element of life on Earth, more and more, this way reaching an irrational and inadequate consumption that made this resource become polluted.

In our country, around 31% of utilized waters are evacuated without being purged, 41% are insufficiently purged and 28% are purged correctly.

Water pollution represents the alteration of physical, chemical and biological water qualities, made directly or indirectly, in a natural or anthropogenic way, that can happen continuously or discontinuously, temporary or accidentally.

Water purging represents the decrease of pollutant concentrations at enough low concentrations not to pollute reception waters. It is realized with the help of numerous machinery that make up the purging stations from which result purged waters and sludges, that can be used as fertilizers in agriculture. The EU legislation and policy impose that the pressure impact on water should be decreased significantly.
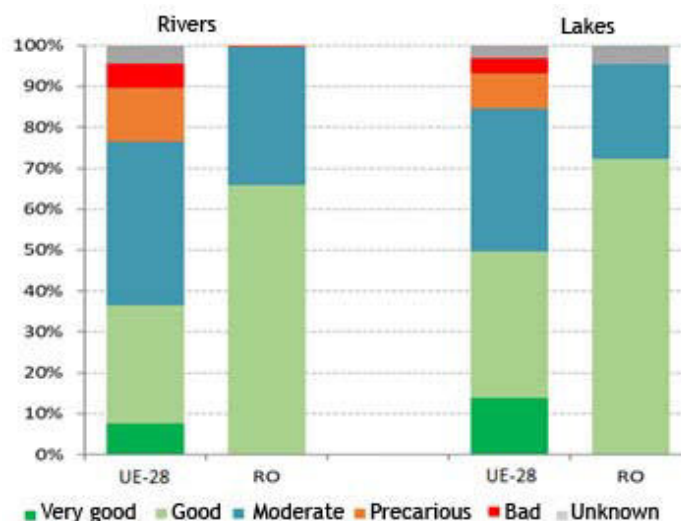
Fig. 1. The ecological status or potential of surface water bodies in Romania [8].

2. Processes and methods of depollution of industrial wastewater

Purging processes are of physical-mechanical, chemical and biological nature. They have the role to obtain an yield as high as possible of impurities elimination that exist in wastewaters, with the goal of giving them back to the surface water circuit at normal parameters in terms of legal norms.
In every purging station exist three stages:
➢ Primary stage (mechanical) with role of retaining coarse substances with the help of grills, sieves and decanters.
➢ Secondary stage (biological) where remaining organic matter break down using microorganisms.
➢ Third stage (biological, mechanical or chemical) that doesn't exist all the time and where mineral and organic non-biodegradable substances are eliminated using neutralization, precipitation, coagulation and flocculation reactions.
More and more are utilized modern wastewater depollution methods such as:
➢ Intensification of the electrochemical processes for the treatment of the residual sludge,
➢ Elaboration and utilization of coagulants
➢ Utilization of membranous matter
When normal functioning of the purging station is not affected it is recommended to purge in the same time the industrial wastewater and the sewage, because they have some advantages, such as: [2]
➢ Optimal development of the purging process, due to the nutritive substances contained by the industrial wastewater
➢ The existence of one wastewater treatment plant, in which both types of wastewater are treated, can reduce the purification costs and increase the cooperation between industry and populated center for water purification
➢ The existence of only one plant responsible for the purification of the entire water in the populated center, giving an increased efficiency of exploitation.

3. Advanced wastewater treatment methods through adsorption

Advanced purification consists of supplementary processes meant to remove substances in suspension and the dissolved ones that remained after the two conventional purification stages. It can be incorporated in the biological process or removed after the secondary stage.
The principal wastewater pollution removal processes are: [3]
➢ Biodegradation- low-cost technology that requires optimal environment conditions
➢ Coagulation- simple technology that produces high quantities of waste that are hard to remove
➢ Membrane separation- allows the removal of a wide range of pollutants, but allows the treatment of a big volume of wastewater
➢ Processes based on biomass- cheap but slow processes
➢ Absorption- big efficiency but doesn't remove pollutants in very small or very big concentrations
➢ Ion exchange- has limitations regarding the species that can be purified
➢ Oxidation- fast and efficient process but with a high cost
➢ Advanced oxidation processes- don't produce waste, are efficient, but in some cases appear toxic by-products

3.1. Purification through absorption with active carbon

Adsorption is a surface phenomenon. After absorption, the grade of pollutants in solutions decreases but doesn't disappear completely. When the quantity of unpurified pollutant is small, it is carried downstream in the emissary. Absorption is much utilized because of its variety of absorbents and the possibility of reutilization in multiple absorption-desorption cycles. Adsorbents can be capillary systems or powders in suspension. From all the adsorbent materials the most common are the vegetal, artificial or animal active carbons, the clays, the synthetic resins, the polymers etc.
Active carbon is utilized on a large scale for wastewater purification. It has the specific surface extremely big, because of the pores, being able to reach hundreds of m^2/gram.

Another important feature of active charcoals is the affinity for various types of pollutants. They have medium efficiency in removing heavy metals, which can be increased through the optimization of the period in which the wastewater comes in contact with the adsorbent.
After some researches it was revealed that the utilization of active charcoal in industrial wastewater purification disolves partially or totally solid impurities according to the quantities and requires a big capacity of oxygen, as shown in figure 2.
Active charcoal can be reutilized by heating it at 900 $^{\circ}$C, temperature at which it was created and when all the impurities that were adsorbed are released.
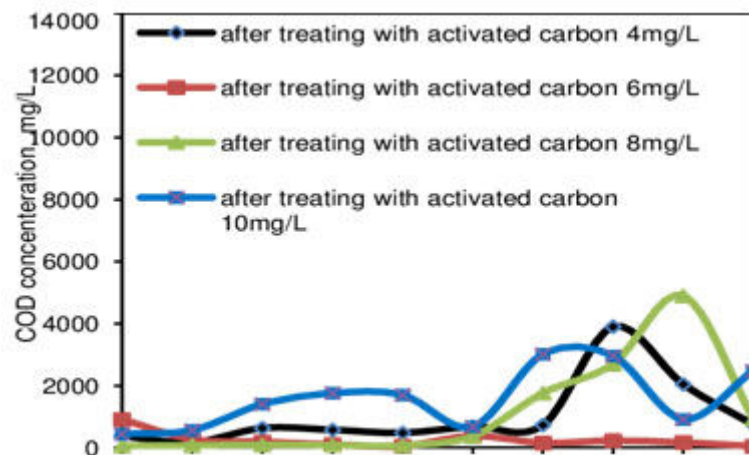

Fig. 2. Chemical concentration of oxygen depending on the amount of activated carbon [4]

In figure 3 it is shown a simplified model of the interaction of the 4 A factors (active charcoal, dissolved oxygen, microorganisms and pollutants). The reaction between the active charcoal and pollutants is the adsorption effect of the active charcoal, and the reaction depends of their characteristics.
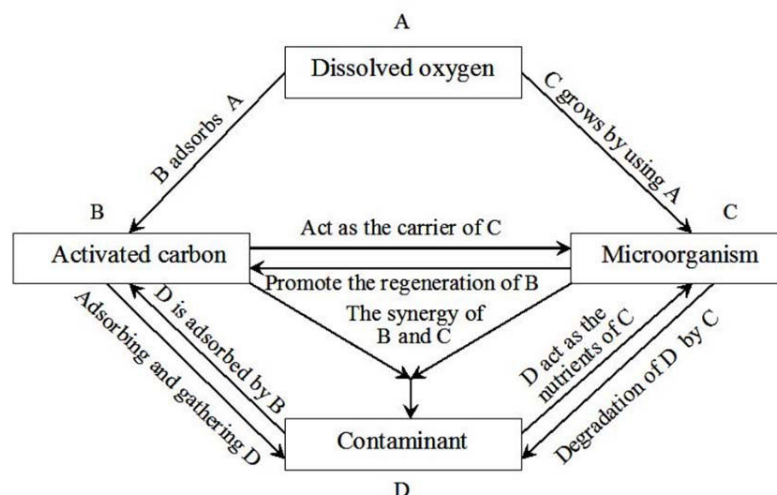
Fig. 3. Simplified interaction model of factors in BAC process [5]

3.2. Ion exchange adsorption on cationites

Ion exchange adsorption refers to the replacement of some ions from the solution with the adsorbents ions.
Very important for this method is the fact that some ions retained on the exchanger can be put back into the solution and the regenerated exchanger can be reutilized. [6]
An ionic species situated into an aqueous electrolyte solution interacts with an adsorbent solid material.

4. Case studies

4.1. Pure oxygen utilization in the decanting technique

Pure oxygen is the concentrated oxygen without nitrogen ballast that can be released into the water fast and at low costs.

Such a supply of pure oxygen has numerous advantages, including the economic one if it is being used through an adequate installation technology, taking into consideration the utilization and local conditions (ex. Special evacuation installations with hose, injectors and oxidizers) as it is represented in figure 4. To fix a problem that shows up when at the decantation installation appears oxygen shortage, serious odor problems, an Emscher decantation installation was introduced, with spillage and an additional supply of pure oxygen.

Fig. 4. The charging procedure developed by Messer for pure oxygen: gas hose (left), injectors (center), oxidizer (right) [7]

In the biological stage, the traditional aeration was supplemented with oxygen in order to eliminate the nitrogen, figure 5, and lifting the biological mass in the system.
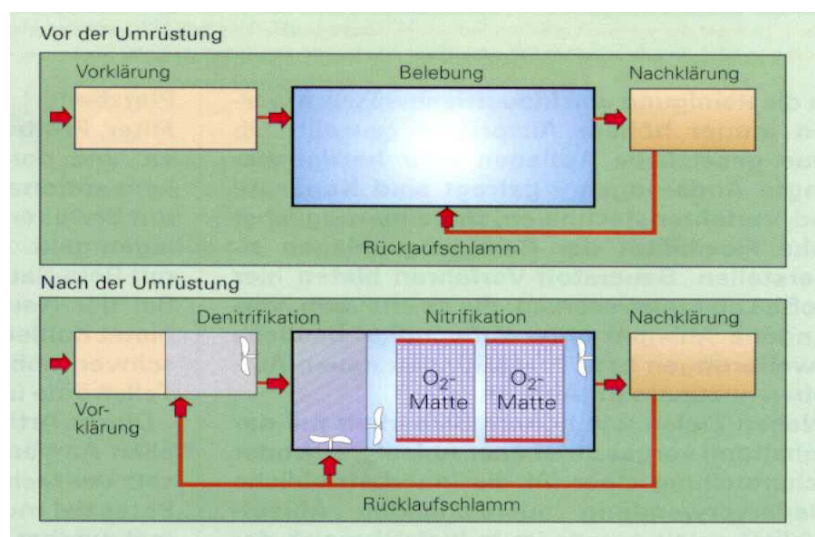
Fig. 5. Schematic representation of the conversion of a clearing installation for the Biox®-N procedure [7]

For low stabile leakage values the biofiltration procedures are utilized, at which the continuous vertical filter uses the quartz sand as a filtering medium.

These are some of the applications in which the oxygen is successfully used in effective purification of industrial wastewater.

4.2. The depollution of waste water from the processing of smoke-free powders and the recovery of ethyl alcohol from them using adsorption / desorption processes on activated carbon

This method is based on the adsorption of ethylic alcohol on two types of materials, carbonic adsorbents, the active charcoal obtained out of ground beech wood charcoal and the Nano carbonaceous powder obtained through laser pyrolysis, followed by its recovery by desorption, which is realized by taking the steam through active charcoal and collecting it in special recipients. From the experimental data resulted the following:

➢ Ethanol adsorption on active charcoal is net superior to the adsorption on carbonic Nano powders.
➢ carbonic Nano powders have different adsorbent capacities compared to ethanol
➢ The chosen method for the determination of adsorbed capacities is advantageous because all the determinations can be made without the need to open the thermostat enclosure and to expose the samples in the atmosphere outside the enclosure. [1]

The process is important because: the toxic substances from the waste water, which can be recycled, are eliminated, the recovered ethanol is reintroduced into the technological process, and the activated carbon is regenerated and reused. The use of this process at industrial level leads to lower costs of producing smoke-free powders and implicitly to the protection of the environment.

5. Conclusions

The biggest problem of pollution is the disposal of industrial waste water in natural water resources due to non-compliance with the legislation in force and insufficient treatment resources.

In the few industrial enterprises that our country still has wastewater treatment should be carried out through a combination of complex biological, chemical and physical procedures.

To eliminate these problems, that are quite serious, Romania should invest much larger amounts for the introduction of wastewater treatment plants from different industrial fields in order to ensure the discharge of clean water in the rivers that cross our country.

Another solution would be the reopening of research institutes, which could find modern and inexpensive solutions designed to help purify industrial wastewater.

Perhaps the most important thing that could be done in Romania would be for all citizens to be aware of the consequences of water pollution and to try by any means to help stop this.

References

[1] Petrea, Nicoleta. *Ecological depollution of industrial wastewater containing toxic substances / Depoluarea ecologică a unor ape uzate industriale conţinând substanţe toxice*. PhD Thesis, Technical University of Civil Engineering of Bucharest, 2012.
[2] Vișan, S., A. Angelescu, and C. Alpopi. *The environment. Pollution and protection / Mediul înconjurător. Poluare şi protecţie*. Bucharest, Economic Publishing House, 2000.
[3] Baciu, D. *Water pollution. Depollution technologies*. Cluj-Napoca, Risoprint Publishing House, 2003.
[4] https://www.researchgate.net/publication/315552769_Industrial_Wastewater_Treatment_Improvements_Using_Activated_Carbon.
[5] https://www.intechopen.com/books/biomass-now-cultivation-and-utilization/biological-activated-carbon-treatment-process-for-advanced-water-and-wastewater-treatment.
[6] http://www.amac.md/Biblioteca/data/17/08/Romania/78-Analize-Fizico-chimice-Si-Metode-Avansate-de-Epurare-a-Apelor-Uzate.pdf.
[7] http://www.messer.ro/Aplicatii/Protectia_mediului_si_reciclarea_deseurilor/Purificarea_apelor_uzate/Epurarea.pdf.
[8] Report_en_en.pdf, AEM, WISE indicator table.

From Classical Systems Thinking to Modern Dynamic Systems Theory: Beyond the System Structure and Properties

Phd. stud. eng. inf. **Bogdan CIORUȚA**[1]

[1] Technical University of Cluj-Napoca - North University Centre of Baia Mare, Department of Informatics, Office of Information and Communication, str. Victor Babeș 62A, 430083, Baia Mare; bogdan.cioruta@staff.utcluj.ro

Abstract: As a natural continuation, of defining and understanding the concept of system, there followed a series of works that later resumed the subject, among them, of particular importance being the work of the Ludwig von Berthalanffy (1950), which represents a beginning of the Classical Systems Thinking zone, in which the system is defined as "a meeting of interdependent elements that work together in order to achieve a common objective through the use of a set of material, information, energy and human resources". In the same context, the present paper presents a natural continuation into the gradual transition from Classical Systems Thinking to Modern Dynamic Systems Theory, focusing on structure, properties and classification for different types of systems, mostly found in the specialized literature.

Keywords: Dynamic Systems Theory, system structure, system general & specific properties.

1. Introduction

The Modern Dynamic Systems Theory (MDST) as a field of research, by itself, follows the study of the properties of various types of systems or "systemic approach", as well as the enunciation of sets of principles, independent of domain, substance, type or time [1-4].

By the emergence of the General Systems Theory (GST), which includes Systems Theory (ST) - classical and modern, respectively post-modern, the ways of designing and developing the modelling of the environment or of the various structures considered, as part of MDST, have been opened [5-7]. The MDST is the symbiotic result between applied mathematics and "Systemology", its origins, as a mathematical theory [8], are especially situated through the multidisciplinary vision and the use of mathematical language and other specialized disciplines (see Fig. 1).
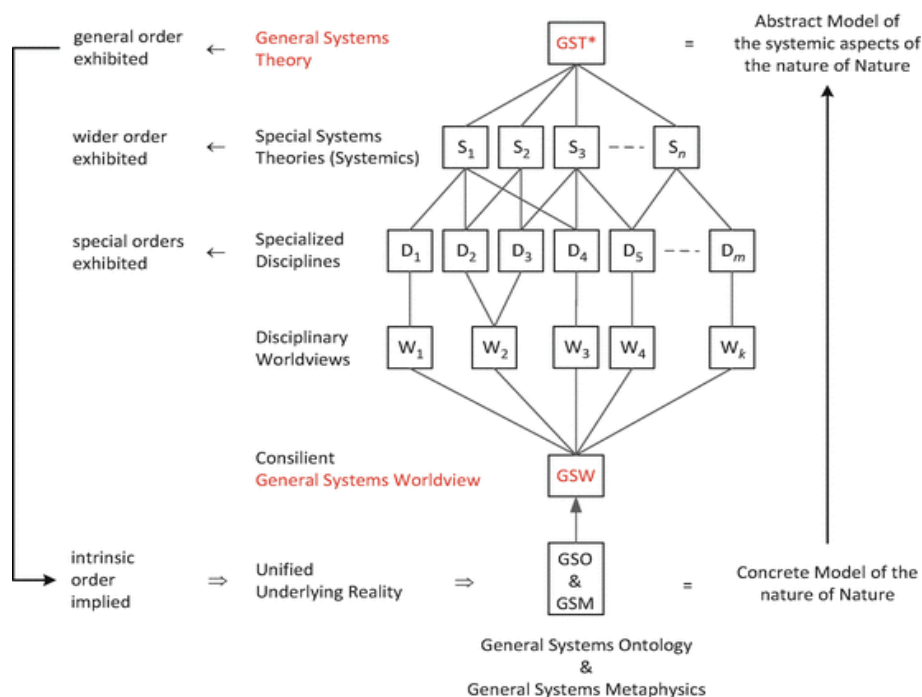
Fig. 1. The Modern Dynamic Systems Theory concept and its relationship with GST, GSO & GSM

As an interdisciplinary epistemological model, the GST represents a "*set of concepts, knowledge, methods and principles of independent applications, necessary and useful for the study of the structure, properties and characteristics of systems with variable degree of complexity*" [5-7, 9].

An extremely important notion, for the following approaches, which subscribes to the GST, is the notion of *system*. As it was natural, the notion of system appeared and developed over time, as a result of highlighting common features and behaviors for a number of processes and phenomena in different fields [8, 9], which allowed their identification, analysis and treatment from a structural-functional point of view, and not only, in a unitary way, from a systemic perspective [10].

In the specialized literature there are various definitions of the concept of system, some reflecting the tendency to define the system in a broader generality [11, 12], others the tendency to specialize in a certain field of knowledge [13-15]. The system, at least from a strictly conceptual point of view, appeared in an embryonic form, for the first time, in ancient Greek philosophy, thus, stating that "*the whole is more than the sum of the component parts*", Aristotle was the one who gave a first definition of the notion of system.

The notion of system therefore has a relative character, in the sense that any system can be decomposed into subsystems and, in turn, can be regarded as a subsystem of a more complex system; on this principle, of decomposing the real system (physical, mechanical) into subsystems, the system analysis is based to study the connections between subsystems, in relation to their objectives and according to the existing resources.

In the analysis of any system it must be taken into account that it cannot be separated from the environment to which it belongs as a subsystem, and that one system only functions as a subsystem within another more complex system. The detachment of a system from its environment can only be realized as an abstraction technique, the existence of a system itself takes place through a permanent exchange of substance, energy and information, which takes the form of the inputs and outputs of the system.

The notion of system has, as we have seen, a very broad sphere of understanding, being frequently encountered both in science and in technique (in all areas of human thought and action), but almost always in association with a "specification attribute". For example, we can mention:

- ➢ in mathematics and related fields: "*axiomatic system*", "*equation system*", "*coordinate system*", "*numbering system*" etc.;
- ➢ in physics and related fields: "*physical system*", "*atomic system*", "*system of forces*", "*reference system*", "*system of material points*", "*system of measurement*", "*system of units*", "*system crystallization*" etc.;
- ➢ for chemistry and related fields: "*chemical system*", "*periodic system*" etc.;
- ➢ in politics, public administration and related areas: "*social system*", "*political system*", "*voting system*", "*parliamentary system*", "*presidential system*", "*monarchic system*" etc.;
- ➢ in biology, medicine and related areas: "*biological system*", "*nervous system*", "*circulatory system*", "*bone system*", "*digestive system*" and so on;
- ➢ in linguistics and related fields: "*writing system*", "*grammar system*", "*philosophical system*", "*communication system*" and so on;
- ➢ in computer science, cybernetics and related areas: "*computer system*", "*file system*", "*database management system*", "*operating system*", "*binary system*", "*autonomous system*", "*expert system*", "*interconnection system*", "*information system*" etc.;
- ➢ in technique and related fields: "*technical system*", "*digital system*", "*energy system*", "*electronic system*", "*hydraulic drive-system*", "*navigation system*", "*heating / cooling system*", "*transport system*", "*pneumatic system*", "*transmission system*" etc.

2. Systems structure and elements

A system is structured as a connection of elements (see Fig. 2), each element in turn constituting a system (subsystem). The interaction between the elements of a system can give the system new properties, characteristics and behaviors, different from those of each component element. In the case of real systems, the interaction is performed on the basis of general physico-chemical laws, through mass and energy flows, which are information bearers.
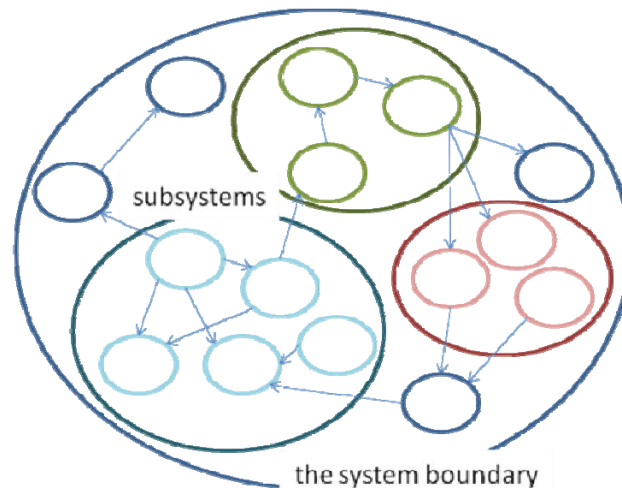
Fig. 2. The system and its relationship with subsystems

In the acceptance of the present work, through the system we will understand "*a set of elements that interact with each other and with the outside, based on and respecting certain rules, laws and principles, in order to achieve an objective, a functionality*". The fundamental characteristic of the physical systems is their materiality; this implies the movement and objective existence in space and time of physical systems.

The study of physical systems and processes is based on the principle of causality: each state in the objective world is the effect of causes that uniquely determine the respective state. Physical systems have mechanical, thermal, electrical properties etc., which can be analyzed in successive stages. In the analysis phase of the system, the model construction is in a sequence of stages, resulting, finally, the mathematical model associated with the physical system:

- *defining the "boundaries" of the system*, given that all physical systems work in interaction with other systems. For this reason it is necessary to define these boundaries.
- *defining simplifying hypotheses* or *defining the allowed approximations* - the model must include what is essential in the physical system. If the system is too complicated its utility becomes questionable.
- *establishing the equilibrium* or *balance equations* for the considered system (the dynamic system) or for the component subsystems, ending with the definition of the additional conditions, taking into account also the specificity of each type of system.

As we have already mentioned, Systems Theory operates with the concept of abstract system, in the form of a *mathematical model*, which allows the description of the characteristics and behavior of systems. Below we highlight some basic features of the systems, respectively:

- the *structural-unitary character* reflects the property of a system to be represented as a connection of subsystems whose action is oriented towards a certain meaning (purpose);
- the *causal-dynamic character* reflects the property of a system to evolve in time under the action of internal and external factors, respecting the principle of causality (according to which, any effect is the result of a cause, the effect is delayed to the cause and, in addition, identical causes generates the same effects under the same conditions);
- the *informational character* reflects the property of a system to receive, process, store / store and transmit information.

In the sense of Systems Theory, information means any factor that contributes qualitatively and / or quantitatively to the description of the behavior of a system. In technical systems, the physical quantities used as a support for the transmission and storage of information are called signals. The variable (state) sizes associated with a system, regardless of its nature, have two essential properties, namely the mediation of the input-output transfer ($I \rightarrow O$), which thus becomes an input-state-output transfer ($I \rightarrow S \rightarrow O$), respectively of accumulation in a concentrated (synthetic) form of all the useful information regarding the previous evolution of the system, that is to say of the past history of the system, being of three types:

- input sizes - independent system sizes (so of type cause), which influence from outside the system status and evolution;
- state quantities - sizes dependent on the input quantities (thus effect type), having the role of characterizing and describing the current state of the system;
- output sizes - sizes dependent on the state and / or input size (so effect type), having the role of transmitting information (especially to neighboring systems) on the current state of the system; some output sizes may be state sizes at the same time.

A system interacts with neighboring systems only through input and output sizes. Output sizes of a system are input sizes for neighboring systems. Output sizes of technical systems are measurable, while status sizes are not always accessible for measurement.

Systems Theory, as mentioned above, operates with two system concepts: I-S-O system (input-state-output) and I-O system (input-output). The I-S-O systems contain input sizes, state sizes, and output sizes, while I-O systems explicitly contain only input sizes and output sizes. Classic systems theory operates with type I-O systems, while modern and post-modern systems theory operate with type I-S-O systems. An abstract system (model) of type I-S-O and an abstract system (model) of type I-O can be associated to a physical system. In I-S-O systems, the input-output information transfer (I→O) is performed indirectly through the state. The input-state transfer (I→S) takes place with strict delay, following a system-specific dynamic, while the state-transfer (S→O) is instantaneous. In the case of systems that follow the principle of causality, the output size has a component that instantly tracks the changes in the input size. In these systems there is a direct input-output channel (I→O), through which the transfer is made instantly.

The Systems Theory also operates with trivial systems, where the output size, as a whole, instantly tracks the changes in the input size. Systems of this type (called static systems), do not contain state sizes, and the input-output transfer is performed only on the direct channel I→O. nontrivial systems where the output size is late for changes in the input size are called dynamic systems. For I-O systems, the input-output transfer is performed directly, with strict delay (on dynamic systems) or instantly (on static trivial systems).

When the variables of a system are separated into cause-type variables and, respectively, into effect-type variables, we say that the system is called oriented. In the abstract systems, the orientation is formal, while in the real systems, the orientation results from the application of the specific physico-chemical laws, with the unconditional observance of the principle of causality. Physical (engineering) systems are based on a series of material components whose properties and interrelationships can change over time, thus the system inputs and outputs can be classified into three categories: matter, energy and information.

3. General & specific system properties

A system can be defined as a set of components interconnected between them (an organized ensemble), so that two gateways exist there: *input gateway* and *output gateway*. For example, in the case of an electrical (and/or electronic) system, the nature of the components is the one mentioned, the gateways are also called *input circuits*, respectively *output circuits*.

Physical quantities involved in the operation of a system can be classified into: *quantities with independent variation* (*input quantities* or *excitations*) and *quantities dependent on those of input* (*output quantities* or *responses*). It should be noted, however, that the system response is not uniquely determined by excitation. For example, the current charged by a capacitor (condenser) depends both on the value of the voltage applied to the terminals, but also on the electrical charge existing in its dielectric ,when the voltage is applied. It turns out that the system also depends on a third size, called its state when the excitation is applied.

The knowledge of the general and specific properties of the systems is particularly useful in the investigation, analysis, modeling, design and control phases of the systems. The following properties characterize the vast majority of systems, both in relation to the external environment (*external properties*) and in the relation of subsystems (*internal properties*).

The external properties are generated by the relationships that the system has with (creates with) the environment, considering the non-trivial nature of inputs and outputs. *The internal properties*

depend on structure and the nature of the relationships, practically depending on the interlinked conditions of the subsystems that make up the system.

According to system classification we take into consideration the following properties:

a) *System sensitivity* refers to the possibility of the state vector to respond or not to certain input/output modifications. This property is extremely important to leadership and control systems, that will have superior performances proportional to how high the sensitivity is, so there is a possibility to influence the states by commands. Sensitivity can be enhanced in a special way by using design techniques when creating the leadership system.

b) *The open/partially open character of systems* - shows us that a system that has links to the environment through at least one input and an output is considered an *open system* (see Fig. 3), while the absence of one connection determines the *partially open* character. In the absence of both links to the environment, we are talking about an *isolated system*.
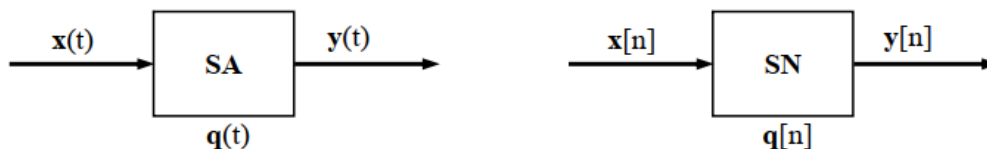

Fig. 3. Schematic representation of analogical and numerical systems

c) *Random character of the systems* - property determined by the way in which a system chooses from a set of possible states, a certain state. The choice of a state for the evolution of the system depends on its internal structure, its objectives, the nature of internal and external interactions, the turbulence of environmental factors, previous decisions made for its management.

d) *System dynamics* - general property of systems in which time is a basic parameter, which captures the transformations that take place inside the system, as well as those that take place outside, between the system and its environment. Every system (subsystem) has an internal time, which is system specific, and which is viewed as an invariable time (technological time) in relation to the processes nature, and internal and external connections that characterize it.

e) *System complexity* - general property that has an *objective character* that is related to the specificity of the analyzed system and *subjective character*, generated by the observer's report to the investigated system, by the way that system is investigated. The complexity can be defined according to *a set of causes and factors*, such as: the number of component elements (subsystems), the non-deterministic behavior of the component subsystems, the possibility of responding to some non-deterministic disturbances and the orientation of the systems towards the realization multitudes of purposes, competing or even contradictory.

f) *Observability* is the property through which the state successions that the system has can be partly or totally deducted knowing the input and output quantities. Regarding the acknowledgment of the states the system can be in, this can be achieved by using the associated model, knowing the system structure and interconnections or using a tracking system, by knowing all the parameters.

g) *Time invariance* - a deterministic and causal system is time invariant if the applications λ and μ are independent of time t (in case of analogic systems) and independent of variable n (in case of numeric systems). In many cases linearity and time invariance represent simplifying hypothesis used to obtain ideal systems.

From this point of view they should be applied only in signal variation domains for which the system is quasilinear, respectively for limited time intervals that depend on other properties (environment conditions) of the system or its components.

h) *Self-regulation* - it is the characteristic that expresses the capacity of a system to react by its own means to the internal or environmental disturbances. This property is characteristic to systems that have in their composition an active system and a control block (an regulation block) that can be a subsystem of itself or one from its environment.

i) *The antientropic character* of the systems is related, in particular, to the possibility of improving the management and reducing the degree of internal disorganization of the open systems, by improving the structural and informational - decision-making properties, as well as by intensifying the information exchange and transactions with the environment.

j) *Adaptability* is the property through which systems respond with certain outputs to given inputs. Modifying the internal structure of some systems in the context set by this property is called *self-adaptability*.

k) *Causality* - a system is causal if it's response for $t \geq t_0$ ($n \geq n_0$) depends exclusively on excitation and initial state of the system, usually $t_0 = 0$ ($n_0 = 0$). If the system is initially in a repose state and $x(0) = 0$ ($x[0] = 0$), then $y(0) = 0$ ($y[0] = 0$), which is a causal excitation corresponds a causal response. In this case input quantities are called *cause quantities* and output quantities are *effect quantities*.

By causality we can understand the trivial fact that an effect can't occur before the cause that and independent of it (*non-anticipative system*). A system is *strictly causal* if the effect occurs strictly after the cause. If effects or components that occur simultaneous with the cause exist, the system is called a *borderline causal system*. The following can be stated:

- an application λ (state function) exists and allows the determination of the evolution of the system state in time, if the initial excitation - state pair is known:

$$\{x(t), q(t)\} \xrightarrow{\lambda(t)} \frac{dq}{dt} = \dot{q}(t)\text{, in case of analogic systems}$$

$$\{x[n], q[n]\} \xrightarrow{\lambda[n]} q[n+1]\text{, in case of numeric systems}$$

(1)

- an application μ (*output function*) exists and allows the determination of evolution of the system response in time, if the initial excitation - state pair is known:

$$\{x(t), q(t)\} \xrightarrow{\mu(t)} y(t)\text{, in case of analogic systems}$$

$$\{x[n], q[n]\} \xrightarrow{\mu[n]} y[n]\text{, in case of numeric systems}$$

(2)

l) *Stability* represents the property of a system to recover to a state of equilibrium, having the same set of values for the state vector for a period of time, after the internal (external) cause of perturbation was removed. This property makes it so that at big variances in the inputs little variances in the outputs occur. If a system, during his evolution, goes through a perturbation, it exits the equilibrium state for the given moment, going to another state.

A causal and deterministic system is stable if the characteristic signals (the response and the state) are of the boundary mode, in case of an excitation of the bounded mode:

$$\left|x(t)\right| < M_x < \infty \Rightarrow \begin{cases} q(t) < M_q < \infty \\ y(t) < M_y < \infty \end{cases}, \forall t \geq t_0 \text{ , in case of analogic systems}$$

(3)

$$\left|x[n]\right| < M_x < \infty \Rightarrow \begin{cases} q[n] < M_q < \infty \\ y[n] < M_y < \infty \end{cases}, \forall n \geq n_0 \text{ , in case of numeric systems}$$

Stability can also be found under the name *BIBO* (*Bounded Input*, *Bounded Output*). Ensuring stability is a major goal in systems design and control.

m) *Accessibility* of a state x_k should occur only if an input u_k exists in the interval (t_0, t_k) which leads the system to the output x_0 when in state x_k. *Detectability of an output y_j* in state x_k it's the duality of this concept and it needs to generate a significant output.

n) *Structurability* defines the need for any system to have a lot of intercorrelated component elements, so a specific structure. A system maintains its structure as an expression of maintaining the qualitative nature of the system (*structural invariant systems*); on the other hand, if the systems respond differently by the values taken by their states in relation to the

inputs (commands) and change their structure over time, then we are talking about *structurally variable systems*.

o) *Composability* and *decomposability* refer to the property of a system to compose itself out of a finite number of subsystems and decompose itself in the same way. Decomposability is the base of system analysis and composability is the base of system development, both being important in system analysis and synthesis.

p) Linearity - a dynamic system S has the linearity property (is linear), if two conditions are met, which are: numerical sets U, X, Y, Ω are organized as linear space on the same scalar set G; state equations have the additive property and homogenous property in regards to the pair $\left(x_0, u_{[t_0,t_1]}\right)$ for the explicit form or with the pair $\left(x(t), u(t)\right)$.

q) For *system equivalence* we start considering the following dynamic system

$$S = S(\Omega, f, g) = S(\Omega, f, g, x) \tag{4}$$

in which the state vector is x. Two states $x_a, x_b \in S$ of this system are equivalent at the time moment $t = t_0$ if the outputs deriving from these initial states for the same applied input are equivalent

$$
\begin{aligned}
x^a(t_0) &= (x^a, t_0) \approx x^b(t_0) = (x^b, t_0) \\
\varphi\left(t, t_0, x^a, u_{[t_0,t]}\right) &\equiv \varphi\left(t, t_0, x^b, u_{[t_0,t]}\right) \\
\eta\left(t, t_0, x^a, u_{[t_0,t]}\right) &\equiv \eta\left(t, t_0, x^b, u_{[t_0,t]}\right)
\end{aligned}
\tag{5}
$$

If two states are equivalent at the time t_0 they remain equivalent $\forall t \geq t_0$

$$x^a(t_0) \approx x^b(t_0) \Rightarrow x^a(t) \approx x^b(t) \tag{6}$$

If in a system exist equivalent states that means that the system, moreover the state vector x it's not in a reduced form, meaning that the dimension is greater than necessary to uniquely determine the output when the input is given.

r) *Finitude* is the property of systems to be finite, in regards to the fact that real systems have finite input, output and state spaces; using these properties in system analysis allows to conceptually define categories of systems and using this base to create structural and functional typologies.

s) *Controllability* and also *state controllability* can be achieved if inputs or commands are known or commands and state at a moment is known, only by doing so the state at the next moment can be generated (all outputs or only parts of the outputs). We can say about the system that is a *globally controllable* if for every output there is a class of input functions that generate them. When certain outputs can't be determined applying the input functions or admissible commands, then we say that the system is *partially controllable*.

4. Conclusions

As it was natural, the notion of system appeared and developed over time, as a result of highlighting common features and behaviours for a number of processes and phenomena in different fields of interest or domains of activity. The knowledge of the structure, even of the general and specific properties of the systems is particularly useful in the investigation, analysis, modelling, design and control phases of the systems.

The properties that we mention characterize the majority of systems, in relation to the external environment (external properties) and in the relation with subsystems (internal properties).

Based on the criteria stated above and properties derived from the structural-unitary, causal-dynamic and informational character of the systems, they can be divided - delimited and grouped - into classes. The systems belonging to a class have similar properties and behaviours; so, they

can be more easily investigated in this context, from the Classical Systems Thinking (CST) to Modern Dynamic Systems Theory (MDST).

References

[1] Bertalanfy, L.V. "General systems theory." Chapter book in *General Systems: Yearbook of the society for the advancement of general systems theory* 1 (1956): 1–10.
[2] Ackoff, R. *Redesigning the future: a systems approach to societal problems*. NY, John Wiley, 1974.
[3] Checkland, P.B. "Towards a systems-based methodology for real world problem solving." *Journal of Systems Engineering* 3, no. 2 (1972): 87–116.
[4] Checkland, P.B. *Systems thinking, Systems Practice*. Chichester, John Wiley, 1981.
[5] Dolga, V. *Systems theory / Teoria sistemelor.* Timișoara, Politehnica Publishing House, 2010.
[6] Cîrtoaje, V. *Introduction to systems theory - lecture notes / Introducere în teoria sistemelor - curs universitar*. Faculty of Mechanical and Electrical Engineering, Petroleum-Gas University of Ploieşti, 2012.
[7] Dolga, V. *Theory of automatic systems - lecture notes / Teoria sistemelor automate - curs universitar.* Faculty of Mechanical Engineering, Politehnica University of Timisoara, 2013.
[8] Cioruța, B., and M. Coman. "Considerations regarding the study of dynamic systems (II): the problem of the knowledge of the behavior*"* / "Considerații privind studiul sistemelor dinamice (II): problematica cunoașterii comportamentului acestora." Sesiunea ştiinţifică naţională pentru studenţi şi elevi "O carieră în inginerie" - Zilele Carierei în UTCN, 4th edition, April 26, 2018, Technical University of Cluj-Napoca. *A profession of the future - engineering / O profesie de viitor – ingineria*. Cluj-Napoca, Alma Mater Publishing House (2018): 21-28.
[9] Cioruța, B., and M. Coman. "Considerations regarding the study of dynamic systems (I): their (re)definition, classification and modeling" / "Considerații privind studiul sistemelor dinamice (I): (re)definirea, clasificarea și modelarea acestora." Sesiunea ştiinţifică naţională pentru studenţi şi elevi "O carieră în inginerie" - Zilele Carierei în UTCN, 4th edition, April 26, 2018, Technical University of Cluj-Napoca. *A profession of the future - engineering / O profesie de viitor – ingineria*. Cluj-Napoca, Alma Mater Publishing House (2018): 13-20.
[10] Cioruța, B., and M. Coman. "Considerations on the dynamic system study: from definition and classification to analysis and interpretation of behavior." Paper presented at the 20th International Conference "Scientific Research and Education in the Air Force" (AFASES[®]), Brașov, Romania, May 22-27, 2018.
[11] Novikov, D.A. "Systems theory and systems analysis. Systems engineering." Chapter book in *Cybernetics. Studies in Systems, Decision and Control* 47 (2016): 39-44.
[12] Hieronymi, A. 'Understanding systems science: a visual and integrative approach." *Systems Research and Behavioral Science* 30 (2013): 580-595, 10.1002/sres.2215.
[13] Jackson, M. "The nature of soft systems thinking: the work of Churchman, Ackoff and Checkland." *Journal of Applied Systems Analysis* 9 (1982): 17-28.
[14] Jackson, M. "Beyond a system of systems methodologies." *Journal of the Operational Research Society* 41, no. 8 (1990): 657-668.
[15] Jackson, M. *Systems approaches to management*. New York, Kluwer Academic Publishers, 2000.

Program: POC 2014 - 2020, Ctr. nr. 37/ 02.09.2016, MySMIS103396-768

Crearea unui nucleu de competență de înalt nivel în domeniul creșterii eficienței de conversie a energiilor regenerabile și a autonomiei energetice prin utilizarea combinată a resurselor, CONVENER

MODELUL EXPERIMENTAL DE SISTEM COMBINAT ELECTRIC

### CONSTRUCȚIA

Componența acestui model experimental este următoarea:

- 1 turbină eoliană (tip DARRIEUS sau tip SAVONIUS), montată pe un ax vertical;
- 1 generator electric, de curent continuu, acționat de turbina eoliană prin intermediul axului vertical, cu o putere de 0,5-1 kW, turația maximă de 500 rot/min și tensiunea de 12 V;
- 2 panouri fotovoltaice, înseriate electric;
- 2 baterii electrice (acumulatoare), pentru înmagazinarea energiei electrice captate, având o capacitate de 260 Ah la tensiunea de 12 Vcc;
- 1 controler electric compus din controler de încărcare solară, încărcător de baterii de la rețea, invertor de 230 Vca și un redresor - încărcător al generatorului eolian.
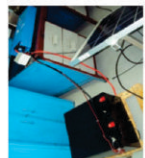
Modelul experimental de sistem combinat electric asociază două surse de energie regenerabilă, prin captarea și conversia energiei termice solare și a energiei eoliene, în scopul asigurării continuității livrării de energie electrică.

În cazul sistemului combinat electric s-au elaborat 2 modele experimentale, și anume:
- modelul experimental de sistem combinat electric ce conține ca elemente principale o turbină eoliană Darrieus și două panouri solare fotovoltaice;
- modelul experimental de sistem combinat electric ce conține ca elemente principale o turbină eoliană cu pale Darrieus combinată cu un rotor Savonius și două panouri solare fotovoltaice.

Așadar, turbina eoliană este componenta care face diferența între cele două sisteme combinate electrice.

Model experimental de sistem electric combinat fără rotor Savonius

Turbina eoliană Darrieus

CONCLUZII PRIVIND REZULTATELE EXPERIMENTALE

- cele două modele experimentale de sistem combinat electric corespund funcțional cu cerințele documentației tehnice, realizând scopul pentru care au fost gândite;
- producția de energie electrică a sistemului combinat este dependentă într-un grad ridicat de condițiile atmosferice, viteze ale vântului și /sau cer senin;
- în cazul unor variații mari ale radiației solare sau a vitezei vântului invertorul este capabil sa compenseze fluctuațiile de energie electrică, până la un prag al descărcării celor 2 baterii de stocare a energiei;
- testarea experimentală a sistemului combinat eolian - solar a evidențiat faptul că este nevoie de o capacitate de producție solară mai mare necesară pentru consum și pentru a încărca complet bateriile de stocare, în special pentru acoperirea necesarului în zilele mai noroase și când viteza vântului nu este suficientă pentru ca turbina să funcționeze la capacitate maximă;
- pentru modelul experimental cu turbină având rotor Savonius s-a constatat o comportare mai bună, în sensul că producția de energie a crescut față de modelul experimental fără rotor Savonius deoarece axul turbinei se pune în mișcare la viteze mai mici ale vântului, sub 6 m/s;
- din analiza tabelului de date numerice, se poate observa că regulatoarele de tensiune solar și eolian asigură tensiunea de încărcare a bateriilor de stocare, curentul variind în funcție de gradul de încărcare al bateriilor și de puterea livrată la consumator.

Pentru prototip, este necesară creșterea puterilor la ambele subsisteme electrice, pentru a avea o rezervă de putere, dacă se dorește garantarea unei anumite producții minime de energie electrică, în cazul condițiilor atmosferice nefavorabile.

Generator P_max = 1 kW

Panouri solare policristaline

Acumulatoare electrice

Model experimental de sistem combinat electric cu rotor Savonius

Turbina eoliană cu rotoare Savonius și Darrieus

Program: POC 2014 - 2020, Ctr. nr. 37/ 02.09.2016, MySMIS103396-768

Crearea unui nucleu de competență de înalt nivel în domeniul creșterii eficienței de conversie a energiilor regenerabile și a autonomiei energetice prin utilizarea combinată a resurselor, CONVENER

MODELUL EXPERIMENTAL DE SISTEM COMBINAT TERMIC

Modelul experimental de sistem combinat termic asociază două surse de energie regenerabilă, prin captarea și conversia energiei termice solare și a energiei termice generate prin arderea biomasei, în scopul asigurării continuității livrării de energie termică, indiferent de factorii atmosferici.

Sistemul combinat termic se dorește a fi utilizat de către companii de stat și private, precum și de către persoane private, în mod special din zonele izolate, care vor să-și asigure independența energetică termică prin utilizarea energiilor regenerabile.

În principiu, modelul experimental de sistem combinat termic grupează un panou termic solar și un modul energetic pentru biomasă de putere mică (3 kW), care este o centrală termică tip TLUD, la care se adaugă componenetele necesare pentru controlul funcționării în bune condiții a sistemului combinat.

Modelul experimental de sistem combinat termic: vedere din față și din lateral

CONSTRUCȚIA

Componența modelului experimental de sistem combinat termic, pentru energie solară și biomasă, precum și caracteristicile tehnice principale, sunt următoarele: mini panou termic solar cu 4 tuburi vidate de 400/500 mm, presiunea de 6 bar; modul energetic pentru biomasă, compus, în principal, dintr-o centrală termică pe biomasă (gazogen tip TLUD de 3 kW și un rezervor de apă caldă); electropompă de circulație apă caldă gazogen, cu debitul 05-06 l/min; boiler mixt de 120 l, la 10 bar, cu două serpentine și rezistență electrică; panou electro-pompă de circulație; panou termic, cu elemente de reglare și securitate; sistem de monitorizare a funcționării, cu senzori de temperatură, traductoare de debit și contor de măsurare a volumului de apă caldă.

Mini panou termic solar | Boiler mixt de 120 l, la 10 bar | Modul energetic pentru biomasă | Panou electropompă de circulație

Sistem de monitorizare a temperaturilor din instalație | Electropompă de circulație apă și debitmetru

CONCLUZII PRIVIND REZULTATELE EXPERIMENTALE

- modelul experimental de sistem combinat termic corespunde funcțional cu cerințele documentației tehnice, realizând scopul pentru care a fost gândit;

- testarea experimentală a subsistemului termic bazat pe biomasă a evidențiat faptul că generatorul termic pe bază de biomasă este funcțional, însă din punct de vedere dimensional s-a dovedit a fi prea mic și, deci, pentru prototip trebuie redimensionat crescător pentru o putere de circa 10-12 kW;

- alimentarea cu peleți, precum și evacuarea cenușei rezultate în urma arderii, durează mult, fapt ce duce la pierderea căldurii acumulate. Din acest motiv, pentru prototip trebuie gândită o altă soluție, care să micșoreze timpii auxiliari;

- testarea experimentală a subsistemului termic bazat pe un panou termic solar, în tandem cu stația solară, care include pompa de circulație, dar și controlerul de funcționare, s-a dovedit o soluție bună.

FLUIDAS

NATIONAL PROFESSIONAL ASSOCIATION OF HYDRAULICS AND PNEUMATICS IN ROMANIA

NATIONAL PROFESSIONAL ASSOCIATION OF HYDRAULICS AND PNEUMATICS IN ROMANIA

www.fluidas.ro

fluidas@fluidas.ro